NPL-865

TECHNICAL PROGRESS REPORT

CONTRACT DE-AC02-76ER00535

November 1, 1980

COO/535-768

NOTICE

This report was prepared as an account of work sponsored by the United States Government. Neither the United States nor the United States Department of Energy, nor any of their employees, makes any warranty, express or implied, or assumes any legal liability or responsibility for the accuracy, completeness, or usefulness of any information, apparatus, product or process disclosed, or represents that its use would not infringe privately owned rights.

DISCLAIMER

TABLE OF CONTENTS

		Page
I.	INTRODUCTION	1
II.	EXPERIMENTAL PROGRAM	2
	A. Nuclear Physics	2
	1. Nuclear Reaction Studies	2
	a. Single-Nucleon Transfer Reactions	2
	i. Proton Stripping to High Spin States of ^{13}N	2
	ii. Proton Stripping to ^{14}N	3
	iii. Neutron-hole States in ^{77}Kr	4
	iv. A Study of ^{79,81}Rb via Proton Stripping Reactions	5
	v. The ^{103}Rh(^{3}He,d)^{104}Pd Reaction at 33.0 MeV	8
	vi. The ^{208}Pb(p,d)^{207}Pb and ^{120}Sn(p,d)^{119}Sn Reactions at 26 MeV	9
	vii. Core-coupled States Excited in the ^{208}Pb(d,t)^{207}Pb Reaction	11
	viii. Search for Stretched 8$^-$ States in ^{52}Cr	12
	ix. Proton Stripping on ^{9}Be	13
	x. Spectroscopy of A=12 in the Ex=19 MeV Region	14
	xi. The ^{11}B(d,n)^{12}C Reaction	18
	b. Two-Nucleon Transfer Reactions	21
	i. The ^{208}Pb(p,t)^{206}Pb Reaction at 26.2 MeV	21
	ii. The Energy Dependence of the (p,t) Reaction on ^{54}Fe	24
	iii. Study of the (p,t) Reaction on Krypton Isotopes	31
	iv. One and Two Step Processes for the ^{208}Pb(^{3}He,p)^{210}Bi Reaction	32
	v. Survey of the (t,p) Reaction on Medium-mass Nuclei	34
	vi. Investigation of the Forbidden 4$^-$ State via the ^{206}Pb(t,p)^{208}Pb Reaction	39
	vii. Proton Pairing Strength in ^{91}Nb, ^{115}Sb, and ^{117}Sb	40
	viii. Excitation of High-lying States by the (^{3}He,n) Reaction	46
	c. Three or More Nucleon Transfer Reactions	50
	i. The (^{4}He,p) Reaction on ^{13}C and Other Light Nuclei	50

Page

ii. The (α,n) Reaction on Light Nuclei..... 51
iii. High Spin States in the $^{46,48}Ti(\vec{p},\alpha)^{43,45}Sc$ Reactions..... 53
iv. The $(\vec{d},^{6}Li)$ Reaction..... 57
v. Evidence of Non-statistical Mechanisms in Low-energy $(^{9}Be,n)$ Reactions..... 57

d. Charge Exchange Reactions..... 59

i. The 1^{+} Strength Distribution in ^{58}Co..... 59
ii. The $^{86}Sr(^{3}He,t)^{86}Y$ Reaction..... 61

e. Elastic and Inelastic Scattering..... 63

i. A Survey of the Octupole States in Even-Even Nuclei and the $^{104}Pd(\alpha,\alpha')$ Reaction at 34.9 MeV..... 63
ii. Alpha Scattering on ^{9}Be..... 66
iii. Isospin Mixing in ^{14}N near 9 MeV..... 68
iv. Inelastic Alpha Particle Scattering on ^{10}B and ^{11}B..... 69

f. Isoscalar and Isovector Transition Amplitudes in A=13..... 72
g. Compound Reaction Mechanism Studies..... 75

2. Gamma Ray Studies..... 80

a. Gamma Ray Spectroscopy in the A=90 Region..... 80
b. The Level Structure of ^{64}Ge..... 83
c. The Tetraneutron Revisited..... 84
d. Aligned Octupole Bands in Deformed Nuclei..... 86
e. In-beam Gamma Ray Spectroscopy in the Rare Earth Region..... 87

3. Other Activities..... 93

a. A Method for Determining the Isotopic Abundance of Lithium..... 93
b. Determination of the Fluorine Content of Oil Shale Samples from the Piceance Creek Basin..... 95
c. Thick Target Measurements of Thermonuclear Reaction Rates..... 99
d. Proton Spectrum Analysis by Thick Target Radioactivation..... 100
e. Mineral Analysis by X-Ray Fluorescence..... 101
f. Neutron Spectral Studies Using the Bonner Sphere System..... 102

Page

B. Intermediate Energy Physics..... 104

1. Elastic and Inelastic π^+, π^- Scattering on ^{7}Li..... 104
2. $\pi\pm$D Comparison at 143 MeV..... 110
3. Excitation of Giant Resonances in ^{118}Sn by 130 MeV Pion Scattering (Experiment 522)..... 114
4. New Proposals to LAMPF..... 116
5. Study of Giant Resonances via the (p,n) Reaction..... 118
6. Neutron Matter Distributions from Quasi-Elastic (p,n) Reactions..... 121
7. Analyzing Powers for the ^{13}C and ^{208}Pb($\vec{p}$,d) Reaction at T_p=123 MeV..... 123
8. Energy Dependence of the $\tau\cdot\tau$ and $\sigma\cdot\sigma\tau\cdot\tau$ Effective Interactions..... 125
9. The ^{4}He($\vec{p}$,d)^{3}He Reaction at 200 and 400 MeV..... 126
10. Analyzing Power Measurements for the ^{13}C($\vec{p}$,d)^{12}C Reaction at 200 and 400 MeV..... 127
11. Proton Radius Determinations from the Ratio of π^+ Elastic Scattering from ^{11}B and ^{12}C..... 131
12. Elastic Scattering of 13.9 MeV Positive Pions from ^{12}C..... 136

C. Apparatus and Facility Development..... 139

1. Accelerator Development Studies..... 139

   a. Introduction..... 139
   b. Storage Ring..... 140
   c. The Mini-Cyclotron and Ion Source Testing..... 146
   d. The 52" Cyclotron Development..... 152

2. Neutron Detector Development for TOF Studies..... 158

   a. Very Large Detector (VLD)..... 158
   b. Long Cylindrical Detectors..... 164
   c. The Multiple-Paddle Detector..... 165
   d. Work in Progress..... 167
   e. Detector Shielding for Neutron TOF Studies at Colorado..... 169
   f. Anti-Coincidence Paddles for Indiana (p,n) Studies..... 169

3. New Computing Facilities..... 171

   a. Data Acquisition Hardware..... 171
   b. Computer Program Development..... 172
   c. Software Update..... 173

Page

4. Electronics Maintenance and Development..... 176

a. Cyclotron..... 176
b. Experimental Support..... 177

5. Space Usage..... 179
6. Photography..... 180
7. Detector Cooling..... 180
8. A Heavy-ion Detector for the Energy-loss Spectrometer. 181
9. An Evaluation of a CdTe Detector as a Practical Spectrometer for Energetic Charged Particles..... 184
10. Time-of-Flight Spectrometer for EPICS..... 186
11. Energy-Time Distribution of the Cyclotron Beam..... 188

D. Cyclotron Operation..... 192

III. THEORETICAL PROGRAM..... 196

A. A Weak-Coupling Analysis of the $^{205}Tl(p,t)^{203}Tl$ Reaction.. 196

B. Finite-Range Two-Nucleon Transfer..... 198

C. Effects of Deuteron Continuum States in Stripping Reactions..... 202

D. Non-Locality Effects in Nuclear Reactions..... 205

E. Studies of the Sensitivity of the Ratio of π^+ Elastic Cross Sections to the rms Charge Radius of Light Nuclei... 207

F. Systematics of the Intermediate Energy (p,d) Reaction..... 210

G. Failure in the DWBA Analysis of (p,d)..... 213

H. Relativistic Generalization of Simple Pion-Nucleon Models. 219

I. Pion-Nucleon Scattering Calculations..... 221

J. Separable Approximation to the Reid Potential..... 222

K. Computer Program Development..... 224

IV. PUBLICATIONS AND REPORTS..... 225

A. Published Articles..... 225

B. Articles Accepted or Submitted for Publication..... 228

C. Published Abstracts, Conference Presentations and Reports. 231

D. Theses..... 233

V. PERSONNEL..... 234

I. INTRODUCTION

This report summarizes work carried out at the Nuclear Physics Laboratory of the University of Colorado from November 1, 1979 through October 31, 1980 under contract DE-AC02-76ER00535 between the University of Colorado and the United States Department of Energy.

We continued this year to emphasize light ion reaction studies with the AVF cyclotron. The high resolution magnetic spectrometer has allowed studies of nucleon transfer, scattering, and charge exchange reactions throughout the periodic table. More experiments have been run with solid state counters this year than has been the case recently, as we examine broad range spectra of the light nuclei where only moderate resolution is demanded. Several of these experiments were undertaken for more detailed studies of excitations seen with higher energy probes. Multiple coincidence measurements with neutron and gamma-ray counters have opened a new program in pre-equilibrium reactions and provided a new signature for the study of neutron-deficient final nuclei. The neutron time of flight program has expanded to higher excitations and to use of the (d,n) and (α,n) direct nucleon transfer reactions.

Our recent progress in the theory of polarization in nuclear reactions has been impressive, and directions for future studies are increasingly clear. The new PDP 11/60 off-line computer now handles much of our need for DWBA and coupled-channel calculations. Many of these theoretical investigations span both the low energy and intermediate energy regimes.

Three important experiments were completed at the EPICS pion scattering facility at LAMPF, and other low energy pion scattering data were obtained at TRIUMF. Several (p,d) runs at high energies were accomplished, some with polarized beams at TRIUMF. High-lying structures in medium mass nuclei were studied by the (p,n) reaction at Indiana. Interest in the use of polarized beams has been prompted by our theoretical successes in this area. This interest has led to the study of one - and two-nucleon transfer reactions on a range of nuclei at the Los Alamos tandem and at IUCF.

The program in accelerator improvement has followed two main paths. Basic studies of the plasma physics of ion sources have been performed on the model cyclotron, now heavily instrumented. Orbit calculations for our cyclotron have indicated several changes to be made, leading especially toward better time of flight running conditions. A novel r. f. cavity structure has been designed, with qualities that make it promising for a number of nuclear applications.

II. EXPERIMENTAL PROGRAM

A. Nuclear Physics

1. Nuclear Reaction Studies

a. Single-Nucleon Transfer Reactions

i. Proton Stripping to High Spin States of ^{13}N

R. J. Peterson and J. J. Hamill

The $7/2^+$ state at 7.16 MeV, the $5/2^-$ state at 7.38 MeV and a broad peak at 9.0 MeV are clearly noted in the ^{12}C (^3He,d) ^{13}N reaction at 43.6 MeV. The $7/2^+$ state cannot be excited by a single excitation without a very unlikely $\ell=4$ transfer. The flat angular distribution noted in Fig. Al-al indicates a multistep process. The most likely excitation, sequential scattering and $d_{5/2}$ stripping on the large quadrupole deformation known for ^{12}C, is noted in the figure. With three sets of optical potentials the predictions are shown in Fig. Al-al; the solid curve gives the best agreement with the well-known single stripping states of ^{13}N. The same model, computed within the strong coupling limit, gives the three predictions shown in Fig. Al-al for the 9.0 MeV peak, assuming a similar $K=5/2^+$, $J=9/2^+$ state. The shape is correctly predicted, but the magnitude is evidently quite sensitive to the choice of optical parameters.

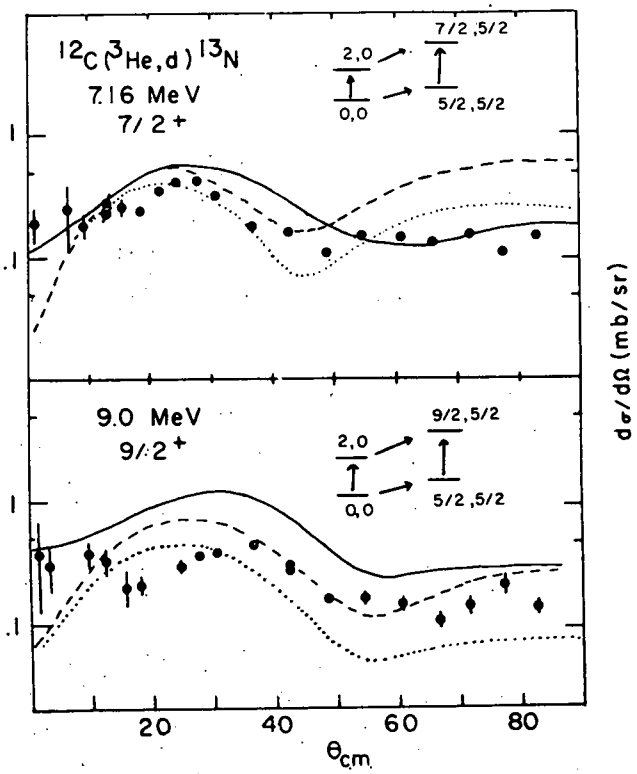

Fig. Al-al.
The pathways for sequential inelastic scattering and stripping to high spin states of ^{13}N are shown. Data are compared to the predictions for these mechanisms for three different sets of optical model distorting parameters which are shown as the three curves for each state.

This state, shown now to be a $9/2^+$ level, is analogous to the 9.50 MeV state of ^{13}C, which is preferentially excited by negative, but not positive, pion scattering.[1] A $9/2^+$ spin assignment has been guessed for this level, and the present work confirms the spin of this important level and establishes its structure as a $d_{5/2}$ proton coupled to the ^{12}C 4.4 MeV 2^+ state.

This work has been accepted for publication in the Physical Review.

---

[1] D. Dehnhard et al., Phys. Rev. Letters 43 (1979) 1091.

ii. Proton Stripping to ^{14}N

R. J. Peterson and J. J. Hamill

The $^{13}C(^3He,d)$ reaction has been studied at 43.6 MeV to measure spectroscopic factors to levels in ^{14}N up to 11.7 MeV. A sample spectrum is shown as Fig. A1-a2, with an overall resolution as good as 35 KeV. The dominant $\ell=2$ proton transfer cross sections are compared to DWBA predictions in Fig. A1-a3, where it is noted that good fits are obtained. The $\ell=1$ spectroscopic factors are observed to be in good agreement with predictions,[1] although several more weak positive parity states are seen than are predicted.

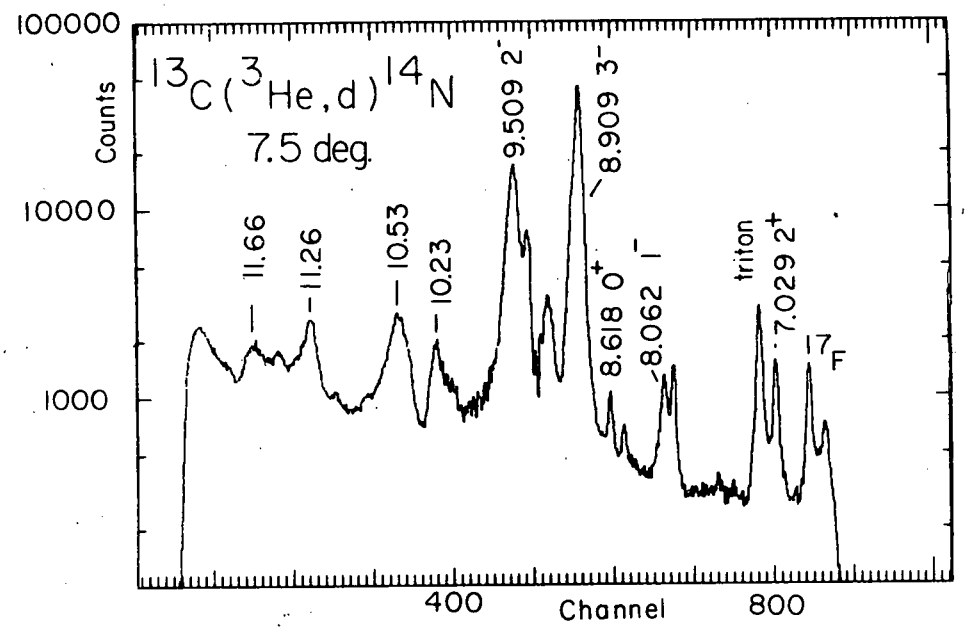

Fig. A1-a2. A sample spectrum, on a logarithmic scale, for proton stripping to ^{14}N at high excitations.

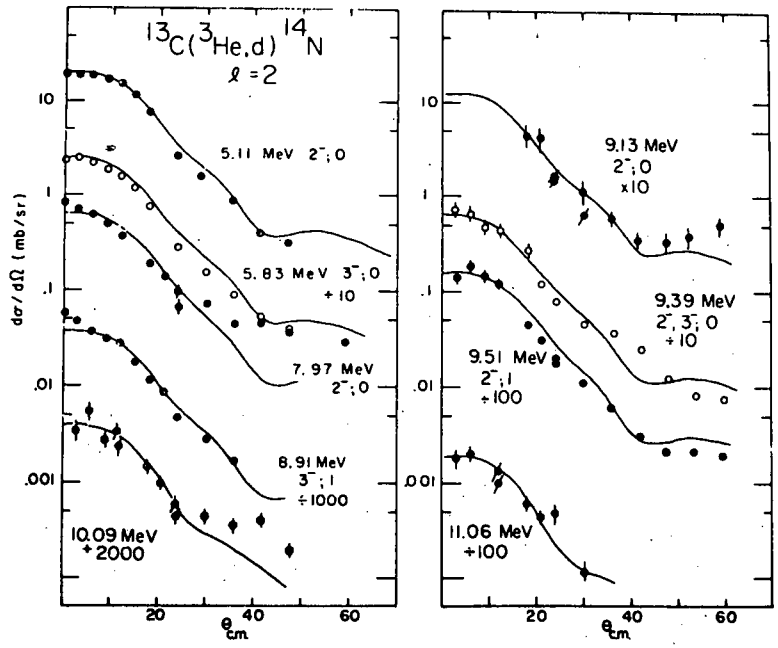

Fig. A1-a3. Angular distributions populating 2^- or 3^- states in ^{14}N by the (^{3}He,d) reaction are compared to DWBA predictions. Reliable spectroscopic factors have been obtained from these comparisons.

The ℓ=1 results provide reassurance of the reliability of the ℓ=0 and ℓ=2 results. We find fair agreement for the ℓ=0 predictions[2] for T=0 states of ^{14}N, but these calculations underpredict the T=1 strength to 0^- and 1^- states, which could be part of the giant dipole state, not included in the calculations. The ℓ=2 strength to the major states is much as predicted[1] but again several more states are seen than predicted.

A number of improved spin and parity assignments are made for states above 10 MeV.[3]

This work has been submitted to Nuclear Physics.

---

1 S. Cohen and D. Kurath, Nucl. Phys. A101 (1967) 1.
2 H. U. Jager et al., Nucl. Phys. A171 (1971) 16.
3 F. Ajzenberg-Selove, Nucl. Phys. A268 (1976) 1.

iii. Neutron-hole States in ^{77}Kr

E. Sugarbaker, B. Diana, C. A. Fields, R. S. Raymond

The $^{78}Kr(p,d)^{77}Kr$ reaction is being studied at Ep=26 MeV.

Comparison of the experimental angular distributions obtained with the University of Colorado energy-loss spectrometer with DWBA calculations will be used to determine the parities and spectroscopic strengths of the low-lying levels in ^{77}Kr. Only tentative spin assignments for the ground state and a few excited levels are currently available from decay and in-beam γ-ray spectroscopic studies. The present pick-up reaction investigation will thus provide a wealth of new spectroscopic information on this neutron deficient isotope of krypton.

iv. A Study of ^{79,81}Rb via Proton Stripping Reactions

B. Diana, R. A. Emigh, C. A. Fields, D. Handschy, R. S. Raymond, E. Sugarbaker, F. W. N. de Boer; W. P. Alford (Western Ontario U.)

The difficulties inherent in the use of a gas target have limited previous stripping reaction studies to only the heaviest Rb isotopes. We recently assembled a small gas cell having 1 mg/cm^2 Ni windows with which 50-60 keV energy resolution in (^{3}He,d) reaction studies is possible. The ^{78,80}Kr(^{3}He,d)^{79,81}Rb reactions have been studied at $E_{^3He}$=25 MeV using this new gas cell.

The University of Colorado energy loss spectrometer was used to analyze the reaction deuterons. Angular distributions from 10^o to 50^o were measured. A sample spectrum of the ^{78}Kr(^{3}He,d)^{79}Rb reaction is shown in Fig. A1-a4. Preliminary analysis of the data indicates that there is sufficient structure in the angular distributions at this bombarding energy with which to extract reliable ℓ-transfers.

The spectra for the two final nuclei are surprisingly similar; a large fraction of the spectroscopic strength appears to be concentrated in the first few hundred keV of excitation. Recent measurements have suggested that the ^{79}Rb ground state spin and parity is $5/2^+$, in disagreement with earlier assignments of $3/2^-$ or $5/2^-$. Based on a preliminary analysis, our data support the most recent assignments, in that the ground state transition appears to have an angular distribution characteristic of an L=2 transfer.

Due to momentum matching, the (α,t) reaction is more sensitive to the high spin transfers. To assist in the identification of high spin states, we have studied the same final nuclei using the (α,t) reaction. A sample spectrum for the ^{78}Kr(α,t)^{79}Rb reaction at E =36 MeV is shown in Fig. A1-a5. The suggestion of Clements, et al.[1] that a $9/2^+$ state is located at 97 keV of excitation in ^{79}Rb may be supported by our data. A strongly populated level is observed at about 100 keV of excitation in our (α,t) spectra.

[1] J. S. Clements, Phys. Rev. C20, (1979) 164.

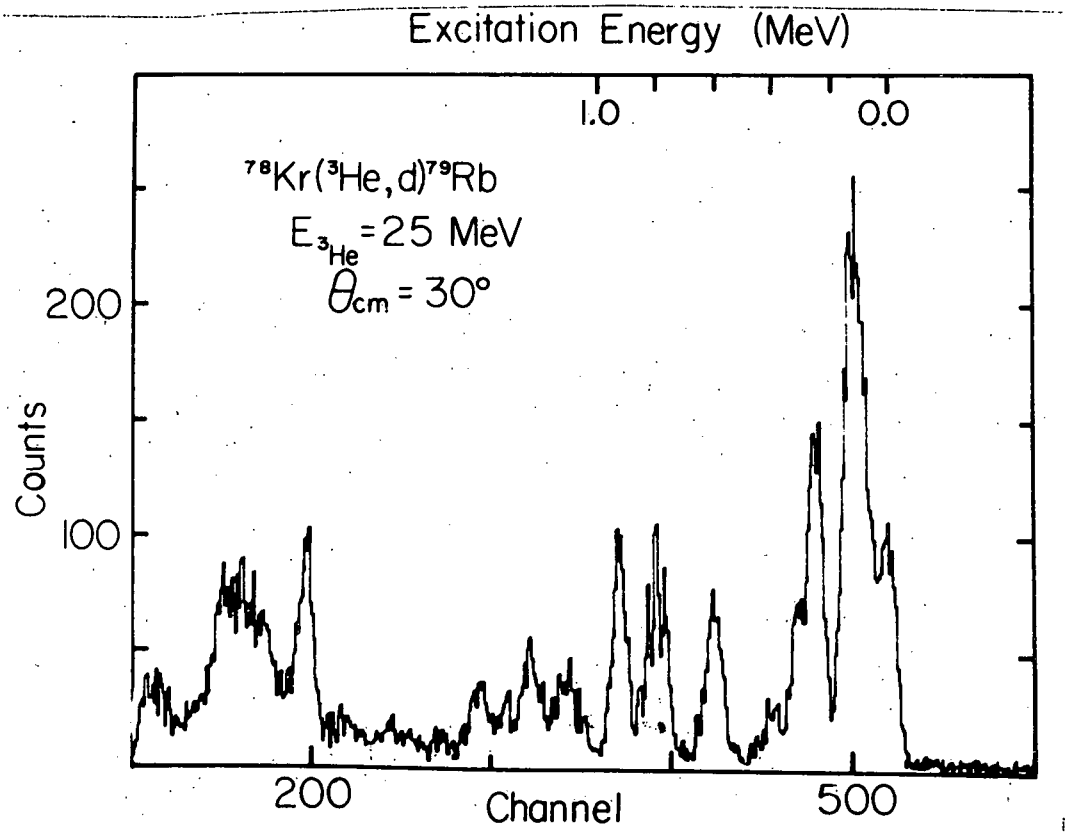

Fig. A1-a4. Sample deuteron spectrum from the $^{78}Kr(^{3}He,d)^{79}Rb$ reaction. The energy scale is approximate.

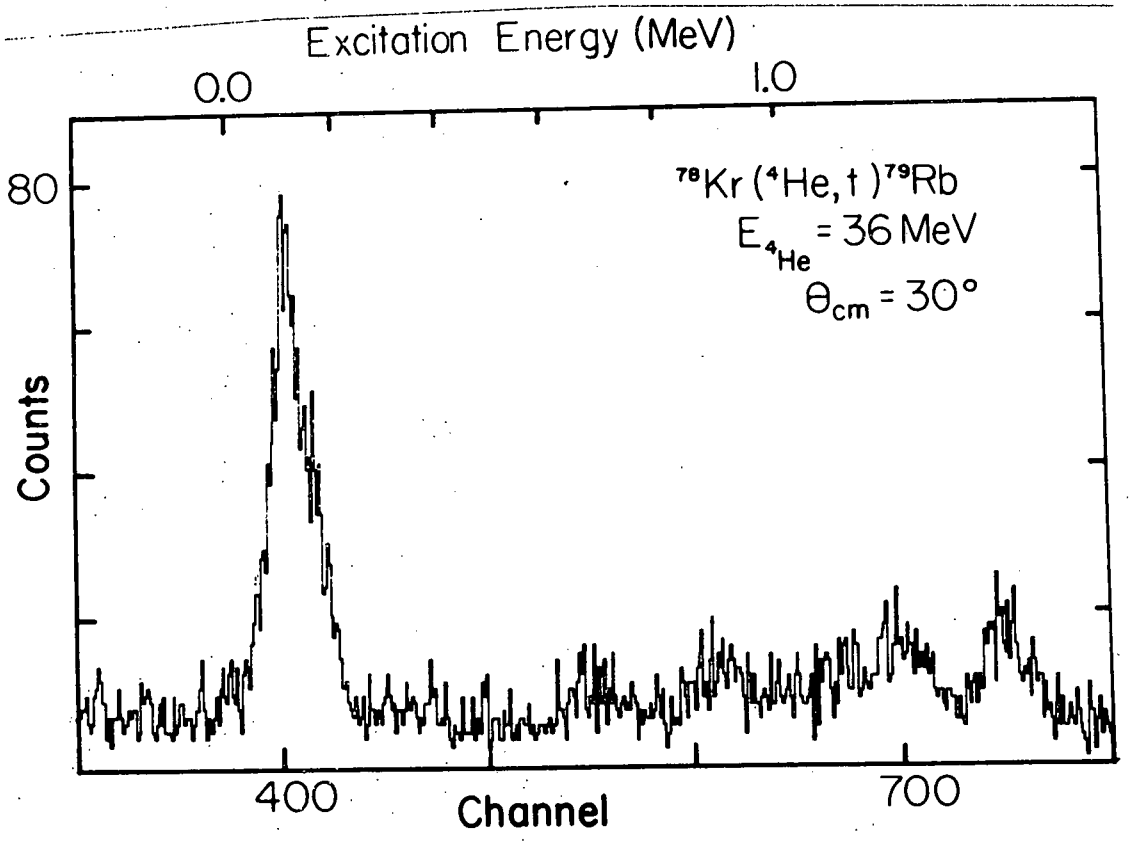

Fig. A1-a5. Sample triton spectrum from the $^{78}Kr(^{4}He,t)^{79}Rb$ reaction. The energy scale is approximate.

v. The $^{103}Rh(^{3}He,d)^{104}Pd$ Reaction at 33.0 MeV

M. Rumore, S. Dickey, J. J. Kraushaar, R. Raymond, R. Sinton and R. Weiss

As part of a continuing effort to determine the proton single particle strengths in nuclei around A=100, data were obtained on the above reaction at scattering angles of 2.5° to 55° in 2.5° steps using the energy-loss spectrometer system. Normalization of the data was achieved by measuring the ^{3}He elastic scattering at seven angles from 20° to 35° and by the use of cross sections from an optical model calculation. The monoisotopic rhodium targets were prepared by evaporation of rhodium onto a salt covered glass slide. The rhodium film was then floated off in warm water and deposited onto a formvar backing. Oxygen and carbon from the formvar were the only contaminants seen. The target thickness was determined to be 140 $\mu g/cm^2$. A deuteron spectrum at 22.5° is shown in Fig. A1-a6.

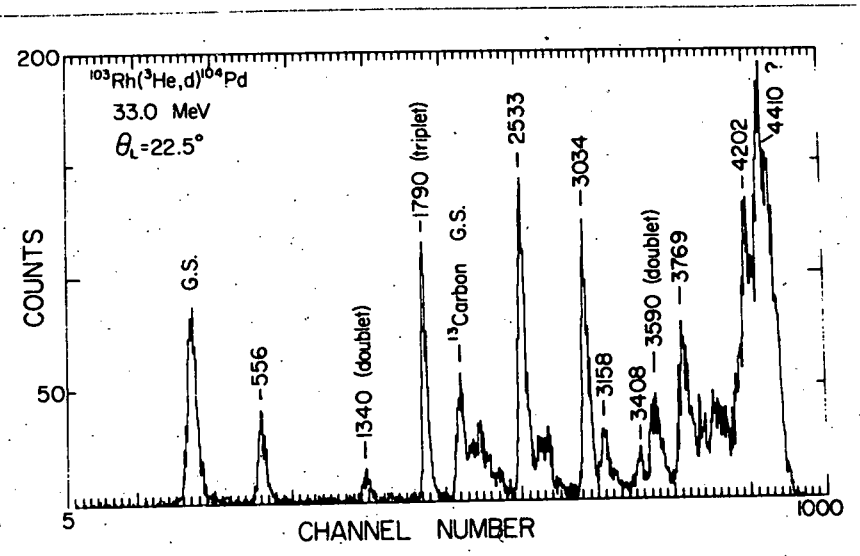

Fig. A1-a6. Deuteron spectrum for the $^{103}Rh(^{3}He,d)^{104}Pd$ reaction at 33.0 MeV.

The data from this experiment are still being analyzed but Fig. A1-a7 shows the angular distributions for the ground and first excited states of ^{104}Pd. Distorted wave calculations have been carried out using the optical model potentials of Emigh and Kraushaar[1] and are shown in Fig. A1-a7. Spectroscopic factors for these and other transitions will be available shortly.

[1] R. A. Emigh and J. J. Kraushaar, Nucl. Phys. A320 (1979) 335.

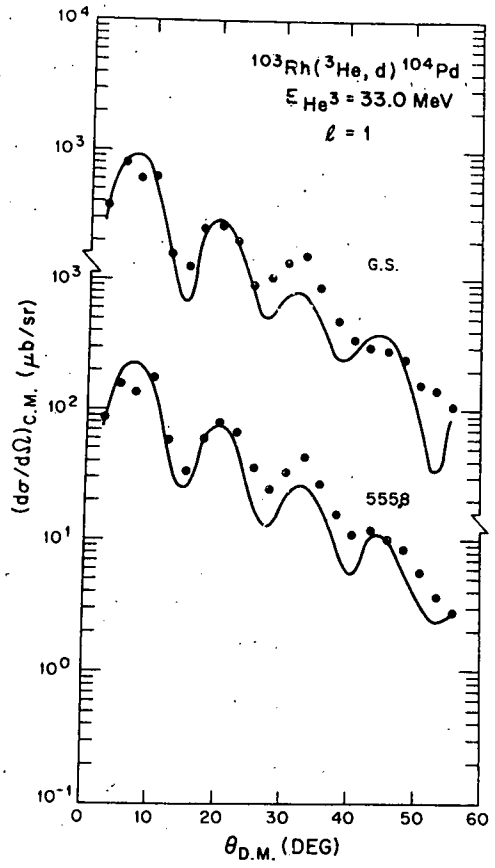

Fig. Al-a7. Angular distributions for the transitions to the ground and first excited states of ^{104}Pd. The solid lines represent DWBA calculations for ℓ=1 transitions.

vi. The $^{208}Pb(p,d)^{207}Pb$ and $^{120}Sn(p,d)^{119}Sn$ Reactions at 26 MeV

S. Dickey, J. J. Kraushaar, R. A. Ristinen, M. Rumore and R. Sinton

Complete angular distributions were taken on the above two reactions using 26.3 MeV protons, self supporting enriched targets and the energy-loss spectrometer. The interest in the $^{208}Pb(p,d)$ reaction stems from a concern for the spectroscopic factors for the five states shown in Fig. Al-a8 which contain essentially all of the single particle strength for the $3p_{1/2}$, $2f_{5/2}$, $3p_{3/2}$, $1i_{13/2}$, $2f_{7/2}$ and $2g_{9/2}$ states. The reaction has been studied previously at several energies ranging up to 121 MeV and a serious discrepancy occurs between the observed spectroscopic factors and the full strength of 2j+1, particularly for the higher ℓ-values. For example, the $i_{13/2}$ excitations with one exception, have been reported to have a spectroscopic factor of around half of the expected 14. The main purpose of the present investigation is to examine the reality and possible causes of this discrepancy. Particular attention will be paid to a precise normalization of the data and a careful examination of the dependence on the bound state and optical model parameters.

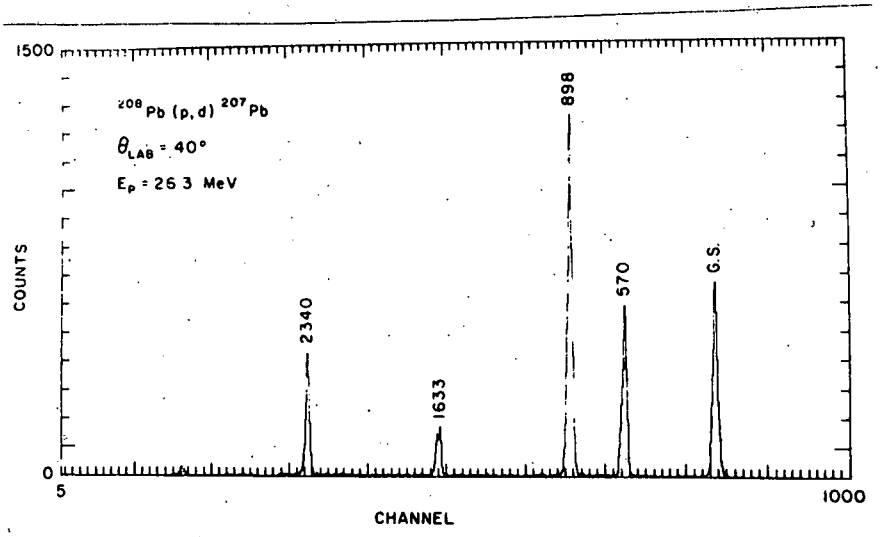

Fig. Al-a8. The $^{208}Pb(p,d)^{207}Pb$ reaction at a scattering angle of 40°. Weaker states seen at higher excitation are now shown.

Both zero range and exact finite range calculations will be carried out. Data were also taken at higher excitations. This was done to include the $1h_{9/2}$ state at 3409 keV in the analysis and to search for weak states that might represent fragments of the strong single particle strengths seen at lower excitation. Comparisons will be made with results from other neutron pickup reactions such as (d,t) and (^{3}He,α).

The ^{120}Sn(p,d) reaction was studied to extract spectroscopic factors for the strong neutron states shown in Fig. Al-a9. A previous investigation at 30 MeV had rather poor resolution and no spectroscopic factors were obtained. The analysis of the data from both these reactions is well under way.

---

[1] P. E. Cavanagh, et al., Nucl. Phys. A141 (1970) 92.

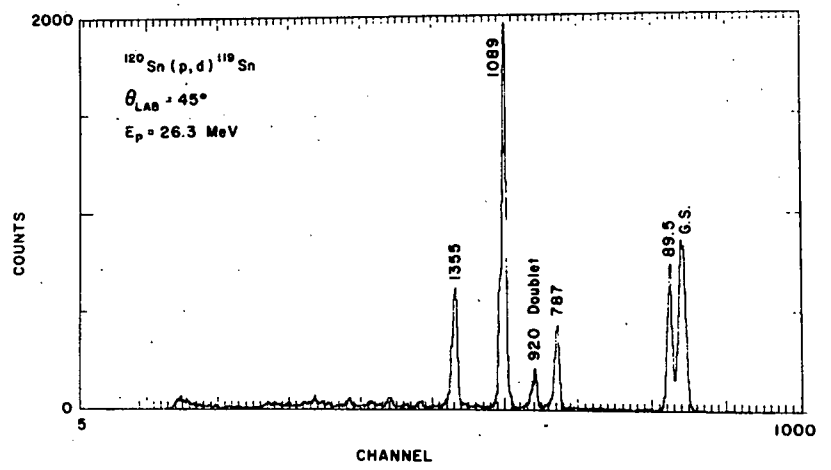

Fig. A1-a9. The $^{120}Sn(p,d)^{119}Sn$ reaction at a scattering angle of 45^{o}. Many additional weaker states seen up to about 2.5 MeV are not labeled.

vii. Core-coupled States Excited in the $^{208}Pb(\vec{d},t)^{207}Pb$ Reaction

E. Sugarbaker; W. P. Alford (U. of Western Ontario); R. N. Boyd (Ohio State); E. R. Flynn and J. Sunier (LASL); J. A. Cameron (McMaster)

Analysis of the $^{208}Pb(\vec{d},t)$ ^{207}Pb reaction at 17 MeV has continued. States up to an excitation energy of 3.8 MeV in ^{207}Pb have been studied. Among the known core excited states in this region are the $(^{208}Pb\ (3^-) \otimes p_{1/2}^{-1})\ 5/2^+,\ 7/2^+$ doublet near 2.6 MeV and the $(^{206}Pb(g.s.) \otimes g_{9/2})$ state at 2.74 MeV. The former should be excited by a two-step process involving inelastic excitation while the latter might be excited by a (d,p)(p,t) sequential transfer two-step reaction. Given the relatively simple structure of these states, it was hoped that measurements of analyzing power as well as cross section would provide a sensitive test of reaction theories for two-step processes.

The poor agreement obtained for the 2.6 MeV doublet was reported last year. Additional attempts involving sequential reaction mechanisms and the Johnson-Soper prescription for the deuteron potential have proved unsuccessful. Further calculations including plausible one-step contributions were also unable to provide a better fit.

More success has been had with the $9/2^+$ state at 2.74 MeV. Its 2h-1p character is established by its strong excitation with ℓ=4 in the $^{206}Pb(d,p)^{207}Pb$ reaction. In such a case it should be described by sequential (d,p)(p,t) transfer, plus a one-step component due to the 2p-2h excitations in the ^{208}Pb ground state. The pure sequential calculations used reaction strengths from the literature and are shown as the dot-dash curves in Fig. A1-a10. The fit (dashed line) to

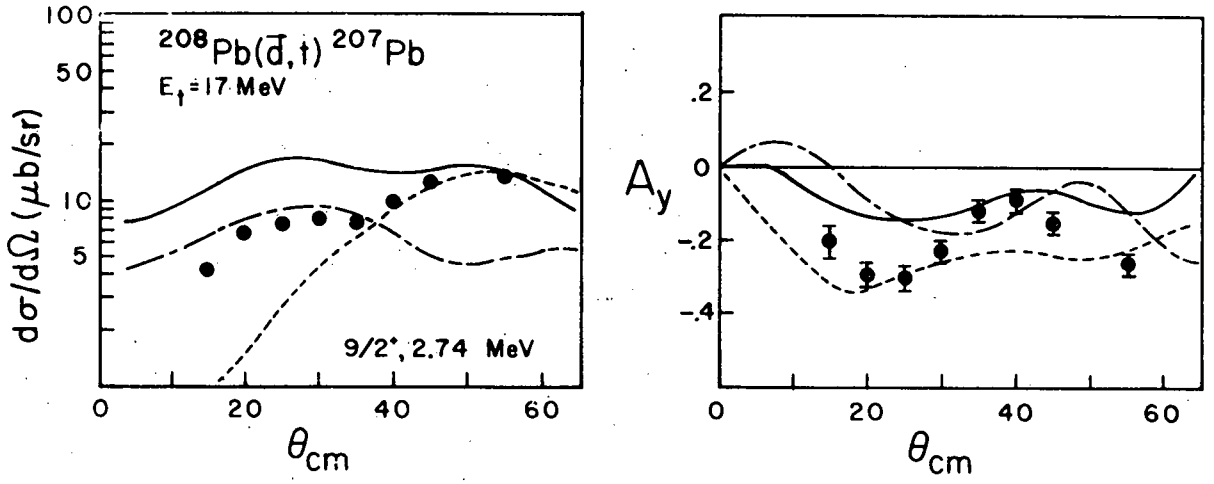

Fig. A1-a10. Angular distributions for the $^{208}Pb(\vec{d},t)^{207}Pb$(2.74 MeV) reaction. The curves are described in the text.

back angle data assuming only a 1-step $g_{9/2}$ pickup gives $C^2S \approx 0.012$, which is a lower value than that obtained in previous studies. The combined 1-and 2-step calculation (solid line) overpredicts the cross sections and provides only a marginal fit to the A_y data. Additional calculations including inelastic excitations are in progress.

viii. Search for Stretched 8^- States in ^{52}Cr

R. S. Raymond, R. J. Peterson, M. A. Rumore

From the shell model we expect the existence of 8^- states in ^{52}Cr, as the result of exciting an $f_{7/2}$ nucleon into the $g_{9/2}$ shell, coupled to the maximum spin of 8. Such 8^- strength has been seen in electron scattering on $^{58}_{28}Ni_{30}$ (1), fragmented among many states with excitation energies from 8 to 13 MeV. If strong, pure 8^- states exist in neutron magic $^{52}_{24}Cr_{28}$, we would have some clue as to the reason for so many 8^- states in nickel. We have searched for proton stretched states using the $^{51}V(\alpha,t)^{52}Cr$ reaction which, with a large negative Q-value and resulting large momentum mismatch, favors high ℓ transfer. We used 35.1 MeV α particles and observed tritons with the energy-loss spectrometer over a range of excitations to 14 MeV.

No tremendous peaks were noted, but two smaller peaks were seen at excitation energies of approximately 7 MeV. Cross sections have not yet been extracted and so the angular momenta associated with these peaks are not known. Good calibration data from a ^{13}C target were also obtained, and reliable excitation energies will be possible. Analysis of the data is continuing.

---

[1] R. A. Lindgren, C. F. Williamson, S. Kowalski, Phys. Rev. Letters 40 (1978) 504.

ix. Proton Stripping on ^{9}Be

M. D. Rayman, R. J. Peterson and J. R. Shepard

Spectroscopic factors for the (d,n), (^{3}He,d) and (α,t) reactions leading to ^{10}B do not agree.[1] This disagreement could be ascribed to isospin-dependent form factors or to inelastic coupling effects. The (α,t) data previously available were obtained at a beam energy of 27 MeV, and a limited excitation function indicated no compound effects. We have remeasured the (α,t) cross sections to several levels of ^{10}B at an energy of 35 MeV as a by-product of the ^{9}Be(α,α') experiment described elsewhere in this report. The angular distribution to the 3^{+} ground state is shown in Fig. A1-a11. At small angles the detector was too thin to stop the more energetic tritons.

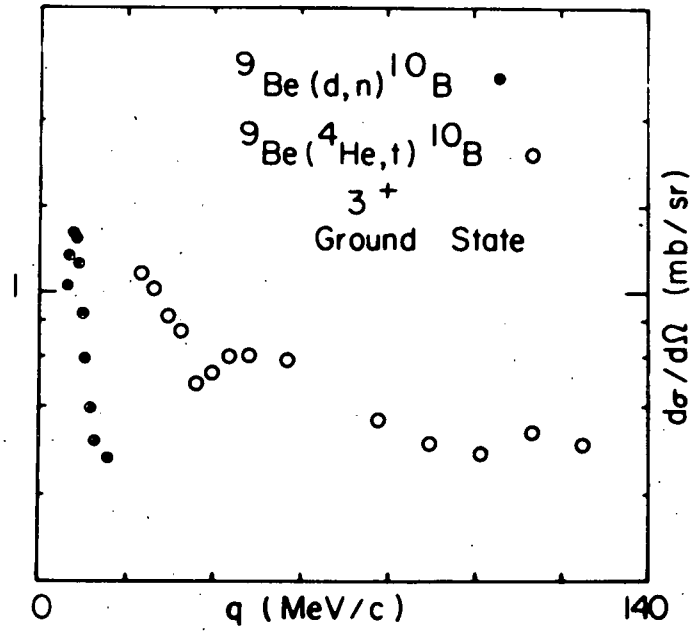

Fig. A1-a11. Proton stripping data to the 3^{+} ground state of ^{10}B are shown for the ^{9}Be(d,n) and (α,t) reactions. The data are plotted against the momentum transfer for each angle, so the stripping peak for the (d,n) reaction is very compressed. A $p_{3/2}$ proton transfer must provide the stripping.

New data for proton stripping by the (d,n) reaction were obtained at 17.6 MeV using a flight path of 9 meters. A sample spectrum is shown as Fig. A1-a12. Angular distributions were measured to 50 degrees (lab). The ground state differential cross sections are shown in Fig. A1-a11, plotted as a function of the momentum transfer.

The two sets of data shown in Fig. A1-a11 indicate the large range of momentum transfers studied. These data will be compared

to DWBA predictions. The more sophisticated CCBA calculations planned will no longer be needed, since the (α,t) cross sections have been measured at 65 MeV and compared to a full-scale coupled channel analysis.[2] It has been concluded that inelastic coupling effects do influence the proton transfer data, but when these are properly included, predictions with the standard spectroscopic factors of Cohen and Kurath[3] suffice to account for the data, and no discrepancy remains for the spectroscopic factors.

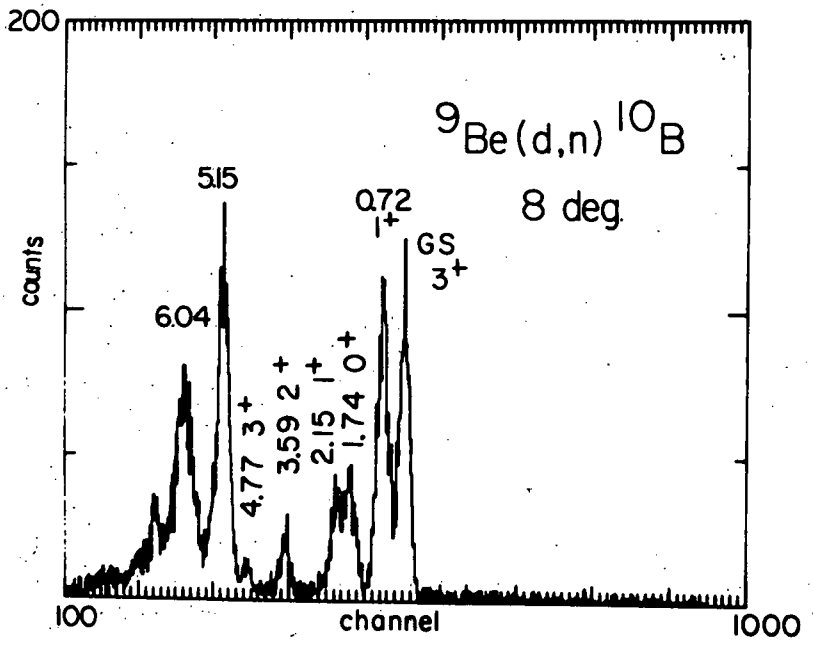

Fig. Al-al2. A sample spectrum at 8 degrees from the (d,n) reaction on ^{9}Be at 17.6 MeV. The triplets at 5.15 MeV and 6.04 MeV were not resolved.

---

1 K. W. Kemper, et al., Nucl. Phys. A222 (1974) 173.
2 M. N. Harakeh, 1979 Progress Report, KVI, Groningen.
3 S. Cohen and D. Kurath, Nucl. Phys. 73 (1965) 1.

x. Spectroscopy of A=12 in the Ex=19 MeV Region
J. R. Shepard, R. J. Peterson, R. A. Emigh, P. A. Smith, M. Rayman; and N.S.P. King (LASL)

A number of recent ^{12}C (e,e') and (π,π') measurements have focused on the region of excitation around 19 MeV where the states, especially those with T=0, are quite poorly known. Some very interesting nuclear structure features have been observed, particularly in the (π,π') work where two strongly isospin-mixed pairs have been

said to have been observed. We have undertaken to test some of the conclusions of these inelastic scattering studies with conventional low-energy measurements.

We have focused our attention on the levels at 19.25 and 19.65 MeV identified by Morris, et al.[1] to be 4^- levels of almost totally mixed isospin so that the lower level takes on the aspect of a proton state and the upper one that of a neutron state. If the leading configuration of these levels is $(p_{3/2}^{-1}d_{5/2})$ relative to a ^{12}C core, then proton stripping reactions on ^{11}B should excite the proton level (19.25 MeV) very strongly compared to the neutron state (19.65 MeV).

We have made extensive measurements of the $^{11}B(^3He,d)^{12}C(Ex\sim19\ MeV)$ reaction at $E(^3He)=43$ MeV using our energy-loss spectrometer. Typical spectra appear in Fig. A1-a13 and the $\theta_{lab}=10^o$ spectrum is very similar to that published by Reynolds, et al.[2] At first glance, this spectrum does not appear to be consistent with the expectations discussed above since there appears to be a concentration of strength at ~19.65 MeV where the neutron level is said to be rather than at 19.25 MeV, the location of the proton state. However, because of the large widths of the structures in the spectrum and because the overall shape of the spectrum changes appreciably with angle (see the $\theta_{lab}=30^o$ spectrum in Fig. A1-a13) it is very difficult to tell even where levels are, much less to identify them with known levels,[3] their analogues[4] or states predicted in nuclear structure calculations.[5] The problem is compounded by the fact that the kinematics of the $^{11}B(^3He,d)$ reaction at this energy cause there to be so little difference between $\ell = 0$, 1, and 2 angular distributions that different multipolarities cannot be readily identified. Such identification would be of obvious value in sorting out the various components of the spectra.

The kinematics of the $^{11}B(d,n)^{12}C(Ex\sim19\ MeV)$reaction at 17 MeV are much more conducive to producing large differences between ℓ=0, 1 and 2 angular distributions. Consequently we have mounted a two pronged attack on the problem of the $^{11}B(d,n)$ reaction. Some preliminary measurements covering the lower regions of excitation ($\lesssim$ 16 MeV) have already been performed and are discussed elsewhere in this report. They will be extended to the Ex~19 MeV region as soon as various technological improvements are completed.

As a complement to these anticipated experiments, we have measured angular distributions for the $^{11}B(d,p)^{12}B$ reaction at E_d= 17 MeV leading to the analogues of the T=1 levels of ^{12}C. These measurements were done with the energy-loss spectrometer with an overall energy resolution of ~ 80 keV(fwhm). A typical composite spectrum appears in Fig. A1-a14. These measurements will be valuable in several ways. First, since the observed levels are generally well resolved, angular distributions can be readily extracted and then used as templates for determining angular momentum transfers in the anticipated $^{11}B(d,n)^{12}C$ data. This is particularly useful since DWBA calculations of stripping cross-sections to unbound levels in light nuclei are usually unreliable, especially for ℓ=0 transitions.

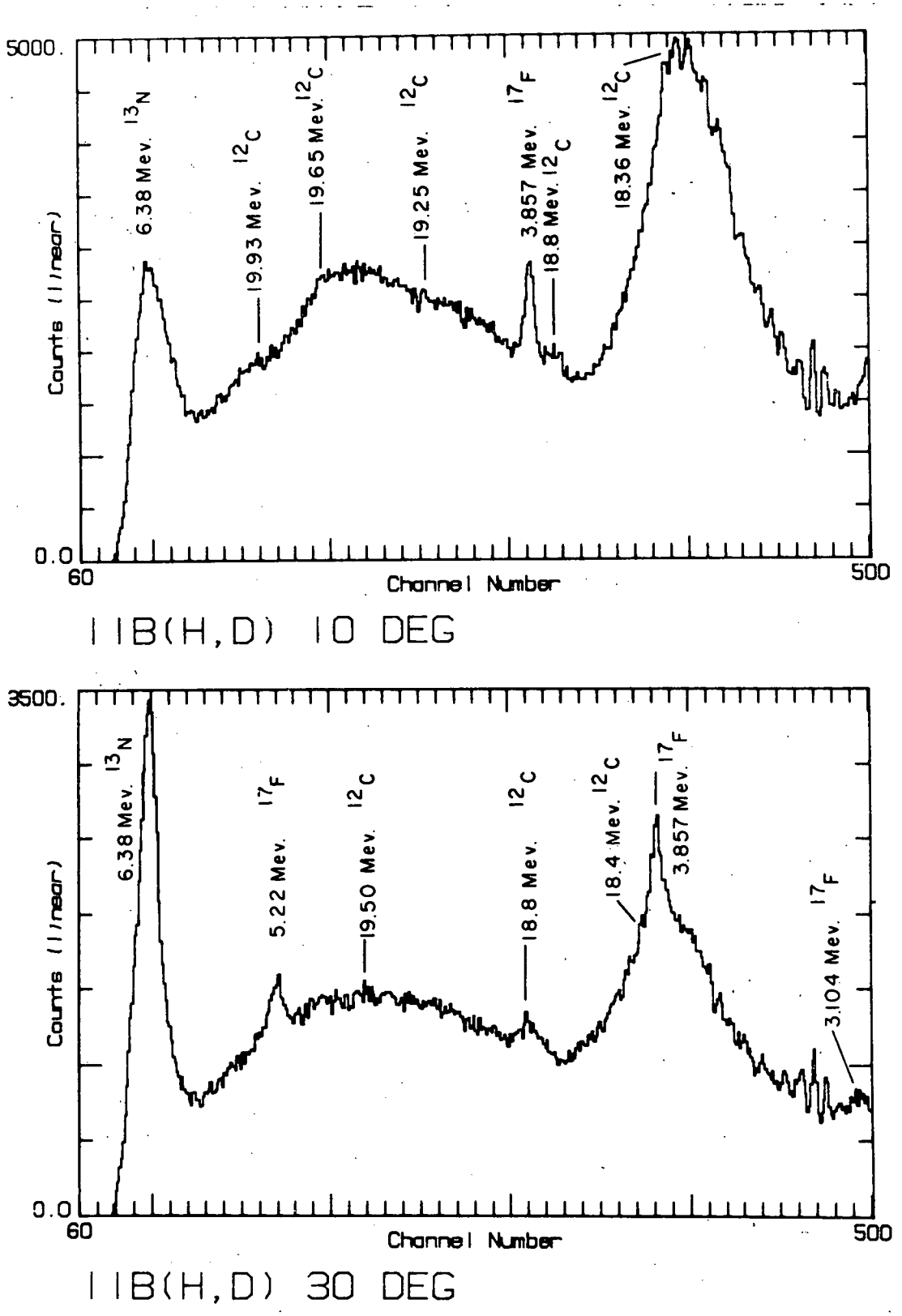

Fig. A1-a13. Energy spectra for the $^{11}B(^{3}He,d)^{12}C$ reaction at $E(^{3}He)=43$ MeV for $\theta_{lab}=10^{o}$ and 30^{o}.

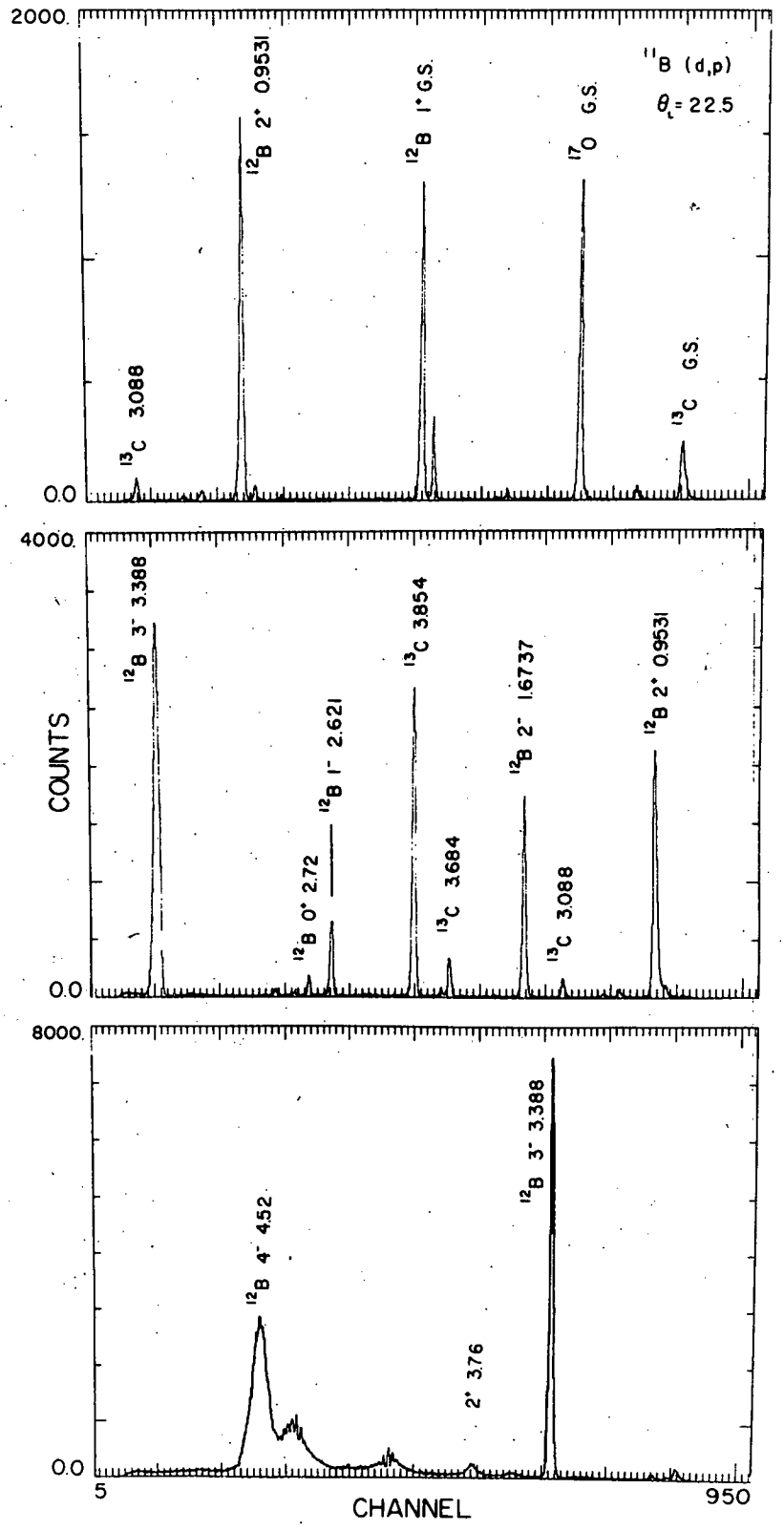

Fig. A1-a14. Energy spectra for the $^{11}B(d,p)^{12}B$ reaction at E(d)=17 MeV. Contaminant peaks are labelled by residual nucleus.

Secondly, these data can serve to test the nuclear structure calculations we will use (e.g., Ref. 5) as a guide in interpreting the $^{11}B(d,n)^{12}C$ data. For instance, the ratios of the strengths of the first 1^+, 2^+ and 0^+ levels are, not surprisingly, roughly consistent with the predictions of Cohen and Kurath. Furthermore, the ratios of strengths for the 1.67 MeV 2^- and 2.62 MeV 1^- levels which are principally ℓ=0 stripping levels and the 3.39 MeV 3^- and 4.52 MeV 4^- levels which are principally ℓ=2 are consistent with the predictions of Millener.[5] More careful checks of these structure calculations are under way.

We have also obtained some $^{10}B(\alpha,d)^{12}C$ and $^{9}Be(\alpha,n)^{12}C$ spectra at E_α=35 MeV, the latter of which are discussed elsewhere in this report. The former measurements especially are potentially very valuable because only T=0 levels are excited and these are the more poorly known of the states in ^{12}C at Ex~19 MeV. Interpretation of our preliminary measurements is hampered by the presence of strong contaminant peaks and poor statistics. Nevertheless, we are able to identify a strong peak at Ex~18.4 MeV. Millener places one of his calculated 2^- T=0 levels at 18.4 MeV on the basis of various π and e^- scattering results. Insofar as he predicts a large (α,d) strength to this level, our measurements support this placement. It should be noted that $^{12}C(\pi,\pi')$ measurements suggest[7] that a 2^- level is present at this excitation energy which is strongly isospin mixed with another 2^- at 19.4 MeV.

More refined analyses of these data are currently underway and further measurements, especially for the $^{11}B(d,n)^{12}C$ and $^{10}B(\alpha,d)^{12}C$ reactions are anticipated.

---

1 C. L. Morris, et al., Phys. Lett. 86B (1979) 31.
2 G. M. Reynolds, et al., Phys. Rev. C3 (1971)445.
3 F. Ajzenberg-Selove and C.L. Busch, Nucl. Phys. A336 (1980) 1.
4 J. E. Monahan, et al., Phys. Rev. C3 (1971) 2192.
5 J. Millener, private communication.
6 S. Cohen and D. Kurath, Nucl. Phys. 101 (1967) 1.
7 H. A. Thiessen, 8th Int. Conf. on High Energy and Nucl. Struct. Phys., Vancouver, B. C., Canada, Aug. 1979.

xi. The $^{11}B(d,n)^{12}C$ Reaction - M. D. Rayman, R. J. Peterson, J. R. Shepard, P. A. Smith

Our continuing interest in the structure of ^{12}C at high excitation has led us to measure proton stripping yields from the (d,n) reaction on an enriched ^{11}B target at 17.67 MeV. This reaction emphasizes low angular momentum transfers, and we hope that it will be particularly sensitive to ℓ=0 transfers to 1^- and 2^- states.

Sample time-of-flight spectra are shown as Fig. Al-al5, using the 9 meter station. Two bias settings were used on the neutron

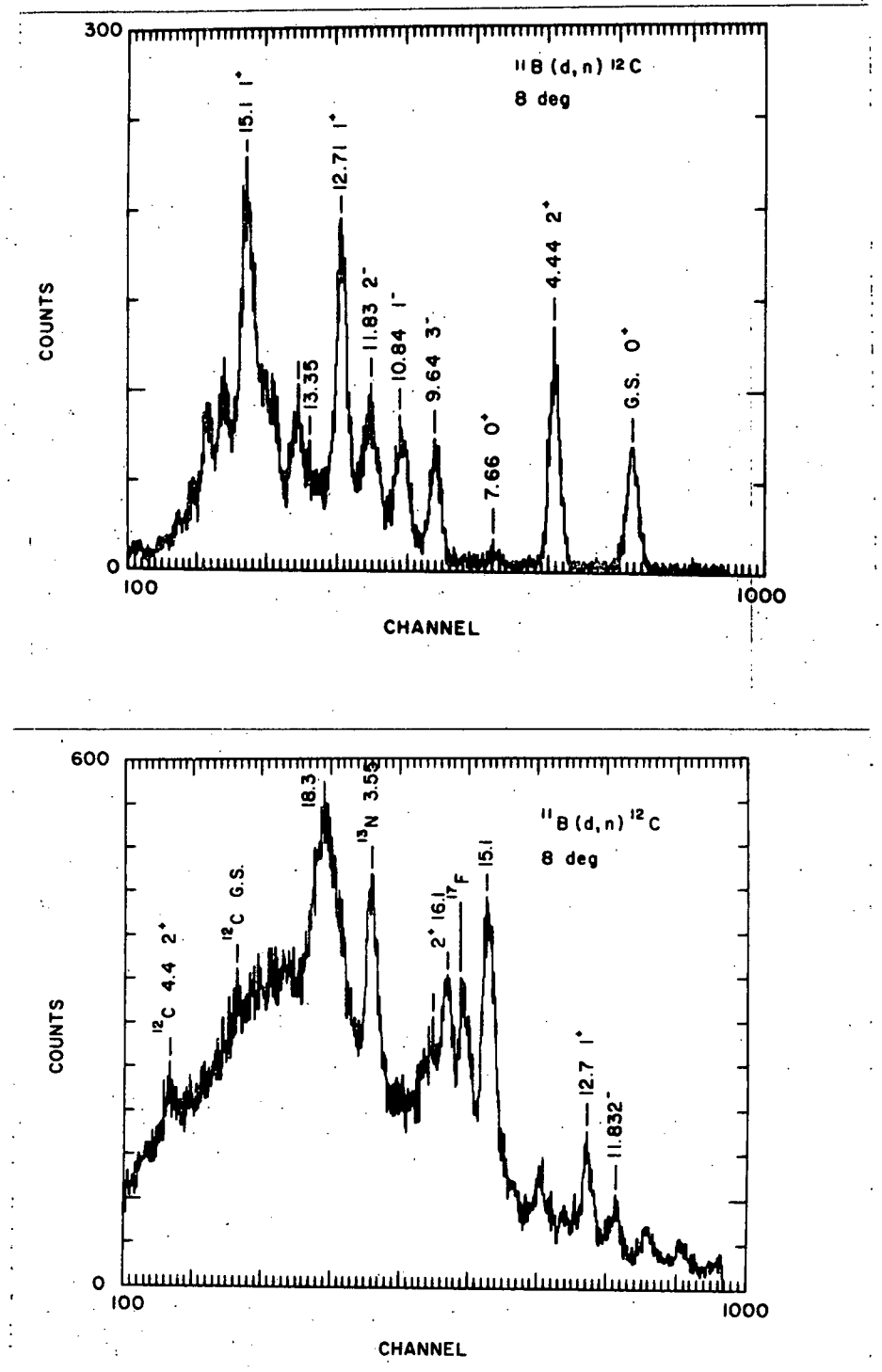

Fig. Al-al5. Sample time-of-flight spectra at 9 meters with different detector bias settings to emphasize high or low excitation energies. Known states of ^{12}C are labelled.

detectors to emphasize two regions of excitation energy. Note that the high excitation spectrum also contains the lowest states from the next beam burst.

Data for the known 2^- state at 11.83 MeV and the 1^- state at 10.84 MeV have been compared to ℓ=0 DWBA predictions using standard optical model parameters. Poor fits are obtained. We plan to search further for good fits to these known states before attempting to analyze the data at higher excitations.

Angular distributions have also been obtained for the $^{12}C(d,n)$ ^{13}N reaction in order to obtain empirical $p_{1/2}$ and $s_{1/2}$ angular distributions.

b. Two-Nucleon Transfer Reactions

i. The $^{208}Pb(p,t)^{206}Pb$ Reaction at 26.2 MeV - R. C. Weiss, J. J. Kraushaar, and R. A. Ristinen; and R. E. Anderson (University of North Carolina)

One of the reasons for studying the $^{208}Pb(p,t)^{206}Pb$ reaction was that it provided a set of well determined energy levels for calibration of the $^{205}Tl(p,t)^{203}Tl$ reaction that was recently studied here. Another reason for interest in this reaction is that it is one of the few examples where the (p,t) reaction has been studied at a sufficient number of energies so that the energy dependence of the reaction can be examined. The energy chosen for the present experiment (26.2 MeV) fills a gap in the energies used so far. Recent studies of the reaction have been completed at 17.8 MeV[1], 35 MeV[2], 40 MeV[3], and 80 MeV[4]. The measured angular distributions are shown in Fig. A1-b1 for the thirteen states observed in this experiment. These include all of the states up to 2659 keV seen in the earlier studies at 35 and 40 MeV, and in addition, the 3^+ state at 1341 keV. The 1^+(1703 keV), 6^-(2384 keV), 4^+(2391 keV) and the 3^-(2648 keV) states have not been excited with any appreciable intensity in any of the (p,t) studies to date.

In order to extract enhancement factors[4] for comparison with $^{208}Pb(p,t)$ data taken at other energies, distorted wave Born approximation (DWBA) calculations were carried out. The proton optical model parameters used in the DWBA calculations were taken from the work of Becchetti and Greenlees[5] and the triton parameters from the work of Flynn, et al.[6]. The binding energies of the neutrons were chosen to be half of the two-neutron separation energy appropriate for the excitation energy of the state in ^{206}Pb. Wave functions for the states in ^{206}Pb were taken from the calculations of True[7] for ^{206}Pb.

The results of the calculations are shown in Fig. A1-b1. For most of the states the data are described reasonably well by the calculations. The angular distribution for the 0^+ state at 1165 keV differs somewhat from either the ground state or the 2315 keV level. The 7^- state at 2200 keV and the 9^- state at 2659 keV are not well described. The reaction mechanism assumed is not appropriate for populating the 3^+ state at 1341 keV since one expects some combination of two-step processes and S=1 components in the picked up neutrons to be important. For this reason, no calculated curve is shown for that state.

The enhancement factors were first extracted using just the leading term in the shell model wave function of True[7] and a value of $D_o^2 = 23 \times 10^4$ MeV^{2}fm^3 and this led to enhancement factors much greater than unity for most of the states. In particular, the 7^- (2200 keV) and 9^- (2659 keV) states have wave functions that are almost entirely due to a single configuration yet the enhancement factors are 4.98 and 4.08, respectively. In order to compare the

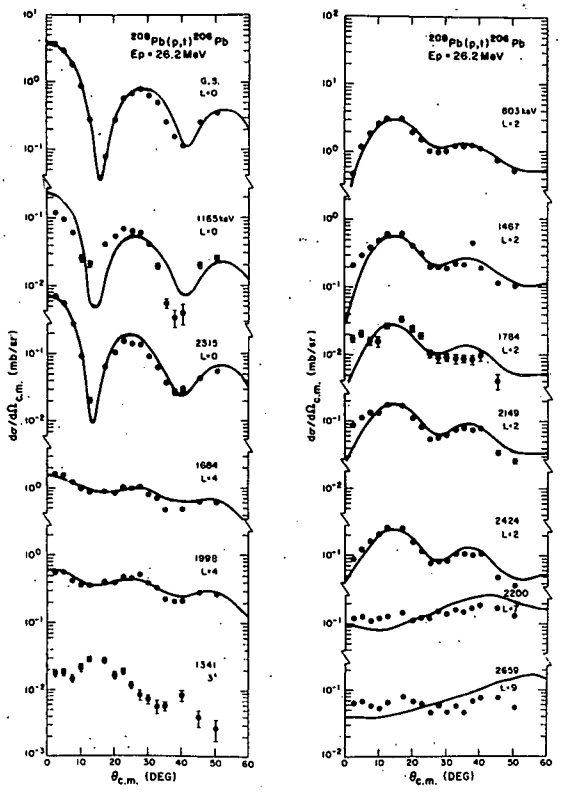

Fig. A1-b1. Angular distributions for the $^{208}Pb(p,t)^{206}Pb$ reaction. The solid lines are the results of DWBA calculations described in the text.

enhancement factors obtained in the present experiment to those from the 17.8, 35, 40 and 80 MeV data of others, zero-range DWBA calculations were carried out at those energies. The optical model parameters used were those in the original papers, and no nonlocality or finite range corrections were included for the distorted waves. Because the enhancement factors were so much greater than unity when just the leading terms of the True wave functions[7] were used, the comparison calculations were carried with all of the terms of the wave functions included. The results of these calculations are shown in Table A1-bI.

The effect of the inclusion of the additional terms in the wave function is remarkably large for the 26 MeV data, the enhancement factors being reduced by factors of about 2.5 to 6. The enhancement factors remain, however, significantly above unity for five of the six states that were chosen for the comparison. The

Table A1-bI

Enhancement factors for the $^{208}Pb(p,t)^{206}Pb$ reaction

Energy level (keV)	J^{π}	Proton Energy (MeV) 17.8[a]	26.2[b]	35[c]	40[e]	80[e]
G.S.	0^+	3.2	3.8	1.0	3.1	0.15
803	2^+	1.5	1.8	0.42	1.6	0.12
1684	4^+	0.93	1.1	0.26	1.1	0.09
1998	4^+	---	4.4	1.05	5.3	0.31
2200	7^-	---	2.0	2.4	1.1	0.08
2659	9^-	---	2.5	1.9	1.2	0.09

a) See Ref. 1
b) Present experiment
c) See Ref. 2
d) See Ref. 3
e) See Ref. 4

enhancement factors for the data at 17.8 and 40 MeV are in rough agreement with the 26.2 MeV data. The first four states, however, for the 35 MeV data have enhancement factors which are about a factor of four lower than those from the 17.8, 26.2 and 40 MeV data. The cause of this discrepancy is unknown but it could have its origins in the particular optical model parameters chosen or possibly a problem in the experimental normalization of the 35 MeV data.

The largest inconsistency is that the 80 MeV enhancement factors are more than a factor of ten smaller than not only those for the 40 MeV data, a fact which has been pointed out previously,[4] but also at least a factor of ten below those for the 17.8 and 26.2 MeV data. The 80 MeV enhancement factors are also about a factor of 4 to 20 less than those for the 35 MeV data. The published[4] 80 MeV enhancement factors differ somewhat from those listed in Table A1-bI because a value of 0.90 fm instead of 0.65 fm was assumed for the bound state diffuseness and only the leading terms of the shell model wave functions of True[7] were used for the published values[4]. For either type of calculation a major discrepancy persists for the 80 MeV data.

The reason for this inconsistency is not known at the present time although there has been speculation[4] that finite range effects may be the cause for the fall off of the enhancement factors at 80 MeV. An exact finite range (EFR) calculation has recently been completed[8] that considered the $^{208}Pb(p,t)^{206}Pb$ reaction at 35 and 40 MeV. Using the triton wave function of Tang and Herndon[9], Takemasa, Tamura and Udagawa[8] performed EFR calculations whose results agreed with the 40 MeV data for the ground state but were up to a factor of 4.4 too high for the excited states. For the 35 MeV data the calculations were too low by a factor of three for the ground state. Unfortunately, the 26.2 and 80 MeV data were not available at the time the EFR calculations were done.

More recently preliminary full finite range DWBA calculations were carried out[10] using the program of P. D. Kunz. The indications were that the discrepancy was reduced from a factor of 12 with the zero range calculations to a factor of about 6 with EFR calculations but a dependence on the detailed optical model potentials was noted.

---

1 K. A. Erb and T. S. Bhatia, Phys. Rev. C 7 (1973) 2500.
2 W. A. Lanford, Phys. Rev. C 16 (1977) 988.
3 S. M. Smith, P. G. Roos, A. M. Bernstein and C. Moazed, Nucl. Phys. A158 (1970) 497.
4 J. R. Shepard, R. E. Anderson, J. J. Kraushaar, R. A. Ristinen, J. R. Comfort, N. S. P. King, A. Bacher and W. W. Jacobs, Nucl. Phys. A322 (1979) 92.
5 F. D. Becchetti, Jr. and G. W. Greenlees, Phys. Rev. 182 (1969) 1190.
6 E. R. Flynn, D. D. Armstrong, J. G. Beery and A. G. Blair, Phys. Rev. 182 (1969) 1113.
7 W. W. True, Phys. Rev. 168 (1968) 1391.
8 T. Takemasa, T. Tamura and T. Udagawa, Nucl. Phys. A321 (1979) 269.
9 Y. C. Tang and R. C. Herndon, Phys. Lett. 18 (1965) 42.
10 P. D. Kunz, J. J. Kraushaar and J. R. Shepard, Bull. Amer. Phys. Soc. 24 (1979) 871.

ii. The Energy Dependence of the (p,t) Reaction on ^{54}Fe

G. N. Hassold, J. J. Kraushaar, P. D. Kunz and P. A. Smith; and E. F. Gibson (Sacramento State College).

There are very few cases where the (p,t) reaction has been studied at a sufficient number of energies so that the direct reaction mechanism can be tested over a wide energy range. Reactions using ^{208}Pb and ^{54}Fe targets are the only ones where high energy (80 MeV) data exist on relatively heavy nuclei. The $^{54}Fe(p,t)^{52}Fe$ reaction has been studied here at 25.2 MeV in order to have a more complete set of data to compare to both zero-range and exact finite-range distorted wave calculations.

The measurements were carried out with a 0.84 mg/cm^2 self-supporting foil of 97% enriched ^{54}Fe. A detector telescope was used that consisted

of a 51 μ ΔE and a 508 μ E surface barrier silicon detector for the tritons. A sample spectrum is shown in Fig. A1-b2 where the states of interest for the study are labeled with their energies. Although the state at 2762 keV (2^+) is shown in Fig. A1-b2 there was insufficient data at most angles to make the angular distribution of much value to the present study. The energy resolution of 90 keV was sufficient to resolve the states shown from the few others in the energy region.

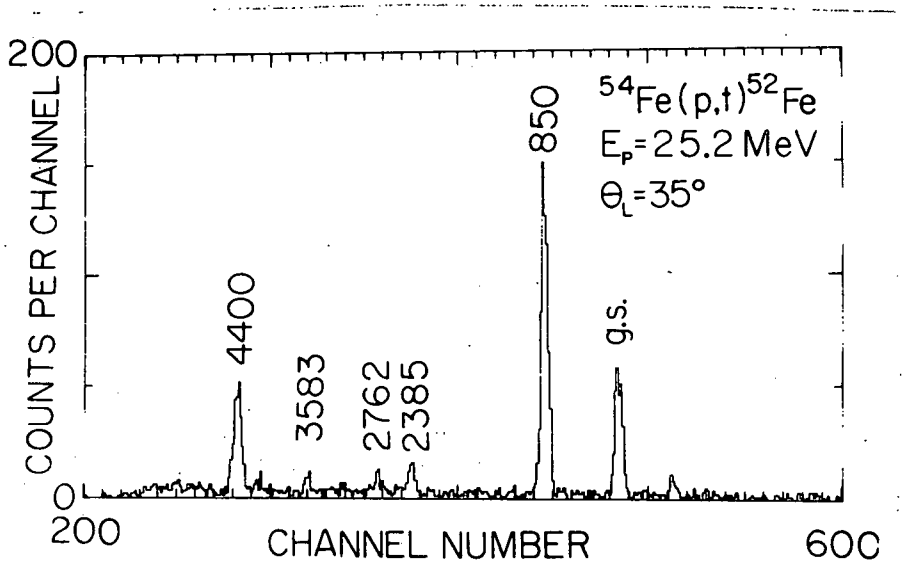

Fig. A1-b2. Triton spectrum for the $^{54}Fe(p,t)^{52}Fe$ reaction at 25.2 MeV and a scattering angle of 35° (lab).

The $^{54}Fe(p,t)$ reaction has been studied previously at 40 MeV[1], 45 MeV[2], 51.9 MeV[3] and 80 MeV[4]. Unfortunately the data at 40 MeV were not absolutely normalized and hence were not of direct use in this study. The results of the studies at 45, 51.9 and 80 MeV along with the present data are shown in Figs. A1-b3 - A1-b7.

Both zero-range and exact-finite range calculations were carried out to extract enhancement factors at the various energies for the five states of ^{52}Fe of interest. The zero-range calculations were done using the program DWUCK 4. It was assumed that a pair of neutrons coupled to S=0 with zero relative angular momentum were simultaneously transferred. Both finite-range and non-locality correction factors were set equal to zero. The other details of the calculations are outlined in reference 5. Sets of consistent optical model potentials were sought for the protons and tritons at the several projectile energies that would give an adequate description of the ground state transitions. The radii of the real part of the potentials for the protons and tritons were made to be about equal. The triton potential is from the so called deep family. The

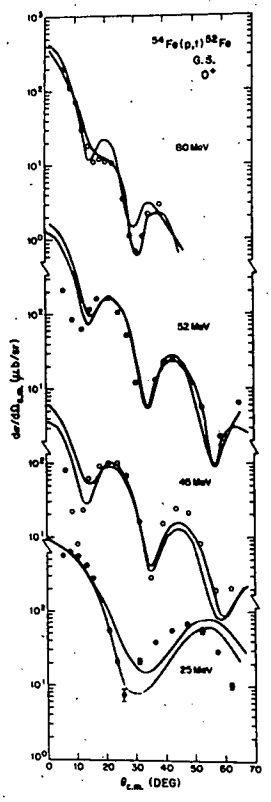

Fig. A1-b3. Angular distributions for the ground state transition. The solid lines are zero-range and the dashed lines are exact finite-range calculations.

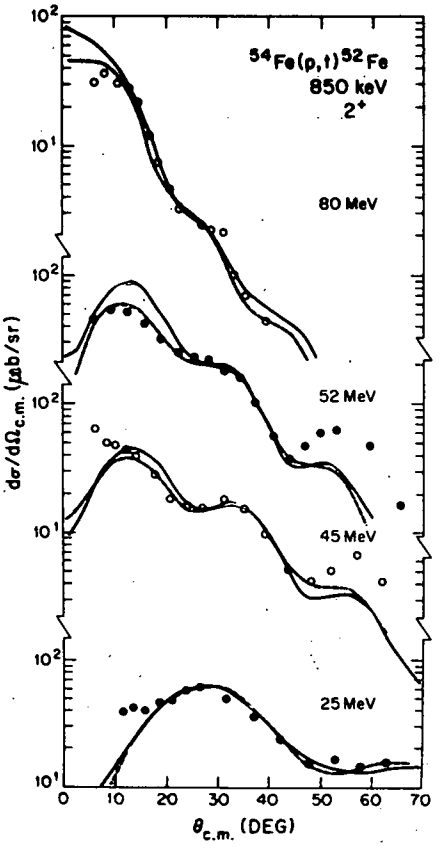

Fig. A1-b4. Angular distributions for the 850 keV, 2^+ state in ^{52}Fe. The solid lines represent zero-range DWBA calculations and the dashed lines exact finite-range calculations.

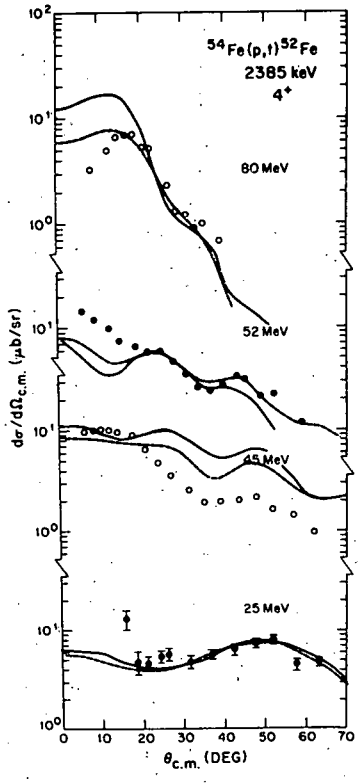

Fig. A1-b5. Angular distributions for the 2385 keV, 4^+ state in ^{52}Fe. The solid lines represent zero-range DWBA calculations and the dashed lines exact finite-range calculations.

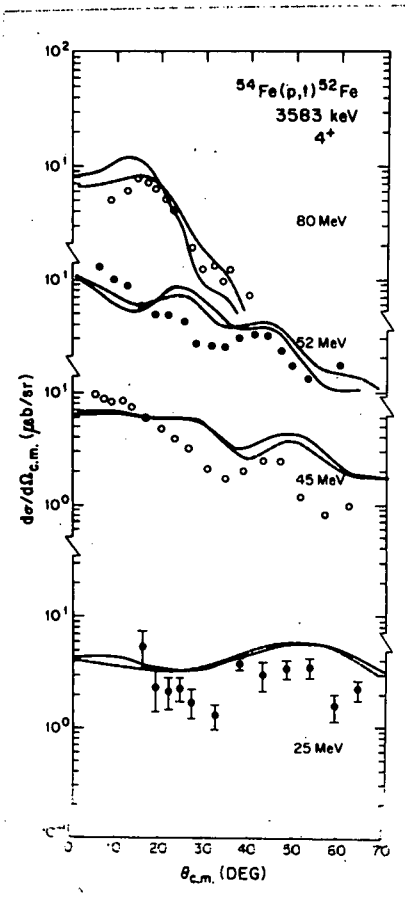

Fig. A1-b6. Angular distributions for the 3583 keV, 4^+ state in ^{52}Fe. The solid lines represent zero-range DWBA calculations and the dashed lines exact finite-range calculations.

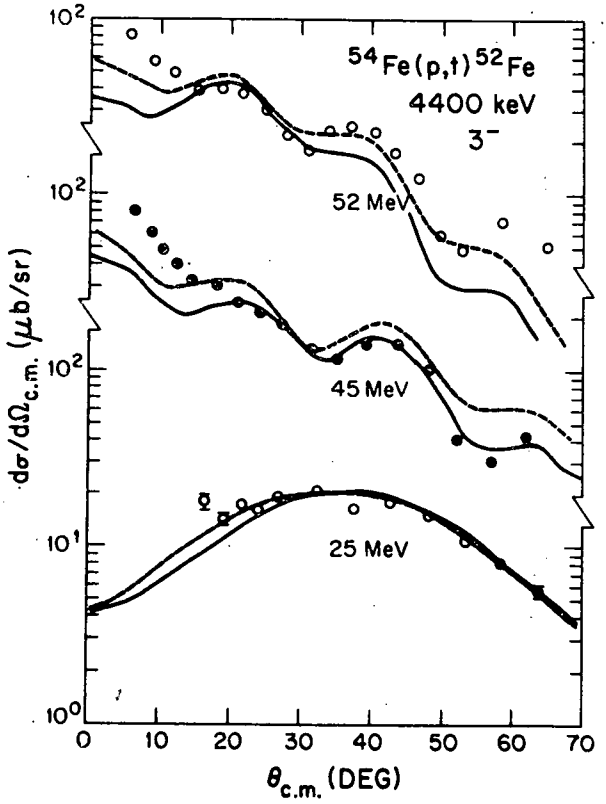

Fig. Al-b7. Angular distributions for the 4400 keV, 3^- state in ^{52}Fe. The solid lines represent zero-range DWBA calculations and the dashed lines exact finite-range calculations.

parameters used are listed in Table Al-bII, as are the parameters for the bound state calculation. The binding energies of the neutrons were chosen to be one half of the two-neutron separation energy appropriate to the excitation energy of the final state. For most of the calculations the two neutrons were assumed to be in a $(1f_{7/2})^2$ configuration. For the 3^- state a $1f_{7/2}$ and a $1d_{3/2}$ neutron were assumed.

The zero-range calculations are shown as the solid lines in Figures Al-b3 - Al-b7. The ground state calculations shown in Fig. Al-b3 appear to describe adequately the data, although some of the behavior at the low angles at 52 and 45 MeV is missed. A zero-range normalization constant, D_o^2 of 21.5 x 10^4 MeV^2 fm^3 was assumed to extract an enhancement factor, ϵ . These enhancement factors are shown in Table Al-bIII. The angular distributions for the four excited states are shown in Figs. Al-b4 - Al-b7. Reasonably good agreement between the experimental results and the calculations is evident for the shapes of the angular distributions for the 2^+ state at 850 keV and the 3^- state at 4400 keV but rather disturbing differences occur, particularly for the 4^+ states at 2385 and 3585 keV with the 45 MeV data.

Table A1-bII

Optical model potential parameters used in the DWBA calculations

E_p(MeV)	Particle	V(MeV)	r_o(fm)	α_o(fm)	W_v(MeV)	$4W_s$(MeV)	r_o'(fm)	α_o'(fm)	V_{so}(MeV)	r_{so}(fm)	α_{so}(fm)
25.2	p	-45.58	1.22	0.72	-2.84	23.78	1.32	0.54	-6.20	1.06	0.68
	t	-165.4	1.16	0.75	-16.4	0.0	1.498	0.817			
45	p	-39.24	1.22	0.72	-7.2	3.98	1.32	0.54	-6.20	1.06	0.68
	t	-163.2	1.20	0.67	-20.88	0.0	1.48	1.01	0.0		
52	p	-30.20	1.23	0.76	-7.29	0.0	1.456	0.505	-4.46[c]	1.052	0.61
	t	-163.2	1.20	0.67	-20.88	0.0	1.475	1.01	0.0		
80	p	-30.2	1.23	0.76	-7.29	0.0	1.456	0.505	-4.46[c]	1.05	0.61
	t	152.0	1.24	0.69	-18.45	0.0	1.59	0.72	0.0		
Bound state	2n	a)	1.25	0.65					b)		

a) well depth adjusted to give correct neutron separation energy

b) Thomas-Fermi form with λ=25

c) An imaginary term was also used that had a depth of 0.4 MeV with radius and diffuseness as shown.

Table Al-bIII

The enhancement factor, ϵ, for the zero-range calculations at the various proton energies. The calculations were carried out for the transfer of $(1f_{7/2})^2$ neutrons except for the quantities in brackets, where complete wave functions were used.

Excited State		Proton Energy			
E_x(keV)	J^π	25.2 MeV	45 MeV	52 MeV	80 MeV
0.0	0^+	3.3(2.66)	1.9(1.56)	5.2(4.89)	2.8(1.91)
850	2^+	0.92	0.33	0.57	0.88
2385	4^+	0.22	0.10	0.38	0.13
3583	4^+	0.21	0.042	0.050	0.073
4400	3^-	1.9	0.30	0.34	---

The enhancement factors shown in Table Al-bIII show a rather large amount of scatter but there does not seem to be any marked trend with energy. The factor of 4 depression in the 80 MeV enhancement factors compared to those at the 45 MeV noted earlier[4] is certainly not evident in the present analysis. The enhancement factors for the 4^+ states at 45 MeV are subject to large uncertainties due to the poor fits.

Calculations were also carried for the ground state transitions with the more complete wave functions listed by Suehiro et al.[3] for the ground state transition in zero range. The shapes of the angular distribution were only very slightly changed. The enhancement factors are listed in parenthesis in Table Al-bIII. As might be expected, there is generally a reduction in the enhancement factors but again no general trend with energy is noted.

Over the past year an exact finite-range two-nucleon-transfer program has been written and is described under the theoretical section of this and last years report. Calculations using this program and the optical model potentials listed in Table Al-bII have been carried out for the various transitions. The results at this time are preliminary but are shown as the dashed curves in Figs. Al-b3 - Al-b7. The differences between the two calculations are not great but detailed differences are apparent. Overall, the quality of the description of the data has not been improved.

The normalization factors required to multiply the calculations to obtain agreement with the experimental cross sections are shown in Table Al-bIV for the ground and first excited states of ^{52}Fe for the two assumptions made concerning the wave functions for the transferred neutrons. Again a rather marked scatter is noted but there appears to be no overall trend with energy. The values at 80 MeV are actually a factor of 4 to 5 greater than those at 45 MeV.

Table Al- bIV

Normalization factors for the exact finite-range calculations for the ground state and first excited state transitions in the ^{54}Fe $(p,t)^{52}$Fe reaction.

Wave Function	Proton Energy			
Ground state	25.2 MeV	45 MeV	52 MeV	80 MeV
$(f_{7/2})^2$	1.53	0.49	1.34	2.4
complete	1.35	0.45	1.12	2.45
850 keV 2^+ / $(f_{7/2})^2$	0.91	0.17	0.62	0.33

1 J. B. Viano, Y. DuPont and J. Menet, Phys. Lett. 34B (1971) 397.
2 P. Decowski, W. Benenson, B. A. Brown and H. Nann, Nucl. Phys. A302 (1978) 186.
3 T. Suehiro, K. Miura, Y. Hiratate, H. Yokomizo, K. Itonaga and H. Ohnuma, Nucl. Phys. A282 (1977) 53.
4 J. R. Shepard, R. E. Anderson, J. J. Kraushaar, R. A. Ristinen, J. R. Comfort, N. S. P. King, A. Bacher, and W. W. Jacobs, Nucl. Phys. A322 (1979) 92.

iii. Study of the (p,t) Reaction on Krypton Isotopes

E. Sugarbaker, B. Diana, C. A. Fields, R. J. Peterson, R. S. Raymond

A study of the Kr(p,t) reactions at E_p=26 MeV has been initiated. The purpose of the study is to investigate the collective excitations of the even-even Kr isotopes, which undergo a smooth transition from

an axially symmetric rotor to a triaxial shape in the upper half of the N=28-50 shell. The (p,t) reaction can probe from the middle (^{76}Kr) to the end of this major neutron shell. Preliminary measurements on targets of ^{78}Kr and ^{86}Kr are being made.

Recently the Interacting Boson Approximation (IBA) has been proposed which describes even-even nuclei in terms of a system of interacting bosons. While in general these bosons define a SU(6) symmetry, three subgroups have provided useful analytic solutions capable of describing nuclei in various regions of a major shell. While many examples of two of these symmetries, SU(5) and SU(3), have been identified in nuclei at the beginning and middle respectively, of major shells; only a few examples of the remaining symmetry, O(6), have been suggested. Arima and Iachello[1] have shown that the O(6) symmetry approximately describes a rigid triaxial rotor with $\gamma=30^{o}$. Such γ-vibrational structure is characteristic of nuclei near the end of major shells. Evidence of O(6) symmetry at the end of the N=82-126 shell has been suggested by Cizewski, et al.[2]. Since the heavy Kr isotopes should exhibit similar symmetry at the end of the N=28-50 shell, a comparison of the strengths observed in the (p,t) reactions with those predicted by the IBA will be of interest.

---

[1] A. Arima and F. Iachello, Phys. Rev. Lett. 40 (1978) 385.
[2] J. A. Cizewski, et al., Phys. Rev. Lett. 40 (1977) 167

iv. One and Two Step Processes for the ^{208}Pb(^{3}He,p)^{210}Bi Reaction

R. J. Peterson

Previous data, shown on p.33 of the 1976 Progress Report and p.41 of the 1977 Progress Report, had been compared to strictly one step two-nucleon stripping calculations and to two-step predictions, computed as ^{208}Pb(^{3}He,d)^{209}Bi(g.s.) followed by ^{209}Bi(d,p)^{210}Bi. Only fair success was reported for the one-step calculations, and grave troubles were encountered in the two-step analysis.

Since that report a new 1^{-} state has been noted in our data at 563 keV[1]. This is responsible for the forward angle rise noted for the data to the 580 keV 8^{-} and the 548 keV 6^{-} states, resolving a problem in the fitting of the angular distributions.

One-step double stripping and two-step sequential stripping predictions have now been coherently combined in a non-local, zero-range calculation. Satisfactory fits to the shapes of the 0^{-}, 1^{-}, 2^{-}, 3^{-}, 4^{-}, 6^{-}, 8^{-} and 9^{-} members of the p $h_{9/2}$ - n $g_{9/2}$ multiplet are found, and are best when the relative phase is selected that would correctly provide the coherence for ground state

to ground state calculations between doubly-even nuclei. Sample predictions are compared to the 0^- and 1^- data in Fig. Al-b8.

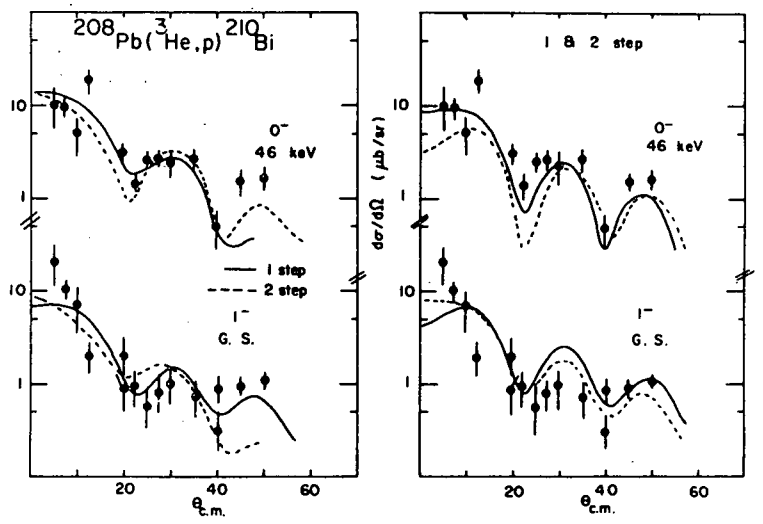

Fig. Al-b8. Angular distributions of the (^{3}He,p) data to the 0^- and 1^- levels of ^{210}Bi are compared on the left to a purely one-step double stripping as the solid curve and to two-step predictions as the broken curve. On the right are shown the coherently mixed predictions, with the solid as the correct choice. The factors needed to provide the magnitudes shown are listed in the table.

The factors necessary to provide the proper magnitudes at the predictions are listed in Table Al-bIV. The two-step prediction is far too small by itself, but provides an important modification to the coherently added one- and two-step calculations. The 9^- state is much weaker than predicted, but a factor of 2 ± 0.5 suffices to bring the properly added prediction into agreement with the other states, excepting the unresolved and untreated doublet of 5^- and 7^- levels.

Also shown in Fig. Al-b8 are the predictions with the incorrect relative phase between one- and two-step amplitudes. This is intended to demonstrate the sensitivity to the mixing. The 0^- data are fit less well and a larger and less constant factor is required to bring the predictions into accord with the data for all the members of the multiplet.

The factor of 2 ± 0.5 required to reconcile the data and predictions may be compared to the ^{208}Pb(^{3}He,d)^{209}Bi ground state spectroscopic factor of 1.2, not unity[2], and the sum of 1.06, not unity observed for ^{209}Bi(d,p)^{210}Bi to the lowest multiplet[3]. Evidently the

Table A1-bV

Factors required to reconcile the magnitudes of the predictions to the $^{208}Pb(^{3}He,p)^{210}Bi$ data.

	Factors to multiply predictions			
J^{π}	1-step	2-step	both	wrong
0^-	5.8	39	1.7	3.3
1^-	1.8	26	0.9	1.5
2^-	5.0	46	2.0	2.8
3^-	4.6	31	1.9	2.9
4^-	4.8	44	2.6	2.3
5^-	---	--	---	---
6^-	0.94	47	2.3	2.3
7^-	---	--	---	---
8^-	5.4	16	3.0	2.9
9^-	0.07	21	0.077	0.077

standard optical-model and bound-state parameters underpredict one-nucleon transfer probabilities a bit, and this effect shows more strongly in two-nucleon transfer.

This work is written up and ready to submit for publication.

[1] H. T. Motz, et al., Phys. Rev. Letters 26 (1971) 854.
[2] B. H. Wildenthal, et al., Phys. Rev. Letters 19 (1967) 960.
[3] C. K. Cline, et al., Nucl. Phys. A186 (1972) 273.

v. Survey of the $(\vec{t},p)$ Reaction on Medium-mass Nuclei

E. Sugarbaker; W. P. Alford (University of Western Ontario); R. N. Boyd (Ohio State); E. R. Flynn, R. N. Brown, J. Cizewski and J. Sunier (LASL); and D. Ardouin (University of Nantes)

Analysis of the differential cross sections and analyzing powers

A_y has been completed for the $(\vec{t},p)$ reactions on $^{70,72}Ge$, $^{96,100}Mo$, ^{106}Pd, and ^{126}Te. Additional data also acquired using the 17 MeV polarized triton beam and Q3D spectrometer at LASL have been measured for the $^{130}Te(\vec{t},p)^{132}Te$ reaction. Data were obtained at angles from 15° to 60° in 5° steps with beams having typical polarizations of 0.75.

The $^{96,100}Mo$ reactions have been studied to investigate the sensitivity of two-nucleon transfer strengths and A_y to the shape transition which occurs in the heavy Mo isotopes. The proton spectrum of the reaction on ^{96}Mo is shown in Fig. A1-b9. While the ground state transitions are populated with comparable strength in these two nuclei, the distribution of excited 0^+ and 2^+ strengths are significantly different. The 0.787 MeV 2^+ state in ^{98}Mo dominates the low-lying excitation region. This 2^+ strength is fragmented in ^{102}Mo, with 87% of the ^{98}Mo strength occuring in levels at 0.296, 0.850 and 1.215 MeV. In addition an excited 0^+ state at 699 keV is seen in the ^{102}Mo spectrum which appears with almost half of the strength of the ground state transition. We conclude that while ^{96}Mo and ^{98}Mo have similar spherical ground state configurations, ^{100}Mo and ^{102}Mo are becoming increasingly deformed. This is supported by a comparison of

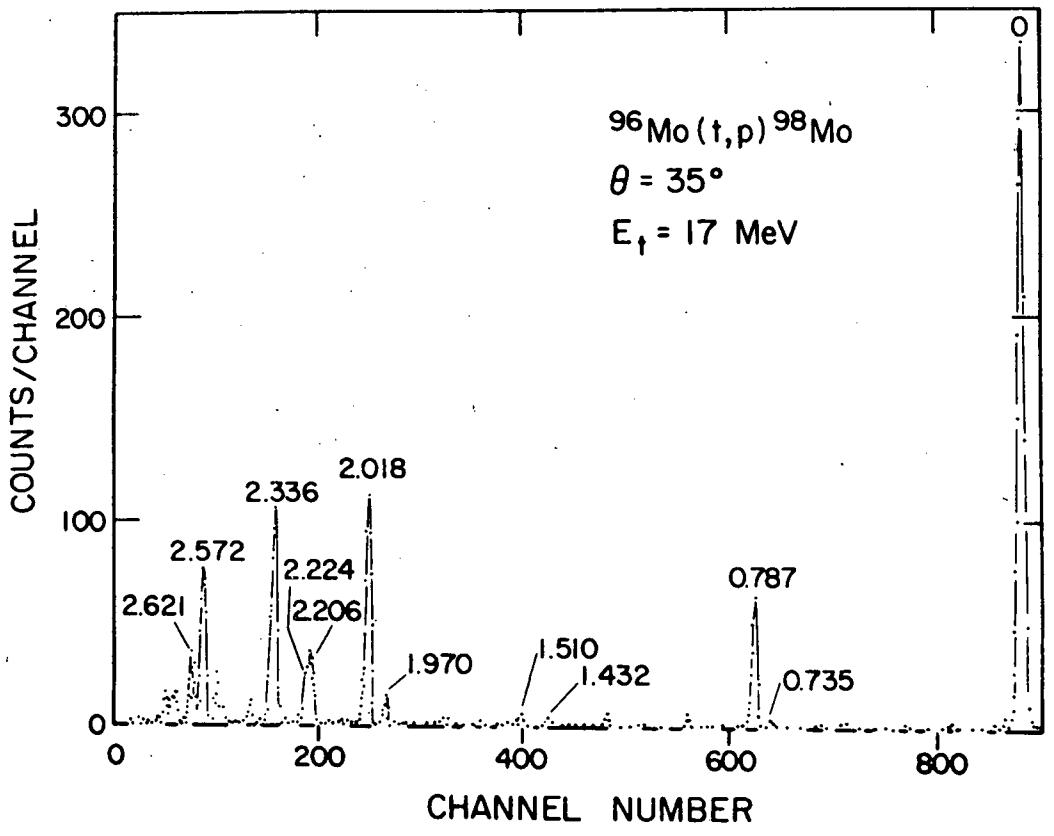

Fig. A1-b9. A sample spectrum of the $^{96}Mo(\vec{t},p)^{98}Mo$ reaction at E_t=17 MeV.

the (t,p) and (p,t) transition strengths for the 0.735 MeV 0^+ state in ^{98}Mo. The (p,t) strength is 16.9% of that of the ground state, while the (t,p) is only 1.5%. Thus the present data clearly indicate that ^{100}Mo is beginning to deform. These results have been published.

The search for anomalous A_y for 2^+ states in this mass region due to interference between one- and two-step processes in the reaction mechanism continues. The $\vec{(p,t)}$ A_y data show differences in A_y between Pd and Te nuclei which have been attributed to increased ground state correlations in Pd[1]. Similar effects have not been seen in the $\vec{(t,p)}$ reaction targets of Mo, Pd and ^{126}Te. A report of this negative result has been published. A recent study of the ^{130}Te(t,p)^{132}Te reaction is presently under analysis. The A_y for the first 2^+ state may deviate from those observed in the lighter Te isotopes.

Angular distributions of the cross sections and A_y for states populated in ^{72}Ge and ^{74}Ge are shown in Figs. A1-b10 and A1-b11, respectively. While the 3^- cross sections exhibit a similar angular distribution for these two nuclei, the A_y are markedly out of phase. This difference may reflect a change in the microscopic structure of the octupole strength. For instance, between N=40 and 42 the $f_{5/2}$ state falls below the $p_{7/2}$ state, modifying the inelastic contributions to the 3^- strength. Thus, A_y measurements or octupole transitions may prove to be a valuable tool in the investigation of collective excitations. This data and a preliminary microscopic interpretation has also been published.

---

[1] K. Yagi, et al., Phys. Rev. Lett. 40 (1978) 161.

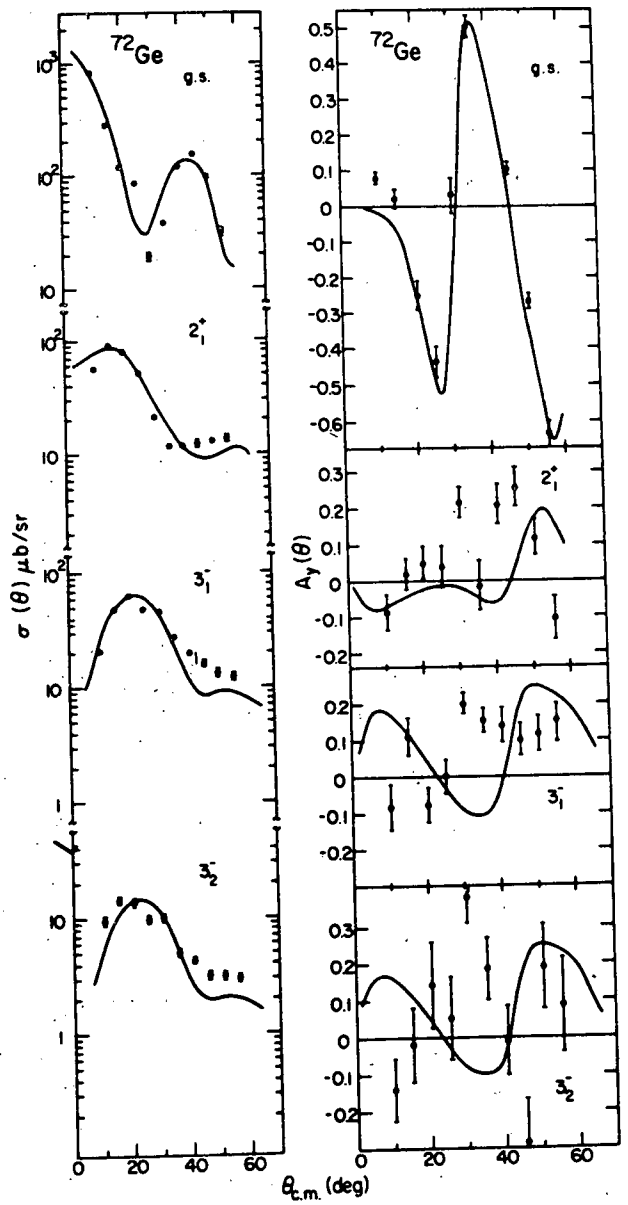

Fig. A1-b10. Angular distributions for the $^{70}Ge(\vec{t},p)^{72}Ge$ reaction.

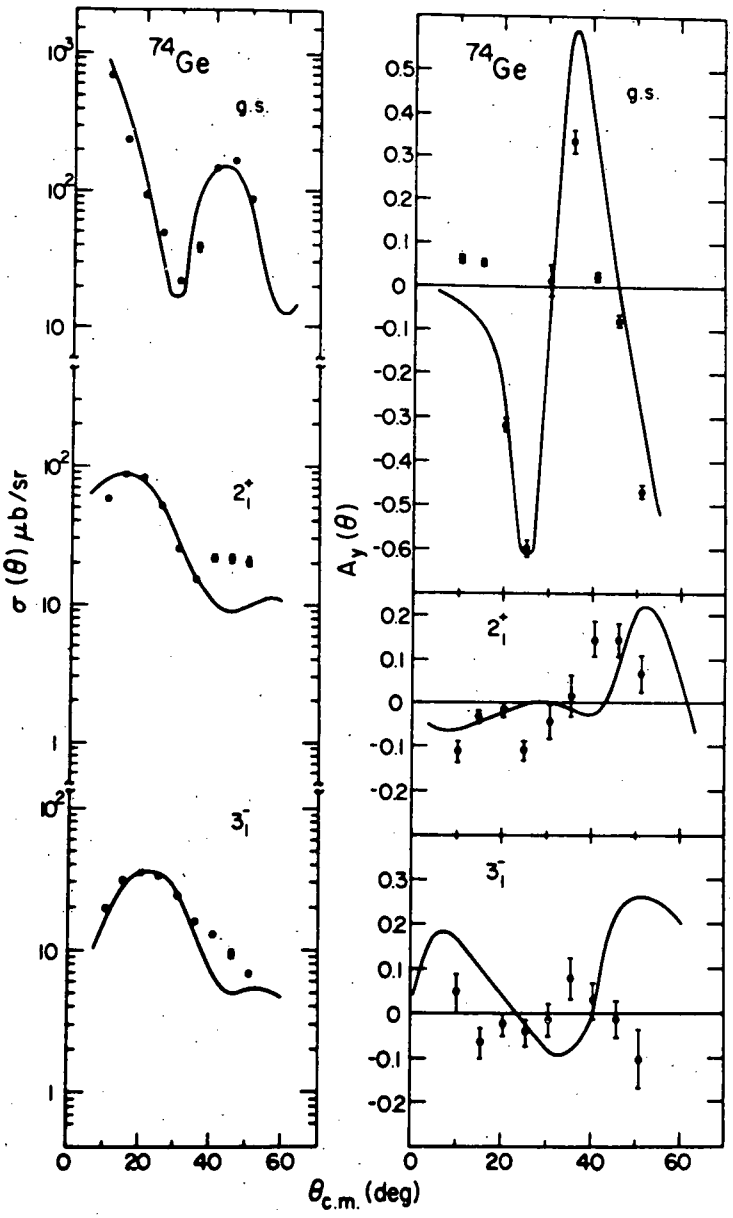

Fig. A1-b11. Angular distributions for the $^{72}Ge(\vec{t},p)^{74}Ge$ reaction.

vi. Investigation of the Forbidden 4^- State via the $^{206}Pb(\vec{t},p)\ ^{208}Pb$ Reaction - E. Sugarbaker and F. W. N. de Boer; W. P. Alford (Western Ontario); R. N. Boyd (Ohio State); R. Brown and E. R. Flynn (LASL).

There has been considerable interest in the nature of the two-neutron transfer reactions, (p,t) and (t,p), populating "forbidden" transitions such as the 3^+ state in ^{206}Pb. Early studies indicated that the cross section data could be reproduced assuming a two-step sequential transfer reaction mechanism. An alternate approach which also provided a fit to the data included finite-range effects within a single-step reaction process. Recently, the analyzing power data for the $^{206}Pb(3^+)$ state could not be fit assuming only a sequential transfer mechanism. We have measured angular distributions of the cross sections and analyzing powers in the $^{206}Pb(\vec{t},p)^{208}Pb$ reaction leading to the 4^-(3.475 MeV) and 5^-(3.198 MeV) states belonging to the $(p_{1/2}^{-1}\ g_{9/2})$ doublet in the hope that the reaction mechanism might be determined.

Data were acquired from 10^o to 65^o using the 17 MeV polarized triton beam at LASL. The angular distributions for the doublet of interest are shown in Fig. A1-b12. The curves are the result of

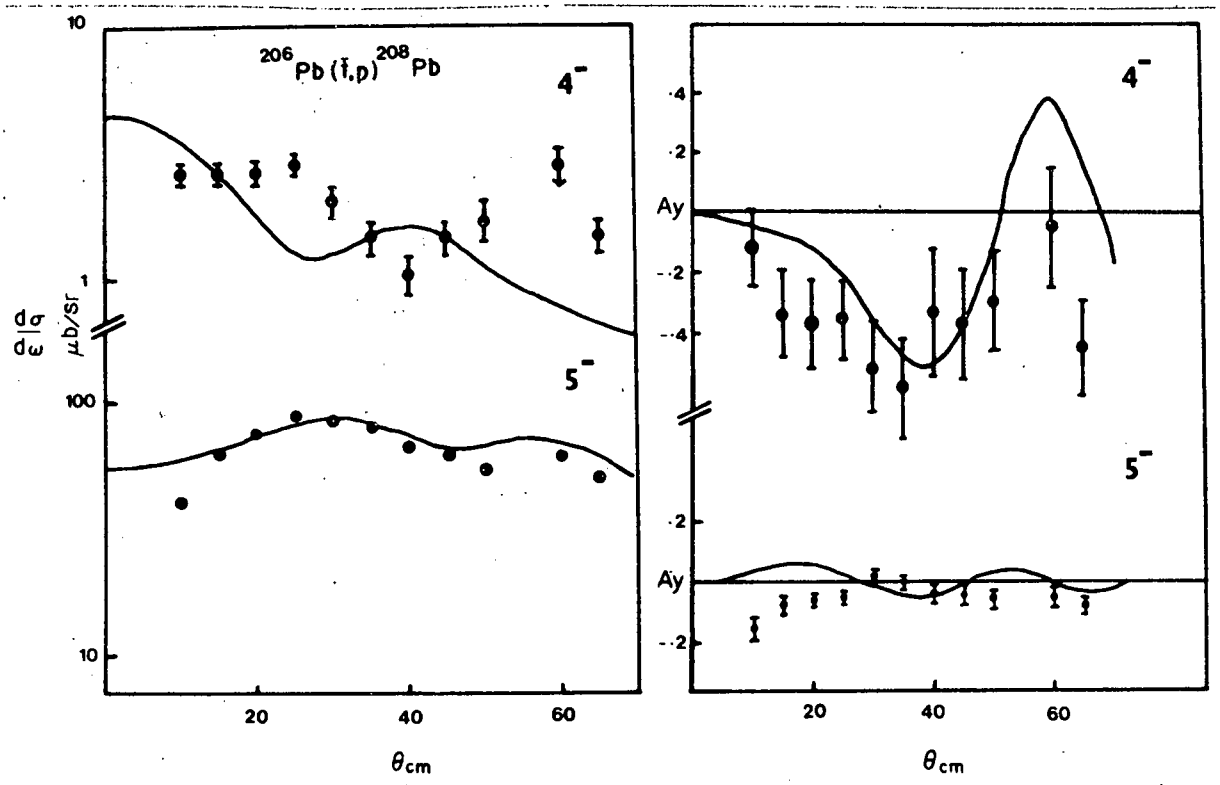

Fig. A1-b12. Angular distributions of the $(p_{1/2}^{-1}\ g_{9/2})$ doublet in the $^{206}Pb(\vec{t},p)^{208}Pb$ reaction.

calculations performed using the zero-range code CHUCK. The 5^- state can be populated directly via a single-step reaction, and for it an expected $(p_{1/2}g_{9/2})$ form factor was assumed. While these calculations provide good agreement with the measured cross section data, the analyzing powers are not well described. Since two-step contributions cannot be ruled out for the 5^- state, this discrepancy might be expected.

The 4^- state was assumed to be populated only via a sequential (t,d)(d,p) reaction. This led to the predictions shown in Fig. A1-b12. In this case the analyzing powers are well reproduced, while only the magnitude of the cross section distribution is correctly predicted.

Further calculations are being performed to investigate whether inclusion of additional small components of the wave functions would provide a better fit to these data.

vii. Proton Pairing Strength in ^{91}Nb, ^{115}Sb and ^{117}Sb

R. A. Emigh, D. A. Lind, P. A. Smith and C. D. Zafiratos; W. P. Alford (Western Ontario University); R. E. Anderson (University of North Carolina); P. A. Batay-Csorba(Schlumberger Research Center); and I. Brissaud(Institut de Physique Nucléaire)

An important characteristic of the (^{3}He,n) two-proton transfer reaction is the preferential population of states with strong proton pairing correlations. This reaction has been used previously at this laboratory to study the regions near Z=40, 50 and 82.[1,2,3] Simple pairing theory qualitatively predicts many of these results although it does not, for example, predict the relatively strong excited L=0 strength seen in the Sn(^{3}He,n) Te reactions for the heavier tin isotopes. A more realistic monopole pairing calculation generally removes these deficiencies and even predicts the observed hot orbit states seen in the Kr(^{3}He,n) Sn studies.[4]

The purpose of the present study is three-fold. First, using the simple pairing model, the (^{3}He,n) results for even N-odd Z nuclei should be similar to those obtained for nearby even N-even Z nuclei. However, in previous (^{3}He,n) studies on odd N-even Z nuclei we have observed anomalously large L=0 intensities. This phenomenon is not well understood at present.

Second, the energy centroids for excited L=0 transitions in the Cd(^{3}He,n)Sn reactions are lower than predicted by a harmonic pairing vibrational model. Flynn and Kunz[5] have shown that this difference arises from a large Coulomb contribution to proton-hole interactions. They also showed that this correction scales linearly with the number of holes and particles, using our preliminary ^{115}In(^{3}He,n)^{117}Sb results. This work completes the ^{115}In study and extends this theoretical consideration to the ^{113}In(^{3}He,n)^{115}Sb and ^{89}Y(^{3}He,n)^{91}Nb reactions.

Third, γ-ray studies of light-mass odd A antimony isotopes indicate the presence of a low-lying rotational band with a $9/2^+$ band head. The L=0 (^{3}He,n) transitions from In to Sb should be sensitive to possible mixing of the spherical $9/2^+$ state into this deformed state.

Spectra for the two Indium targets are shown in Figs. A1-b13 and A1-b14. The two prominent low-lying states contain a great deal of L=0 strength. Angular distributions and DWBA calculations for ^{89}Y, ^{113}In and ^{115}In targets are shown in Figs. A1-b15 - A1-b17.

The strengths of the observed transitions are summarized in Table A1-bVI. The results for ^{89}Y(^{3}He,n) are similar to previous

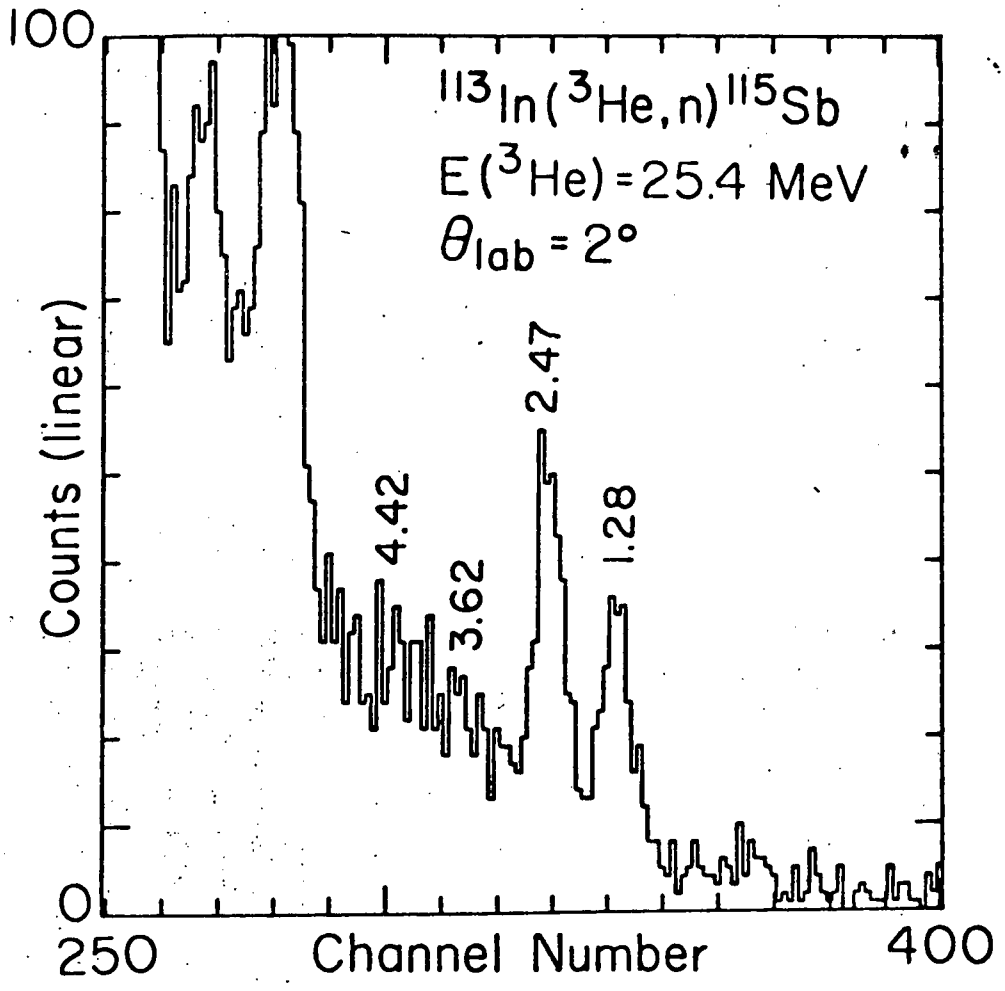

Fig. A1-b13. Neutron time-of-flight spectrum of the ^{113}In(^{3}He,n)^{115}Sb reaction at 2°. Energies are in MeV and time per channel is 0.179 ns.

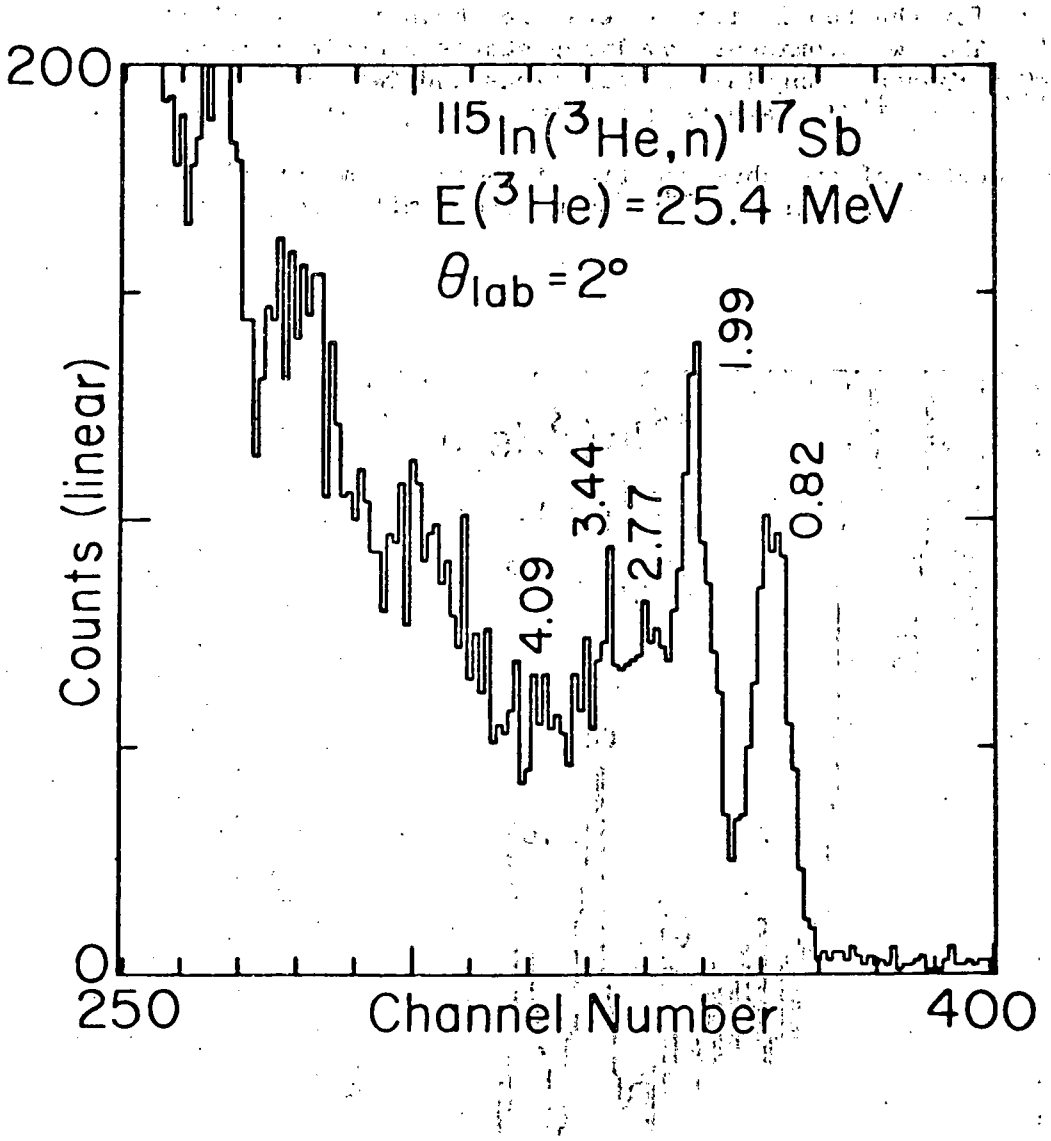

Fig. A1-b14. Neutron time-of-flight spectrum of the $^{115}In(^{3}He,n)^{117}Sb$ reaction at 2°. Energies are in MeV and time per channel is 0.179 ns.

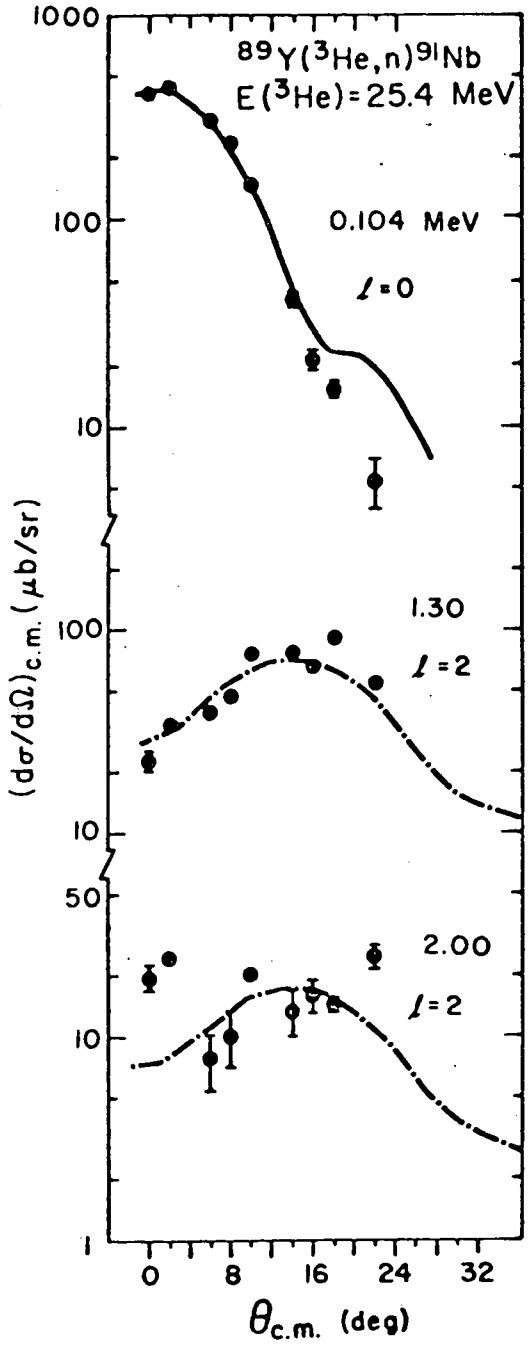

Fig. Al-b15. Angular distributions of neutron groups observed in the $^{89}Y(^{3}He,n)^{91}Nb$ reaction. The solid curves are the results of DWBA calculations described in the text.

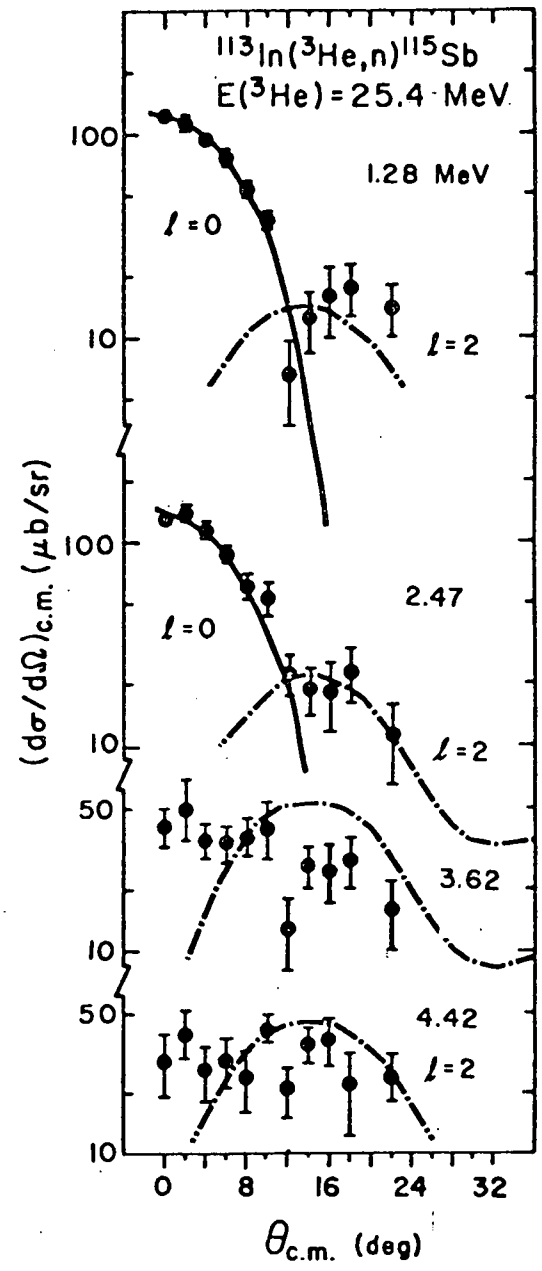

Fig. Al-b16. Angular distributions of neutron groups observed in the $^{113}In(^{3}He,n)^{115}Sb$ reaction. The solid curves are the results of DWBA calculations.

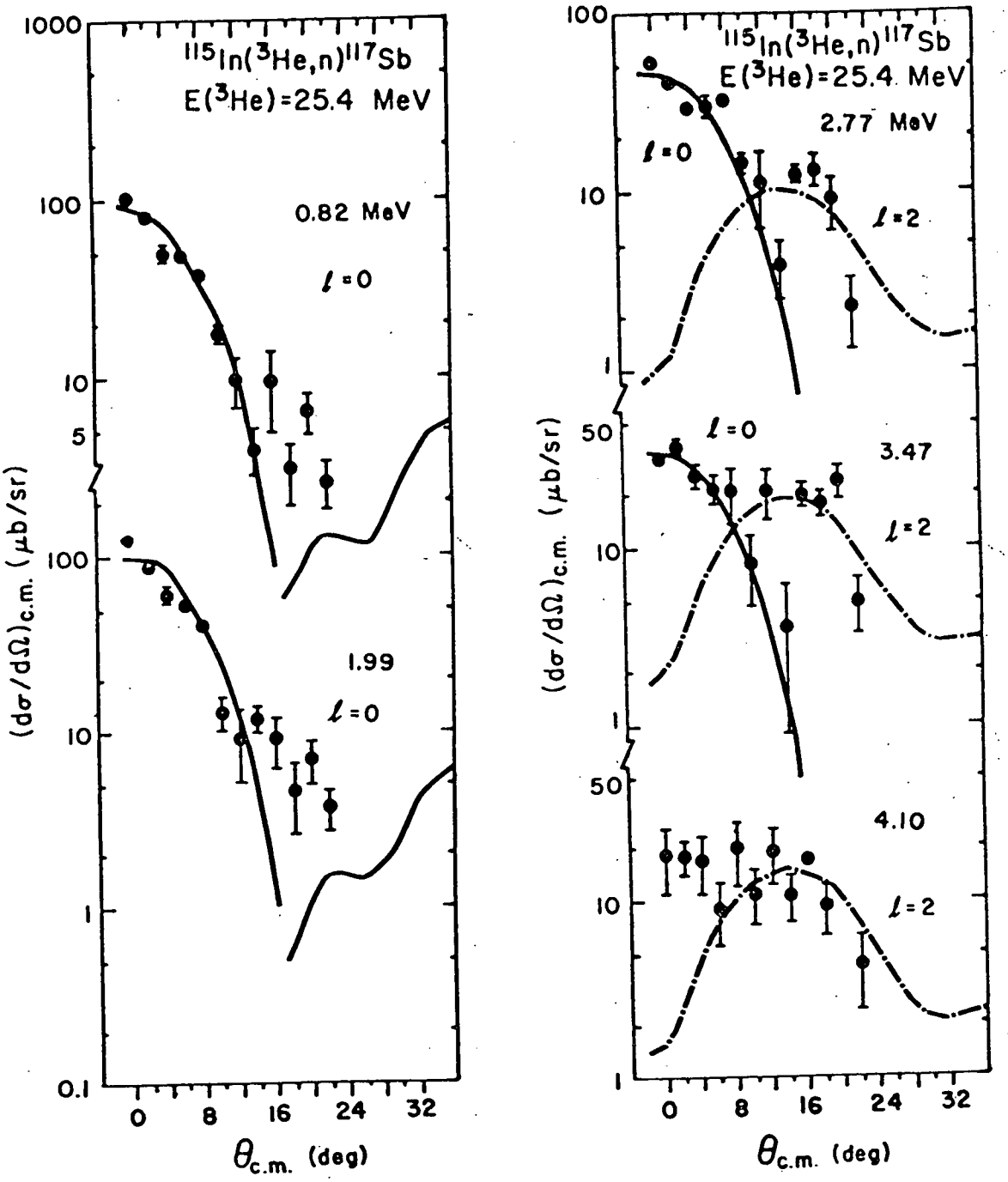

Fig. A1-b17. Angular distributions of neutron groups observed in the $^{115}In(^{3}He,n)^{117}Sb$ reaction. The solid curves are the results of DWBA calculations.

Table A1-bVI

Transition Strengths

Target Nucleus	Final Nucleus	Excitation (MeV)	Uncertainty (MeV)	L-transfer	σ_{max} (mb/sr)	enhancement
^{89}Y	^{91}Nb	0.104	---	0	0.440	5.34
		1.30	0.09	2	0.095	2.36
		2.00	0.19	2	0.020	0.46
^{113}In	^{115}Sb	1.28	0.10	0+2	0.125	1.34
		2.47	0.20	0+2	0.130	1.30
		3.62	0.15	0(+2)	0.025	0.23
		4.42	0.17	(2)	0.035	1.44
^{115}In	^{117}Sb	0.82	0.11	0	0.110	1.42
		1.99	0.18	0	0.120	1.44
		2.77	0.20	0+2	0.050	0.57
		3.44	0.19	0+2	0.035	0.38
		4.09	0.22	2(+0?)	).020	1.00

$^{88}Sr(^{3}He,n)$ and $^{90}Zr(^{3}He,n)$ measurements and can be interpreted in terms of a weak-coupling picture. In contrast, two strong low-lying L=0 transitions are seen in the $^{113,115}In(^{3}He,n)$ studies. The total strengths and energy centroids are as expected from $(^{3}He,n)$ studies on light tin isotopes and monopole pairing calculations. It appears that the two observed states correspond to strongly-mixed spherical and deformed $9/2^{+}$ states in the antimony isotopes.

This work is now being prepared for publication.

1 H. W. Fielding, R. E. Anderson, D. A. Lind, C. D. Zafiratos and W. P. Alford, Nucl. Phys. A269 (1976) 125.

2 H. W. Fielding, R. E. Anderson, P. D. Kunz, D. A. Lind, C. D. Zafiratos and W. P. Alford, Nucl. Phys. A304 (1978) 520.

3 R. E. Anderson, P. A. Batay-Csorba, R. A. Emigh, E. R. Flynn, D. A. Lind, P. A. Smith, C. D. Zafiratos and R. M. De Vries, Phys. Rev. C, 19 (1979) 2138.

[4] W. P. Alford, R. E. Anderson, P. A. Batay-Csorba, R. A. Emigh, D. A. Lind, P. A. Smith and C. D. Zafiratos, Nucl. Phys. A330 (1979) 77.
[5] E. R. Flynn and P. D. Kunz, Phys. Lett. 68B (1977) 40.

viii. Excitation of High-Lying States by the (^{3}He,n) Reaction - W. P. Alford, P. Craig, D. A. Lind, T. Masterson, R. Raymond, C. D. Zafiratos

In a preliminary survey searching for $2\hbar\omega$ pairing vibrations, it was noted that light targets showed large cross-sections to states at 10-15 MeV of excitation in the residual nucleus. These states were observed over a continuum since the nuclear level density is far too high to be resolved in these measurements. Nonetheless, some of the strongly excited states exhibited angular distributions that appear to represent well-defined single values of angular momentum transfer.

The preliminary results reported here were obtained for ^{26}Mg and ^{27}Al targets using the 9-meter flight path facility. The incident beam energy was 25.4 MeV. Figures Al-b18 and Al-b19 show spectra taken at zero degrees for ^{26}Mg and ^{27}Al.

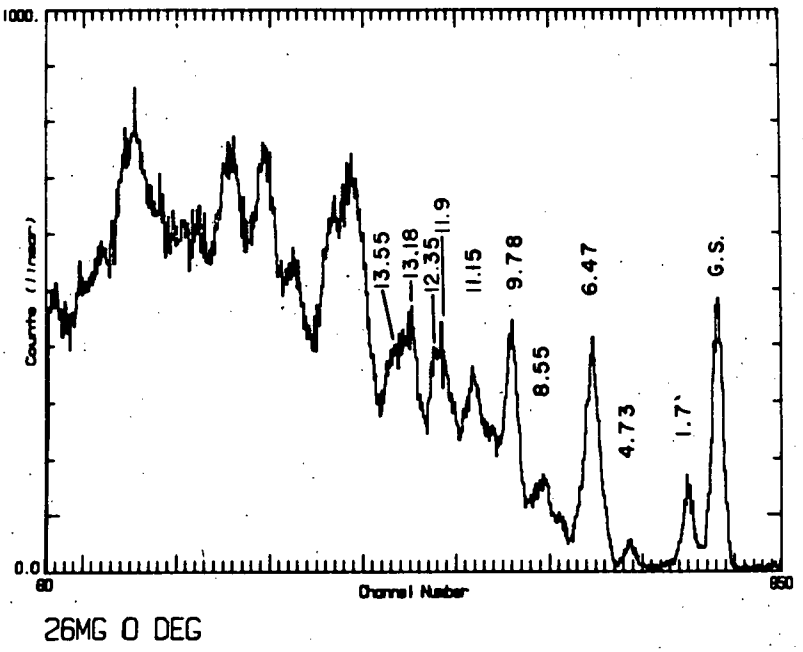

Fig. Al-b18. A time-of-flight spectrum for ^{26}Mg(^{3}He,n)^{28}Si at zero degrees and an incident energy of 25.4 MeV. The time dispersion is 0.09 ns/channel.

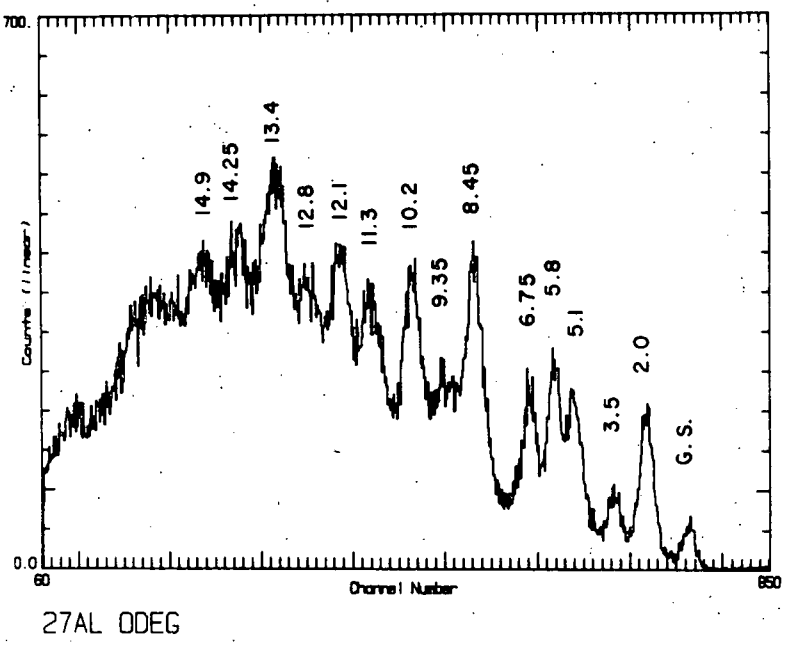

Fig. Al-b19. A time-of flight spectrum for $^{27}Al(^{3}He,n)^{29}P$ at zero degrees and an incident energy of 25.4 MeV. The time dispersion is 0.09 ns/channel.

The angular distribution shown in Fig. Al-b19 is for the 8.45 MeV state in ^{29}P. A preliminary DWBA calculation, also shown in Fig. Al-b19 indicates that this state is reached predominantly through L=0 transfer. Similarly, other states at high excitation energy have angular distributions resembling the empirical L=2 angular distribution seen for the ^{28}Si first-excited state.

These data are being further analyzed and DWBA calculations are being made.

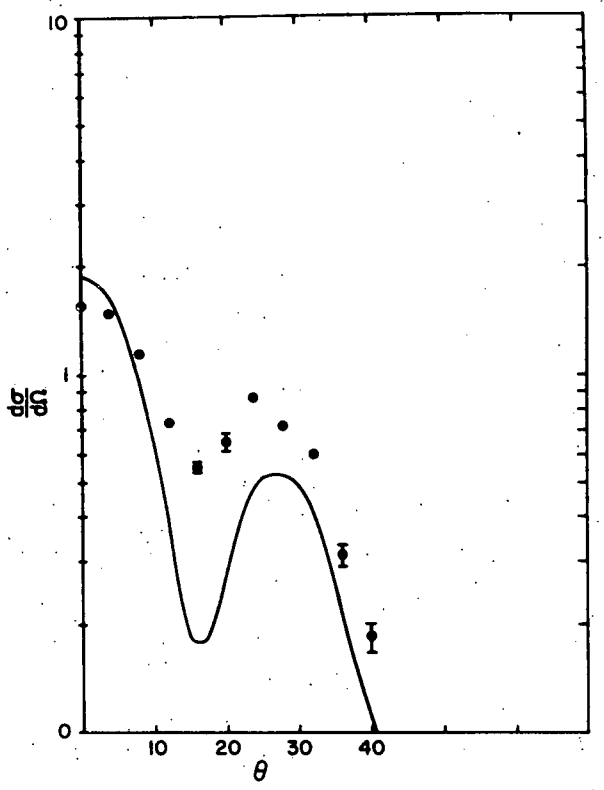

Fig. A1-b20. An angular distribution for the state at 8.45 MeV excitation in ^{29}P. The solid curve is an unnormalized L=0 DWBA calculation with optical model parameters which are not quite appropriate for this energy.

THIS PAGE
WAS INTENTIONALLY
LEFT BLANK

c. Three or More Nucleon Transfer Reactions

i. The (^{4}He,p) Reaction on ^{13}C and Other Light Nuclei - J. Hamill, R. S. Raymond, R. J. Peterson, D. Murdock, C. D. Zafiratos, D. Haynes, and T. G. Masterson

We have studied the (α,p) reaction at 35.5 MeV on ^{13}C to complement the (α,n) study, in particular to distinguish T=0 and T=1 levels in A=16. The experiment was performed with solid state detectors to obtain broad range spectra. A sample spectrum is shown as Fig. Al-c1. The ground state quartet of weak levels in ^{16}N has previously been studied at high resolution with the beam swinger and spectrograph.

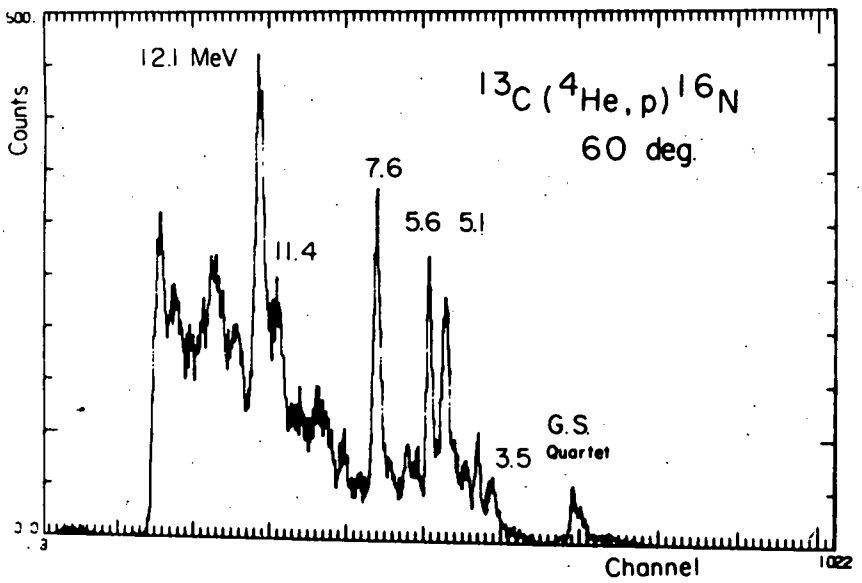

Fig. Al-c1. A sample spectrum from the (α,p) three nucleon stripping reaction on ^{13}C. The large angle will emphasize the excitation of high spin states, with the 11.4 and 12.1 MeV peaks candidates for 6^- or 7^- states populated by $(d_{5/2})^3\,13/2$ transfer.

Excitation energies labelled in Fig. Al-c1 are taken from ref. 1, where energy systematics are used to suggest spins and parities of 6^- or 7^- for the 11.4 and 12.1 MeV peaks. We have obtained data for more precise energy calibration and for angular distributions to test if these are indeed states of such high spin.

Data on ^{24}Mg, ^{12}C, and ^{9}Be have also been obtained with the (α,p) reaction to provide test cases for DWBA calculations to states of definite angular momentum transfer. The ^{9}Be(α,p) data will complement the (α,n) data, and again allow us to distinguish between T=0 and T=1 states in ^{12}C. These data have been taken to lab angles as large as 140°.

---

[1] N. T. Burtebaer et al., Sov. J. Nucl. Phys. 24 (1976) 457.

ii. The (α,n) Reaction on Light Nuclei - J. J. Hamill, D. H. Haynes, D. A. Lind, T. G. Masterson, P. A. Smith, E. Sugarbaker, and C. D. Zafiratos

Recent intermediate energy studies with pion and nucleon probes have discovered new features at high excitation energies in light nuclei. Most of this new spectroscopy was previously unobserved in low energy studies. It is desirable, if possible, to observe these new features with low-energy reactions with reasonably well-understood reaction mechanisms.

We have begun a study of light nuclei with the (α,n) reaction for a number of reasons. First, we expect to observe larger momentum transfers and higher spin states than have been previously found with light-ion reaction studies. Second, the (α,n) reaction has not previously been studied extensively at direct reaction energies. Third, a comparison of (α,n) cross sections with (α,p) cross sections on mirror and analogue cases can be an interesting test of isospin and reaction models. Finally, a study of the (α,n) reaction must begin with light nuclei because experimental difficulties currently make studies of heavy targets difficult.

Currently, data have been obtained at E_α=28 MeV for ^{9}Be, ^{12}C, ^{24}Mg, ^{40}Ca, and ^{142}Nd with a 9 m flight path. The beam was pulsed so that one burst in three reached the target. After pulsing 150 nA was obtained on target. In a second run at E_α=36 MeV data were obtained for ^{9}Be, ^{12}C, and ^{13}C targets. Sample spectra from the ^{9}Be, ^{12}C, and ^{13}C 36 MeV data are shown in Fig. A1-c2. The beam on target after pulsing was also about 150 nA for this energy.

Sample angular distributions which illustrate the strong j-dependence normally observed in the (α,p) reaction are shown in Fig. A1-c3. As usual the $1/2^-$ transfer has obvious minima while the $3/2^-$ transfer is rather featureless. A strong j-dependence is also observed for the ℓ=2 pair. This j-dependence is a reassuring feature in that it suggests a direct reaction mechanism.

Initial attempts at cluster DWBA calculations to predict the angular distribution shapes are underway. A reasonable fit to the $1/2^-$ transfer has been obtained. However, simultaneous fits to all the states observed have not yet been realized. A great deal of sensitivity to both the alpha and neutron optical parameters has been observed.

Further studies are currently in progress. These include optical model searches on existing α-scattering data and acquisition of more data on the (α,n) reactions. The analogous (α,p) reactions have been investigated and are described elsewhere in this Progress Report.

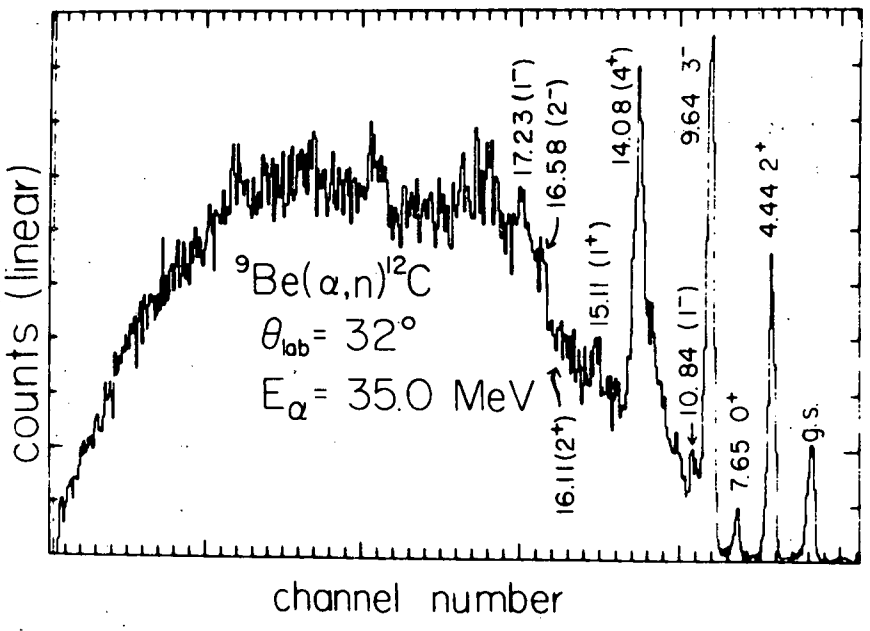

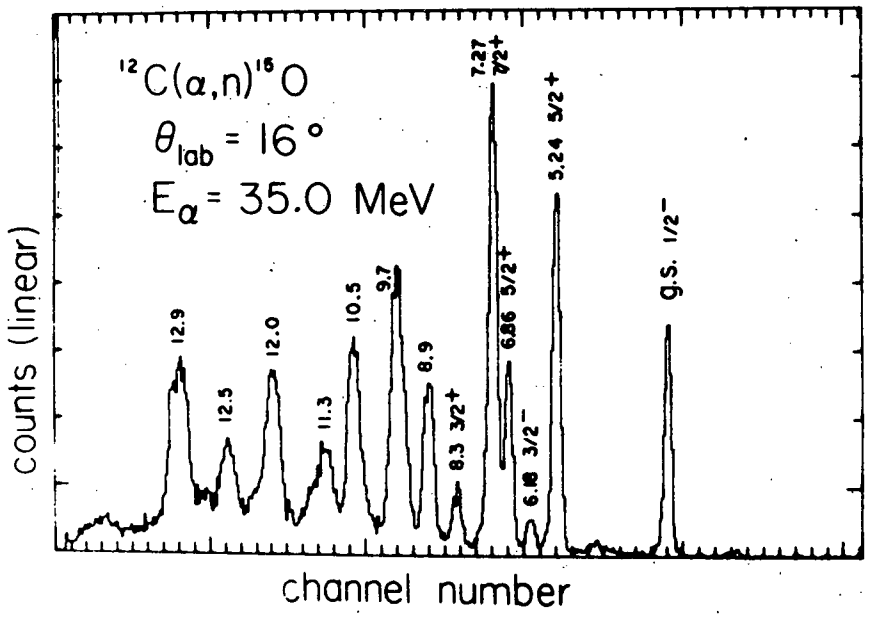

Fig. Al-c2. Time-of-flight spectra for the (α,n) reaction on several targets. The flight path was 9 meters and the time dispersion is 3.1 channels/ns.

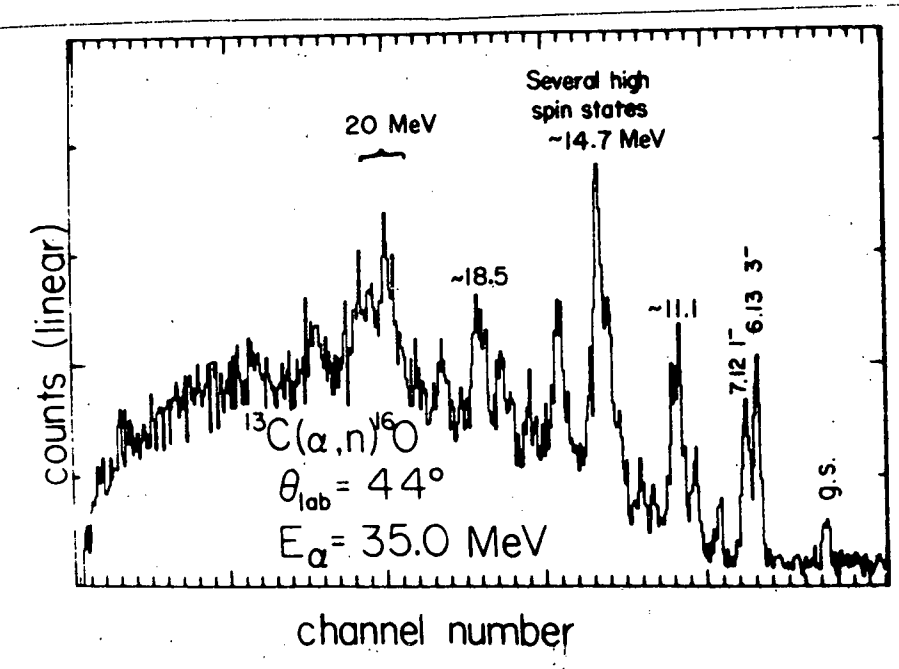

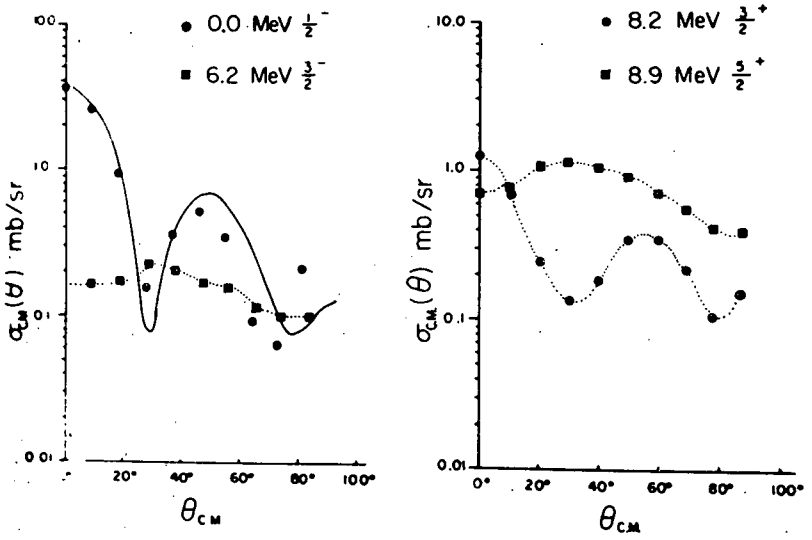

Fig. A1-c3. Four angular distributions for the $^{12}C(\alpha,n)^{15}O$ reaction at E_α=35.0 MeV. Error bars are not given, but non-systematic errors are in all cases smaller than 15%. The dotted curves serve only to guide the eye; the solid curve is the result of a DWBA calculation scaled to agree with the data at small angles. These angular distributions show that $\Delta\ell$=1 and $\Delta\ell$=2 transfers have a strong Δj dependence.

iii. High Spin States in the $^{46,48}Ti(\vec{p},\alpha)^{43,45}Sc$ Reactions - E. Sugarbaker; R. N. Boyd, S. L. Blatt, T. Donoghue and H. Hausman (Ohio State); S. Vigdor and P. Schwandt (IUCF); H. Fulbright (U. of Rochester)

The study of the $(\vec{p},\alpha)$ reaction on $^{46,48}Ti$ targets continues. Additional data have been obtained at IUCF to complete the angular distributions of the analyzing powers. The striking j-dependence of these analyzing powers suggested in last year's report has been confirmed. Momentum matching at $E_p \approx 80$ MeV requires that this reaction will selectively populate high spin states. Thus, the analysis has concentrated on the high spin $\nu f_{7/2}^2\, \pi f_{7/2}$ configuration states and on a few more complex states.

Data for levels populated in ^{43}Sc and ^{45}Sc are presented in Fig. Al-c4 and Fig. Al-c5, respectively. The curves shown with the data are the result of DWBA calculations in which a cluster form factor has been used in the transfer mechanism. These one-step calculations reproduce the qualitative features of the data of the known high spin states. An exception occurs for the 4.36 MeV level in ^{43}Sc, which has been suggested as a $17/2^-$ state. The one-step calculation shown in Fig. Al-c4 assuming such an assignment does not reproduce the data. However, the agreement for the level at 5.20 MeV is quite good using a $17/2^+$ assignment. This assignment is in agreement with the range of $3/2^+$ to $17/2^+$ suggested by a (p,t) reaction study.

An additional level was observed at high excitation in ^{45}Sc. The level observed is probably the state at 5.42 MeV which has been assigned a spin of either $21/2^-$ or $23/2^-$.[1] The curves shown in Fig. Al-c5 are the result of a $23/2^-$ calculation which included a 19/2 transfer and L=2 inelastic excitation. While the fit to the cross section is not good, the $21/2^-$ calculation underpredicts the data by more than an order of magnitude. The $23/2^-$ calculation does provide a reasonable fit to the analyzing powers, and we conclude that the most likely assignment for the 5.42 MeV state in ^{45}Sc is $23/2^-$.

Cluster spectroscopic factors have been calculated using $(f_{7/2})^3$ shell model wave functions[2], using the code MICRO[3]. The normalization of preliminary DWBA curves (defined to be 1.0 for the $19/2^-$ states) is compared with these cluster spectroscopic factors (again relative to that for the $19/2^-$ states) in Table Al-cI. For the high spin states, for which it is correct to assume $(f_{7/2})^3$ wavefunctions, we find excellent agreement with the predictions. The enhancement of the $j_>$ member for a given ℓ-transfer is well described. The lower spin states should contain significant contributions from the $p_{3/2}$ orbital and as such would not be reproduced by the above model wavefunctions.

Table A1-cI

Comparison of experimental and predicted spectroscopic factors for the $^{46,48}Ti(p,\alpha)^{43,45}Sc$ reactions.

	^{43}Sc			^{45}Sc		
J^{π}	E_x (MeV)	S_{exp}	$S_{pred.}$	E_x (MeV)	S_{exp}	$S_{pred.}$
$19/2^-$	3.12	1.0	1.0	3.69	1.0	1.0
$17/2^-$	--	--	0.085	--	--	0.07
$15/2^-$	2.99	0.53	0.49	(4.69)	(0.31)	0.166
$13/2^-$	--	--	0.024	--	--	0.008
$11/2^-$	1.83	0.18	0.19	1.24	0.04	0.026
$9/2^-$	2.87	(0.14)	0.013	--	--	0.001
$7/2^-$	0.0	0.75	1.57	0.0	0.21	0.51
$5/2^-$	0.84	0.21	0.012	--	--	0.001

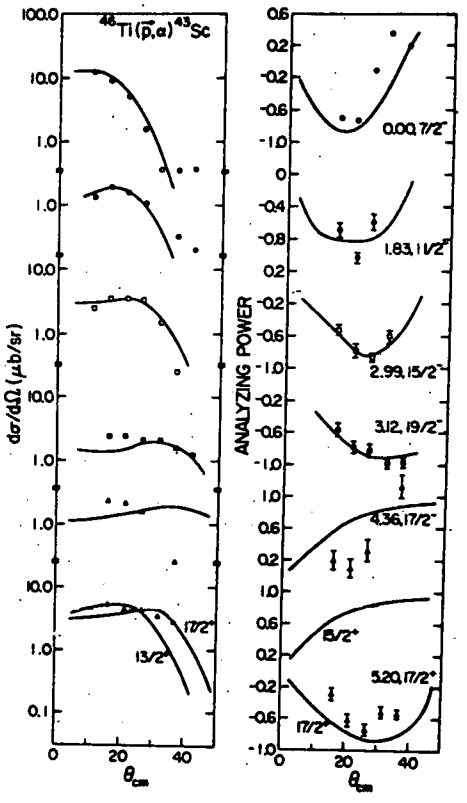

Fig. A1-c4. Angular distributions of states observed in the $^{46}Ti(\vec{p},\alpha)^{43}Sc$ reaction.

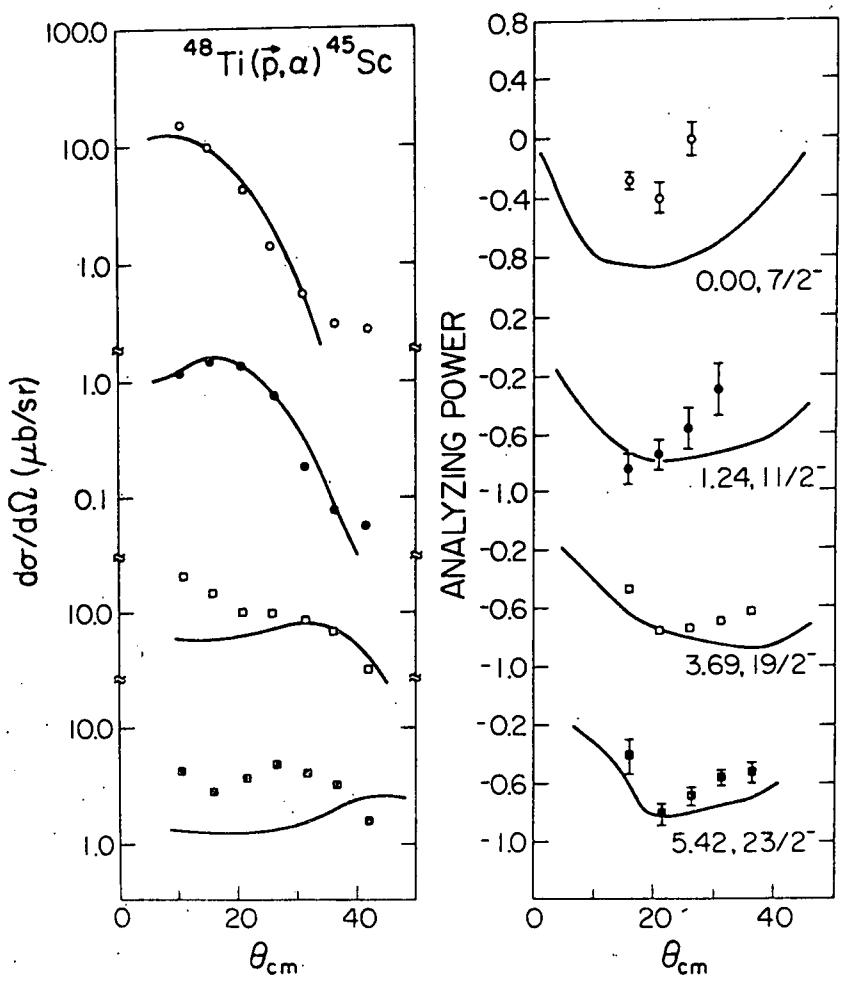

Fig. A1-c5. Angular distributions of states observed in the $^{48}Ti(\vec{p},\alpha)^{45}Sc$ reaction.

1. P. G. Bizzetti, et al., Nuovo Cim. 26A (1975) 25.
2. W. Kutschera, B. A. Brown, K. Ogawa, private communication.
3. P. A. Smith, private communication.

iv. The $(\vec{d}, {}^{6}Li)$ Reaction - E. Sugarbaker; R. N. Boyd, S. L. Blatt, T. R. Donoghue and H. J. Hausman (Ohio State); R. E. Brown and N. Stein (LASL); C. C. Foster and S. E. Vigdor (IUCF)

The study of the $(\vec{d}, {}^{6}Li)$ reaction at IUCF is still in the beginning stages. It is hoped that the sensitivity of the vector analyzing powers to the transferred L and to the ^{6}Li spin-orbit potential will provide interesting results for nuclei in the sd and fp shells. However, at present only preliminary data on ^{24}Mg and ^{40}Ca have been obtained. Some levels did exhibit strong analyzing power effects, suggesting that extraction of the above information might indeed be possible with more complete data.

v. Evidence of Non-statistical Mechanisms in Low-Energy $(^{9}Be,n)$ Reactions - E. Sugarbaker; D. Elmore and H. Gove (U. of Rochester); R. N. Boyd (Ohio State)

We reported last year on the selectivity observed in the $^{12}C(^{9}Be,n)^{20}Ne$ reaction at 16 and 24 MeV bombarding energies. Members of the band belonging to the (8,8) representation in the SU(3) model are seen with enhanced strength with respect to members of bands of different configuration. A typical spectrum at 24 MeV is shown in Fig. A1-c6. Statistical compound and finite range direct reaction calculations have not reproduced this effect.

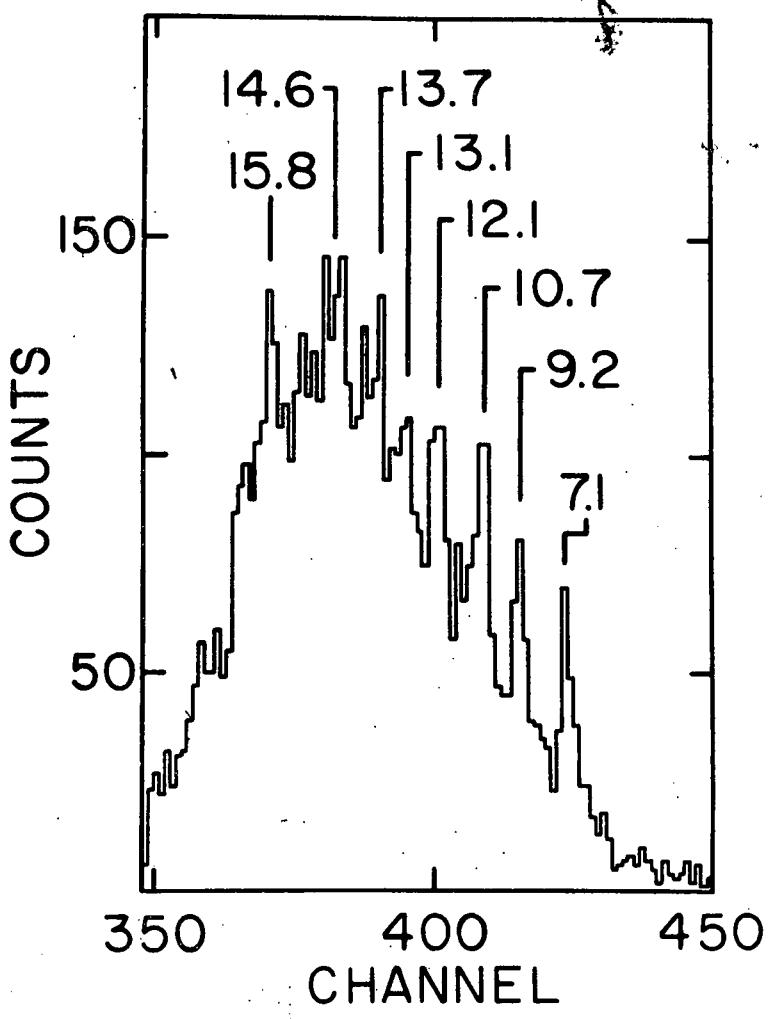

Fig. Al-c6. The $\theta_{lab}=130°$ $^{12}C(^{9}Be,n)^{20}Ne$ neutron time-of-flight spectrum at $E_{^{9}Be}$ = 24 MeV.

The enhanced strength with which this 8p-4h band is populated in the (^{9}Be,n) reaction may be due to a mechanism similar to that described by Middleton et al.[1] and by Carlson and Johnson[2]. They argue that enhanced strength in ^{12}C and ^{7}Li induced reactions might arise from a "semidirect" mechanism involving intermediate states containing the cluster fragments of the breakup of the projectile. The more loosely bound the clusters in the projectile, the more likely the formation of such doorway states. This is consistent with the observation that the (^{12}C,α) reaction has exhibited greater selectivity than the (^{14}N,^{6}Li) reaction, since ^{12}C has a breakup energy (into ^{8}Be plus other) of 7.37 MeV compared with 16.17 MeV for ^{14}N. The breakup energy of ^{9}Be into ^{8}Be plus a neutron is only 1.67 MeV, which may account for the rather significant selectivity observed in the present study. Even at the low center-of-mass energies studied, "doorway" states could be easily formed which would have a potentially strong overlap with final ^{20}Ne states having a configuration based on two α-particles outside a ^{12}C core.

This work has been completed and accepted for publication.

1. R. Middleton et al., Phys. Rev. Lett. 27 (1971) 950.
2. R. R. Carlson and D. J. Johnson, Phys. Rev. Lett. 25 (1970) 172.

d. Charge Exchange Reactions

i. The 1^+ Strength Distribution in ^{58}Co - E. Sugarbaker, R. A. Emigh, C. A. Fields, and P. A. Smith

Analysis of the $^{58}Fe(^3He,t)^{58}Co$ reaction at $E_{^3He}$=43 MeV is proceeding. This investigation was undertaken in the hope that the disagreement in the M1 strengths observed in the $^{58}Ni(e,e')$ and $^{58}Ni(t,^3He)$ reactions might be better understood. Since a subsequent $^{58}Fe(p,n)$ study agreed with the (e,e') results, the $(t,^3He)$ strengths remain suspect. A discrepancy between (e,e') and $(t,^3He)$ results might arise from the more complex reaction processes to which the latter reaction is subject. The $(^3He,t)$ reaction should be subject to the same problems, and it is surprising that the agreement with the (e,e') and (p,n) results is as good as was reported last year. The major disagreement at that time, which was associated with the 3.29 MeV level, has now been removed. The $(^3He,t)$ relative 1^+ strength for this level is now 0.7, in excellent agreement with the value of 0.5 obtained in the (p,n) study.

The j-dependent shapes of the angular distributions obtained in the present $(^3He,t)$ reaction also seem to indicate that the reaction mechanism is not overly complex. Fig. A1-d1 shows the data for some peaks of known spin. Fig. A1-d2 shows the angular distributions for the levels previously identified as 1^+ states in ^{58}Co. Note that the data for the 1.05 MeV level are not particularly characteristic of a low J transfer. This is expected, since the adopted level scheme places at least four levels near an excitation energy of 1.05 MeV. We can therefore not expect to extract more than an upper limit on the 1^+ strength in this region. Since the $(t,^3He)$ study had comparable energy resolution, it is likely that contributions from these other states led to an excessive strength assignment for this level, and subsequently to erroneously small relative strengths for the higher 1+ states.

We are proceeding with a macroscopic DWBA analysis of these data.

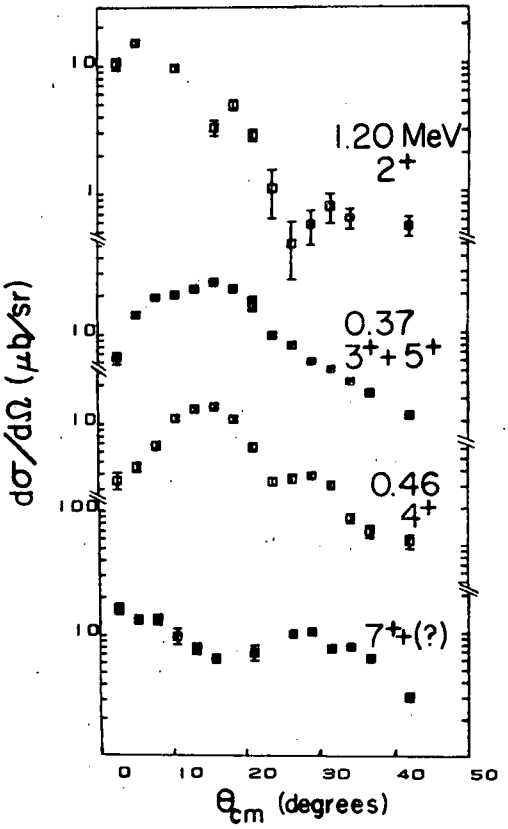

Fig. Al-dl. Sample angular distributions for J>1 transitions in the $^{58}Fe(^{3}He,t)^{58}Co$ reaction.

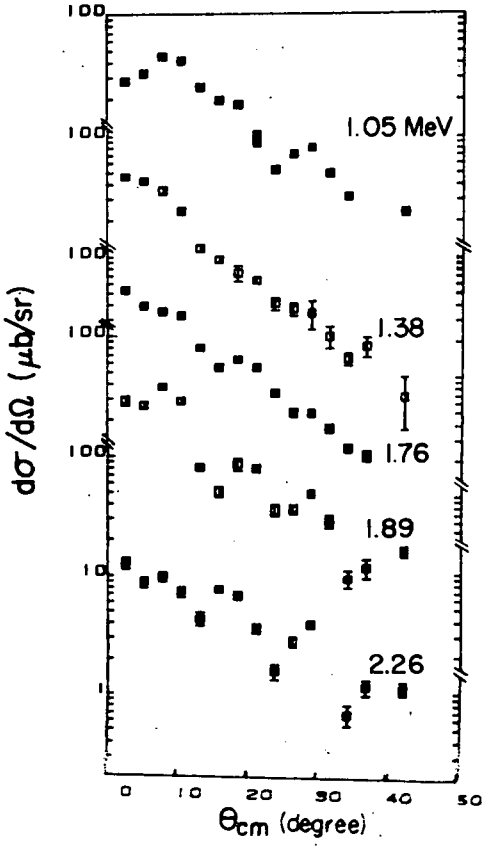

Fig. Al-d2. Angular distributions for known 1^{+} states populated by the $^{58}Fe(^{3}He,t)^{58}Co$ reaction.

ii. The $^{86}Sr(^{3}He,t)^{86}Y$ Reaction - C. A. Fields, F. W. N. de Boer, R. A. Emigh, J. J. Kraushaar, R. A. Ristinen, and E. Sugarbaker

A study of the $^{86}Sr(^{3}He,t)^{86}Y$ reaction has been undertaken in order to establish the locations of the $\pi(p_{1/2})\nu(g_{9/2})^{-3}$ and $\pi(g_{9/2})\nu(g_{9/2})^{-3}$ multiplets in this nucleus. This work complements previous studies of the ($^{3}He,t$) reaction of ^{88}Sr (ref. 1), ^{90}Zr (ref. 2-4), and ^{92}Mo (ref. 5). Furthermore, the direct reaction provides level locations which are useful in the analysis of γ-ray spectroscopic results on ^{86}Y (presented elsewhere in this report).

A 30 $\mu g/cm^2$ thick ^{86}Sr target was bombarded by 42.8 MeV ^{3}He ions from the cyclotron. The outgoing tritons were momentum-analyzed with the magnetic spectrometer and detected in a helical-cathode proportional counter. The overall energy resolution of the system was about 40 keV FWHM.

Angular distributions were obtained between 7.5° and 40° for all states below 1.3 MeV. Above 1.3 MeV the density of populated states increases very quickly, and only a few states could be resolved.

Tentative J assignments can be made to several of the observed states of ^{86}Y by comparing their ($^{3}He,t$) angular distributions to those of known[4] states of ^{90}Nb. Fig. A1-d3 shows a preliminary level scheme for ^{86}Y obtained in this way along with the known[6] states of ^{86}Y.

Distorted-wave Born approximation calculations for this reaction are in progress. Shell model calculations for the expected particle-hole multiplets will also be carried out.

---

1 J. R. Comfort et al, Phys. Rev. C4, 803 (1971).
2 R. C. Bearse et al, Phys. Rev. Lett. 23, 864 (1969).
3 S. I. Hayakawa et al, Nucl. Phys. A139, 465 (1969).
4 C. A. Fields et al, CUNPL Report 845, 49 (1979).
5 S. I. Hayakawa et al, Nucl. Phys. A199, 560 (1973).
6 J. W. Tepel, Nucl. Data Sheets 25, 553 (1978).

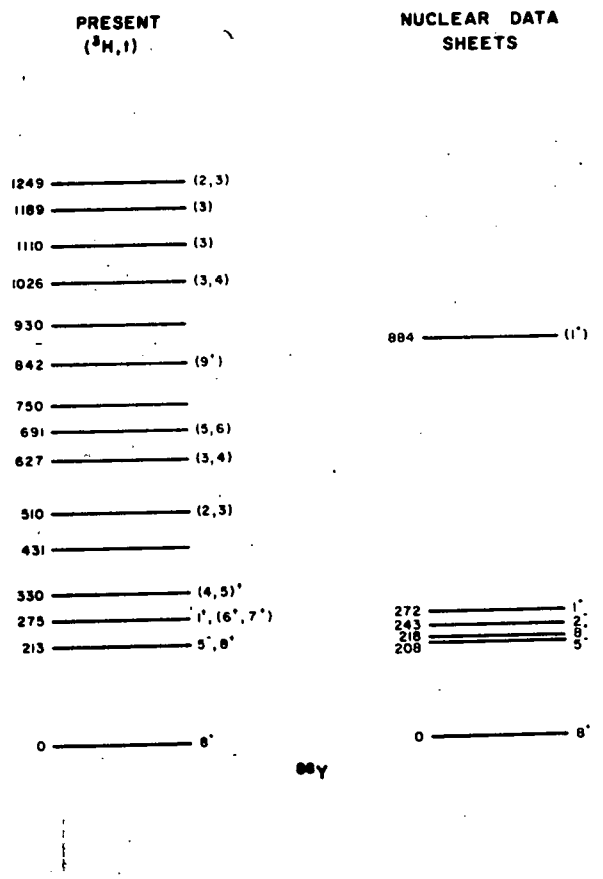

Fig. A1-d3. Levels of ^{86}Y observed in the 43 MeV $^{86}Sr(^{3}He,t)^{86}Y$ reaction compared with the previously known[6] level scheme for ^{86}Y. The J^{π} assignments based on the present work are tentative.

e. Elastic and Inelastic Scattering

i. A Survey of the Octupole States in Even-Even Nuclei and the ^{104}Pd(α,α') Reaction at 34.9 MeV. - R. Sinton, S. Dickey, J. J. Kraushaar, R. S. Raymond, M. Rumore, and R. Weiss.

An effort was made over the summer to find out what the current status of octupole states was beyond the 1970 survery of Bernstein. It became evident that even though a rather large number of inelastic studies had added to our knowledge of the positions and strengths of excitations (deformation parameter β_3, for example) there were a surprisingly large number of even-even nuclei that had never been investigated by inelastic scattering and hence there is no knowledge of the octupole states. The medium weight nuclei ^{54}Cr, ^{96}Ru, ^{98}Ru, ^{102}Pd, and ^{104}Pd fall into this category. A much larger number of nuclei need study as one goes higher in mass. It is the intention to continue the survey of octupole states in order to provide additional information on the systematics of octupole states and to bring forth nuclei that need studying to answer particular questions concerning the nature of the octupole mode.

Initially it appeared useful to obtain data on ^{102}Pd and ^{104}Pd since no data were available and these nuclei fall in a transitional region. Elastic and inelastic data at 34.9 MeV were taken on ^{104}Pd. A 1.60 mg/cm^2 thick target of 90% enriched ^{104}Pd was used. A single surface barrier silicon detector was employed with a solid angle of 0.35 msr. The resolution of 60 keV was sufficient to resolve the strongly excited 2^+ state at 0.556 MeV and the 3^- state at 2.19 MeV. The elastic angular distribution is shown in Fig. Al-d1 with a first attempt at an optical model fit. The cross sections for the excitation of the 2^+ and 3^- states are shown in Fig. Al-d2 where the solid lines are the usual collective-model DWBA calculation. The fits are reasonably good and the values of β_2 and β_3, also shown in Fig. Al-d2, were extracted. The energies of the lowest 3^- states are shown in Fig. Al-d3 in the mass region of 90 to 120. The new ^{104}Pb value continues the rather smooth increase in excitation energy as the number of neutrons decreases toward the magic number of 50. The deformation lengths, βR, shown in Fig. Al-d4 show a less easily interpreted pattern for the various isotopes in the mass region. The value of βR for the present experiment on ^{104}Pd (0.76), for example, is less than the value for ^{106}Pd.

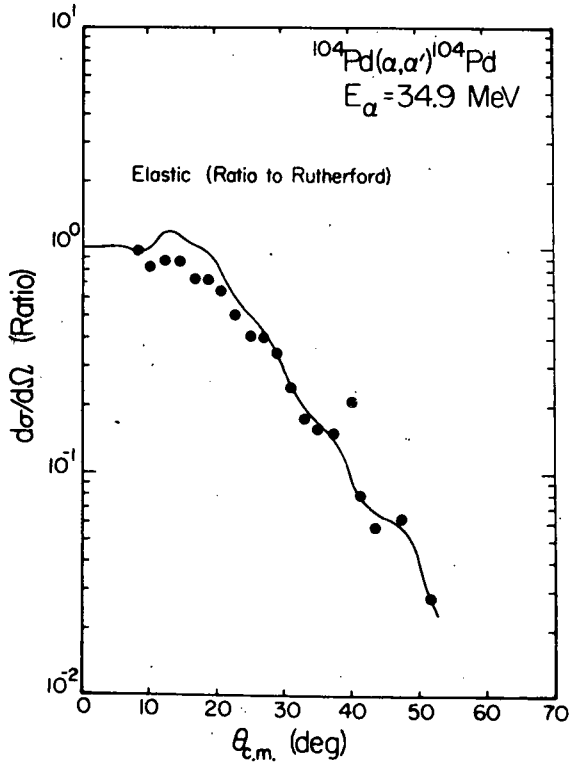

Fig. Al-d1. Elastic angular distribution for 34.9 MeV alphas on ^{104}Pd.

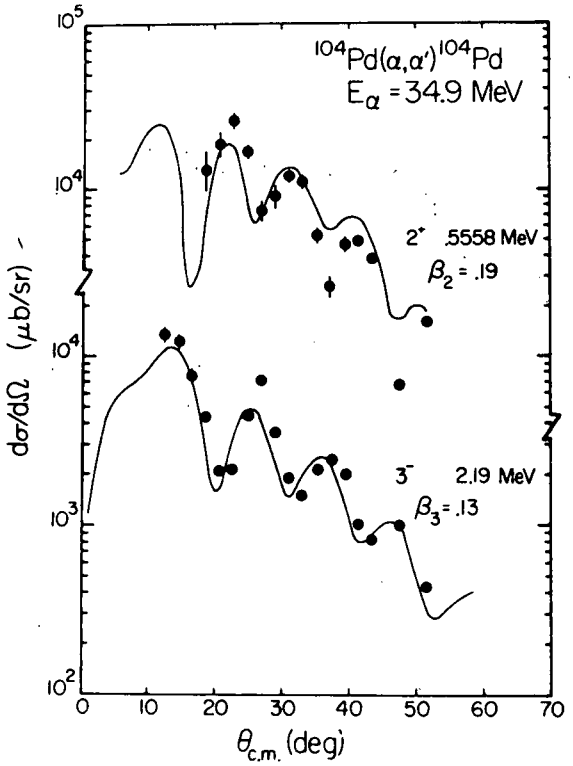

Fig. Al-d2. Inelastic cross section for the excitation of the 2^+ and 3^- states in ^{104}Pd. The solid lines are distorted wave calculations

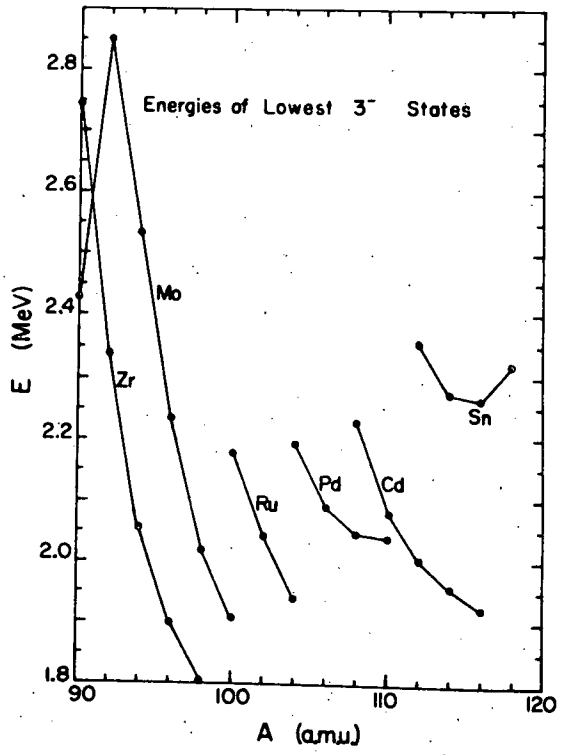

Fig. A1-d3. Energies of the lowest 3^- states for even-even nuclei in the mass region from 90 to 120.

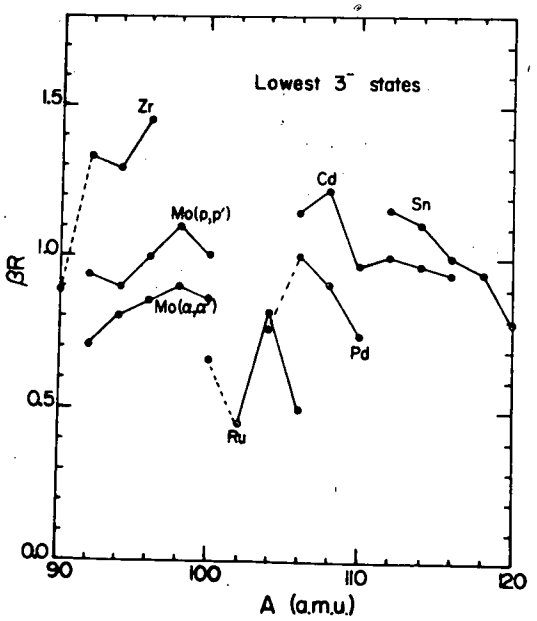

Fig. A1-d4. The deformation lengths for the excitation of the 3^- states shown in Fig. A1-c3.

ii. Alpha Scattering on ^{9}Be - D. Haynes, J. J. Hamill, and R. J. Peterson

Elastic and inelastic scattering of 35.5 MeV ^{4}He by ^{9}Be has been studied with a solid state detector out to 70 degrees (lab). The recoiling ^{9}Be ions were also detected, extending the elastic scattering data to 153° (c.m.).

The sample spectrum shown in Fig. Al-d5 shows the ground state band, with the 2.43 MeV $5/2^-$ and 6.76 MeV $7/2^-$ states. These and the elastic data will be analyzed within the strong coupling CCBA.

These data are the first for scattering to the positive parity band, 1.68 MeV $1/2^+$, 3.05 MeV $5/2^+$ and 4.70 MeV $3/2^+$ states. The broad 2.78 MeV $1/2^-$ state is very weakly excited, although an L=2 transition is allowed.

Sharp states at high excitations are also seen, and the (α,t) and $(\alpha,{}^{3}He)$ states will provide an excellent calibration, but this is not yet complete. These isoscalar excitations in ^{9}Be will be compared to ^{3}He and pion data for the extraction of isovector to isoscalar nuclear matrix elements, as described for A=13 elsewhere in this report.

Fig. Al-d6 shows the angular distributions for the $1/2^+$ and $5/2^+$ levels. Characteristic $\Delta L=1$ and $\Delta L=3$ shapes are found, but the DWBA predictions shown fit very poorly. Several sets of optical model parameters gave equivalent shapes and magnitudes, with $\beta_1=0.10$ for the 1.68 MeV $1/2^+$ state and $\beta_3=0.25$ for the 3.05 MeV $5/2^+$ state. No sign of a $\Delta L=1$ contribution is found for the $5/2^+$ state, although this is allowed.

This weak $\Delta L=1$ transition is consistent with the Nilsson scheme. The $3/2^-$ ground state is due to the [101] orbital, and the $1/2^+$ ($K=1/2^+$) band head is from the [220] orbital. These orbitals are near one another for large positive deformations. For such deformations the N_Ω quantum number is very good, with no oscillator quanta aligned with the symmetry axis for the ground state and two for the $K=1/2^+$ band. A change of two oscillator quanta cannot proceed by a transfer of only $\Delta L=1$, but can for $\Delta L=3$.

This reaction analysis will be continued.

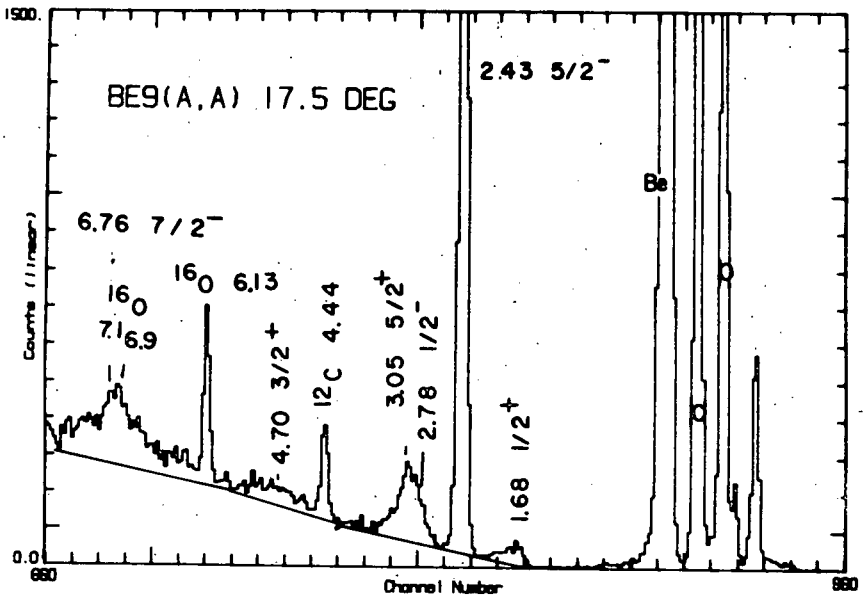

Fig. A1-d5. A sample spectrum of 35.5 MeV alpha scattering from ^{9}Be. The broad 6.76 MeV state lies beneath small sharp ^{16}O peaks. The 2.78 MeV $1/2^-$ state (Γ=1.08 MeV) is much weaker than the 3.05 MeV $5/2^+$ state (Γ=0.28 MeV).

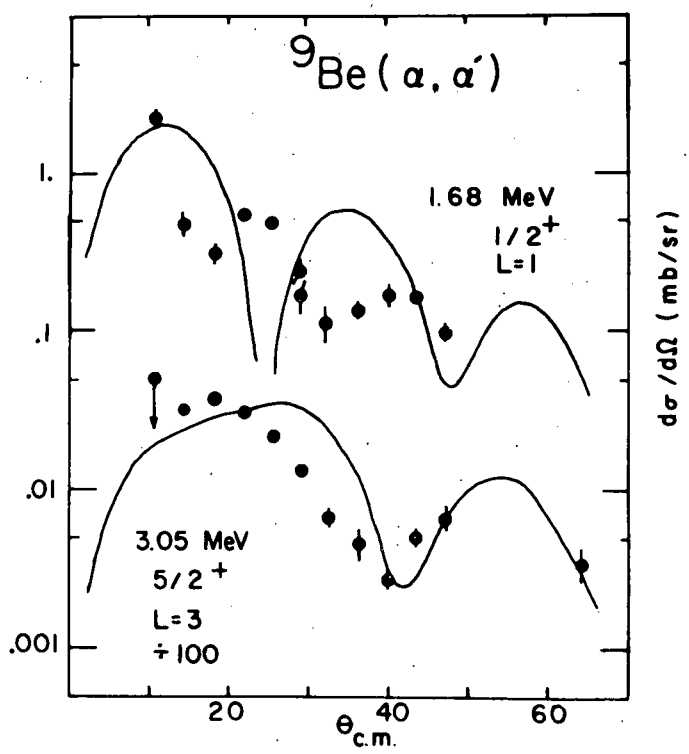

Fig. A1-d6. Data for the first two positive parity states of ^{9}Be are compared to DWBA predictions for collective excitations. Only $\Delta L=1$ can excite the $1/2^+$ state from the $3/2^-$ ground state, but both $\Delta L=1$ and 3 can populate the $5/2^-$ state.

iii. Isospin Mixing in ^{14}N near 9 MeV - R. J. Peterson

States of spins and isospins $2^-;0$ and $2^-;1$ are listed[1] at excitations of 9.129 MeV and 9.509 MeV. The $3^-;1$ level at 8.909 MeV may have a 3^- partner in the $2^-,3^-;0$ level at 9.386 MeV. The 8.909 and 9.509 MeV levels are more strongly excited by proton stripping on ^{13}C (see section A.1.a.i.) than the other two. If the states were anti-analog pairs, this would indicate appreciable isospin mixing. States of the same structure and T=0 or T=1 should be equally populated by proton stripping. Although the T=0 2^- and 3^- levels near 5 MeV are expected to be the anti-analogs of the T=1 states, there are nonetheless two extra T=0 states near 9 MeV, with small separations from the T=1 states.

Inelastic alpha scattering on ^{14}N can excite only T=0 states. Data were taken at an alpha energy of 35.5 MeV on a melamine target using a solid state detector at several angles. A sample spectrum is shown as Fig. A1-d7.

Overall strength limits on the T=1 states are $\leq$ 1/5 of the 9.386 MeV state for the 8.909 MeV state and $\leq$ 1/5 of the 9.129 MeV state for the 9.509 MeV state. If the 9.386 MeV level is taken to have a spin of 3^-, these limits and the observed energy splitting provide isospin-mixing matrix elements of < 195 keV for the 3^- and < 155 keV for the 2^- states.

Since the problem is largely one of energy resolution, this work will be repeated with the magnetic spectrograph.

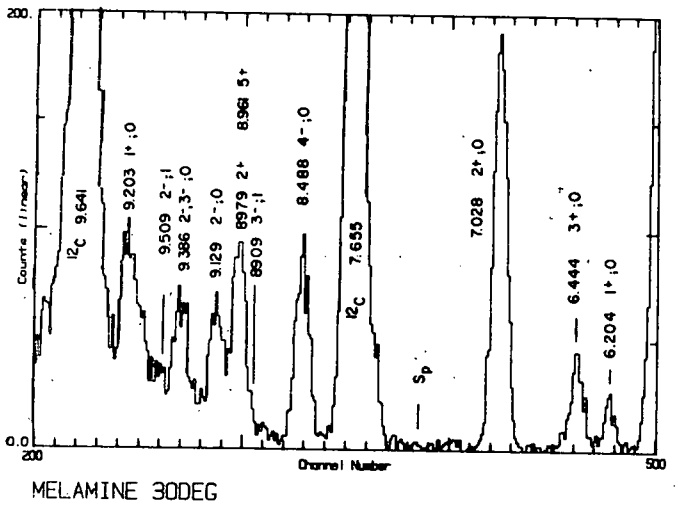

Fig. A1-d7. A sample spectrum of alpha scattering from melamine, using a Si detector. The T=1 states at 9.509 and 8.909 MeV are the subjects of this study of isospin mixing in ^{14}N.

[1] F. Ajzenberg-Selove, Nuclear Physics, to be published.

iv. Inelastic Alpha Particle Scattering on ^{10}B and ^{11}B -
E. F. Gibson, T. Herbert, J. J. Kraushaar,
T. G. Masterson, P. A. Smith, and C. Somps

In the analysis of the data from the π^+ scattering on ^{11}B and ^{12}C, corrections had to be made for the contributions of the first excited states of ^{10}B and ^{11}B to the elastic cross section of ^{11}B. It became evident that values for the deformation parameter (β) for the excited states of these two nuclei were either not available in the literature or serious discrepencies existed between the various quoted values. For this reason and because of an interest in the structure of these nuclei, inelastic alpha particle scattering measurements were carried out at 35.2 MeV. The measurements were made with a detector telescope that consisted of a 97 μ thick ΔE and a 5000 μ thick E surface barrier Si detector.

The enriched ^{10}B target was about 100 $\mu g/cm^2$ thick and was deposited onto a Au backing. The ^{11}B target, also enriched and about 100 $\mu g/cm^2$ thick was on a formvar backing. Spectra taken at 50° for the two targets are shown in Figs. Al-d8 and Al-d9. The presence of the contaminants complicated the analysis of the data especially at forward angles, but useful angular distributions are being extracted for most of the excited states.

For ^{10}B the states at 0.71, 2.15, 3.59, and 6.03 MeV were sufficiently resolved to extract useable cross section data. The elastic angular distribution was fit using the search code OPUCK with resulting parameters V_0 = 54.17 MeV, r_0 = 1.66 fm, a_0 = 0.708 fm, W = 14.01 MeV, r_i = 1.86 fm and a_i = 0.463 fm for the real and imaginary part of the potential, respectively. Collective-model distorted wave calculations were then carried out in order to obtain values of β_2 for the various states. The results are shown in Table Al-dI where the values of both β and βR are shown for the present experiment and two others. For the inelastic proton and alpha data R was taken as the radius of the real part of the potential while for ^3He the imaginary radius was used. There is a surprisingly large scatter in the various values of either β or βR for the three experiments. The present value of β (0.56 $\pm$ 0.07) falls between the 0.37 $\pm$ 0.04 and 0.67 $\pm$ 0.05 values for ^3He and proton scattering, respectively.

Considerably less information exists in the literature on inelastic scattering from ^{11}B. The present experiment is currently being analyzed and results for the low-lying collective states should be available soon.

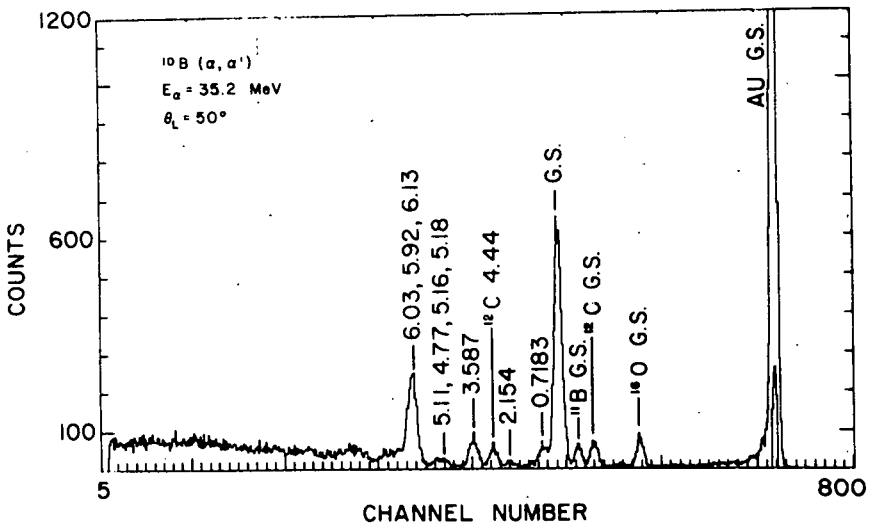

Fig. A1-d8. Inelastic alpha particle spectrum for ^{10}B at a scattering angle of 50° and an alpha energy of 35.2 MeV.

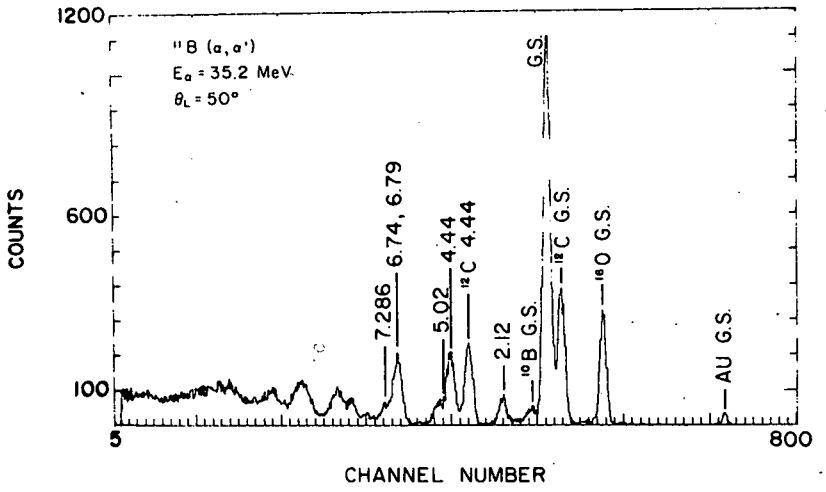

Fig. A1-d9. Inelastic alpha particle spectrum for ^{11}B at a scattering angle of 50° and an alpha energy of 35.2 MeV.

---

[1] G. T. A. Squier et al., Nucl. Phys. A119 (1968) 369.
[2] R. de Swinearski, F. G. Resmini, C. Glashausser, and A. D. Bacher, Helv. Phys. Acta 49 (1976) 227.

Table Al-dI. Deformation Parameters from Inelastic Scattering on ^{10}B

E_x (MeV)	J^π	T	L	$(^3He,^3He')^1$ r_0=1.32 fm β	R	βR	$(p,p')^2$ r_0=1.10 fm β	R	βR	$(^4He,^4He')$ r_0=1.66 fm β	R	βR
0.0	3^+		-	-	-	-	-	-	-	-	-	-
0.71	1^+		2	0.37 ± 0.04	2.85	1.05 ± 0.11	0.67 ± 0.05	2.37	1.59 ± 0.12	0.56 ± 0.07	3.58	2.00 ± 0.25
1.74	0^+	1	(3)	(0.69 ± 0.09	"	1.97 ± 0.26	-		-	-		-
2.15	1^+		2	0.36 ± 0.04	"	1.03 ± 0.11	0.49 ± 0.04	"	1.16 ± 0.10	0.32 ± 0.04	"	1.15 ± 0.14
3.59	2^+		2	0.36 ± 0.04	"	1.03 ± 0.11	0.45 ± 0.04	"	1.06 ± 0.09	0.35 ± 0.04	"	1.25 ± 0.14
4.77	3^+		-	-		-	-					
5.11	2^-		3	-			0.45 ± 0.04	"	1.07 ± 0.10			
5.17	2^+	1	2	-		-	-		-			
5.18	1^+		-	-		-	-		-			
5.92	2^+		2	-		-	0.28 ± 0.03	"	0.66 ± 0.07			
6.03	4^+		2	0.62 ± 0.03	"	1.77 ± 0.09	0.95 ± 0.04	"	2.25 ± 0.09	0.68 ± 0.06	"	2.43 ± 0.21
6.13	3^-		3	-		-	0.58 ± 0.03	"	1.37 ± 0.07			
6.57	2^-		3	-		-	0.59 ± 0.03	"	1.40 ± 0.07			
6.57	4^-		3	-		-	0.46 ± 0.04	"	1.09 ± 0.09			

f. Isoscalar and Isovector Transition Amplitudes in A=13 - R. J. Peterson, J. R. Shepard, R. A. Emigh; and D. Dehnhard (Univ. of Minn.)

Comparisons of positive and negative pion inelastic scattering on ^{13}C show clear enhancements of states of single neutron or single proton character.[1] When recast into an isospin representation, as described in last year's Progress Report, we may use isospin matrix elements reduced in the projections of the projectile to write, for scattering through formation of the 3-3 resonance,

$$\frac{d\sigma(\pi^-)}{d\sigma(\pi^+)} = \left|\frac{M_1 + 2M_0}{M_1 - 2M_0}\right|^2,$$

with isovector M_1 and isoscalar M_0 nuclear transition amplitudes. The same analysis for (^{3}He,t) and ^{3}He scattering gives for target states of isospin 1/2

$$\frac{d\sigma(^3He,t)}{d\sigma(^3He,^3He')} = 2\left|\frac{M_1}{M_1 - \sqrt{3}\, M_0}\right|^2,$$

and for ^{4}He scattering

$$\frac{d\sigma(^4He,^4He')}{d\sigma(^3He,^3He')} = 6\left|\frac{M_0}{M_1 - \sqrt{3}\, M_0}\right|^2,$$

while for mirror electromagnetic transition rates

$$\frac{B(EL)\ (^{13}N)}{B(EL)\ (^{13}C)} = \left|\frac{M_0 - M_1}{M_0 + M_1}\right|^2.$$

In principle the ratios of M_1/M_0 may be determined from any of these comparisons. Two electromagnetic lifetimes have been compared for ^{13}N and ^{13}C,[2] and we have measured the ^{3}He and ^{4}He scattering to many levels of ^{13}C and the (^{3}He,t) yields to their analogs in ^{13}N. This equips us for a large scale study of the validity of the simple isospin arguments.

The ^{3}He and ^{4}He scattering yields were compared by their deformations β extracted by comparison to DWBA predictions. These scatterings were measured at 43.5 MeV and 35.5 MeV, with very similar momenta. The ^{3}He scattering and charge exchange data were obtained simultaneously with silicon counters (with poor resolution and statistics) as well as

separately with the spectrometer. The equations assume perfect mirror symmetry, which is not true for ^{13}N and ^{13}C due to different binding energies.

Comparisons have been made for 14 transitions up to 16 MeV of excitation. Fig. (1) shows data for the lowest $1/2^+$ states. The ratio of these cross sections gives $M_1/M_0 = 0.31$ or -0.49, with the ambiguity due to the need to take the square root of the ratio of yields. These predict pion asymmetries of -0.46 or 0.31, with the measured value of 0.3 ± 0.1[1] clearly selecting one root.

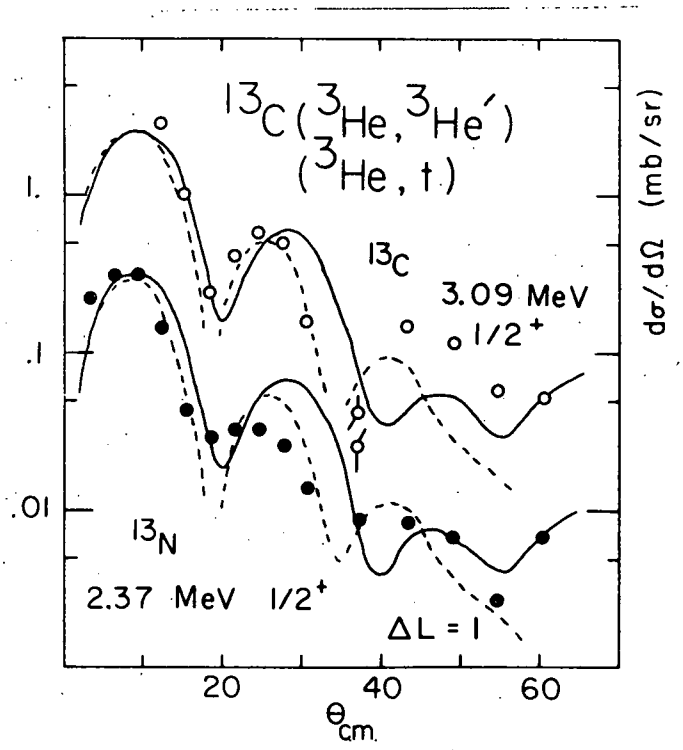

Fig. Al-f1. ^3He scattering data on ^{13}C shown as the open points are compared to solid points for charge exchange data to the analog in ^{13}N. The solid curves are DWBA collective predictions with $\Delta L=1$. The broken curves show microscopic DWBA predictions, including the differences in charge and binding energy for the two transitions. These changes have an effect of less than 5% on the comparison of the magnitudes.

The same ratio of matrix elements predicts ^4He scattering to be stronger than ^3He scattering by 1.21 or 2.96, where the latter choice agrees well with the observed 2.76. The predicted E1 reduced transition rates are in the ratios of 0.12 or 3.60, and are observed to be in the ratio 4.86 ± 0.70. In all cases, the same choice of sign is preferred. These results are all consistent, with four probes.

In general, the same agreement is found for higher states, and lack of agreement is noted only for unresolved doublets or for states exhibiting unusual ^{4}He angular dependences. In particular, data to the $9/2^+$ pure neutron transition are consistent with $M_0 = 0.73\ M_1$. A pure neutron transition has $M_0 = M_1$.

A comparison of the pion and ^{3}He data is shown in Fig. Al-f2, where the pion charge asymmetry is predicted, using the equations above, from the (^{3}He,t) to (^{3}He,^{3}He') ratio. Examples for several states are also shown.

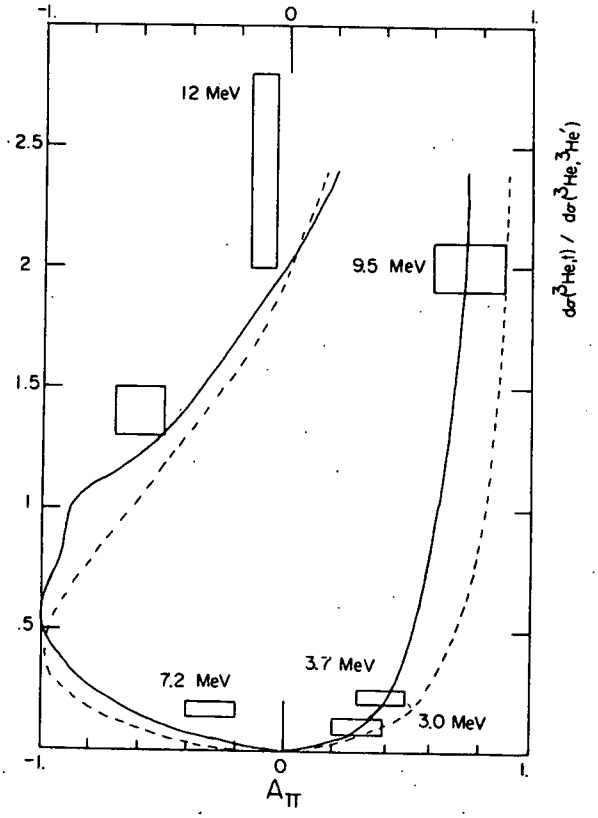

Fig. Al-f2. The equations in the text are used to relate the (^{3}He,t)/(^{3}He,^{3}He') ratio to the pion charge asymmetry, with the solid curve appropriate to 3-3 dominance. Several measurements are shown as the boxes.

This work shows that the relative importance of isovector and isoscalar strength in a T = 1/2 system can be obtained in several ways. This offers a powerful new tool for nuclear structure studies.

We have also compared (t,t'), (^{3}He,t), and (^{3}He,^{3}He') data on ^{13}C at 23 MeV, using the Los Alamos tandem. The preliminary analysis also finds consistency with the present work.

A major paper has been prepared on this work, and we intend to make the same comparisons for other T = 1/2 systems to check the present conclusion on the universal nature of the analysis and to extract isospin information on other nuclei.

---

1 D. Dehnhard et al., Phys. Rev. Lett. 43 (1979) 1091.
2 F. Ajzenberg-Selove, Nucl. Phys. A268 (1976) 1.

g. Compound Reaction Mechanism Studies - C. A. Fields, F. W. N. de Boer, R. A. Ristinen, P. A. Smith, and E. Sugarbaker

Last year a study of the spectra of neutrons emitted in $(\alpha,xn\gamma)$ and $(^3He,xn\gamma)$ reactions was initiated. Preliminary results of these investigations have been presented at meetings of the American Physical Society in Knoxville (Oct. 1979) and Washington (April 1980). A paper dealing with the use of neutron time-of-flight spectroscopy for identifying γ-rays with specific $(\alpha,xn\gamma)$ and $(^3He,xn\gamma)$ reactions has been published in Nuclear Instruments and Methods.

Neutron time-of-flight (TOF) spectra are measured with 5 cm x 20 cm (dia.) NE224 liquid scintillator detectors. These detectors are placed at 60 cm from the target. The neutron detection angle can be varied from 20° to 125° with respect to the beam. The 60 cm flight path gives an energy resolution of about 1 MeV at a neutron energy of 10 MeV. All measurements have been made on the cyclotron γ-ray beam line. Exclusive neutron spectra from specific α- and ^3He-induced reactions are obtained by measuring the neutron TOF spectra in coincidence with specific γ rays. The multiparameter coincidence data are written on tape in event mode and analyzed off-line.

In the past year we have acquired a new high-resolution γ-ray detector and a variety of additional fast electronic modules. Significant improvements in on-line multiparameter data acquisition have also been made. Together, these improvements have increased our ability to study compound reactions.

Exclusive neutron spectra from the $^{150}Nd(^3He,4n\gamma)$ reaction at three different beam energies are shown in Fig. Al-gl. A distinct change in spectrum shape with increasing beam energy is apparent. This kind of spectrum shape transition is also observed in α-particle induced reactions, and is due to the dominance of pre-equilibrium neutron emission in the early stages of compound reactions induced by high-energy projectiles. By measuring n-n coincidence spectra, we have found that in these pre-equilibrium reactions, the dominant mechanism involves the emission of one very energetic neutron followed by equilibration. The competing processes which involve the emission of several particles with moderately high energy are relatively unlikely.

We have developed a technique for the analysis of the γ-ray spectra coincident with specific groups of neutrons which allows the determination of the lowest spin value populated in the final nucleus by those neutron decays. In its most general form this technique is independent of knowledge of the γ-ray multiplicities de-exciting the entry states, and depends only on the assumption that the line describing the average entry-state population in U-J space (the "entry line") is roughly parallel to the yrast line. This assumption is based on consideration of the spin-dependent density of nuclear states and has recently been demonstrated to be correct by γ-ray multiplicity measurements.[1] Gamma-ray spectra are obtained in coincidence with neutrons of various energies E_n. For the reaction of interest a reference neutron energy E_0 and a reference gamma ray γ_0 are selected; E_0 is the lowest neutron energy for which the

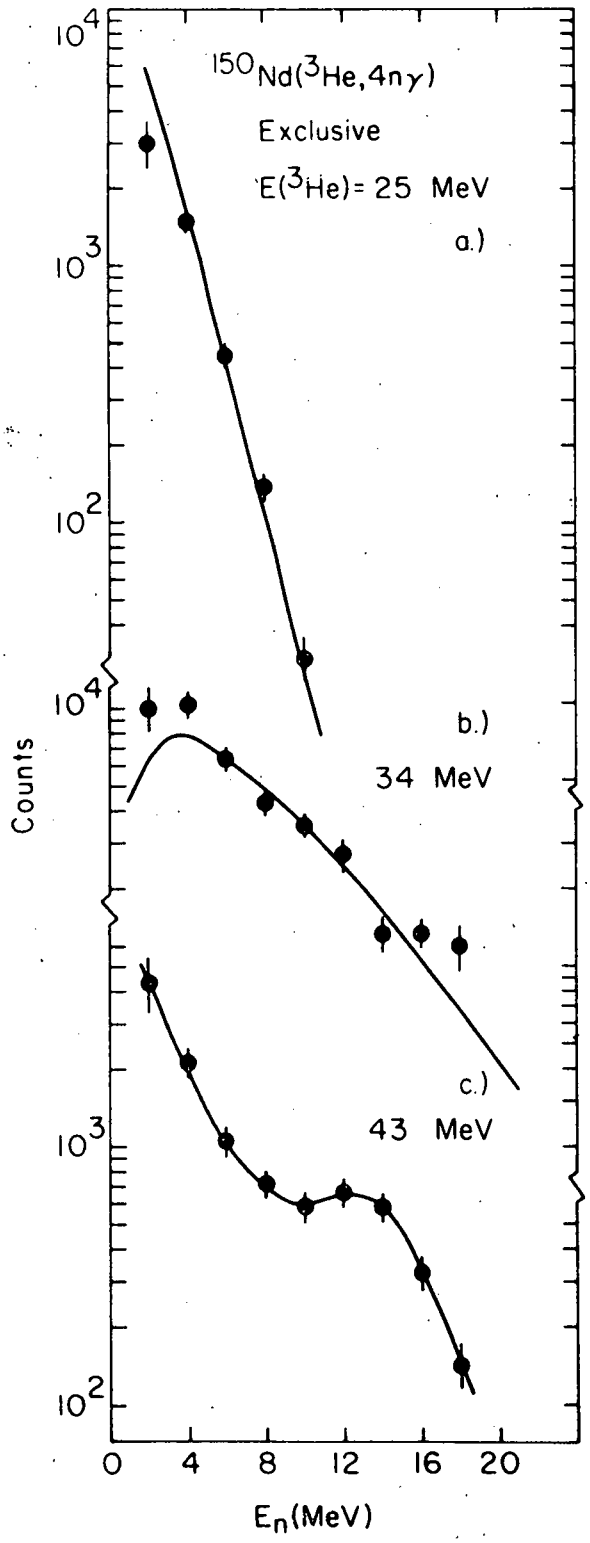

Fig. Al-g1. Exclusive neutron spectra from the ^{150}Nd(^{3}He,4nγ) reaction at E(^{3}He)=25,34, and 43 MeV. The change from equilibrium to pre-equilibrium behavior is apparent. The curves have no theoretical significance.

γ rays from the appropriate reaction are statistically significant and γ_0 is the lowest-lying statistically significant γ ray from that reaction. The intensities of the yrast-cascade γ rays with respect to that of γ_0 are obtained from the coincident gated spectra. The function:

$$R_\gamma = \frac{I_\gamma(E_n)}{I_{\gamma_0}(E_n)} \Big/ \frac{I_\gamma(E_0)}{I_{\gamma_0}(E_0)}$$

is then plotted with respect to gating neutron energy E_n.

Plots of R_γ versus E_n are shown along with the exclusive neutron energy spectra for $(\alpha,2n\gamma)$ reactions on several targets in Fig. Al-g2. As can be seen in the figure, the values of R_γ for γ rays depopulating high-spin states fall off steadily with increasing E_n in reactions (such as $^{120}Sn(\alpha,2n\gamma)$ at 35 MeV) for which the neutron spectrum is nearly Maxwellian.

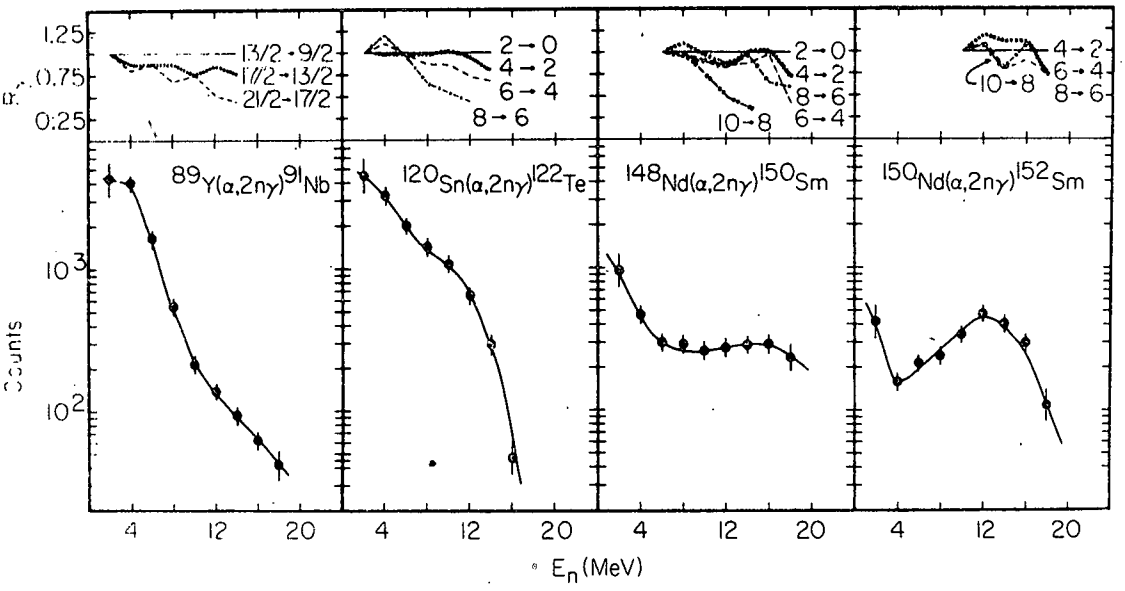

Fig. Al-g2. Plots of R_γ versus E_n and exclusive neutron spectra for 35 MeV $(\alpha,2n\gamma)$ reactions on ^{89}Y, ^{120}Sn, ^{148}Nd, and ^{150}Nd. The R_γ curves approach a constant value of unity as the neutron spectrum approaches an extreme pre-equilibrium shape (as in $^{150}Nd(\alpha,2n\gamma)$). The curves in the neutron spectra have no theoretical significance.

However in reactions such as the 35 MeV $^{150}Nd(\alpha,2n\gamma)$ reaction for which the neutron spectrum has a distintly pre-equilibrium shape, the R_γ curves are constant at unity for even the highest observed spins.

The highest yrast state spin for which the R_γ curve is flat at unity is the lowest yrast spin which is fed directly by the γ-decay of the entry states. Lower-spin yrast states are fed either by the yrast cascade or by side bands. This critical yrast spin provides a lower limit on the spin of the entry states.

If the average γ-ray multiplicity of the entry state to yrast line cascade is known, the minimum entry state spin can be deduced from the measured R_γ curves. With assumptions regarding the angular momentum removed from the compound nucleus by neutron decay, the range of angular momentum states of the initial compound nucleus which decay by any particular reaction channel can be deduced.

The total energy available for the decay of a compound nucleus is given by the initial compound nucleus (CN) excitation minus the binding energy difference between the CN and final nucleus ground states. This quantity Δgs is thus an upper limit on the energy of any single neutron involved in the decay. We have found that the neutron spectra for reactions with the same Δgs may have very different shapes. This indicates that the value of Δgs alone does not determine the point at which pre-equilibrium processes dominate a given reaction, although the spectra shown in Fig. A1-g1 prove that the beam energy (and hence Δgs) is one of the relevent parameters.

In order to understand more fully the transition from equilibrium to pre-equilibrium decay, we have measured exclusive neutron spectra from the $(\alpha,2n\gamma)$ and $(^3He,3n\gamma)$ reactions on a wide range of targets at several different beam energies. We have found that the transition from Maxwellian to non-Maxwellian spectrum shape occurs along a well-defined straight line if the data are plotted against Δgs and the neutron skin thickness t introduced by Myers and Swiatecki.[2] Such a plot for the $(\alpha,2n\gamma)$ reaction is given in Fig. A1-g3 with observed spectra indicated by crosses showing Δgs and the value of t for the target. The spectrum shape transition shown in Fig. A1-g1 occurs in the region between the two dashed lines in Fig. A1-g3.

Since the minimum entry-state spin increases as the pre-equilibrium processes become stronger, these pre-equilibrium processes must occur in the outer edge of the target nucleus. The systematic decrease in the beam energy (or Δgs) required to induce pre-equilibrium reactions as shown in Fig. A1-g3 suggests strongly that it is the excess neutrons in the outer region of the nucleus which are emitted in pre-equilibrium decay.

A similar systematic study of the $(p,2n\gamma)$ reaction is planned. The combined results of studies of proton-, ^3He-, and α-induced reactions should enable us to form a coherent phenomenology for light-ion induced, low-multiplicity pre-equilibrium neutron emission.

A scattering chamber is currently under construction which will allow the measurement of the spectra of charged particles emitted in compound reactions. The chamber will allow one or two detector telescopes to be placed at variable angles relative to the beam, and operated in coincidence with one or two Ge(Li) detectors and an arbitrary number of neutron

detectors. With this system we plan to make systematic measurements of proton spectra from the $(\alpha,pn\gamma)$, $(^3He,pn\gamma)$, and $(^3He,p2n\gamma)$ reactions in the coming year.

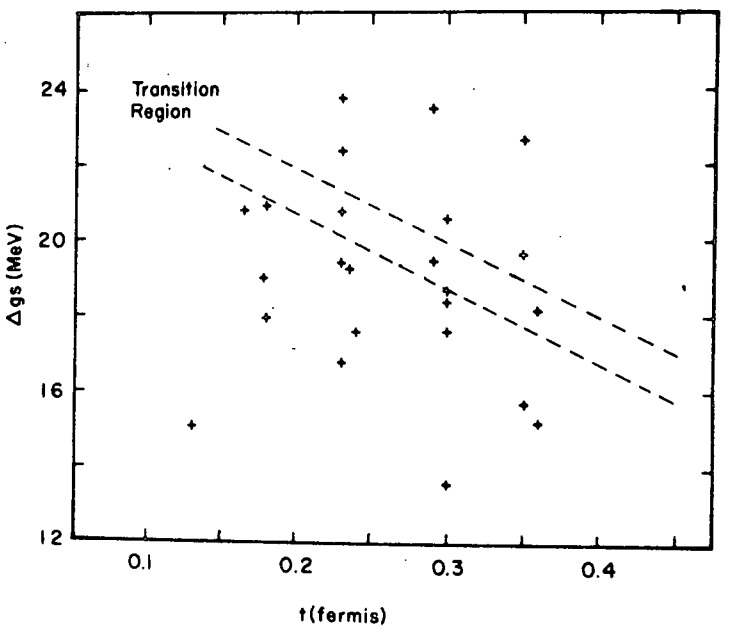

Fig. Al-g3. Crosses indicate the positions of observed exclusive $(\alpha,2n\gamma)$ spectra in the plane defined by the total energy available for neutron decay Δgs and the Myers-Swiatecki neutron skin thickness t of the target. The spectrum shape transition shown in Fig. Al-g1 occurs as the reaction moves from the lower left to the upper right in the figure. The region between the dashed lines in the figure corresponds to the shape of the 35 MeV $^{120}Sn(\alpha,2n\gamma)$ spectrum shown in Fig. Al-g2.

[1] M. J. A. de Voigt et al., Nucl. Phys. A323, (1977) 403.
[2] W. D. Myers and W. J. Swiatecki, Nucl. Phys. A336, (1980) 267.

2. Gamma Ray Studies

a. Gamma-Ray Spectroscopy in the A=90 Region - F. W. N. de Boer, B. Diana, C. A. Fields, J. J. Kraushaar, R. A. Ristinen, E. Sugarbaker, and P. M. Walker (Daresbury Lab., England)

Our investigations of the high-spin states of nuclei in the A=90 region by γ-ray spectroscopic methods are being continued. This study has two major objectives. The first is the identification of high-spin high-seniority states, the locations of which provide a strict test of the shell model. The second is the study of shape transitions and shape co-existence near the N=50 shell closure.

The use of n-γ coincidence methods for reaction identification, presented in last year's progress report, has proven quite worthwhile in this mass region. These techniques are especially helpful in identifying the gamma rays from reactions induced by high-energy ^{3}He ions. Our progress in γ-ray spectroscopy has also been aided by the acquisition of the computer code ALICE,[1] which calculates compound reaction cross-sections, and by the purchase of a new high-resolution GAMMA-X detector.

i. The Strontium Nuclei

The $^{A}Kr(\alpha,2n\gamma)^{A+2}Sr$ reactions have been studied at 28 MeV for A = 78, 80, 82, and 84. Singles, γ-γ coincidence, and γ-ray angular distribution measurements were made using enriched Kr gas targets. Preliminary results of this study were presented at the International Conference on Band Structure and Nuclear Dynamics in New Orleans, February 1980.

The ^{86}Sr nucleus is expected to be very nearly spherical. The low-lying levels in this nucleus which are populated by the β^{+} decay of the 8^{+} (218 keV) and 4^{-} (g.s.) states of ^{86}Y have been extensively studied. The major objective of the present investigation is the location of the high-spin states formed by the $v \geq 4$ interaction of protons in the $f_{5/2}$, $p_{3/2}$, $p_{1/2}$, and $g_{9/2}$ orbitals with the $g_{9/2}$ neutron holes.

As neutrons are removed from the N=50 shell, the Sr nuclei appear to move through a vibrational region (^{84},^{82}Sr) to a region of quadrupole deformation (^{80}Sr). Calculations will be performed using the Interacting Boson Approximation, which has proven successful in describing a similar shape transition in the Kr isotopes.[2]

ii. The Yttrium Nuclei

The results of our investigations of ^{89}Y and ^{87}Y were published this year. The analysis of the experimental results for ^{88}Y and ^{86}Y is still in progress. Several levels in ^{86}Y have been identified using the direct ^{86}Sr(^{3}He,t) reaction (discussed earlier in this report). These results will aid the construction of a level scheme for ^{86}Y.

iii. The Niobium Nuclei

The halflife of the new iosmeric state of ^{90}Nb reported last year has been found to be 0.44 ± 0.04 μs. All evidence suggests that this state has spin and parity 11$^-$. The decay scheme of this isomeric state is shown in Fig. A2-a1. A search for levels feeding this state by delayed γ-γ coincidence techniques is in progress.

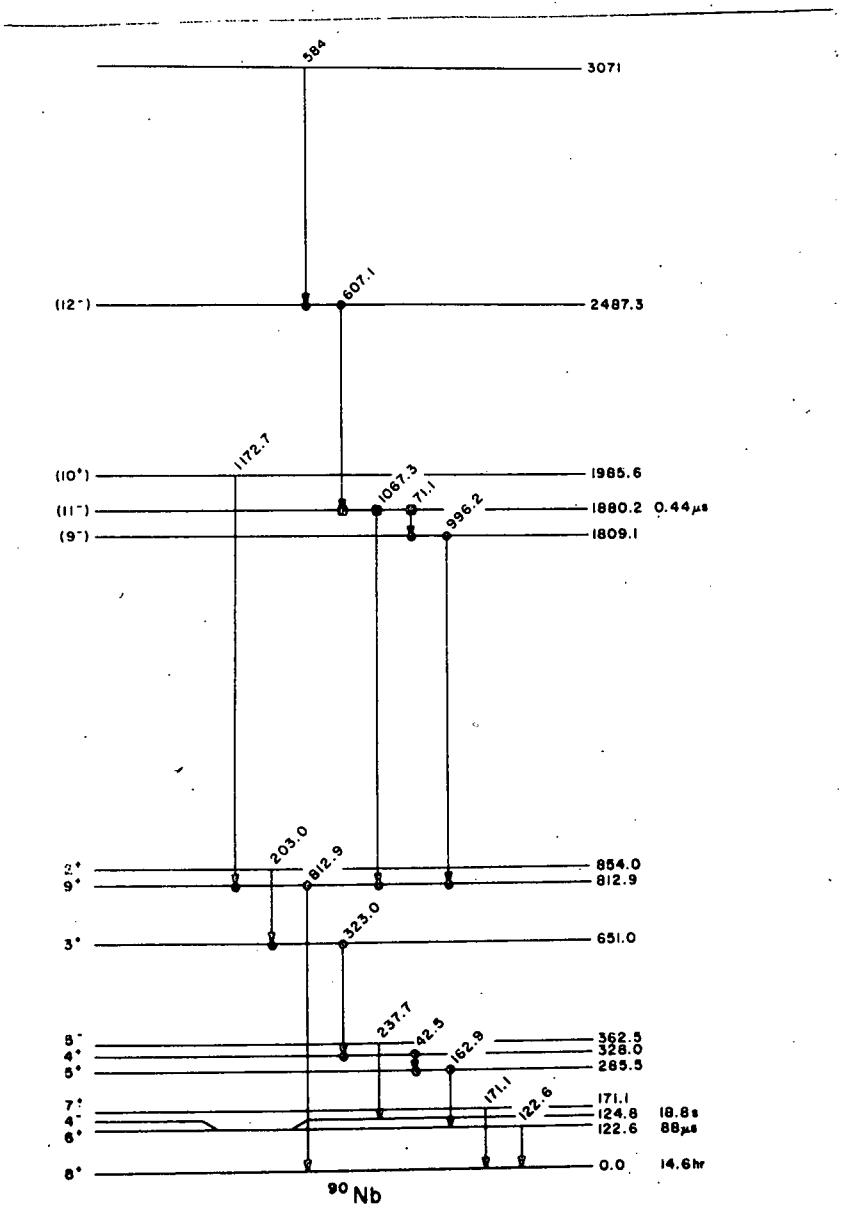

Fig. A2-a1. The decay scheme for the (11$^-$) isomeric ($T_{1/2}$ = 0.44 μsec) state in ^{90}Nb. Circles indicate prompt coincidences; squares indicate delayed coincidences.

An investigation of the high-spin structure of the N = 48 nucleus ^{89}Nb has been initiated. Measurements have been made using the 33 MeV ^{89}Y(^{3}He,3nγ) and the 43 MeV ^{90}Zr(^{3}He,p3nγ) reactions. The results for low-lying states are in agreement with the ^{89}Y(^{3}He,3nγ) results of Spalek et al.[3]

iv. The Molybdenum Nuclei

The study begun last year of ^{89,90}Mo is continuing. The assignments of γ rays to the ^{90}Zr(^{3}He,3nγ)^{90}Mo and ^{90}Zr(^{3}He,4nγ)^{89}Mo reactions were checked using coincident neutron time-of-flight techniques. The transitions feeding the 2875 keV 8^+ isomeric state of ^{90}Mo have been investigated using delayed γ-γ coincidence techniques.

As noted in last year's report, the high-spin level scheme of ^{90}Mo is very similar to that of ^{88}Zr. The locations of states with $J \geq 10$ can be reproduced reasonably well by simple weak-coupling calculations which use the experimentally determined energies of the states consisting primarily of the $\nu(g_{9/2})^{-2}$ and $\pi(g_{9/2})^{2}$ configurations.

An article describing our work on ^{90}Mo is being submitted for publication. The analysis of the data on ^{89}Mo is still in progress.

v. Further Studies

An investigation of the ^{92}Mo(^{3}He,3nγ)^{92}Ru and ^{92}Mo(^{3}He,p2nγ)^{92}Tc reactions has recently been initiated. The ^{92}Ru nucleus is the heaviest N=48 nucleus which can be investigated with low-energy light ions, and the level structure of this nucleus is completely unknown. If this nucleus is spherical, the low-lying structure should be very similar to that of ^{86}Sr, ^{88}Zr, and ^{90}Mo. With eight $g_{9/2}$ particles (6 protons and 2 neutron holes) outside the ^{88}Sr core, however, this nucleus may be deformed. Its study therefore would provide more information about a possibly deformed region which surrounds the N=50 shell closure.

The low-lying states of ^{92}Tc are known from studies of the ^{92}Mo(^{3}He,t)^{92}Tc reaction.[4] Shell model calculations for this nucleus predict a structure similar to that of ^{90}Nb. The aim of the present investigation is to locate the high-spin states corresponding to those found in ^{90}Nb. (see sec. iii. of this report).

---

[1] M. Blann and F. Plasil, USAEC Report C3494-10 (1973); and M. Blann, private communication.
[2] U. Kaup and A. Gelberg, Z. Physik A293, 311 (1979).
[3] Spalek et al., Nucl. Phys. A280, 115 (1977).
[4] S. I. Hayakawa et al., Nucl. Phys. A199, 560 (1973).

b. The level structure of ^{64}Ge - F. W. N. de Boer, C. A. Fields, L. E. Samuelson, P. A. Smith, E. Sugarbaker (Univ. of Colorado), and D. Cline (Univ. of Rochester)

The level structure of the N=Z nucleus ^{64}Ge has been investigated with the ^{64}Zn(^{3}He,3nγ) and the ^{54}Fe(^{12}C,2nγ) reactions using the ^{3}He beam of the University of Colorado cyclotron and the ^{12}C beam of the University of Rochester MP Tandem van de Graaff. The theoretical interest in this nucleus and part of the experiments performed have been described in last year's Progress Report. The analysis of these experiments has been finished.

Four new measurements have been performed during the last year. The first two consisted of measuring the time-of-flight (TOF) of neutrons in coincidence with γ rays at 35 and 44 MeV ^{3}He bombarding energies. Coincidences were recorded event-by-event on magnetic tape. By gating on the higher energy neutrons, the 2n and 3n reaction channels are enhanced considerably with respect to reactions where charged particles (which are in general the hot particles) are also emitted. It should be noted that this method is mandatory for identification of the 3n reaction in this case since the (^{3}He,p2n) reaction leading to levels in ^{64}Ga is a factor 1000 times stronger. A description of this reaction identification method has recently been published.[1] An array of four neutron detectors was placed at a 60 cm distance from the target at 30° with respect to the beam direction and the Ge(Li) detector was placed at 5 cm at 90° to the beam direction. Both experiments took about 12 hours.

Finally, two triple coincidence experiments have recently been performed, simultaneously, in the same experimental setup at a ^{3}He bombarding energy of 44 MeV. Two Ge(Li) detectors were placed at 90° with respect to the beam at 5 cm from the target and opposite to each other. The same array of four neutron detectors was used as for the n-γ coincidences. In addition, a set of two neutron detectors was placed at back angles as close as possible to the target ($\pm$ 10 cm). Triple coincidences were recorded in event mode on magnetic tape between the two Ge(Li) detectors and any back angle neutron detector (n-γ-γ) or between the two sets of neutron detectors and either one of the Ge(Li) detectors (n-n-γ). The analysis of data from this experiment, which lasted about a week, is still in progress.

---

[1] C. A. Fields et al., Nucl. Instr. and Methods 169 (1980) 173.

c. The Tetraneutron Revisited - F. W. N. de Boer, E. Sugarbaker, C. A. Fields, C. S. Zaidins (Univ. of Colorado); J. J. van Ruyven, A. W. B. Kalshoven, and R.Vis (Free Univ. of Amsterdam)

The analysis of our experiments searching for tetraneutrons (^{4}n) in (^{3}He + Te) interactions (reported in last year's Progress Report) was finished this year. Tetraneutrons, if formed in neutron evaporation reactions, were supposed to be detected in thick tellurium targets by inducing ^{130}Te(^{4}n,2n)^{132}Te reactions. From the absence of γ rays from ^{132}Te decay, we can conclude that we have not found evidence for the existence of tetraneutrons. For the first time, however, we have determined an upper limit for the formation probability of a tetraneutron from four neutrons depending on its half-life ($\tau_{1/2}$). Recently several searches for bound neutral systems in interactions using protons at GeV[1,2] and even multi-GeV[3,4] bombarding energies have led to contradictory results. At these energies it is impossible to estimate the number of neutrons leading to tetraneutrons produced since fission and spallation processes will dominate neutron evaporation. Moreover, weak unexpected secondary processes might obscure possible results.

At our relatively low bombarding energies of 44 and 130 Mev, however, the number of neutrons produced can be calculated quite accurately using the evaporation code ALICE.[5] The cross section for the (^{4}n,2n) reaction was similarly calculated, and it was assumed that the ^{4}n energy spectrum is constant between 0.5 and 10 MeV. By combining the theoretically expected yield of ^{132}Te nuclei with the experimentally determined upper limit and with corrections applied for half-life and detector efficiency the following conclusions could be made:

The formation probability (F) of a tetraneutron per four neutrons is smaller than 1.5×10^{-7} if $\tau_{1/2}(^4n)$ is longer than 10^{-9} s. If $\tau_{1/2} < 10^{-9}$ s, the unknown quantities $\tau_{1/2}$ and F depend upon each other according to the relation $F\tau_{1/2} < 1.5 \times 10^{-16}$ s. The formation probability (F) is displayed versus $\tau_{1/2}$ in Fig. A2-c1. The experimental upper limits for the (^{3}He,^{4}n) cross section are 28 and 19 μb at 44 and 130 MeV bombarding energies, respectively. These limits are two orders of magnitude lower than a positive value reported in ref. 3.

The consistency of our experimental set-up and analysis was checked by comparing experimental and theoretical yields of ^{131}Te nuclei. Gamma rays belonging to 31 h ^{131}Te were always present in our spectra. The experimental yields were compared with theoretical yields of ^{131}Te presumably produced by the ^{130}Te(^{3}He,^{2}He) reactions. Cross sections were calculated with the code DWUCK. The agreement between experiment and theory (within a factor of 3), is quite satisfactory and supports the reliability of our upper limits on our ^{4}n formation. An article describing this study has been accepted by Nuclear Physics.

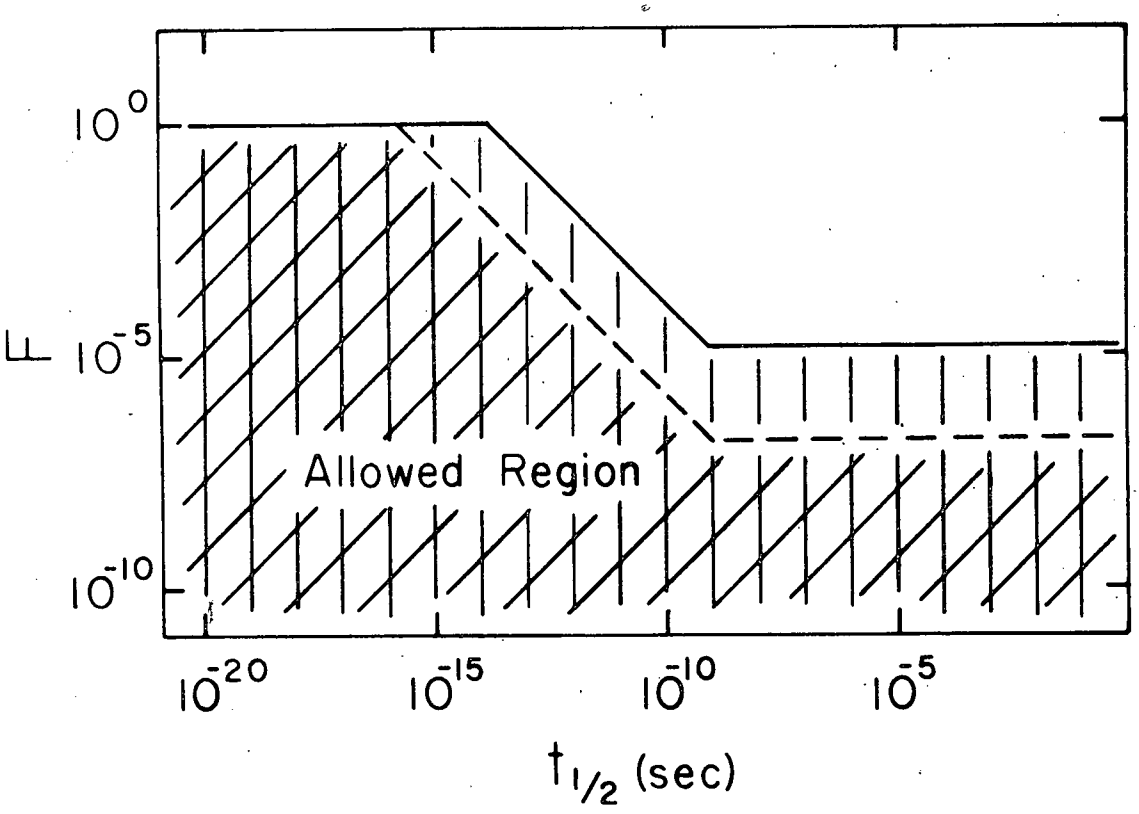

Fig. A2-c1. A plot of the formation probability of tetraneutrons F versus the half-life ($\tau_{1/2}$). A weight factor W(x) was introduced assuming that the chances of ^{4}n formation are higher than unity if more than 4 neutrons per reaction are produced. The vertical lines indicate the allowed region if the weight factor W(x) is taken as unity. The slanting lines indicate the allowed region if W(x) is taken as x!/4!(x-4)!.

[1] A. Turkevich et al., Phys. Rev. Lett. 38 (1977) 163.
[2] D. Chultem et al., Nucl. Phys. A316 (1978) 206.
[3] C. Detraz, Phys. Lett. 66B (1977) 333.
[4] A. Turkevich et al., Phys. Lett. 72B (1977) 163.
[5] M. Blann and F. Plasil, USAEC Report COO-3496-10 (1973).

d. Aligned Octupole Bands in Deformed Nuclei - F. W. N. de Boer, C. A. Fields, G. Marro, E. Sugarbaker (Univ. of Colorado); J. Konijn, H. Verheul (Free University, Amsterdam); and P. M. Walker (Mich. St. Univ.)

Our study of aligned octupole bands in rare earth nuclei and possible phase transitions to aligned two-quasiparticle bands has been continued in the past year. Constant aligned angular momenta ($I_\alpha < 3$) up to the highest spins observed were reported in last year's Progress Report for the negative parity yrast bands (NPB) in ^{152}Sm and ^{156}Dy. These parameters were derived from plots of the spins of GSB and NPB versus the rotational frequency $\hbar\omega$. Due to the constancy of I_α, remarkably good fits were obtained simultaneously for the GSB and NPB levels using the VMI formula with only four parameters. In ^{156}Gd (ref. 1) octupole bands were observed with 2^- and 3^- bandheads. From similar plots of I vs $\hbar\omega$, constant aligned angular momenta of 1.28 and 2.38 respectively were again found, leading to excellent VMI fits to the level energies of GSB and NPB (RMS values of 5.8 and 2.1 keV respectively). The low aligned angular momenta (< 2 or < 3) indicates that in these N = 90 and N = 92 nuclei the NPB's are aligned octupole bands and that transitions to the aligned two-quasiparticle situation do not occur below the highest spins observed (13^-).

Aligned octupole bands have previously been observed in ^{180}W and ^{238}U. The aligned angular momentum varies from 1.0 to 2.3 $\hbar$ in ^{180}W and between 1.7 and 2.3 $\hbar$ in ^{238}U. In the N=88 Sm, Gd, Dy, and Er nuclei, the N=94 and 96 Er nuclei, and the N=100 and 102 Pb, Hf, and W isotopes, values of I_α exceeding 3 $\hbar$ were observed. They are probably caused by a strong contribution of neutrons from the $i_{13/2}$ orbital which for N=82 to N=126 nuclei is the only positive-parity neutron orbital close to the Fermi surface. Bands which involve the $i_{13/2}$ neutrons are strongly aligned by the Coriolis force. This alignment tends to increase with increasing spin and generally exceeds 3 $\hbar$. Since the bands under consideration exhibit constant alignment, smaller than 3 $\hbar$, it is likely that two-quasineutrons do not play an important role in their structure. The aligned octupole bands in the rare earth region are thus probably due to a dominance of two-quasiproton configuration in the octupole structure.

In the actinide region, the $i_{13/2}$ proton orbitals are active. Two-quasiproton bands in this region can thus be expected to be strongly aligned by the Coriolis force. It is thus unlikely that the aligned octupole band observed in ^{238}U is a two-quasiproton band. Recent calculations by Ivanova et al.[2] indeed show that the main intrinsic component of the octupole phonon states in ^{238}U is the $j_{15/2}$ neutron orbital with $\Omega = 7/2$. Although the j value is large, the large value for Ω apparently reduces the Coriolis force such that no transition to particle alignment takes place.

The aligned octupole bands in the N=90 and N=92 nuclei are found to have a constant degree of alignment below the maximum value for a pure octupole phonon. This remarkable constancy of I_α is not well understood.

A letter on these aligned octupole bands has been accepted by Physics Letters.

---

[1] J. Konijn, F. W. N. de Boer, A. van Poelgeest, W. H. A. Hesselink, H. Verheul, and O. Scholten, to be published in Nucl. Phys.
[2] S. Ivanova, A. Komov, L. Malov, and V. Soloviev, Phys. Elem. Part. Al Nucl. JINR, Dubna 7 (1976) 450.

e. In-beam Gamma-ray Spectroscopy in the Rare Earth Region - F. W. N. de Boer, C. A. Fields, E. Sugarbaker (Univ. of Colorado); P. M. Walker (Mich. St. Univ. and Daresbury Laboratory); L. K. Peker (Brookhaven Nat. Laboratory), J. Konijn, and H. Verheul (Free Univ., Amsterdam)

The study of side bands in ^{152}Sm and ^{150}Sm with the ^{150}Nd(α,2nγ) and ^{148}Nd(α,2nγ) reactions, respectively, was continued during the last year. An additional study was started of the level structure of ^{162}Dy using the ^{160}Gd(α,2nγ) reaction. It should be noted that the (α,2n) reaction is often the only reaction with which it is possible to study side bands in neutron rich nuclei up to high spins. Heavy ion and more highly energetic alpha (> 40 MeV) reactions tend to populate mainly yrast positive and negative parity levels.

Singles γ-ray and γ-γ-t coincidence measurements were performed for all nuclei at 24 MeV at this laboratory. Angular distributions were measured for ^{162}Dy. A collaboration was started with J. Konijn and H. Verheul of the Physics Laboratory of the Free University on ^{152}Sm since it was realized that similar level structure studies had been undertaken at both laboratories. At the Free University, gamma-gamma coincidences, angular distributions, timing, and conversion electrons were measured for ^{152}Sm, using the ^{150}Nd(α,2nγ) reactions at 24 MeV.

The following results were obtained:

i. The level structure of ^{152}Sm

The study of the level structure of ^{152}Sm was recently completed. A wealth of new levels were identified and classified in rotational bands.

The following positive parity bands were firmly established: the ground state band (GSB) up to spin 14^+, the gamma-vibrational band up to 9^+, and the beta-vibrational band up to 14^+. A band built upon the "spherical" 0^+ (1082.8 keV) and 2^+ (1297.4 keV) states was tentatively identified up to 10^+. Due to the weak population of its band members, no E2 intraband transitions, which have to compete with M1's to the GSB, were observed.

A total of four negative parity bands were found. The lowest in excitation energy is an aligned octupole band built upon a 3^- bandhead at 1041.2 keV. Members of this band were found up to spin 13^- (see also section d). In a ^{152}Sm(d,d') reaction study,[1] 1^-,3^-, and 5^- levels were strongly excited at 1510, 1578, and 1764 keV. With a 2^- level at 1530 keV, these levels were interpreted by Grigoriev and Soloviev[2] as members of a K=1 octupole vibrational band. In the present study band members up to 14^- were found. A strong odd-even shift is exhibited in this band. Both odd and even spin members have large aligned angular momenta which exceed 3 and 2, respectively, around spin 6 ($I_\alpha \approx 4.3$). It seems apparent that around this spin value a transition occurs from octupole alignment to particle alignment. This is probably due to the presence of $i_{13/2}$ neutrons which tend to align strongly with the rotation of the core (see section d) in the intrinsic structure of these levels. The most probable two-neutron configuration is the $\{[660]\uparrow - [521]\uparrow\}$, which was shown by two-quasiparticle calculations to exist at low excitation energy in ^{152}Sm. This configuration can very well account for the irregular behaviour of the level energies. The odd levels mainly decay to members of the GSB, whereas the even spin ones show, besides intraband decay, decay to the gamma band. This can be explained by assuming K=0 admixtures in the odd levels and K=2 admixtures in the even levels, through $\Delta K=1$ interaction with nearby K=0 and K=2 levels. Direct $\Delta K=1$ E1 transitions to the GSB and to the gamma band are hindered by a factor of 100 with respect to $\Delta K=0$ E1's. Levels at 1803.9 (5^-), 1920.4 (6^-), 2057.3 (7^-), and 2214.6 (8^-) keV were found by Hirning and Burke[3] to be members of the 5^- $\{[413]\downarrow + [532]\uparrow\}$ two-quasiproton state. In the present work members of this band up to 12^- were identified.

A 7^- level, presumably the $\{[505]\uparrow + [651]\uparrow\}$ state, decays with delayed 63.7 and 200.6 keV M1 transitions to the 6^- and 7^- levels of the $K=5^-$ band. Hindrance factors with respect to the Weisskopf estimate are ≈ 400 which is quite normal for one time K forbidden M1 transitions. Members of the rotational band built upon the $K=7^-$ state were found up to 11^-. Through the strong population of the lower members of the 5^- band in the ^{183}Eu(τ,α) reaction[3], the $\{[413]\downarrow + [513]\uparrow\}$ configuration can be inferred as being the main component in their wavefunctions. However some mixing with lower K configurations has to exist in order to explain the decay to the GSB and the gamma band. At higher spin values mixing occurs with the $\{[660]\uparrow + [505]\uparrow\}_{6^-}$ two neutron configuration. This is reflected by strong M1 transitions between the ($I \rightarrow I-1$, $I > 9$) levels in the two bands.

---

[1] E. Veje, B. Elbek, B. Herskind, and M. C. Olesen, Nucl. Phys. A109 (1968) 668.

[2] E. P. Grigoriev and V. G. Soloviev, Structure of Even Deformed Nuclei, (Nauka Press, Moscow, 1974).

[3] C. R. Hirning and D. G. Burke, Can. J. Phys. 55 (1977) 1137.

ii. The level scheme of ^{150}Sm

Levels of the GSB of ^{150}Sm were reported by de Voigt et al.[1] up to spin 14^+ and members of the NPB up to spin 14^-. The low spin level scheme was thoroughly investigated by Becvar et al.[2] via ^{149}Sm(n,γ) reactions. In

that study the 0^+, 2^+, and 4^+ members of the beta band, 0^+, 2^+, and 4^+ members of a "deformed" band, and 2^+, 3^+, 4^+, and 5^+ members of the gamma-vibrational band were reported.

In the present work, the beta band was excited up to 10^+, the "deformed" band up to 12^+, and the gamma band up to 8^+. An additional (8^+) level (bandhead?) was found at 2089 keV. A strong odd-even shift is displayed in the gamma vibrational band.

The deformed band exhibits a very irregular behaviour in the level energies. The $8^+ \rightarrow 6^+$ spacing especially is very low (270 keV), compared to the $6^+ \rightarrow 4^+$ (424 keV) spacing. Mixing of the 6^+ and 8^+ levels with the nearby 6^+ and 8^+ levels of the gamma and beta bands, and of the 8^+ also with the 2089 keV 8^+ level may very well account for this irregular behaviour. The deformed band shows a regular but eccentric decay pattern. Its levels primarily decay to the I + 1 levels of the negative-parity band. The difference in deformation will inhibit decay to the ground state. Decay to the octupole shape can apparently compensate for the different deformation.

---

[1] M. J. A. de Voigt et al., Phys. Lett. 59B (1978) 137.
[2] F. Becvas, R. E. Chrien, and B. A. Watson, Nucl. Phys. A236 (1974) 173.

iii. The Level Structure of ^{162}Dy

The low spin level structure of ^{162}Dy has been extensively studied in beta decay and (n-γ) capture studies.[1] Levels of the ground state band were recently found up to 18^+ in a Coulomb excitation experiment.[2] A number of bands, proposed by ref. 1, could be extended to higher spin values in the present study, and some new bands are proposed.

Members of the ground state band were confirmed up to spin 16^+. Members of the gamma band were identified up to spin 13^+. A strong odd-even shift, typical for gamma vibrational bands due to ΔK=2 admixture with levels of the GSB and excited K=0 bands, is exhibited. Two aligned octupole bands with 2^- and 3^- bandheads were identified up to spin 12^- and 13^- respectively. The aligned angular momenta I_α[1] exceed the values 3 and 2 around spin 11 and 10 for the odd and even members, respectively. This indicates that around these spin values the character of these bands change from being collective octupole aligned to being particle aligned. In N=90 and 92 nuclei (see section d.) this transition does not take place up to the highest spin values observed. We argued that this is due to the dominance of two proton configurations in the octupole structure of the N=90 and N=92 nuclei. Conversely, the large aligned angular momenta (around spin 10) in ^{162}Dy is due to the presence of $i_{13/2}$ neutrons in the octupole structure. Indeed the strongest component in the $K=0^-$ octupole phonon projection was calculated[3] to be the $\{[642]\uparrow - [523]\downarrow\}_{0^-}$ 2-quasineutron configuration.

Recently it has become fashionable[4] to analyze rotational bands in terms of the Routhian $H' = H - \omega I_x$ instead of the Hamiltonian H of the system. The Routhian is the Hamiltonian in a frame of reference rotating with an angular frequency ω about the x-axis. Experimental energies are represented in the form of the experimental Routhian $E'(\omega)$ defined by $E'(\omega) = E(\omega) - \omega I_x(\omega)$. The ground-state band is normally taken as the frame of reference, so the members of this band have zero energy under the transformation. The following quantities are now introduced:

$$e'(\omega) = E'(\omega) - E'_g(\omega)$$
$$\text{and} \quad i(\omega) = I_x(\omega) - I^x_g(\omega)$$

The quantity $i(\omega)$ is equal to the aligned angular momentum I_α. The Routhians of the rotational bands near the yrast line have been compared with the low lying part of the theoretically calculated[4] two-quasiparticle spectrum of H' for the N=96 nucleus ^{164}Er. Since ^{162}Dy also has 96 neutrons it seems appropriate to apply the calculations and interpretations of ref. 4 to this nucleus.

The lowest odd parity configurations that can be constructed are those involving the [642]↑ and [523]↓ 2 neutron levels. Because of the invariance of a deformed nucleus with respect to a rotation of π about the intrinsic axis, each quasiparticle can be characterized by the signature quantum number α which can have the values $\pm 1/2$. On one quasiparticle two $\Delta I=2$ rotational bands can be constructed with $I = \alpha + 2n$. Since signature quantum numbers are additive the total signatures can be -1, 0, and 1. Four different configurations can be constructed for the [642]↑ and [523]↓ neutron levels, namely

a) [642 5/2:1/2][523 5/2:1/2] with α_t=1 (odd I)
b) [642 5/2:1/2][523 5/2:-1/2] with α_t=0 (even I)
c) [642 5/2:-1/2][523 5/2:1/2] with α_t=0 (even I)
d) [642 5/2:-1/2][523 5/2:-1/2] with α_t=-1 (odd I)

The first particle comes from the $i_{13/2}$ neutron orbit which tends, depending on the value of Ω, to align partially with the rotational axis and is therefore called rotationally aligned (RA). The second particle is strongly coupled to the deformation axis and is called deformation aligned (DA). Following the nomenclature of ref. 5, combinations of two such particles are called semi-aligned bands.

At low frequency, the largest K value of the $K = K_1 \pm K_2$ possibilities is the lowest in energy, the splitting energy being of the order $2K_1K_2/K$, with K being a good quantum number. At higher frequencies, there is a gain in energy from the Coriolis effect which mixes K on the first ($i_{13/2}$) particle over the K splitting energy. Since the difference in signature of the second particle only changes the energy of the system slightly, at higher frequency two different $\Delta I=1$ bands, (a+b) and (c+d), can be expected. These bands have the signature of the $i_{13/2}$ particle as real quantum number rather than K. The first band (a+b) was observed up to spin 24 ($\hbar\omega \simeq 0.35$ MeV) in ^{164}Er.[6]

In the present work a $K^\pi=5^-$ band was identified up to spin 13^-. The band head at 1486 keV was found to be mainly the $\{[523]\downarrow + [642]\uparrow\}_{5^-}$ configuration as it is fed in the allowed unhindered $\beta+$ decay from the $\{[523]\uparrow$

+ [642]↑$\}_{6^-}$ configuration. A ΔI=1 sequence similar to that in ^{164}Er is observed in this band, indicating that we are indeed dealing with a band of type (a+b).

From the α value of −0.49 ± 0.12 of the $8^- \rightarrow 7^-$, 124 keV transition, a g_K value for the band of −0.30 ± 0.33 could be derived, consistent with the value of ≈ 0 expected for the [523]↓ + [642]↑ two neutron configuration. The odd levels show decay to the GSB, whereas the even spin levels show mainly intraband decay. This is due to mixing of the odd spin levels with K=0 components of the octupole vibration which is, in the extreme, absent in the even spin levels.

The level spacing in this 5^- band is regular up to the 11^- level. The aligned angular momentum varies between 2.7 and 3.7 ħ, giving rise to an anomalously high apparent moment of inertia (see Fig. A2-e2). This is consistent with the semi-aligned character of the band. The small level spacings are caused by the $i_{13/2}$ particle, whereas the $h_{9/2}$ particle has to be considered as a spectator.

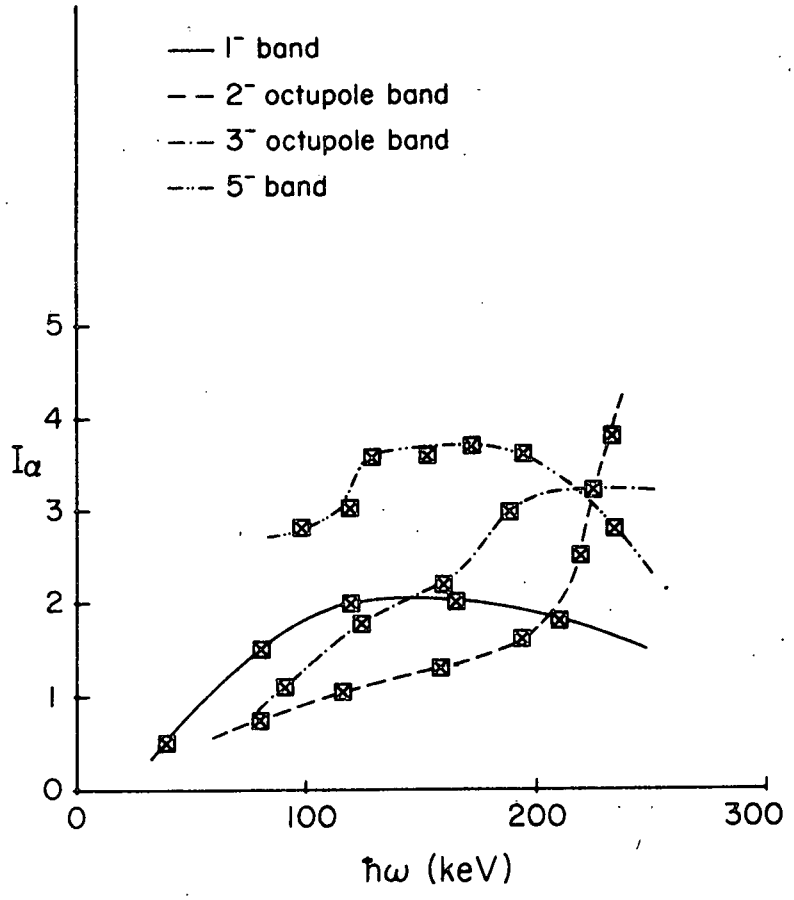

Fig. A2-e2. The aligned angular momentum I_α plotted versus the rotational frequency for the 2^- and 3^- octupole bands, the $K=1^-$ two-quasiproton band, and the $\{[523]\downarrow+[642]\uparrow\}_{5^-}$ two-quasineutron band with signature +1/2 for the [642]↑ particle.

The lowering of the 11^- level is explained by mixing with the nearby 2232 keV (11^-) state of the odd spin octupole/particle aligned band. Possible candidates for levels built upon combination a) were observed from 5^- to 11^-. Levels built upon the $\{[505]\uparrow + [642]\uparrow\}_{8^-}$ two-neutron configuration were predicted[4] and weakly observed in ^{164}Er. Possible candidates were now found in ^{162}Dy, together with members of the $\{[404]\downarrow + [523]\uparrow\}_{7^-}$ two-quasiproton band. A timing experiment is planned in order to search for the half-lives of the bandheads since K isomerism has to be expected.

A $\Delta I=2$ level sequence was identified up to 11^-, built upon a 1^- 1276.6 keV level. This is probably a band built upon the $\{[532]\downarrow-[411]\uparrow\}_{1^-}$ two-quasiproton configuration, since the aligned angular momentum never exceeds 2. It should be noted, however, that the categorization of the earlier discussed 2^- and 3^- bands as aligned octupole bands at $I \leq 11$ and the 1^- band as an aligned two-quasiproton band is a simplified picture. A considerable amount of mixing must exist between the levels of the 1^- and 3^- bands which are in turn reasonably mixed with the odd spin levels of the 5^- band.

---

[1] A. Buyrn, Nucl. Data Sheets 17 (1976) 1.
[2] M. W. Guidry et al., Phys. Rev. C 20 (1979) 1816.
[3] P. Vogel, private communication.
[4] R. Bergtsson and S. Fravendorf, Nucl. Phys. A327 (1979) 139.
[5] S. W. Yates et al., Phys. Rev. C 21 (1980) 2366.
[6] P. M. Walker et al., Nucl. Phys. A363 (1980) 45.

3. Other Activities

a. A Method for Determining the Isotopic Abundance of Lithium - T. Chenevert, R. A. Ristinen and W. R. Smythe

Recently the U.S. Geological Survey[1] expressed interest in the development of an accurate method of measuring the ratio of ^{7}Li to ^{6}Li in geological samples. Mass spectrometers, typically accurate for heavier elements, are known to have widely varying results when used to measure lithium isotopes due to fractionation occurring in the ion source. One method free of fractionation has been developed by a group at the Department of Terrestrial Magnetism.[2] It uses the deuteron induced reactions $^{6}Li(d,\alpha)^{4}He$ and $^{7}Li(d,\alpha)^{5}He(n)^{4}He$. The latter reaction, as a result of its three body final state, yields a continuum of alpha energies. This continuum is integrated and compared with the monoenergetic alpha peak of the ^{6}Li reaction to yield a $^{7}Li/^{6}Li$ ratio. Our approach involves comparison of two monoenergetic peaks. It employs alpha scattering from lithium and detection of the recoiling lithium nuclei.

By virtue of their low atomic mass, ^{6}Li and ^{7}Li recoiling from an alpha collision at 10° from the incident alpha direction acquire 94% and 91% of the alpha energy, respectively. For 31 MeV incident alphas a Si surface barrier detector need only be ≈ 160 μm thick to stop completely the ejected lithium nuclei.

A stacked pair of silicon detectors was used in coincidence, the first detector being 105 μm thick and the second 68μm thick. Recoiling nuclei and reaction products heavier than lithium stop in the relatively thick first detector and fail to produce a coincidence. Alpha particles and light reaction products which pass through both detectors generally produce small pulses and are easily eliminated by non-critical discriminator settings. Thus, this relatively simple arrangement provides very clean lithium energy spectra in spite of the very large elastic alpha particle flux. A typical spectrum obtained with this arrangement is shown in Fig. A3-1. The targets were prepared by evaporating ≈100 $\mu g/cm^2$ of LiF onto 50 $\mu g/cm^2$ carbon foils. It was reasoned that evaporation of the tightly bound LiF molecules of relatively large molecular weight (26) would be less likely to produce isotopic fractionation than would evaporation of metallic lithium. Isotopically pure ^{6}Li and ^{7}Li targets were also prepared by evaporation of metallic lithium. Observation of spectra from these targets verified that there is no cross contamination of the peaks used for analysis.

These preliminary results are very encouraging, indicating that a very good signal-to-noise ratio can be obtained. Future efforts will need to demonstrate that small variations in beam energy and detector angle do not significantly change the relative sensitivity to the two isotopes, that isotopic fractionation does not occur in the target preparation process, and that the method can be calibrated with sufficient precision.

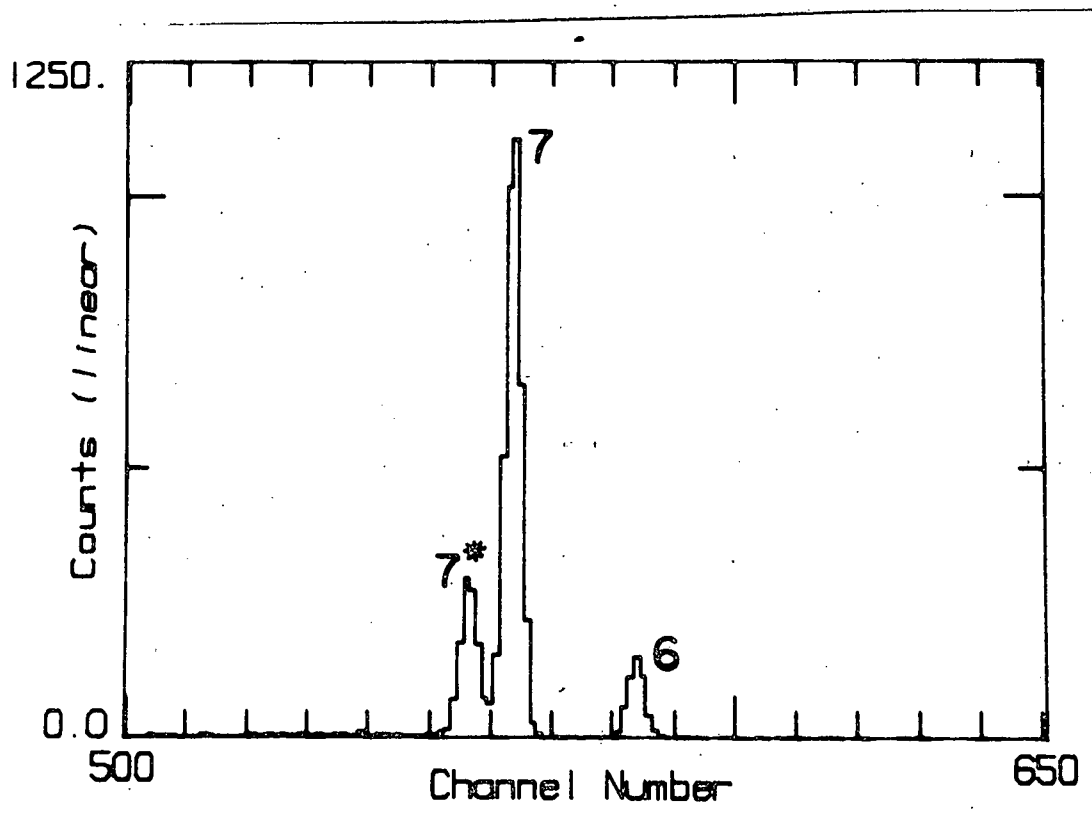

Fig. A3-1. Energy spectrum of recoiling lithium nuclei from natural lithium fluoride bombarded by 31 MeV alpha particles. The right hand peak is from the less abundant isotope, ^{6}Li, while the central peak is from ^{7}Li. The left hand peak is produced by inelastic scattering from ^{7}Li leaving the recoil in the 0.478 MeV excited state. Note that the peak from the less abundant (7.5%) isotope is conveniently on the high energy side of the ^{7}Li peaks, avoiding low energy tail problems.

---

1. J. R. Dooley and J. D. Vine, personal communication.
2. A New Method for Determining the Isotopic Composition of Lithium, L. Brown, R. S. Rajan, R. B. Roberts, F. Tera and D. J. Whitford, Nucl. Inst. and Meth. 156 (1978) 541-546.

b. Determination of the Fluorine Content of Oil Shale Samples from the Piceance Creek Basin - R. A. Ristinen, W. R. Smythe, and O. M. Saether and D. D. Runnells (Dept. of Geological Sciences)

Several years ago workers in this laboratory developed a method[1] for the determination of trace amounts of fluorine in various types of samples of environmental interest. This technique has now been applied to the analysis of density fractions of oil shale samples obtained by core drilling in the Piceance Creek Basin of northwestern Colorado. The individual density fractions were separated by density gradient centrifugation.

Because the mass of each density fraction was too small for standard wet-chemical analysis for fluorine, the sensitive analytical technique of nuclear inelastic scattering was employed. The samples, which weighed only 300 μg were irradiated by a beam of 5.9 MeV protons from the University of Colorado cyclotron. An approximately uniform flux of protons was obtained by diffusing the beam by small angle Coulomb scattering in a 2 mg/cm^2 aluminum foil located 35 cm upstream from the sample position. This uniform flux irradiated the entire sample, thus tolerating non-uniformity in the sample areal density and greatly simplifying sample preparation. The fluorine nuclei were excited by inelastic proton scattering to the first or second excited states at 100 keV or 197 keV. By detecting the de-excitation gamma rays and measuring their energies accurately with a hyper-pure germanium gamma-ray detector the presence of fluorine in the sample can be unambiguously determined. An example of the spectra obtained by this method with the detector located about 5 cm from the sample is presented in Fig. A3-2. An aluminum absorber 4 mm thick was placed between the sample and detector to reduce the high counting rate due to x-rays at the lower end of the energy spectrum. The method is made quantitative by use of calibration samples which we made from NaF for the fluorine mass range of 80 to 1280 ng and from CaF_2 for the range of 74 to 296 μg. This calibration curve is shown in Fig. A3-3 for the 110 keV gamma ray. The method was found to be linear, with no indication of a zero offset, over four orders of magnitude; this range includes the fluorine content of all samples considered in this work. The results for the 197 keV gamma ray are not shown in this figure because the analysis involving this gamma ray is not as straightforward as for the 110 keV gamma ray due to the much longer half-life of the 197 keV state. This is because the fluorine nuclei can be driven out of the sample by the proton collisions which produce the nuclear excitations. In the case of the much more prompt 110 keV transition, the gamma emission takes place before the target nucleus moves significantly from its original position, but for the longer-lived 197 keV state, the target nucleus may actually leave the field of view of the gamma ray detector before the gamma emission occurs. This effect will obviously reduce the number of 197 keV gamma rays reaching the detector. The probability of the recoiling nuclei in the 197 keV excited state escaping from the target before gamma emission depends on the sample mass. The recoiling excited nucleus will most probably be brought to a stop in a thick sample whereas a thinner sample will tend to allow it to

escape from the detector's field of view. Thus, for the 197 keV gamma ray, the probability of gamma-ray detection per nuclear interaction is a function of sample mass. In the case at hand, all sample masses were approximately 300 μg so a calibration appropriate to this sample mass was employed. The calibration for the 110 keV gamma ray is independent of sample mass.

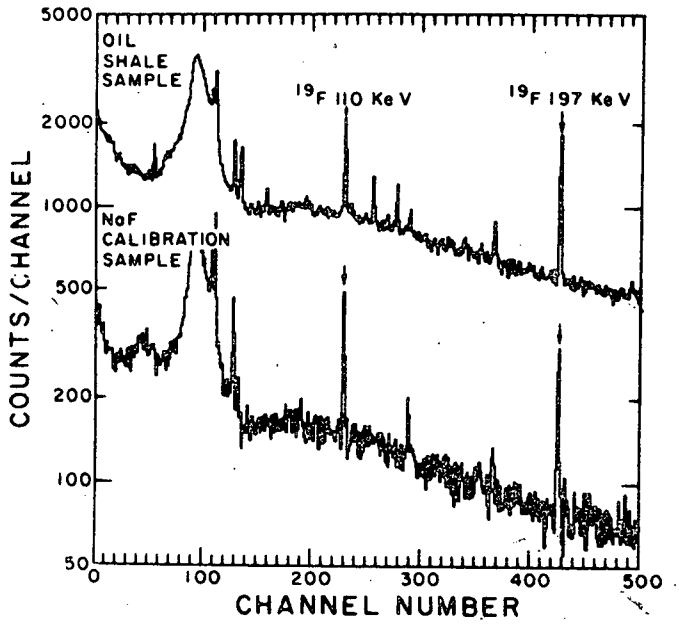

Fig. A3-2. Gamma-ray spectra obtained in the nuclear method of fluorine analysis. The lower spectrum was obtained from a calibration sample known to contain 640 ng of fluorine as sodium fluoride. The upper spectrum is from a typical oil shale sample. The running time for this sample was approximately five minutes at a proton beam current of 50 nA. The sample was found to contain 735 ng at a concentration of 2200 ppm by weight. The fluorine 110 keV and 197 keV peaks are labelled; the other peaks are due to elements other than fluorine in the sample and in the beam collimation apparatus. The counts near channel 100 are from x-rays produced by proton interactions in the sample.

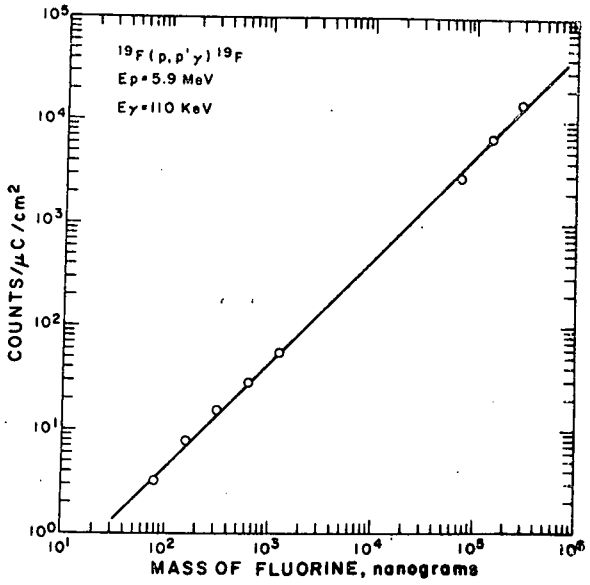

Fig. A3-3. Calibration and linearity check of the nuclear inelastic scattering method of measuring fluorine. The number of counts in the 110 keV gamma-ray peak per microcoulomb of proton beam per square centimeter at the target location is plotted as a function of the mass of fluorine in each calibration sample. The plot covers approximately four decades, from 80 ng to 296 μg. The straight line corresponds to the adopted calibration of 1.79×10^8 counts per microcoulomb per gram of fluorine.

It is interesting to compare the results obtained on bulk oil shale samples by this nuclear technique and by a new molecular absorption technique[2]. A comparison for six samples is shown in Fig. A3-4. The nuclear method was applied to 300 μg splits from the much larger samples analyzed by the chemical method. While the values obtained by the two methods are seen to be linearly related, the least squares straight line fit to these data displays a zero offset of 310 μg/g and a slope of 0.65, substantially different than the slope of 1.0 expected for a perfect correlation. The non-zero intercept may be due to the fact that the lowest fluorine values shown in Fig. A3-4 were near the limits of detection for the molecular absorption method. The calibration of the nuclear method shown in Fig. A3-3 indicates that the method yields results in strict proportion to the amount of fluorine present in the sample, and we therefore believe that the method of nuclear inelastic scattering is the more reliable method in this case. The method of molecular absorption requires a difficult step of wet digestion of the oil shale, and this step is avoided in the analysis by nuclear inelastic scattering.

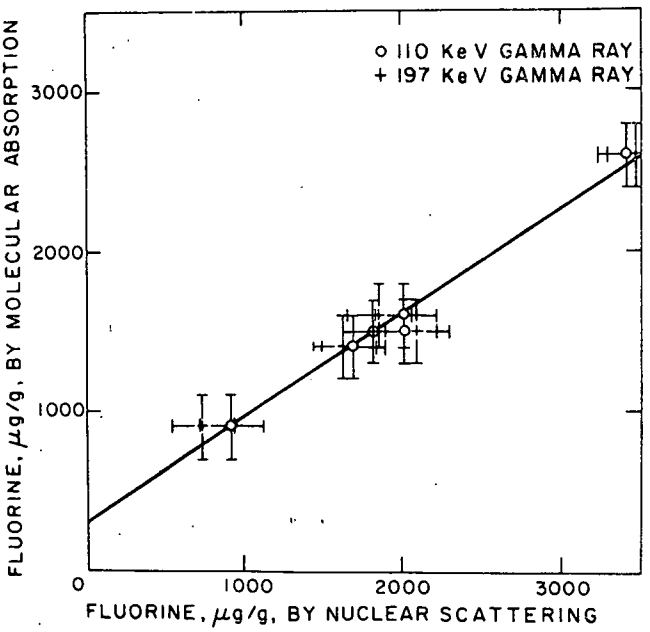

Fig. A3-4. A comparison of two methods of fluorine analysis: molecular absorption and nuclear inelastic scattering. Two values are shown for the nuclear analysis of each of the six samples, one obtained from the 110 keV gamma ray, the other from the 197 keV gamma ray. The split of the sample used for the nuclear method consisted of about 300 μg. The straight line, a linear least squares fit to the twelve data points, indicates that the two methods give results linearly related by y=310+0.65 x where y is the chemical and x the nuclear result, both in μg/g. The two sigma (95% confidence level) experimental uncertainty for each data point is estimated independently for each method as ±200 μg/g.

The results of these measurements indicate that the fluorine in oil shale is associated with the ubiquitous illitic clay minerals of the shale and that the shales which yield the highest amount of oil will leave residual waste shale with the highest concentrations of fluorine.

---

1. H. Rudolph, J. J. Kraushaar, R. A. Ristinen, and R. Meglen. Determination of Trace Elements of Fluorine by Nuclear Inelastic Scattering. Published in Trace substances in Environmental Health VII, D. D. Hemphill, Editor, University of Missouri, Columbia, MO, pp 313-321 (1974).
2. R. B. Meglen and A. Krikos. The Determination of Fluorine in Oil Shale Related Matrices using Graphite Furnace Molecular Absorption. Proceedings EPA Oil Shale Sampling Analysis and Quality Assurance Symposium, Denver, CO, March, 1979.

c. Thick Target Measurements of Thermonuclear Reaction Rates - C. S. Zaidins, R. J. Peterson, T. Intrator; N. A. Roughton (Regis College); C. J. Hansen, (JILA, Univ. of Colo.)

We have completed our program of measuring ^{4}He induced reactions at energies as high as 35 MeV and a paper to describe this work is in preparation. The analysis for previously measured yields has been completed and several new targets were measured in these experiments. The final list of reactions is shown in Table A3-I. Our analysis schemes were standardized once more and converted to the laboratory's new PDP-11/60 computer with a translation of the programs from BASIC to FORTRAN.

One experimental measurement of particular interest was on a boron nitride target. We were able to measure the $^{14}N(\alpha,\gamma)^{18}F$ and $^{14}N(\alpha,n)^{17}F$ rates which are of interest in processes other than explosive synthesis in supernovae. There has been much interest lately in variations of the isotopic abundance ratios of C, N, and O with galactic location. It is possible that an understanding of this problem will require the introduction of nuclear reactions not previously considered important in contributions to these sparse elemental abundances.

In addition to the techniques used previously, a new method to find a parametric fit to the temperature-dependent thermonuclear reaction rates has been developed. This analysis will not be included in the paper currently being written, but will be discussed elsewhere along with any systematics that we discover in the overall family of parametric fits.

The general development of the thick target yield data follows the discussion in the two previous annual progress reports and this particular phase of the astrophysical measurements is at an end. The experiment to measure the $^3He + ^4He \rightarrow ^7Be + \gamma$ reaction rate, which was discussed in last year's report, has been postponed for a year. The attempt to measure and understand the prompt γ-ray spectrum for the ^{4}He and ^{1}H bombardment of thick targets will be the first order of experimental priority in the coming year.

Table A3-I

^{4}He Induced Reactions Studied to Extract Thermonuclear Reaction Rates.

$^{10}B(\alpha,n)^{13}N$	$^{58}Ni(\alpha,p)^{61}Cu$
$^{14}N(\alpha,n)^{17}F$	$^{60}Ni(\alpha,n)^{63}Zn$
$^{14}N(\alpha,\gamma)^{18}F$	$^{62}Ni(\alpha,n)^{65}Zn$
$^{25}Mg(\alpha,p)^{28}Al$	$^{63}Cu(\alpha,n)^{66}Ga$
$^{26}Mg(\alpha,p)^{29}Al$	$^{65}Cu(\alpha,n)^{68}Ga$
$^{27}Al(\alpha,n)^{30}P$	$^{64}Zn(\alpha,n)^{67}Ge$
$^{40}Ca(\alpha,n)^{43}Sc$	$^{64}Zn(\alpha,p)^{67}Ge$
$^{46}Ti(\alpha,n)^{49}Cr$	$^{66}Zn(\alpha,n)^{69}Ge$
$^{48}Ti(\alpha,n)^{51}Cr$	$^{70}Zn(\alpha,p)^{73}Ga$
$^{49}Ti(\alpha,p)^{52}V$	$^{70}Ge(\alpha,n)^{73,73m}Se$
$^{50}Ti(\alpha,p)^{53}V$	$^{72}Ge(\alpha,n)^{75}Se$
$^{51}V(\alpha,n)^{54}Mn$	$^{73}Ge(\alpha,p)^{76}As$
$^{50}Cr(\alpha,n)^{53}Fe$	$^{74}Ge(\alpha,n)^{77m}Se$
$^{53}Cr(\alpha,p)^{56}Mn$	$^{76}Ge(\alpha,p)^{79}As$
$^{55}Mn(\alpha,n)^{58}Co$	$^{76}Ge(\alpha,n)^{79m}Se$
$^{54}Fe(\alpha,p)^{57}Co$	$^{92}Mo(\alpha,n)^{95}Ru$
$^{54}Fe(\alpha,n)^{57}Ni$	$^{94}Mo(\alpha,n)^{97}Ru$
$^{59}Co(\alpha,n)^{62}Cu$	

d. Proton Spectrum Analysis by Thick Target Radioactivation - T. Intrator, R. J. Peterson, C. S. Zaidins; N. A. Roughton (Regis College

Analysis of the data reported in the past two progress reports is complete. The numerical methods for fitting the yield from a brass thick target to a histogram representing the proton spectrum are complete and tested. Data were taken for protons degraded and broadened in energy by passing through a foil before stopping in a brass foil. The histogram obtained by our diagnostic method is in fair agreement with that predicted by energy straggling.

A Master's thesis has been written on this work and a publication is being prepared.

e. Mineral Analysis by X-Ray Fluorescence – W. R. Smythe, C. R. Stern (Geological Sciences), and C. A. Crouch

Previous efforts to analyze geological samples with the small sample x-ray fluorescence equipment developed in this laboratory have met with mixed success and disappointment. It now appears that the problem was a lack of homogeneity in the samples. In the process of examining some carefully selected samples, results which consistently agree with other measurements of the major constituents have been achieved. However, x-ray fluorescence also yields measurements of the trace elements.

The geological objects under study here are samples of the earth's mantle from a depth of 100 to 200 km below the earth's surface. These samples have been rapidly transported to the earth's surface by volcanic action, without melting. They were collected in the Pali-Aiki volcanic field in southern Chile. Small individual mineral crystals were removed from the sample under a microscope. Only crystals which appeared to be clean and pure under the microscope were analyzed. The samples were ground into a fine powder and prepared for x-ray fluorescence analysis using methods previously described. A typical x-ray spectrum is shown in Fig. A3-5, and the results of the analysis of that spectrum are presented in Table A3-II.

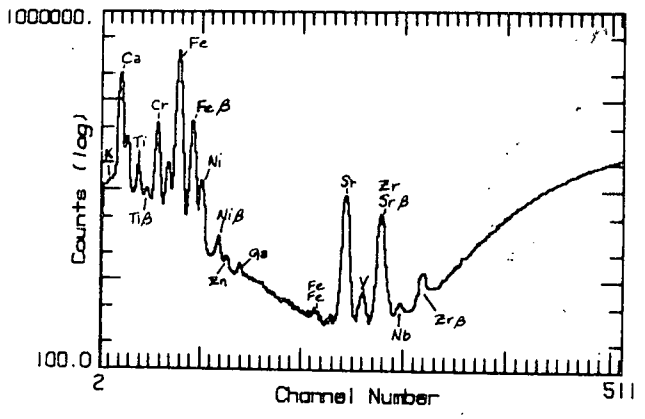

Fig. A3-5. X-ray fluorescence spectrum of a powdered 269 microgram sample of clinopyroxine. A filtered 55 kV x-ray beam was used to excite the sample, and a 5 mm thick Si(Li) detector was used to detect the x-rays.

It has been found by other methods that the major element composition of these mineral separates is very consistent from sample to sample. Because of the small size of the available crystal grains and the ability of the x-ray fluorescence system to achieve part-per-million sensitivity with these small samples, XRF does appear to be an ideal analytical tool for investigating trace elements in these minerals.

Table A3-II. Results of X-ray Fluorescence Analysis of Clinopyroxen

Element	Concentration By XRF (PPM)	Concentration (by other methods)
K	3810	
Ca	127000	13.5%
Ti	3410	0.39%
V	156	
Cr	6550	0.56%
Mn	702	0.07%
Fe	23200	2.4%
Ni	373	0.02%
Cu	8.0	
Zn	10.9	
Ga	9.8	
Sr	84	
Y	4.0	
Zr	32.9	
Nb	0.3	

f. Neutron Spectral Studies Using the Bonner Sphere System - C. S. Zaidins

The annual progress report for 1979 discussed the reasons for reactivating the Bonner Sphere Neutron Spectral System. The major achievements for the year in this project fall into two categories:

1) Improvement of the electronics system, and
2) Modification of the analysis programs.

Our original plans for the year included a collaborative effort with the University Radiation Safety Office to do a complete survey of the nuclear physics laboratory environs under different beam conditions. This has had to be postponed because of the major personnel changes that occured in the Health Physics department, but we plan to carry this out in the future.

There was a fairly straightforward change in the electronic modular equipment used on the Bonner Sphere system. The modified system was used for a project in the Health Physics courses offered by the Department of Physics. The system is now easier to set up reliably and it is easier to control the time used in counting each sphere flux measurement.

The modification in the program, NFLS, has made this data analysis program far easier to use also. The use of punched cards has been eliminated completely. There are choices of the energy bin regions and response spheres. At the moment there are only two choices, but with the modifications in the RIJ program it is considerably easier to generate new fit schemes. All input is now via the local terminals on the PDP-11/60 system and the format is easy to use. The output is recorded on the line printer.

Although we were unable to carry out the survey of the building or the Be target measurements this year, the system is now arranged to operate in a significantly simpler mode and these measurements and the associated analysis can be done with a minimum of equipment or computer problems.

B. Intermediate Energy Physics

1. Elastic and Inelastic π^+,π^- Scattering on ^{7}Li - E. F. Gibson (Sacremento State College); J. J. Kraushaar, T. G. Masterson, R. J. Peterson, R. S. Raymond, R. A. Ristinen; and R. L. Boudrie (Los Alamos Scientific Laboratory)

Under LAMPF proposal 391, data were taken in February 1980 on the ^{7}Li ($\pi\pm,\pi\pm$) reaction at 143 MeV using the EPICS facility. The angular range of 22° to 120° was covered with good statistics for the ground, 0.478, 4.630, and 6.68 MeV states and with usable data on the states at 7.456 and 9.67 MeV.

Two ^{7}Li targets were used; a thin target (90 mg/cm^2) for the small angles and a thicker (251 mg/cm^2) target for the larger angles. Cross sections for the elastic scattering of $\pi\pm$ on ^{2}H and ^{1}H were measured at a number of angles during the experiment as a means of normalizing the data. The ^{7}Li experiment followed directly the $\pi\pm$ ^{2}H experiment where careful proceedures for normalizing the data to $\pi\pm$ ^{1}H cross sections were worked out. This is discussed elsewhere in this Progress Report.

The magnetic tapes for the ^{7}Li experiment have all been played back with a 3 degree acceptance angle chosen in the reaction plane and cross sections obtained. Figure B1 shows a positive pion spectrum at a lab angle

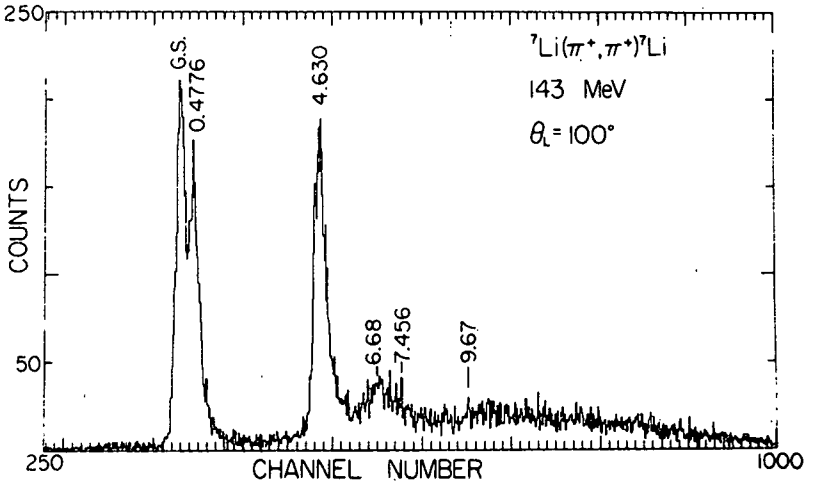

Fig. B1. Inelastic π^+ spectrum at a scattering angle of 100° and 143 MeV.

of 100°. The 0.478 MeV state can be seen to be clearly resolved from the ground state. The elastic angular distributions are shown in Figs. B2 and B3 for π^+ and π^-, respectively. The optical model codes in use such as DUMIT do not include contributions from the quadrupole interaction. Since the ground state of ^{7}Li has a spin of 3/2, it is necessary to correct the

elastic cross sections for the contribution for the quadrupole interaction. The nearby 0.478 MeV state would be expected to be excited primarily by the quadrupole interaction and calculations have shown that it

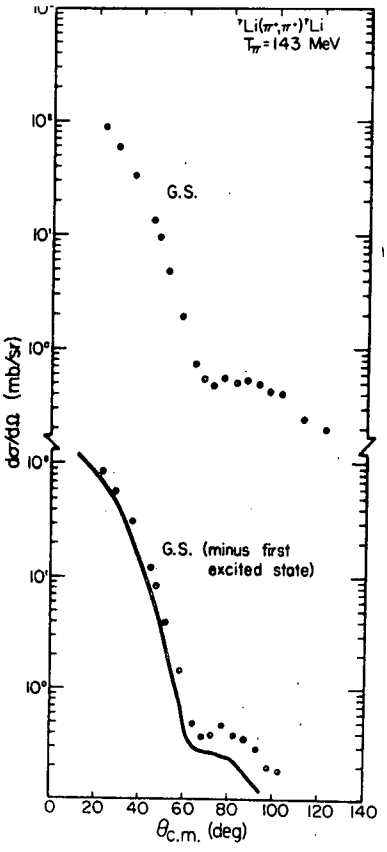

Fig. B2. The elastic angular distributions for π^+ scattered from ^{7}Li. The data in the lower part of the figure had the first excited state cross sections subtracted. The solid line is an optical model calculation as described in the text.

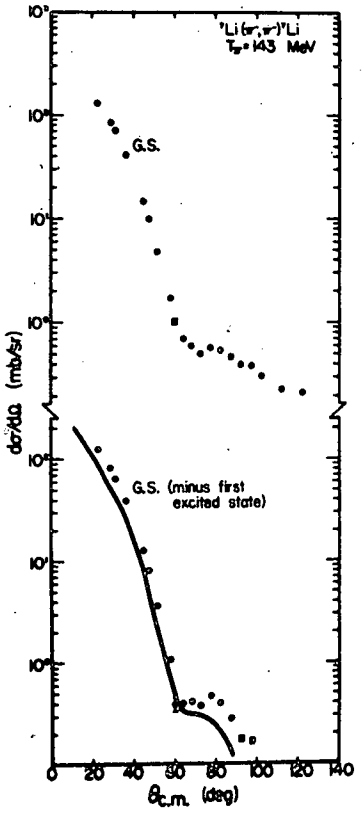

Fig. B3. The elastic angular distributions for π^- scattered from ^{7}Li. The data in the lower part of the figure had the first excited state cross sections subtracted. The solid line is an optical model calculation as described in the text.

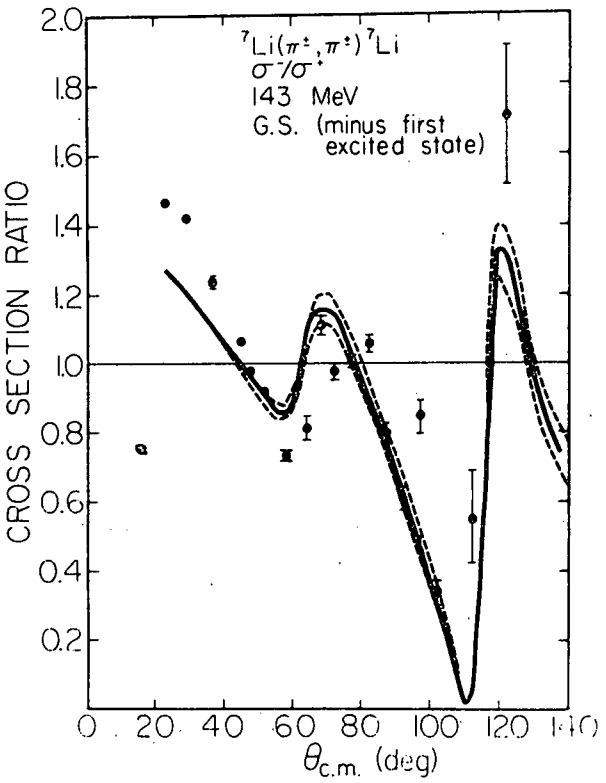

Fig. B4. The ratio of the cross sections for π^+ to π^- elastic scattering after the subtraction of the cross sections for the first excited state. The solid line represents the ratio of optical model calculations with a, the neutron radius, adjusted for a best fit.

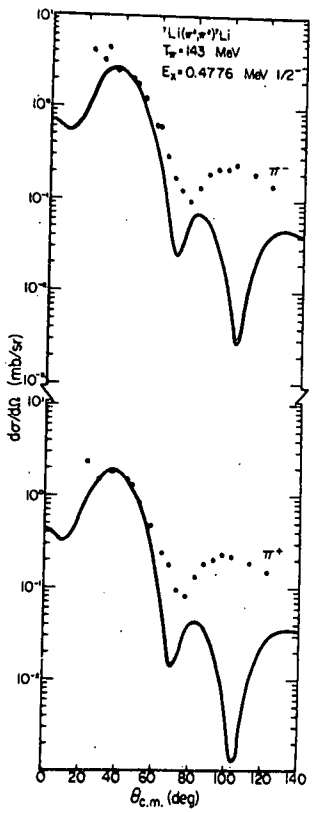

Fig. B5. Inelastic cross sections for the excitation of the 0.478 MeV state by 143 MeV π^- and π^+.

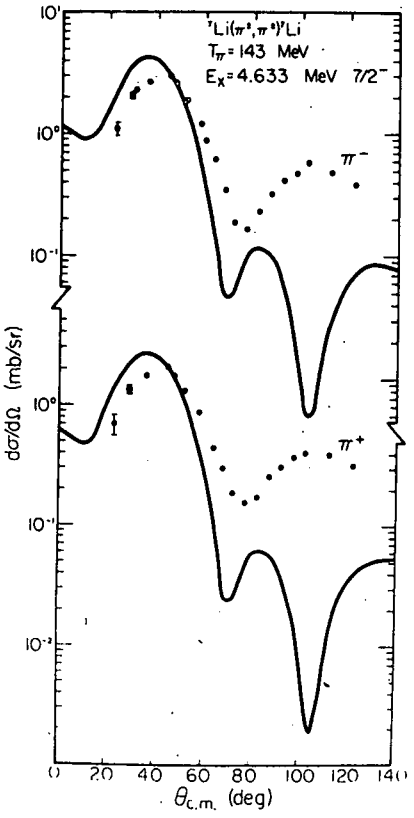

Fig. B6. Inelastic cross sections for the excitation of the 4.63 Mev state by 143 MeV π^- and π^+.

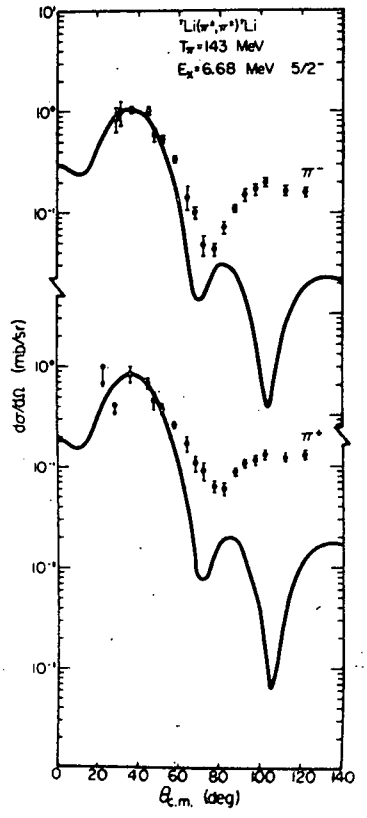

Fig. B7. Inelastic cross sections for the excitation of the 6.68 MeV state by 143 MeV π^- and π^+.

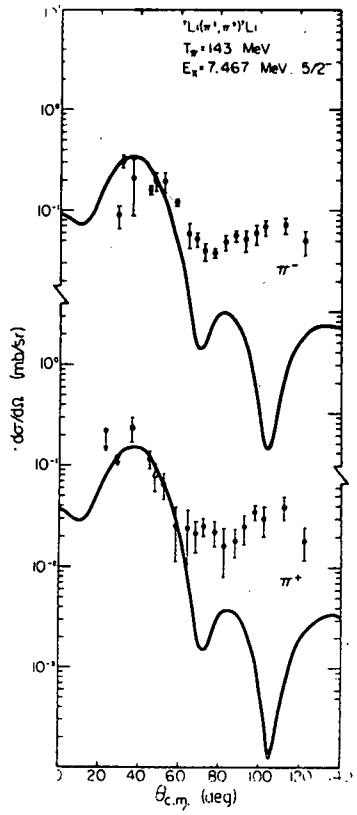

Fig. B8. Inelastic cross sections for the excitation of the 7.47 MeV state by 143 MeV π^- and π^+.

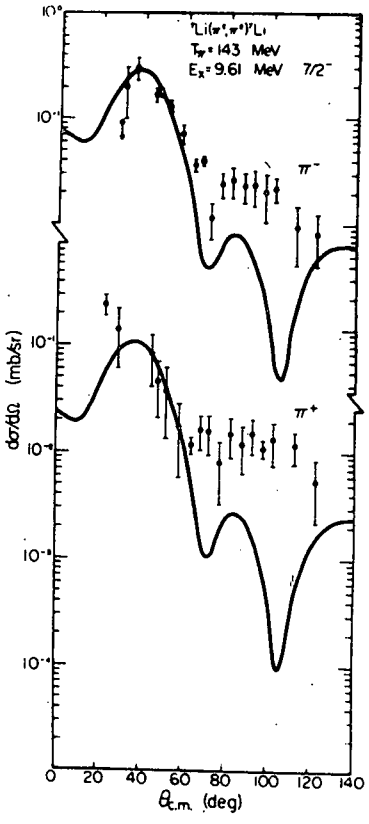

Fig. B9. Inelastic cross sections for the excitation of the 9.61 MeV state by 143 MeV π^- and π^+.

would be a reasonable approximation to use the cross section for the excitation of that state as a close estimate of the contribution of the quadrupole interaction. In the bottom half of Figs. B2 and B3 the elastic cross sections are shown with the cross section for the 0.478 MeV state (see Fig. B5) subtracted. A variety of optical model calculations were carried out to try to obtain an adequate description of this corrected elastic data. The LOFIT π-N phase shifts were finally used, with the s and p wave absorption from the thesis of Rosenthal, the Pauli blocking value from Thies, and the Lorentz-Lorentz parameter set equal to 1. It was found that the second order terms that went as ρ^2 had very little effect on the calculated cross section. The proton density distribution was taken from electron elastic scattering measurements. It was in the form of a modified harmonic oscillator with a=1.77 and α=0.327. This corresponds to an rms charge radius of 2.39 fm for ^{7}Li. The DUMIT program was modified so that a search could be performed for the best values of a and α for the neutron distribution to give a minimum χ^2 for the ratio of π^- to π^+. The data and the resulting optical-potential fit to the ratio are shown in Fig. B4. While the general shape of the ratio of angular distributions is obtained, there are detailed differences, particularly at the forward angles. The dashed curves on either side of the solid line represent calculations for neutron radii where the value of χ^2 is 1 greater than the minimum. The value of a for the neutron distribution was determined to be 1.85 $\pm$ 0.02 and α=0.282. These correspond to an rms matter radius of 2.60 $\pm$ 0.02 fm for the neutrons. The corresponding optical potential calculations are shown in Figs. B2 and B3 for the individual π^+ and π^- elastic angular distributions. The fact that the calculations in both cases are somewhat below the data has been of some concern. At this time there appears to be no valid reason to question the normalization of the data and there has been no reasonable variation in any of the optical model parameters that affects the forward angle behavior of the calculations to any degree.

Figs. B5 thru B9 show the inelastic angular distributions for the 0.478, 4.63, 6.68, 7.47, and 9.61 MeV states for both π^- and π^+. As yet no detailed theoretical calculations have been performed, but some preliminary collective model ℓ=2 DWBA results obtained using the program CHOPIN and the potentials previously discussed are shown as the solid lines in the various figures. The deformation parameters, β_2, were extracted from these calculations for the first four states and these are shown in Table BI. The values of β_2 are consistently larger for π^- than for π^+ scattering. The calculations were repeated using coupled channels and the effects on either the shapes of the angular distributions or the values of β_2 were quite small.

Table BI

Deformation Parameters, β_2, for the excitation of the excited states of ^{7}Li using 143 MeV π^+ and π^-.

E_x	J^π	π^-	π^+
0.478	$1/2^-$	1.26 ± 0.17	1.21 ± 0.15
4.63	$7/2^-$	1.05 ± 0.23	0.95 ± 0.17
6.68	$5/2^-$	0.49 ± 0.09	0.48 ± 0.08
7.46	$5/2^-$	0.27 ± 0.05	0.21 ± 0.05

2. π±D Comparison at 143 MeV - T. G. Masterson, R. L. Boudrie (LAMPF), E. Gibson (Sacramento St.), J. J. Kraushaar, D. A. Lind, R. J. Peterson, R. Raymond, R. A. Ristinen

Charge symmetry implies that the nuclear interaction should be unchanged by the inversion of the T_3 component of the isospin of every part of the system. Thus the n-n and p-p nuclear interactions should be identical. This classical example is plagued by a Coulomb correction of more than a factor of two which changes the p-p scattering length from -7.8 fm to -17.2 fm. The comparison n-n system is still unavailable to the experimenter and must be deduced from n-D scattering, resulting in a large experimental error (16.1 ± 1.0 fm).

The intermediate energy πD system minimizes these problems. The inversion of the T_3 component of the isospin of the π^+D system gives the π^-D system and both are experimentally available. The Coulomb corrections are small (≈2%). A π±D comparison provides a direct test of charge symmetry.

A comparison[1] of the total cross sections for π±D has indicated possible charge-symmetry violations at the several-percent level even after electromagnetic corrections.[2] If this effect occurred entirely in the elastic channel, the effect would be enhanced by the ratio of the total to the elastic cross sections (183 mb/47 mb) and would be seen as a 10-25% difference between π^+D and π^-D differential cross sections.

This experiment was carried out to look for possible violations of charge symmetry, and to obtain the first π^-D differential cross sections. The experiment was done on the EPICS channel at LAMPF. The target was 194 mg/cm^2 CD_2. Background subtraction was made with a 131.5 mg/cm^2 C target while a 152.7 mg/cm^2 CH_2 target provided a reference to the πp cross sections.[4] The π^+ and π^- cross sections were measured sequentially at each angle.

The measured π^+D and π^-D differential cross sections are shown in Figs. B10 and B11. The angles at which forward angle data were measured were selected to minimize interference from inelastic scattering from ^{12}C. The resolution of the EPICS spectrometer was a crucial factor in allowing us to do this. The angles were also selected to match those at which Bussey et al.[4] have measured the $\pi^{\pm}p$ differential cross section. This gave us two independent reference cross sections: The experimental πp data and the theoretical calculations of the πp differential cross section. Three different sets of theoretical πp cross sections were available to us: the Dodder,[5] SCATPI[6] and CROSS phase shift codes. For most angles, these codes agreed with each other and with the Bussey data to within ± 2%. We used the reference cross sections calculated from the CROSS computer code. Statistical errors were usually $\leq$ 1.5%. The 0° points shown in Figs B10 and B11 are determined from the total cross section data. The 180° data are from Holt et al.[8] at 140 MeV. Systematic errors associated with μ and e contamination of the pion beam, the absolute pion flux, the spectrometer acceptance and electronic dead times were minimized by the procedure of using the πp reference cross section.

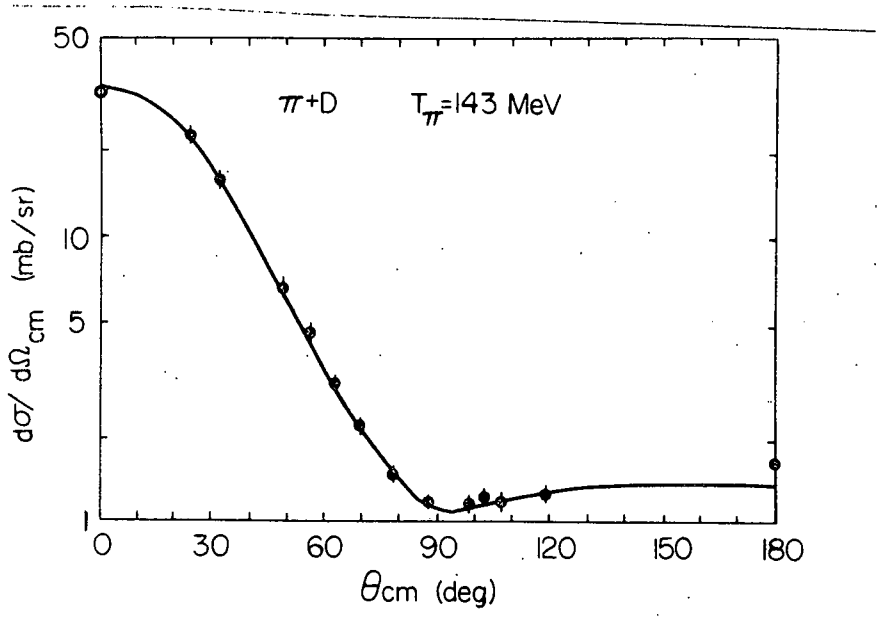

Fig. B10. π^+D differential cross section at 143 MeV. The 0° and 180° data points are from refs. 1 and 4 respectively. The 3-body calculation is from ref. 7 and includes all πN s- and p-wave channels.

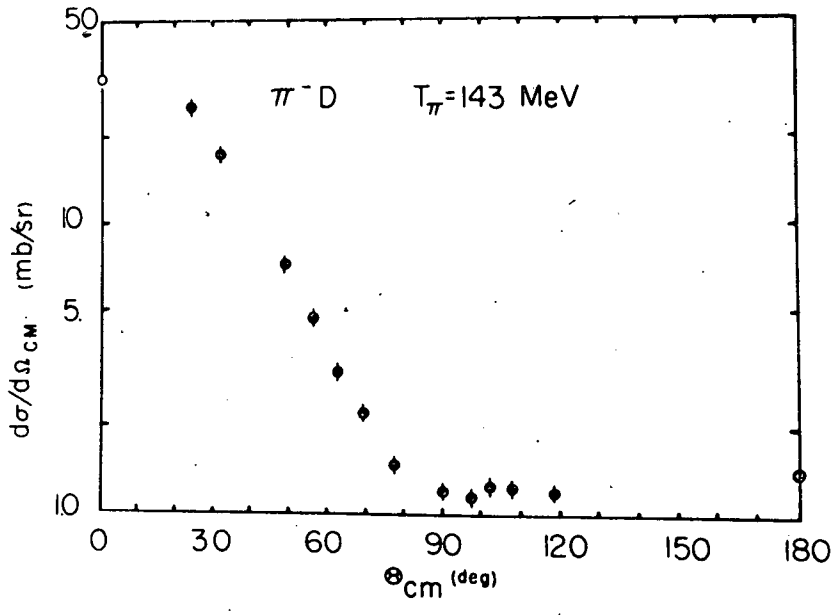

Fig. B11. π^-D Differential cross section at 143 MeV. The 0° and 180° data points are from refs. 1 and 8 respectively.

The π^+D cross sections agree very well with the 3-body Faddeev calculations of Girraud et al.[7] when all s- and p-wave πN channels are included. Their calculations would be identical for both π^+D and π^-D as charge symmetry is assumed. Our π^+D cross sections also agree very well with the preliminary SIN data of Gabathuler et al.[3]

The π^-D data shown in Fig. B11 represent the first accurate π^-D measurements between 100 and 300 MeV. The only previous data were the bubble chamber data of Pewitt et al.[9] which had large angular bins and poor statistics.

The difference between π^-D and π^+D divided by their sum is shown in Fig. B12. This ratio method is a very powerful tool for reducing systematic uncertainties. Effects of chamber inefficiencies and different possible πp phase shifts were also reduced by this procedure. All πp calculations and data ratios agree well in the medium angle range. A maximum difference occurs at far backward angles where the SCATPI π^-p calculation differs from the CROSS π^-p calculation by enough to raise the last 2 points by $\approx$0.02.

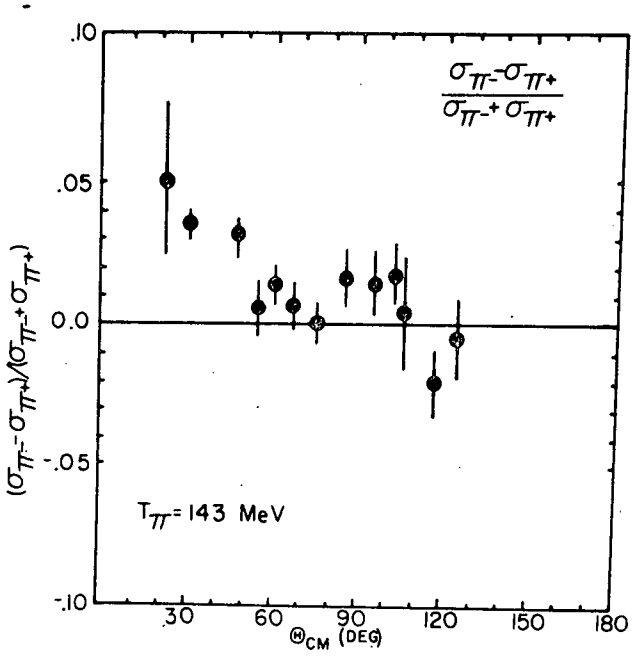

Fig. B12. The ratio $[\sigma_{\pi^-}(\theta) - \sigma_{\pi^+}(\theta)]/[\sigma_{\pi^-}(\theta) + \sigma_{\pi^+}(\theta)]$ at T_{π}=143 MeV. No Coulomb corrections have been included. They will lower the first three points. The use of different $\pi^{\pm}p$ calculations could raise the back two points by as much as 0.02.

No Coulomb corrections have been included in the data shown in Fig. B12. These calculations are in progress and their net effect will be to lower the first 3 points to about +0.01. The errors shown are statistical and it is unlikely that any residual systematic effect could change the median value of the ratio by more than ± 0.01.

The median charge-symmetry deviation as shown here corresponds to $\sigma_{el}(\pi^-) - \sigma_{el}(\pi^+) = +0.5 \pm 1.0$ mb. and is consistent with no violation of charge symmetry. This is to be compared with a difference of approximately -3 ± 2 mb seen in the total cross section measurements of Pedroni et al.[1] The difference in sign of the two measurements puts them outside of each other's uncertainties. There are at present no calculations of the effect on the differential cross section of any of the electromagnetic charge-symmetry-violating terms. The effect should however change sign at energies above the resonance and an experiment at higher energy is part of our continuing investigation of the $\pi^{\pm}D$ system.

[1] E. Pedroni et al., Nucl. Phys. A300 (1978) 321.
[2] F. Myhrer and H. Pilkuhn, Z. Phys. A276 (1976) 29.
[3] K. Gabathuler et al., Nucl. Phys. B55 (1973) 397.
K. Gabathuler et al., SIN Preprint PR 80-011 (1980).
[4] P. J. Bussey et al., Nucl. Phys B58 (1973) 363.
[5] D. C. Dodder, private communication.
[6] J. B. Walter and G. A. Rebka, LA-7731-MS (1979) (Unpublished).
[7] N. Giraud et al., Phys. Rev. C19 (1979) 465.
N. Giraud, C. Fayard, and G. H. Lamont, Phys. Rev. C21 (1980) 1959.
[8] R. J. Holt et al., Phys. Rev. Lett 43 (1979) 1229.
[9] E. G. Pewitt et al., Phys. Rev. 131 (1963) 1826.

3. Excitation of Giant Resonances in ^{118}Sn by 130 MeV Pion Scattering (Experiment 522) - T. G. Masterson, R. J. Peterson, R. S. Raymond, R. A. Ristinen; R. E. Anderson (LASL); J. Piffaretti (Neuchatel); R. L. Boudrie and N. S. P. King (LASL)

Both positive and negative pion scattering from ^{118}Sn have been studied at high excitations with the EPICS system. Several angles were examined to differentiate between the expected multipolarities. An energy of 130 MeV was used, which allowed time-of-flight rejection of the muon continuum.

Fig. B13 shows sample spectra, corrected for the acceptance across the focal plane. The elastic and low excitation region was excluded by a hardware gate to avoid filling up the tapes too quickly. The accepted locations and widths of several giant resonances are indicated on the figure. The isoscalar E2 is the most strongly excited, but the high excitation shoulder shows the greatest difference between π^+ and π^- scattering. The excitation energy corresponds to either the isoscalar E0 or isovector E1 giant states.

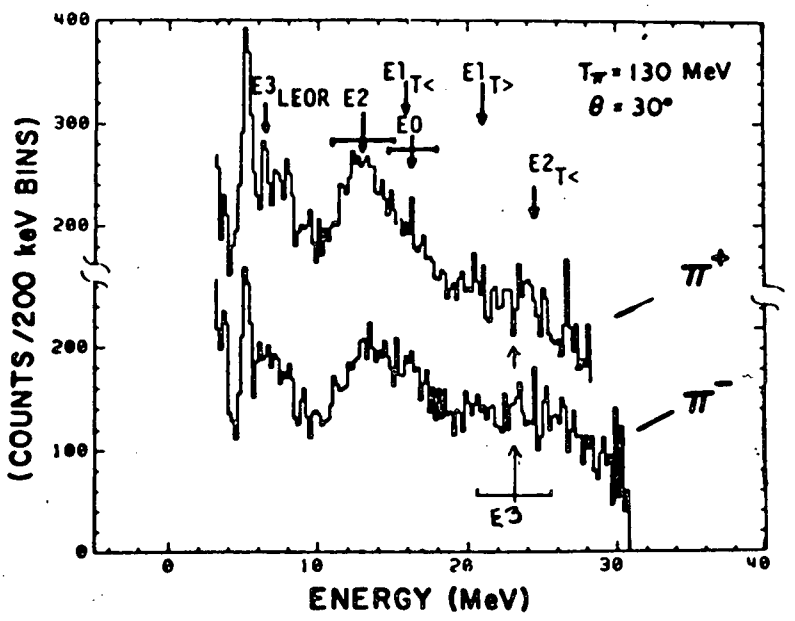

Fig. B13. Inelastic scattering spectra on ^{118}Sn at 30 degrees, corrected for the acceptance of the spectrometer. Known giant resonance regions are indicated.

An E3 giant resonance has been found recently with the HRS, at 22.9 MeV (110 $A^{-1/3}$ MeV) in ^{116}Sn.[1] The location and width of this peak are indicated in the pion spectrum, where some excess of counts may be indicated. A similar E3 state has been located in ^{208}Pb at 17.5 MeV (104 $A^{-1/3}$ MeV) by ^{4}He scattering[2], indicating an isoscalar degree of freedom, interpreted as the 3 $\hbar\omega$ octupole state.

The sample spectrum also shows a partially resolved low energy octupole resonance. Angular distributions of the E2 state confirm the expected L=2 angular distribution. Further angular distributions are being analyzed.

Preliminary runs on targets of ^{40}Ca, ^{90}Zr and ^{208}Pb also show clear excitation of peaks in the giant resonance region, but no angular distribution studies have been attempted.

Pion scattering charge asymmetries would be zero for either strictly isoscalar or isovector scattering, but are very sensitive to mixing of these modes[3]. For a small mixing $\epsilon=M_0/M_1$ of isoscalar excitation in a primarily isovector transition,

$$\frac{d\sigma(\pi^-)}{d\sigma(\pi^+)} = \left|\frac{1+2\varepsilon}{1-2\varepsilon}\right|^2$$

For ε=0.1, or a 1% loss of the T=1 summed transition strength, this ratio is 2.25. For a primarily isoscalar excitation with a bit of isovector, ε=10, the ratio is 1.22. This greater sensitivity to the mixing of nominally isovector excitations may be the cause of the enhanced π^- yield near 15 MeV, where the E1 ΔT=1 giant resonance is known to reside.

More beam time has been requested to pursue this important project.

---

1. T. A. Carey et al., Phys. Rev. Lett. 45 (1980) 239.
2. H. P. Morsch et al., Phys. Rev. Lett. 45 (1980) 337.
3. R. J. Peterson, Nucl. Phys. A335 (1980) 365.

4. New Proposals to LAMPF - R. J. Peterson, T. G. Masterson, J. J. Kraushaar, R. S. Raymond, and R. A. Ristinen

This list of experiments proposed to be run at LAMPF includes those with University of Colorado personnel as spokesmen or planned participants.

Experiment 575

A proposal to study ^{50}Ti, ^{51}V, and ^{52}Cr by 800 MeV proton inelastic scattering has been submitted in collaboration with a group from South Carolina, Gary Blanpied as spokesman. The states of known seniority four in ^{52}Cr will be investigated as the first examples of shell model double excitation. A search will also be carried out for the $f^{-1}g$ stretched 8^- states.

Experiment 581

This proposal concerning $\pi^\pm$ scattering from deuterium at 237 MeV addresses the fundamental question of charge symmetry. T. G. Masterson is spokesman. Total cross section calculations[1] and experiments[2] have indicated a possible several percent violation in charge symmetry in the πD reaction. The $\sigma_T(\pi^-D) - \sigma_T(\pi^+D)$ difference is negative below the (3,3) resonance and positive above. Our experiment #478 (see section II.B.2.) measured the differential cross section difference at 143 MeV to better than 5% accuracy. This new proposal will

make a similar careful comparison of the differential cross section difference at 237 MeV. The experiment has been approved for 180 hours of EPICS time and is scheduled for beam in early 1981.

---

[1] F. Myhrer and H. Pilkuhn, Z. Phys. A276 (1976) 29.
[2] E. Pedroni et al. Nucl. Phys. A300 (1978) 321.

Experiment 608

Our success in observing giant resonances in both π^+ and π^- inelastic scattering (see section II.B.3.) has led us to propose a continuation on other targets and at a larger range of angles. N. S. P. King, R. E. Anderson, and R. L. Boudrie are the spokesmen. We intend to vary:

1. Beam energy from 100 to 290 MeV to select the optimum bombarding energy,

2. Isotopic sequences to use the sensitivity of π scattering to examine the predicted (N-Z) variation,

3. Higher excitations for a better look at the 3 $\hbar\omega$ octupole state,

4. The mass range, to guarantee that we see giant resonances with excitation energies that vary as $A^{-1/3}$.

Experiment 538

J. R. Shepard and N. S. P. King (LASL), co-spokesmen. We have proposed to measure ^{4}He($\vec{p}$,d)^{3}He cross-sections and analyzing powers at energies between 500 and 800 MeV. These would be the highest energy (p,d) Ay measurements in existence and would complement previous measurements done at TRIUMF. This proposal was approved in Jan. 1980 and an update to include ^{13}C(p,d) at the lowest energy was approved in July 1980. We hope to learn about the intermediate energy (p,d) reaction mechanism from these measurements.

5. Study of Giant Resonances via the (p,n) Reaction - E. Sugarbaker, T. Masterson, D. Lind, and R. Raymond; C. Goodman and C. Foster (IUCF); D. J. Horen (Oak Ridge); J. Rapaport and T. Taddeucci (Ohio Univ.); C. Goulding and M. Greenfield (Florida A & M); S. Austin, A. Galonsky, and W. Sterrenburg (MSU); C. Gaarde and J. Larsen (Niels Bohr Institute); D. Bainum (Emporia State)

We have continued the survey of the (p,n) reaction at intermediate energies, utilizing the beam-swinger facility at the IUCF. In the past year we have obtained additional data on targets from lithium to lead at proton energies of 80, 120, and 200 MeV. Flight paths ranged from 45 m to 90 m. Angular distributions from 0° to a maximum $\theta_{lab} \leq 48°$ have been acquired for most of the targets studied. Implementation of additional neutron detectors and anti-coincidence detectors (discussed in sect. IIC) for background reduction facilitated these measurements. With this detector array we should be able to proceed in the coming year with an investigation of analyzing powers in the $(\vec{p},n)$ reaction.

At zero degrees the most prominent peaks are the Gamow-Teller (GT) resonances. The angular distributions for these $\Delta\ell=0$ transitions are the same as those for the ground state isobaric analog (IAS) resonances. Examples of these distributions are shown in fig. B14. In light elements

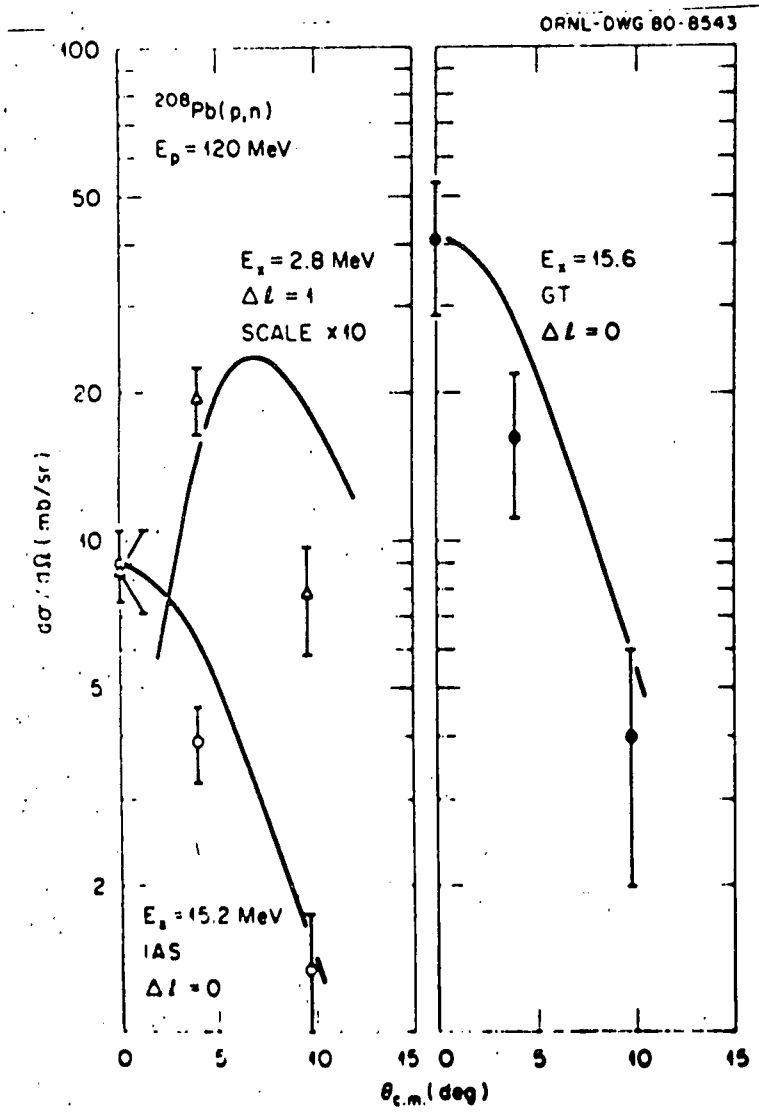

Fig. B14. Angular distributions for the ^{208}Pb(p,n)^{208}Bi reaction at 120 MeV.

the GT strength is concentrated in two peaks. However, in the heavy elements, the component at lower excitation appears very weakly. In the $^{208}Pb(p,n)^{208}Bi$ reaction we see about 40% of the total predicted GT strength in a broad resonance (4.1 MeV FWHM) located 0.4 MeV above the IAS. The energy separation between the giant GT and the IAS is a function of (N-Z)/A, an effect easily seen in the Zr and Sn isotopes. The GT is 1, 2.1, and 3 MeV above the IAS in $^{124,116,112}Sb$, respectively. Using data for all nuclei having $A \geq 90$, we find that

$$E_{GT}-E_{IAS} = -30.0(N-Z)/A + 6.7 \text{ MeV}. \quad (1)$$

This is in surprisingly good agreement with an early prediction of Fujita et al.[1], who estimated a dependence of -30.7 (N-Z)/A based on residual p-$\bar{n}$ interactions.

In excellent agreement with the predictions of Love[2], the 0° cross sections of the GT resonance relative to the IAS continued to rise with increasing proton energy. This ratio is about 10 at 160 MeV and 18 at 200 MeV. This can be related to the energy dependence of the spin dependent and independent terms in the nucleon-nucleus interaction (see sect.II.B.8.)

Another resonance having a proton energy dependence similar to that of the GT has been observed at an excitation above both the IAS and the GT resonance. This energy dependence suggests that it is also populated via a spin-flip transition. Its angular distribution is sharply peaked near 5°, characteristic of $\Delta\ell=1$ transitions (see Fig. B14). Time-of-flight spectra at 4.5° for a few heavy nuclei are shown in Fig. B15. The energy separation between this $\Delta\ell=1$ resonance and the GT is approximately constant, suggesting that they exhibit similar (N-Z)/A dependence. Indeed the Sn, Tm, and Pb data define an energy difference given by

$$E_{\Delta\ell=1}-E_{IAS} = -33.0\ (N-Z)/A + 13.6 \text{ MeV}. \quad (2)$$

Since the GT resonance involves L=0, S=1 transitions between p-$\bar{n}$ states within the same oscillator shell, we suggest that the $\Delta\ell=1$ resonance represents L=1, S=1 transitions between p-$\bar{n}$ states in different shells. This would explain the comparable (N-Z)/A dependence for the two resonances, due to the operation of the same residual interactions in each case. The larger constant term in equation 2 probably represents the additional energy required for the shell crossing associated with the $\Delta\ell=1$ resonance. The $\Delta\ell=1$ resonance is observed in the Zr isotopes at a larger energy separation from the IAS, although the (N-Z)/A dependence appears to be about the same as in the heavier nuclei. This deviation for the Zr nuclei may reflect a higher average energy splitting between L shells in medium mass nuclei.

---

1. Fujita et al., Phys. Rev. 133 (1964) B549.
2. W. G. Love, in Proc. Conf. on the (p,n) Reaction and Nucleon-Nucleon Forces, Telluride, CO, March, 1979, p. 23.

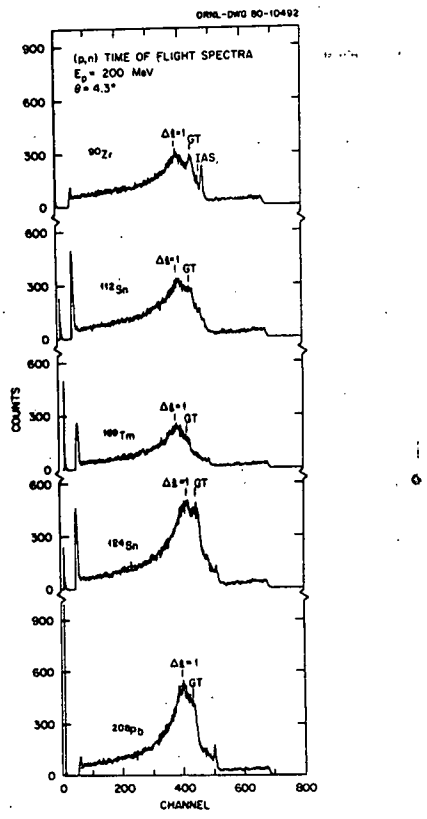

Fig. B15. Time-of-flight spectra at E_p=200 MeV.

6. Neutron Matter Distributions from Quasi-Elastic (p,n) Reactions - R. S. Raymond, D. A. Lind, T. G. Masterson, E. Sugarbaker, C. C. Foster (Indiana University)

In a continuation of studies of the sensitivity of the (p,n) reaction to neutron distributions,[1] we measured angular distributions of the quasi-elastic (p,n) reaction to ground-state isobaric analog states of ^{90,92,94}Zr and ^{112,116,124}Sn for a proton energy of 79.2 MeV. These measurements were made at the Indiana University Cyclotron Facility and extended from 0° to 24°. A time-of-flight system was used with a 43 m neutron flight path and plastic scintillator neutron detectors. The neutron detectors were covered by veto scintillator paddles to reduce background due to charged particles from cosmic rays and from the neutron beam. A typical T. O. F. spectrum is shown in Fig. B16. Angular distributions are shown in Fig. B17. Statistical errors in the cross sections are ± 1% at forward angles and ± 5% at back angles. There is a relative uncertainty of ± 5% between spectra due to target thickness uncertainties, and an uncertainty in the absolute cross sections of ± 15% due to uncertainties in the cross section for the ^{7}Li(p,n)^{7}Be reaction,[2] with which the system was calibrated, and in the Li target thickness.

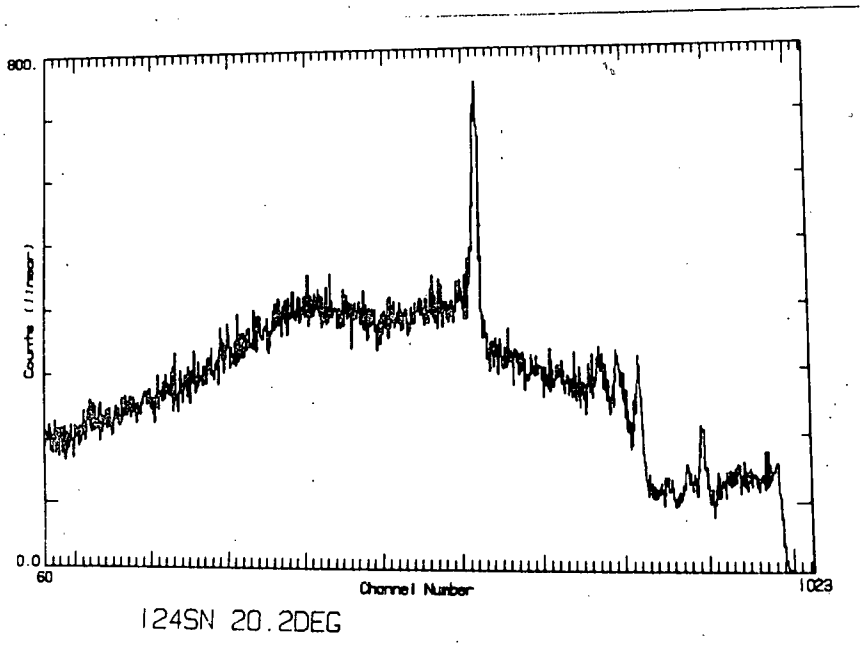

Fig. B16. Neutron T. O. F. spectrum for ^{124}Sn(p,n)^{124}Sb at 79.2 MeV and 20.2°. The prominent peak is the ground-state IAS.

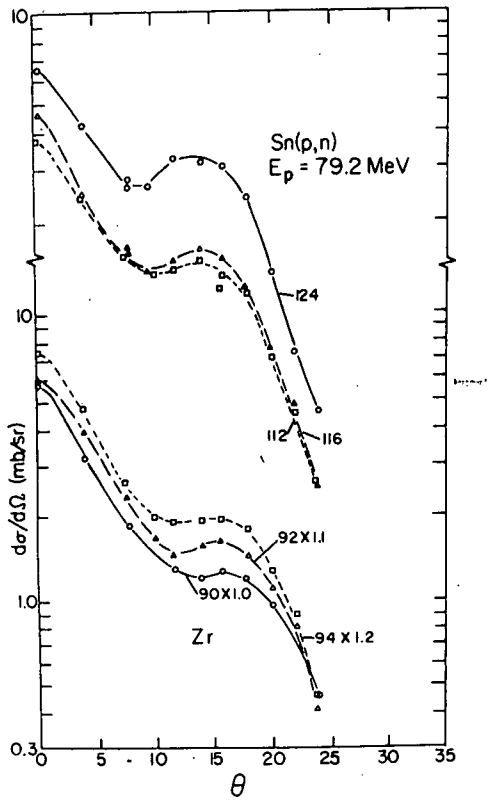

Fig. B17. Angular distributions for ^{112,116,124}Sn(p,n) and ^{90,92,94}Zr(p,n) for a proton energy of 79.2 MeV.

We are using two methods to fit the data. In the first, we use the DWBA code DWUCK4, with distorting potentials by Nadasen et al.[3] For the form factor two assumptions are made. The first is that the potential is the sum of two parts, a repulsive, real, central part due to the protons and an attractive, real, central part due to the neutrons. Second, we assume that the ratios of volume integrals of these potentials is equal to the ratio of neutron and proton numbers. With these two assumptions, the radius of the neutron potential is varied to fit the shape of the angular distribution.

In the second method, the code SMUCK[4] folds neutron and proton distributions with nucleon-nucleon potentials, and then searches on the neutron distribution to fit the data.

Analysis is not complete, but the change in ratios of neutron to proton rms radii in going from ^{112}Sn to ^{124}Sn is approximately 2%, consistent with the change seen for 22.8 MeV protons.[1] We do not yet have estimates on the uncertainties in these ratios and, at least until a satisfactory estimate can be made, the (p,n) reaction will remain of limited use for the determination of neutron distributions.

Cross sections at large momentum transfer needed to resolve the ambiguity at small radii are difficult to obtain. The values are small relative to the background of $T_<$ states and particularly the giant spin flip resonances upon which the IAS state sits. At 120 MeV, the IAS state in Sn is not seen at all beyond about 15°. Considerable calculational effort is needed now to determine whether further data at larger angles or the data we have at E_p=120 MeV will be useful for further analysis.

---

[1] S. D. Schery, D. A. Lind, and H. Wieman, Phys. Rev. C14, 1800 (1976).
[2] C. C. Foster et al, Bull. Am. Phys. Soc. 24, 828 (1979).
[3] A. Nadasen, P. Schwandt, P. P. Singh, A. D. Bacher, P. T. Debevec, W. W. Jacobs, M. D. Kaitchuck, J. T. Meek, Private Communication.
[4] S. D. Schery in "The (p,n) Reaction and the Nucleon-Nucleon Force", edited by C. D. Goodman, S. M. Austin, S. D. Bloom, J. Rapaport, and G. R. Satchler, Plenum Press, New York and London, 1980.

7. Analyzing Powers for the ^{13}C and $^{208}Pb(\vec{p},d)$ Reaction at T_p=123 MeV - J. R. Shepard and J. J. Kraushaar, Univ of Colorado, and D. W. Miller, D. W. Devins, W. Jacobs, and W. P. Jones, Indiana University

We have measured differential cross sections and analyzing powers for the first 2 (6) levels in the $^{13}C(^{208}Pb)$ $(\vec{p},d)$ reactions at T_p=123 MeV using the magnetic spectrograph at the Indiana University Cyclotron Facility. Several preliminary analyzing-power distributions for the latter reaction appear in Figs. B18 and B19.

The $^{13}C(\vec{p},d)^{12}C$ analyzing powers for the transitions to the 0^+ ground state ($p_{1/2}$ pick up) and the 4.44 MeV 2^+ level ($p_{3/2}$ pickup) are quite similar to those observed at 65[1] and 200 MeV,[2] as is discussed elsewhere in this report.[3] The DWBA description of them is quite poor. The failure is comparable to that reported for the T_p=94 MeV $^{24}Mg(\vec{p},d)^{23}Mg$ (2.36 MeV $1/2^+$ level) in another section of this report.

In contrast to the $^{13}C(\vec{p},d)^{12}C$ data, the $^{208}Pb(\vec{p},d)$ analyzing powers show only slight $j_>$ vs. $j_<$ dependence based on comparisons of $p_{1/2}$ vs. $p_{3/2}$ and $f_{5/2}$ vs. $f_{7/2}$ angular distributions. All analyzing-power angular distributions show significant structure which becomes more pronounced for decreasing angular-momentum transfer.

Zero-range DWBA calculations were performed as described in ref 4 using optical potentials P7P and D3P of that reference. Some of these calculations appear as the solid curves of Figs. B18 and B19. Generally there is reasonably good agreement with the analyzing-power data in contrast with the very poor agreement observed for the lighter targets. Only for the 3.409 MeV $9/2^-$ level data shown in Fig. B19 is the agreement qualitatively poor.

Further analysis of these data is currently under way.

---

[1] K. Hosono et al., RCNP (Osaka) Annual Report, 1978, p. 7.
[2] See Section II.B.10, this report, and R. P. Liljestrand et al., to be published.
[3] Section III.F., This report.
[4] R. E. Anderson et al., Nucl. Phys. A311 93 (1978).

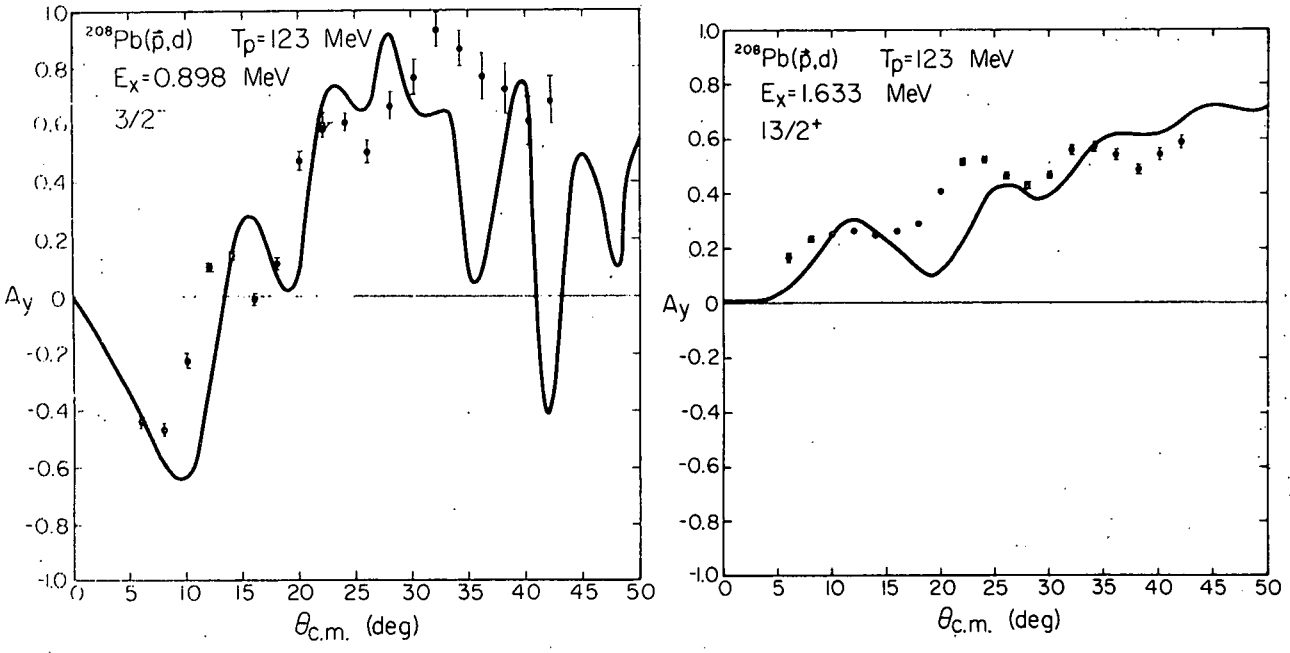

Fig. B18. Analyzing power data for the ^{208}Pb(p⃗,d) reaction at T_p=123 MeV leading to the 0.898 MeV $3/2^-$ and the 1.633 MeV $13/2^+$ levels are compared with zero range DWBA calculations.

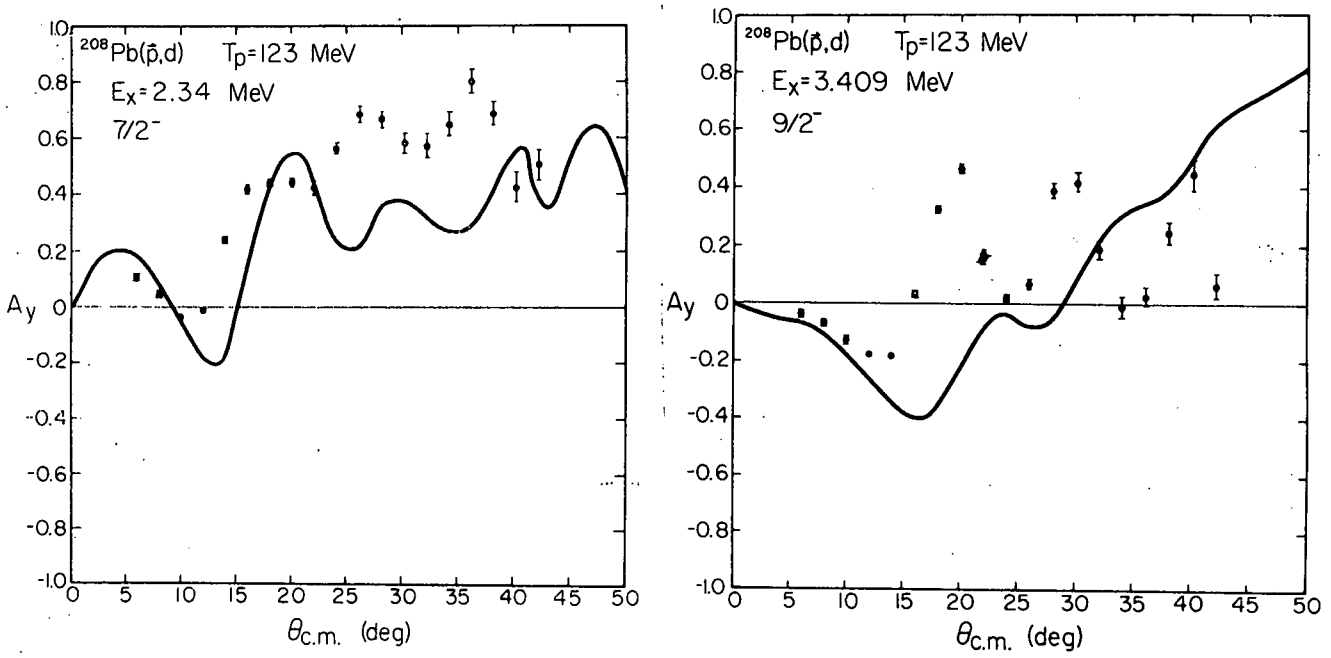

Fig. B19. Analyzing power data for the ^{208}Pb(p̄,d) reaction at T_p=123 MeV leading to the 2.34 MeV 7/2⁻ and 3.409 MeV 9/2⁻ levels are compared with zero-range DWBA calculations.

8. Energy Dependence of the $\tau\cdot\tau$ and $\sigma\cdot\sigma\tau\cdot\tau$ Effective Interactions - E. Sugarbaker and T. Masterson; J. Rapaport and T. Taddeucci (Ohio Univ.); C. Goulding and M. Greenfield (Florida A & M); C. D. Goodman and C. Foster (IUCF); D. J. Horen (Oak Ridge National Lab); D. Bainum (Emporia State)

The study of the (p,n) reaction at intermediate energies continues to provide information on the isospin-spin dependent and independent parts of the nucleon-nucleus interaction. The IUCF beam swinger facility has been used to study the (p,n) reaction at bombarding energies from 80 to 200 MeV. Angular distributions for numerous light to medium nuclei have been measured near zero momentum transfer. Under such experimental conditions it is possible to extract the strengths of the $\tau\cdot\tau$ and $\sigma\cdot\sigma\tau\cdot\tau$ central interactions. Comparison with matrix elements extracted from β-decay measurements has proven very successful and determination of Gamow-Teller (GT) matrix elements for transitions not accessible by other means appears possible[1].

The sensitivity of the (p,n) reaction to various terms of the effective interaction as the bombarding energy is changed has been discussed in detail by Love[2]. Between 100 and 200 MeV the spin-isospin dependent term is predicted to remain nearly constant while the isospin dependent term should decrease significantly. There appears to be experimental support for both predicted trends. The ratio of cross sections for Fermi to GT

transitions is observed to decrease with increasing bombarding energy. In addition the angular distributions of the cross sections for GT transitions when plotted versus momentum transfer appear to be independent of bombarding energy. This suggests that the spin-isospin term may indeed be energy independent in this energy region and that the change in the above ratio is due only to an isospin dependent term which decreases with increasing energy.

---

1. C. D. Goodman et al., Phys. Rev. Lett. 26 (1980) 1755.
2. W. G. Love, in The (p,n) Reaction and the Nucleon-Nucleon Force, edited by C. D. Goodman, S. M. Austin, S. D. Bloom, J. Rapaport, and G. R. Satchler (Plenum Press, New York, 1980), p. 23.

9. The $^4He(\vec{p},d)^3He$ Reaction at 200 and 400 MeV - G. Hassold, J. J. Kraushaar, J. R. Shepard (Univ. of Colo.), D. A. Hutcheon, W. J. McDonald, R. P. Liljestrand, C. A. Miller (Univ. of Alberta), J. Tinsley (Univ. of Oregon), and C. E. Stronach (Virginia State Univ.)

As part of a previous proposal to TRIUMF, the $^4He(\vec{p},d)^3He$ reaction was studied during a run in the first week of June. The measurements were carried out using a beam of polarized protons and the 1.4 GeV/c magnetic spectrometer with a liquid ^4He target. Analyzing powers and cross sections were measured from 23° to 90° in the center of mass at 200 MeV and from 23° to 120° at 400 MeV. The cross sections at both energies fell off very steeply and monotonically with angle. Preliminary DWBA calculations are in general agreement with respect to the magnitude of the cross sections but they show considerably more structure as a function of angle than do the data. The measured analyzing powers at 200 MeV are always positive and rise to a value of 0.55 at θ_{cm}=90°. At 400 MeV there is somewhat more structure inasmuch as the analyzing power starts at about -0.3 and rises rather rapidly to +0.5 at 45° and thereafter stays positive with mild variations. Preliminary DWBA calculations at 400 MeV show a far more oscillatory behavior with angle.

Efforts are being made to obtain final cross sections and analyzing powers. More extensive calculations will be done shortly. The cross sections are compared with the 770 MeV Saclay data[1] elsewhere in this report (Sec. III.F.)

---

[1] G. Bruge, Saclay Internal Report DPh-N/Me/78-1.

10. Analyzing Power Measurements for the $^{13}C(\vec{p},d)^{12}C$ Reaction at 200 and 400 MeV - J. J. Kraushaar and J. R. Shepard (Univ. of Colorado), R. P. Liljestrand, J. M. Cameron, D. A. Hutcheon, W. J. MacDonald, R. McDonald, C. A. Miller, and W. C. Olsen (Univ. of Alberta), J. G. Rogers (TRIUMF), J. T. Tinsley (Univ. of Oregon), C. E. Stronach (Virginia State Univ.)

Data on the above reaction taken at TRIUMF using the 1.5 GeV/c magnetic spectrometer and beams of 200 and 400 MeV polarized protons were partly described in last year's Progress Report. During the past year the rest of the data were analyzed and normalization problems with the cross sections straightened out.

Extensive distorted wave Born approximation calculations have been performed in zero-range (ZR) using the code DWUCK4 and in exact finite range (EFR) using DWUCK5. The EFR calculations were performed as in ref. 1 except that S- and D-wave deuteron contributions were combined coherently. The geometry of the bound state well was determined as discussed in ref. 2. The proton distorting potential for the 400 MeV measurements was generated using the leading term of the optical potential in the KMT multiple scattering theory. The deuteron potential was obtained by doubling the potential strengths of the KMT proton potential at $1/2T_p$. The geometry was altered to account for the finite size of the deuteron. The strengths of the spin orbit potentials are simple estimates based on low energy p + nucleus results. For the 200 MeV calculations, the empirical p + ^{12}C potentials of Comfort and Karp[3] were used; their 183 MeV potential was adopted for the proton distortion while the strengths of the 96 MeV potential were appropriately adjusted to give the deuteron potential. The DWBA calculations were normalized using spectroscopic factors computed with the A=12 and 13 wave functions of Norton and Goldhammer.[4] The values are $C^2S=0.67$ for the transition to the ground state ($1p_{1/2}$ pickup) and $C^2S=1.1$ to the 4.44 MeV 2^+ level ($1p_{3/2}$) pickup.

The calculations are also presented in Figs. B20 and B21. At 200 MeV, Fig. B20 indicates the EFR (or D-state) contributions to the differential cross sections are small, their principal effect being to introduce somewhat more structure into the ground state angular distribution. Comparing the EFR and ZR results gives an effective ZR normalization of $D_0 \approx 85$ MeV-fm$^{3/2}$, compared to the low energy value of ≈ 125 MeV-fm$^{3/2}$. The 200 MeV analyzing powers are not strongly influenced by D-state contributions for $\theta < 30°$ although big effects are seen at larger angles. Contributions from the D-state account for roughly one-half of the differential cross section at 400 MeV and consequently must be treated explicitly.

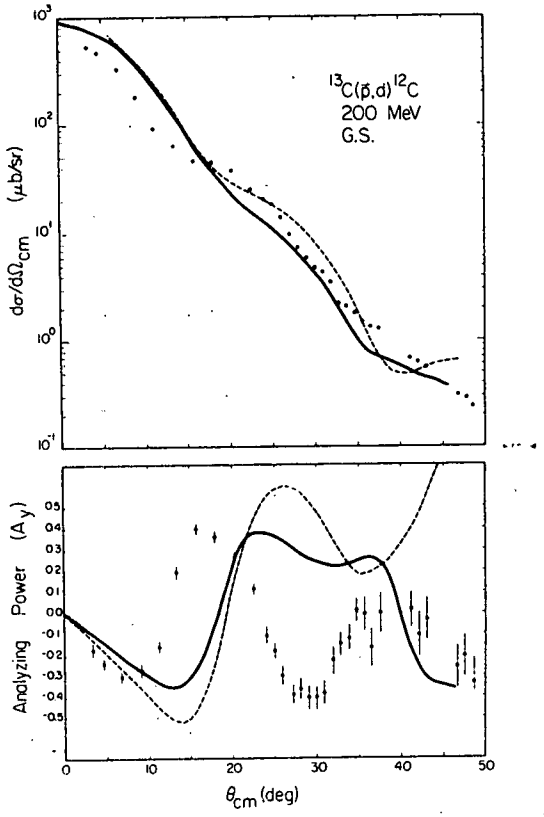

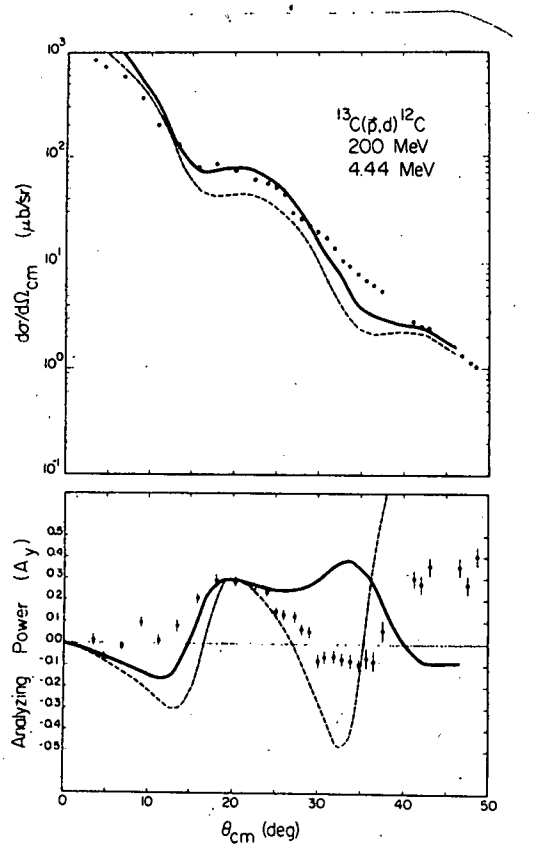

Fig. B20. Cross sections and analyzing powers for the $^{13}C(\vec{p},d)^{12}C$ reaction at 200 MeV. The dashed curves are the results of a zero range DWBA calculation. The solid curves are the results of EFR calculations using the same potentials.

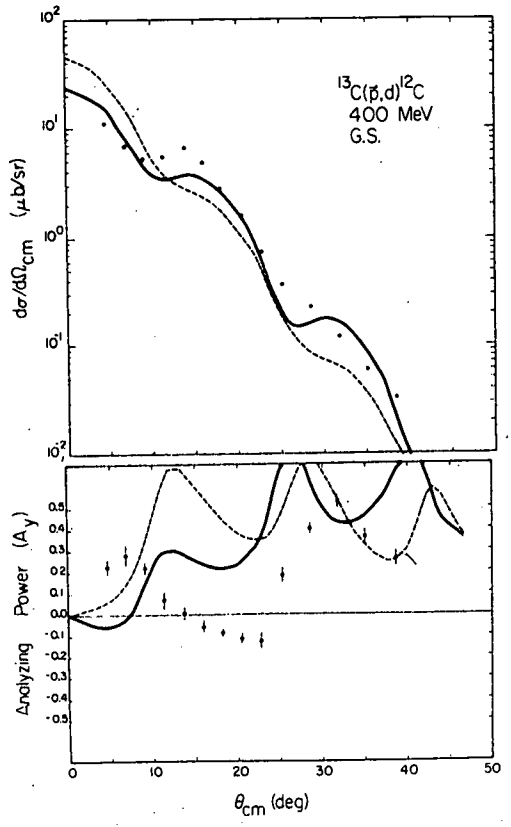

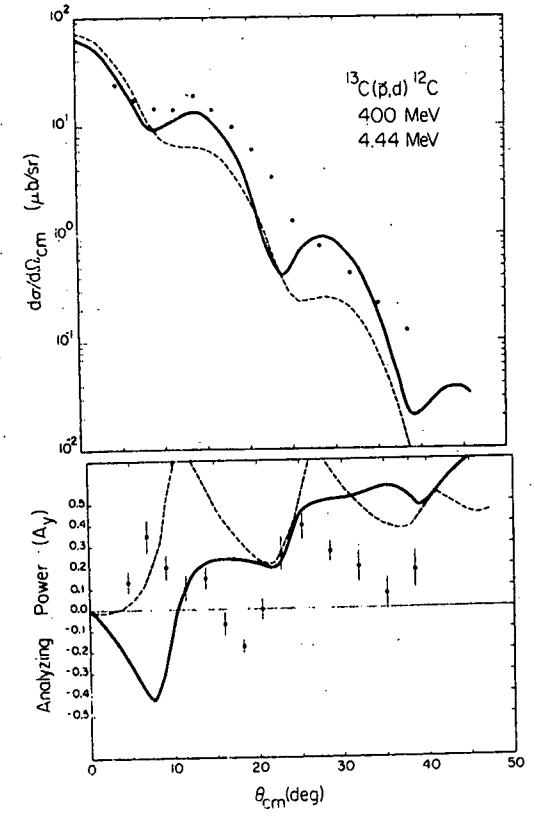

Fig. B21. Cross sections and analyzing powers for the $^{13}C(\vec{p},d)^{12}C$ reaction at 400 MeV. The solid curves are the results of EFR calculations. The dashed curves are also the results of EFR calculations using the same potentials except that the spin-orbit potentials in both the proton and deuteron channels were set equal to zero.

The sensitivity of the 200 MeV calculations to uncertainties in the distorting potentials was explored in some detail and found to be appreciable, particularly for the deuteron channel. Reasonable variations in the deuteron potentials caused changes both in the overall magnitude of the cross sections (results varied by factors as large as three) and in the shapes (rate of fall-off and location of inflection points) of the angular distributions. The calculated analyzing powers did not vary significantly for $\theta < 25°$. These sensitivities coupled with the lack of reliable published analyses of the relevant elastic scattering data, especially for deuterons, introduce many ambiguities into the calculations. The curves shown in Fig. B20 were generated with what we judged to be the most reliable potentials. Arbitrary modification of these potentials did not appreciably improve the agreement with the data. Sensitivity to the spin orbit potentials was found to be considerable in the ZR calculations. Surprisingly, only a slight sensitivity was observed for the EFR calculations, possibly due to averaging over the increased number of spin orientations possible when the D-state is treated explicitly. The 400 MeV calculations in Fig. B21 were done using KMT potentials for both channels. Substituting a deuteron potential based on the 200 MeV p + C had little effect on the calculated cross sections and did not result in improved agreement for the analyzing powers.

The EFR-DWBA is seen to give a reasonable account of the measured cross sections. The differences between the shapes calculated for the two transitions is markedly greater than that observed experimentally, indicating that the DWBA overestimates the j-dependence of the cross section. On the other hand, the calculated analyzing power bears only a vague resemblance to the data. While the calculations do correctly predict a much larger negative analyzing power for the $j=\ell-1/2$ state than for the $j=\ell+1/2$ state at forward angles, the overall agreement is very poor. No reasonable optical model parameter combination could be found which resulted in significant improvement upon the results shown in Fig. B20. The analyzing power calculated for the 2^+ level at 400 MeV is sensitive to the removal of the spin orbit distortion, as shown in Fig. B21. One also sees, however, that in all cases the agreement with data is catastrophic at the higher energy.

At both energies calculations were insensitive to reasonable variations of the binding well geometry which in turn give rise to changes (in configuration and momentum space) in the bound state wave function. This is particularly surprising at 400 MeV where the distorting potentials are relatively small and one might expect to see changes in the predicted oscillatory pattern corresponding to changes in the position of the node in the momentum space bound state wave function, as predicted by the plane wave Born approximation (PWBA). It can thus be inferred that the PWBA is quite unreliable, even qualitatively, at these energies and that information about high momentum components of the nuclear wavefunction is not readily accessible even assuming that distortion effects are correctly treated using the DWBA.

We have presented the first analyzing power measurements for the medium energy $(\vec{p},d)$ reaction. The angular distributions of these quantities for the transitions to the ground and first excited states in the $^{13}C(\vec{p},d)^{12}C$ reaction show a great deal of structure in contrast to the nearly featureless cross sections. These two transitions represent $p_{1/2}$ and $p_{3/2}$ pickup, respectively, and distinctive j-dependence is observed at forward angles for the lower bombarding energies. At higher momentum transfers, the analyzing powers are seen to be roughly independent of energy and j-transfer. The highly structured analyzing power data does provide, as anticipated, a demanding test of the DWBA. Although it reproduces the measured cross sections quite well, the DWBA unambiguously fails this test, reproducing crudely only the most general features of the analyzing powers for T_p=200 MeV. The failure is catastrophic at 400 MeV. While sensitivity to poorly known deuteron optical potentials is appreciable, it does not seem likely that reasonable variation of the optical model parameters can bring about acceptable agreement. The extreme failure of the DWBA, even at 200 MeV where the standard low energy reaction model should still be appropriate, is disconcerting and is being studied further. Identification of the causes of the failure is likely to result in both a greater understanding of the DWBA and a greatly increased utility of the $(\vec{p},d)$ reaction as a spectroscopic tool to be used, for example, in the identification of deep-hole states in nuclei.

---

[1] E. Rost, J. R. Shepard, and D. A. Sparrow, Phys. Rev. C 17 (1978) 1513.
[2] J. R. Shepard and P. Kaczkowski, Univ. of Colorado, Tech. Prog. Rept. 1977, p. 160.
[3] J. R. Comfort and B. C. Karp, Univ. of Pittsburgh, to be published.
[4] J. L. Norton and P. Goldhammer, Nucl. Phys. A165 (1971) 33, and J. L. Norton, Ph. D. Thesis, Univ. of Kansas, unpublished.

11. Proton Radius Determinations from the Ratio of π^+ Elastic Scattering from ^{11}B and ^{12}C - J. J. Kraushaar, S. Lepp, T. G. Masterson and E. Rost; B. M. Barnett, W. Gyles, R. R. Johnson, K. L. Erdman and J. Johnstone, Univ. of British Columbia; D. R. Gill and A. W. Thomas, TRIUMF; J. Alster and I. Navon, Tel-Aviv; R. H. Landau, Oregon State

A new method has been developed for determining nuclear charge radii using a low energy positive pion probe. In a recent publication[1] a method was put forth for the determination of rms radii of the neutron matter distributions in nuclei through the use of low energy π^- elastic scattering from different isotopes. For the cases studied, the neutron radii could be determined to within a few hundredths of a fermi relative to reference nuclei. The elastic scattering of π^+ mesons at low energies from different isotones should demonstrate the same sensitivity to the pro-

ton matter distribution as π^- scattering does to the neutron matter distribution from comparable isotopes. A π^+ elastic scattering experiment should determine proton matter radii which can be compared directly with those found by analysis of electron scattering and muonic x-ray data. The π^+ elastic scattering experiment should therefore provide a more definitive test of the multiple scattering optical potential method of determining matter radii. For this purpose ^{12}C and ^{11}B were selected as target nuclei with π^+ beams of 47.7 and 38.6 MeV.

The experimental apparatus is shown schematically in Fig. B22. The π^+ beam intensity from the TRIUMF M13 channel was about 5×10^5 π^+/sec. Targets were 0.333 gm/cm^2 ^{12}C and 0.377 gm/cm^2 B. The

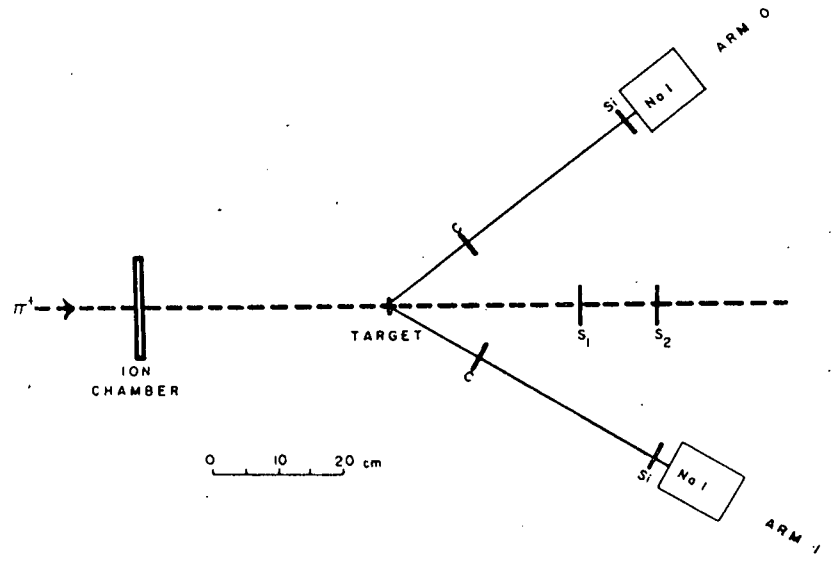

Fig. B22. A schematic view of the detectors and beam monitors.

scattered pions were detected in two counter telescopes each containing a direction defining plastic scintillator, a lithium drifted silicon passing detector, and a NaI stopping detector.

The natural boron target contained 19.2% ^{10}B and 80.8% ^{11}B. The corrections for the presence of ^{10}B in the target were carried out by calculating the ^{10}B and ^{11}B cross sections with the Colorado pion optical potential model. Corrections were calculated at both 38.6 and 47.7 MeV using both global and best fit parameters. The ratio of ^{11}B cross sections to natural boron cross sections ranged from 0.99 to 1.08 from small to large scattering angles. This ^{10}B correction was also calculated with the MSU optical potential[2] with equivalent results.

Since the overall energy resolution of the experiment was 1 to 2 MeV, small corrections also had to be made for contributions from the first excited states of ^{11}B at 2.14 MeV and of ^{10}B at 0.72 MeV. Those corrections were obtained by calculating the inelastic cross sections in a collective-model framework using a coupled channel pion-nucleus computer code

CHOPIN with a value of the deformation parameter, β_2, of 0.25 for ^{11}B[3,4] and 0.67 for ^{10}B [5]. The inelastic cross section contributions were always less than 1% of the elastic cross sections.

The corrected ratios of the elastic cross sections of ^{12}C to ^{11}B are shown in Figs. B23 and B24. The uncertainties shown are a quadrature addition of statistical errors and the estimated error introduced by the correction for the presence of ^{10}B in the target.

The data were analyzed with the MSU and Colorado coordinate space and the Landau-Thomas[6] momentum space optical potential models. For the calculations with the Colorado and MSU potentials both global parameters, internally available in the programs, and best fit parameters were used. The best fit parameters were determined by fitting the 49.9 MeV π^+ on ^{12}C data[7] of Moinester et al. The quality of the fits to the Moinester data was excellent.

For all calculations the rms radii for the neutron matter distributions in ^{11}B and ^{12}C were set equal to the rms radius of the proton distribution in ^{12}C, 2.31 fm. When the finite proton size is folded in this is equivalent to an rms charge radius of 2.44 fm, a measured[8] value for ^{12}C. The cross section ratios were calculated for various proton radii individually for both the 38.6 MeV and 47.7 MeV data. The numerical results of these calculations are listed in table BII and a sample of the predicted cross section ratios displayed with the data in Figs. B23 and B24.

It can be seen in table BII that the agreement among the three optical model calculations is quite good at both 38.6 and 47.7 MeV. The results at 47.7 MeV produced, however, a proton radius that was generally about 0.03 fm smaller than the 38.6 MeV result. Although this difference

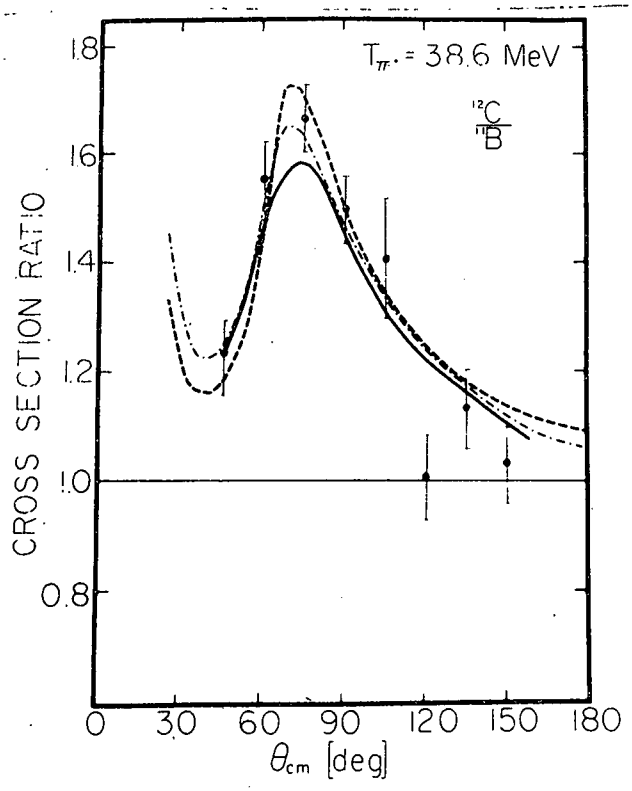

Fig. B23. The ratio of the elastic cross sections of 38.6 MeV π^+ on ^{12}C to ^{11}B. The dash-dot curve is a calculation using the MSU potential with the parameters determined by a best fit to 49.9 MeV ^{12}C data. The solid line is a calculation using the Colorado potential with the best fit parameter set. The dashed curve is a calculation using the momentum space program of Landau and Thomas using global parameters.

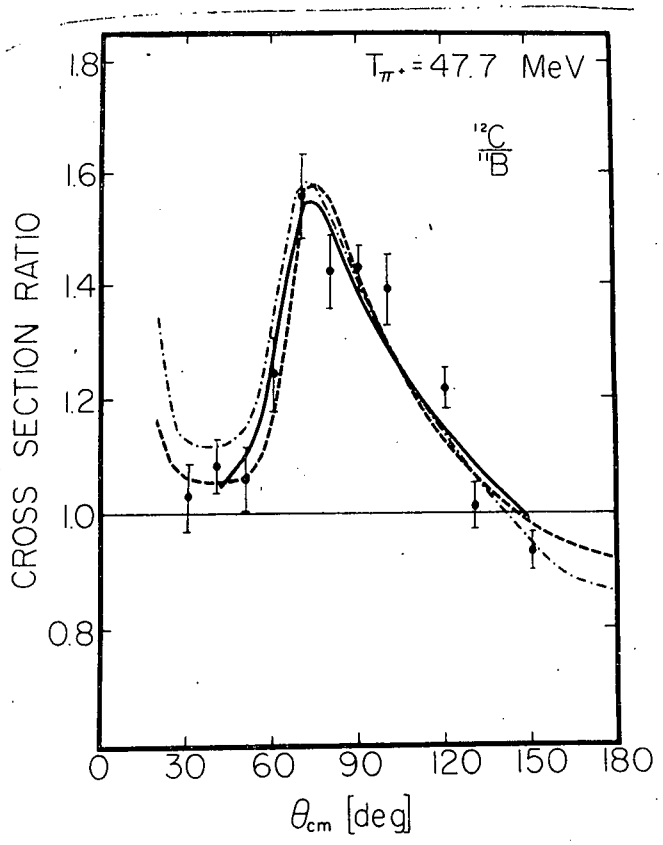

Fig. B24. The ratios of the elastic cross sections of 47.7 MeV π^+ on ^{12}C to ^{11}B. The curves shown are as explained in the caption to Fig. B23.

Table BII

Charge density rms radii (in fermis) for ^{11}B relative to a ^{12}C rms charge radius of 2.44 fm determined by various optical model calculations. The uncertainties shown were determined in the fitting procedure. The final uncertainty is just the standard deviation of the ten combined values.

Potential	38.6 MeV		47.7 MeV
Colo.- global	2.401±0.017		2.360±0.010
Colo. - best fit	2.365±0.022		2.349±0.010
Colo. weighted mean	2.385		2.355
Colo. overall		2.370	
MSU - global	2.391±0.034		2.344±0.016
MSU best fit	2.389±0.026		2.354±0.012
MSU weighted mean	2.390		2.350
MSU overall		2.370	
LT	2.380±0.010		2.350±0.005
Combined mean		2.358±0.021	
$\langle r_p^2 \rangle^{1/2}\ ^{12}C - \langle r_p^2 \rangle^{1/2}\ ^{11}B$		0.072±0.021	

is not significant beyond the experimental uncertainties, it suggests that a test of this point over a wider energy range would be of interest.

From table BII it can be seen that the difference in the rms charge radii of ^{12}C and ^{11}B was determined to be 0.072 fm with a standard deviation of 0.021 fm. Assuming the ^{12}C radius to be 2.44 fm this corresponds to a ^{11}B radius of 2.368±0.021 fm. Unfortunately, there is no electron scattering value as precise as this with which to compare. There are two electron scattering results[8], namely 2.42±0.12 and 2.37 fm. The results from the present experiment are completely compatible with these values, but it is clear that a more precise electron scattering measurement is needed. There have been two Hartree-Fock calculations completed by N. Auerbach[9] that relate to the difference between the ^{12}C and ^{11}B radii. These resulted in values of 0.045 and 0.072 fm, which are in reasonable agreement with the measured value from the present study. The most accurate measurements to date are the pionic x-ray studies by Beer *et al.*[10] which indicate a ^{12}C-^{11}B radius difference of 0.09±0.04 fm, which is in excellent agreement with our results.

In summary, this experiment demonstrates that low energy π^+ elastic scattering can determine proton matter distributions with respect to a reference nucleus in a rather precise way and that the result is insensitive to the details of the optical model calculations. The result of this experiment lends support to the conclusions of the previous experiment[1] involving the determination of the relative neutron radii using π^- elastic scattering.

---

1. R. R. Johnson *et al.*, Phys. Rev. Lett. 43 (1979) 844.
2. K. Stricker, H. McManus and J. Carr, Phys. Rev. C 19 (1979) 929.
3. O. Karban, J. Lowe, P. D. Greaves and V. Hnizdo, Nucl. Phys. A133 (1969) 255.
4. O. Aspelund *et al.*, Nucl. Phys. A231 (1974) 115.
5. R. de Swiniarski, F. G. Resmini, C. Glashausser and A. D. Bacher, Helv. Phys. Acta 49 (1976) 227.
6. R. H. Landau and A. W. Thomas, Nucl. Phys. A302 (1978) 461.
7. M. A. Moinester *et al.*, Phys. Rev. C 18 (1978) 2678.
8. C. W. de Jager *et al.*, At. Dat. and Nucl. Dat. Tables 14 (1974) 479.
9. N. Auerbach, private communication.
10. G. A. Beer *et al.* Contribution 1B27 to Eighth International Conference on High Energy Physics and Nuclear Structure, Vancouver, B. C., Canada, August, 1979, and A. Olin, private communication.

12. Elastic Scattering of 13.9 MeV Positive Pions from ^{12}C - T. G. Masterson (Colorado); D. R. Gill, K. L. Erdman, E. W. Blackmore (TRIUMF); W. Gyles, B. M. Barnett, C. Oram, R. R. Johnson (U. B. C.); N. Grion (Trieste).

The low energy (0 - 100 MeV) region is the testing ground for optical potential theories of pion-nucleus scattering. These theories incorporate pion-nucleon scattering parameters into a multiple scattering framework.[1-3] Absorption parameters have been empirically determined both from pionic atom data and from 50 MeV elastic scattering data.[4,5] They differ by about a factor of two. The lowest-energy measurements[6] had been made at approximately 30 MeV. The present scattering experiment was carried out on ^{12}C at 13.9 MeV to bridge the energy gap between stopped pions and 30 MeV and to look at the absorption parameters.

The experiment was performed on the TRIUMF M13 channel which had a 10^5 π^+ sec^{-1} flux at T_π=15 MeV when 20 μA of protons were delivered to the production target. The π^+:μ^+:e^+ composition of this beam was, respectively, 55:24:21 percent. The scattering apparatus, similar to that used previously,[7] is shown schematically in Fig. B22. Each scattering arm consisted of a sodium iodide (NaI) counter preceded by a 19.5 mm radius x 2 mm thick silicon passing detector which in turn was preceded by a 1 mm thick plastic (NE102) direction-defining scintillation counter.

The overall resolution of this detection system, including the contribution from the channel resolution, was 1-2 MeV FWHM for these experiments. Any pions inelastically scattered from the first excited state of ^{12}C at 4.4 MeV were, therefore, well separated from the elastically scattered pions. Very little evidence of inelastically scattered pions was seen in our spectra. This was due to three circumstances: First, these pions would have had an outgoing energy of about 9.5 MeV and therefore a substantial fraction would be stopped or scattered before reaching the NaI detector, second, a large fraction decayed in the telescope, and, third, the inelastic cross section is small at these energies. The target was 0.1147 gm/cm^2 natural carbon. The pion flux was monitored with an ion chamber and with two plastic scintillators, S1 and S2, in the beam downstream of the scattering target. The use of the Si(Li)-NaI counter combination gave excellent particle identification, as seen in the two-dimensional spectrum shown in Fig. B25, and allowed separation of the scattered pions from the in-flight decay muons at forward angles.

The 13.9 MeV π^+-^{12}C elastic differential cross section is shown in Fig. B26. The error bars are statistical only. The estimate of the systematic error is ± 15%. In addition, the in-flight decay muons cause further uncertainty for the small angle data where the background increased as illustrated in Fig. B25. In the worst case the pion peak-to-valley separation in the E-ΔE spectrum was 4:1. These muons also introduced a large dead time effect (30%) that was corrected for in the 30°, 35°, and 40° data. The overall systematic error for the 30°, 35°, and 40° data points is estimated at ± 25%.

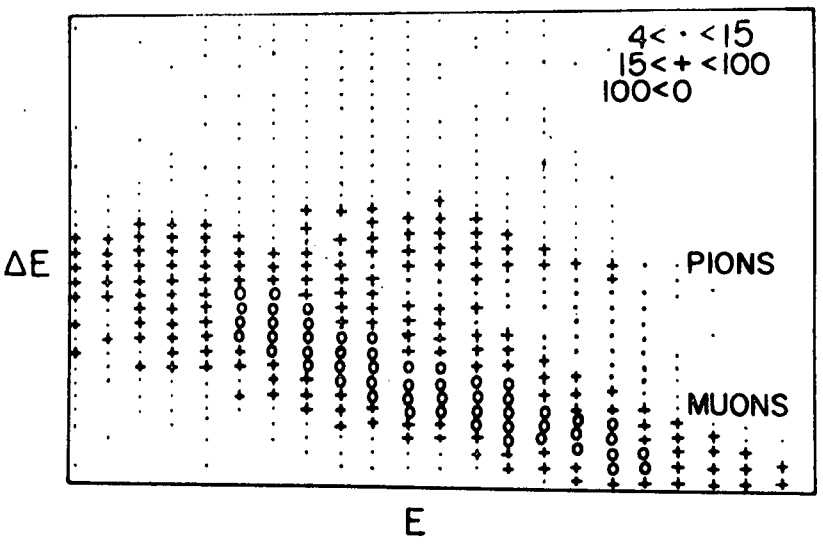

Fig. B25. E vs ΔE spectrum for scattered particles, clearly showing separation between pions and muons.

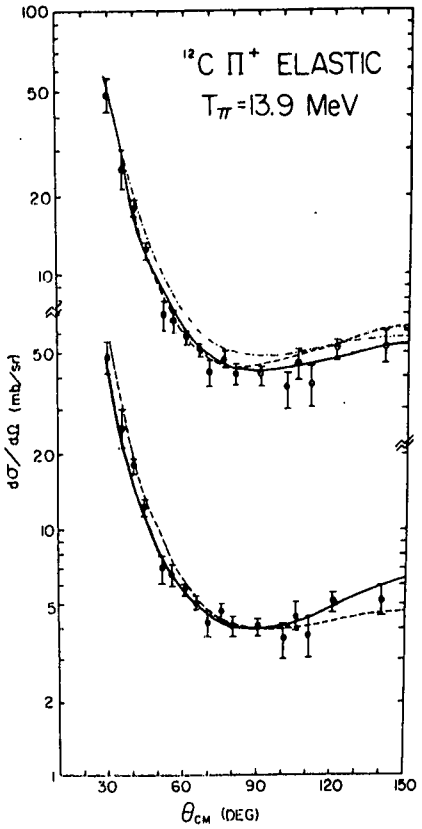

Fig. B26. Top: 13.9 MeV π^+ ^{12}C data compared with calculations with the MSU potential. Solid curve - Set 'A' from ref 8; dashed curve - same without absorption; dash-dot curve - set 1 from ref 1. Bottom: 13.9 MeV π^+ ^{12}C data compared with calculations with the Colorado potential. Solid curve - best fit; dashed curve - standard parameters.

The solid curve in Fig. B26 (top) is the result of a calculation with the Michigan State (MSU) potential using their Set 1 parameters.[1] The dashed curve in Fig. B26 (top) was derived using the same potential and parameter Set A from their latest report.[8] The latter result shows improved agreement with the data. The dot-dash curve in Fig. B26 (top) is the result of calculation again with the MSU potential using the parameter Set A6 with the absorption parameters B_0 and C_0 set to zero. This indicates that pion absorption is necessary in low energy pion optical potentials to reproduce the shape of the angular distribution. The bottom half of the same figure compares the data with calculations made with the Colorado potential of Rost et al[2] using their standard set of parameters (dashed curve). The solid curve was obtained by allowing the absorption parameters to vary to obtain a best fit. The fit is qualitatively improved but the absorption parameters are not statistically well determined by this procedure. The ratio Re B_0/Im B_0 is approximately -0.4 ± 0.3 while pionic atom studies[9] prefer a value of -1 and higher-energy scattering studies suggest a ratio[4] closer to -2. Additional low energy studies will be required to examine the systematics of the energy dependence of the absorption parameters.

In conclusion, the 13.9 MeV data are well represented by optical potential calculations. The absorption parameters are clearly different from both higher-energy and pionic atom data although more data are required to determine their energy dependences.

---

1 K. Stricker, H. McManers, and T. Carr, Phys. Rev C19 (1979) 929.
2 E. Rost, private communication. See also N. J. DiGiacomo, A. S. Rosenthal, E. Rost, and D. A. Sparrow, Phys. Lett. 66B (1977) 421.
3 R. H. Landau and A. W. Thomas, Nucl. Phys. 302 (1978) 461.
4 A. Rosenthal, Thesis, Univ. of Colo. 1978 (Unpublished).
5 A. W. Thomas and R. H. Landau, to be published in Phys. Rev. C.
6 R. R. Johnson et al., Phys. Lett. 78B (1978) 560.
7 B. M. Barnett et al., (submitted to Phys. Lett.).
8 K. Stricker, J. Carr, and H. McManus, preprint.
9 J. Hufner, Phys. Rev. 21 (1975) 1.

C. Apparatus and Facility Development

1. Accelerator Development Studies - P. A. Smith, M. Covey, M. Gordon, D. H. Haynes, D. A. Lind, J. Magyar, R. Rodenburg, W. R. Smythe, R. A. Stern, R. C. Weiss, T. Woolf, C. D. Zafiratos

a. Introduction

Approximately one year ago we requested research and development funds from the DOE to begin research on the production of intense pulsed beams. The motivation for this research lay in the need to have a long flight path for high resolution neutron time-of-flight spectroscopy, which requires both high beam intensity and a greatly reduced duty factor. We proposed to investigate two methods of increasing the charge per beam burst while decreasing the duty factor.

One method involves manipulation of the external beam. The duty-factor reduction can be accomplished without intensity loss by constructing a storage ring in such a way that the storage orbit period is a multiple of the period between beam bursts. Thus every injected burst falls physically within a stored bunch in both space and time. The beam is extracted from the ring at a reduced rate.

A second possible approach involves manipulation of the ion source. We have noted in the past that under certain conditions a pulsed ion source may produce nearly as much average external beam as an unpulsed source. We proposed that it might be possible to optimize this effect if we could understand it. In any event, research into improved source brightness would attack the problem of raising the beam intensity. We proposed to study the physics of the ion source through a collaboration with the plasma physics group in the Physics Department by constructing a scale-model cyclotron and instrumenting this ion source test facility with the necessary plasma diagnostic devices.

Our original proposal was initially funded for six months' work and expanded subsequently through the next year. We have now started the storage ring study. The model cyclotron is in operation and measurements of the source plasma characteristics are under way.

An increase in pulsed-beam capability required a study of the configuration of the present cyclotron so the program was expanded to include improvements of the cyclotron as well. There are a number of motivations for this expansion which may be summarized as follows:

1) Improvement of beam quality so that the energy and time widths of our extracted beam can be reduced.

2) Improvement of the extraction efficiency so that more intense beams can be produced.

3) Possibly some modest increase in maximum energy.

4) Beam line instrumentation and controls are almost 20 years old. Instrumentation for longitudinal phase-space measurement and control is needed. Hence we are making improvements in the instrumentation for these changes as well as for improved ease of operation.

It has taken some time to build up momentum for this development activity. The staff has expanded by two technicians with M. S. degrees in physics. The new electrical engineer has devoted most of the last year to this project. In addition, we have been fortunate enough to obtain a number of bright undergraduate students from Physics and Engineering who have been an immense help during this past summer.

b. Storage Ring

i. The General Concept

Standard techniques for increasing the time between beam bursts on target involve removing pulses from the beam so that an n-fold increase in the time between bursts also results in an n-fold decrease in the current on target. If a reduction of the duty factor of more than 5:1 is required by an experiment, the current on target will generally be too low. Certainly a reduction in duty factor of 100:1 is out of the question. In concept at least, it is possible to avoid most of the current loss by constructing a storage ring, with an orbital period which is an integral multiple of the period between bursts in the cyclotron beam.

An outline of a possible ring that could accomplish "pulse stacking" is shown in Fig. C1. The ring consists of a section of an open-sector cyclotron, including trimming, so that the orbit is isochronous. The size of the ring is determined by a number of considerations: First, the orbit circumference must be an integral multiple of the circumference of the cyclotron that produced the beam. Second, the magnetic field for the most rigid beam must be reasonable. Third, the ring must be big enough to make injection and extraction of the beam possible.

The second consideration rules out storing only a single burst in the storage orbit since the average magnetic field in the ring would have to equal that of the cyclotron, which is not an open-sector machine. Thus the storage orbit has to have four or more beam bursts circulating. This is no problem as long as the ratio of the injection frequency to extraction frequency is not a multiple of four.

Injection into the ring cannot be accomplished simply, because we require the incident burst to join with the phase space of the circulating pulse. This cannot be done with normal conservative forces, as indicated by Liouville's theorem. The solution that is discussed in more detail below is to accelerate negative or partially stripped beams which can be stripped at a point where the circulating beam is also passing through the stripper. Possible entrance paths are indicated in Fig. C1.

Extraction can be accomplished with a pulsed extractor. We are investigating both electric and magnetic extraction systems. The requirements on the extraction system push the state of the art of high power electronics. The pulses must have a short duration (≈50 ns) so that the leading and trailing beam buckets pass unaffected. The repetition rate should be as high as a few hundred kHz. We estimate that a practical extraction design will require an average of 20 kW of power. The extraction will be discussed below in more detail.

Finally we must address the question, "What limits the storage time?" Practically, it is probably the repeated passage through the stripper. Nonetheless, we wish to investigate the space charge limit: "What is the maximum amount of charge that can be put in a single burst?"

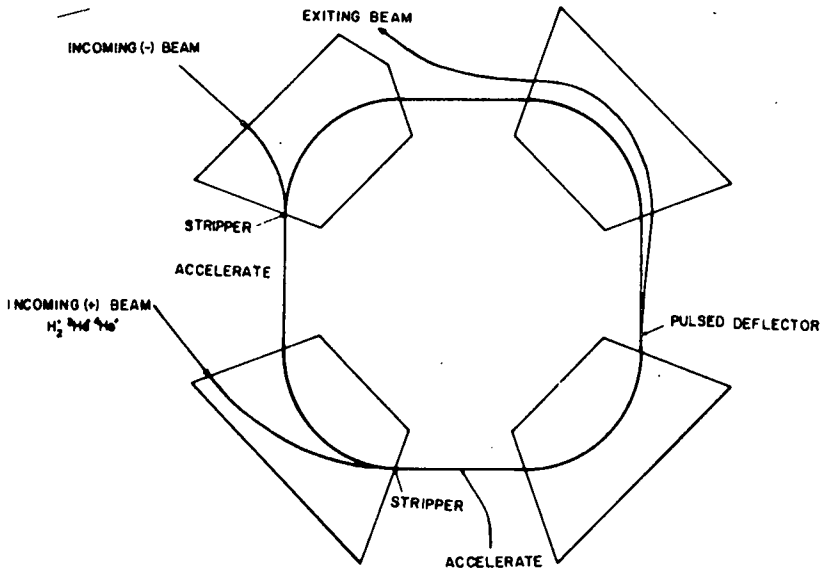

Fig. C1. A schematic layout of a 4-sector storage ring showing possible orbits for stripping negative or positive ion beams into ring.

ii. Orbit Codes for an Open Sector Ring

A FORTRAN program for an open-sector magnet ring has been written and tested. The simple mathematics for describing the orbit radius may be found in a paper by Gordon[1], where a hard edge approximation is used for the field. The orbit optics are also calculated by the program using a first-order transfer-matrix approach as suggested by Gordon[1] or Courant and Snyder[2]. The transfer matrices, including a soft-edge approximation, were taken from the description of the program TRANSPORT[3], by Brown and Howry. The orbit program allows us to determine the size of a ring for an orbit at a specific cyclotron frequency, number of storage pulses and magnet angle. In addition, the maximum magnetic field is determined. The orbit optics may be calculated, yielding focussing frequencies and phase-space ellipse parameters. Resulting graphs for ν_x vs. ν_z for the IUCF and VICKSI rings are compared for various softness parameters in Fig. C2.

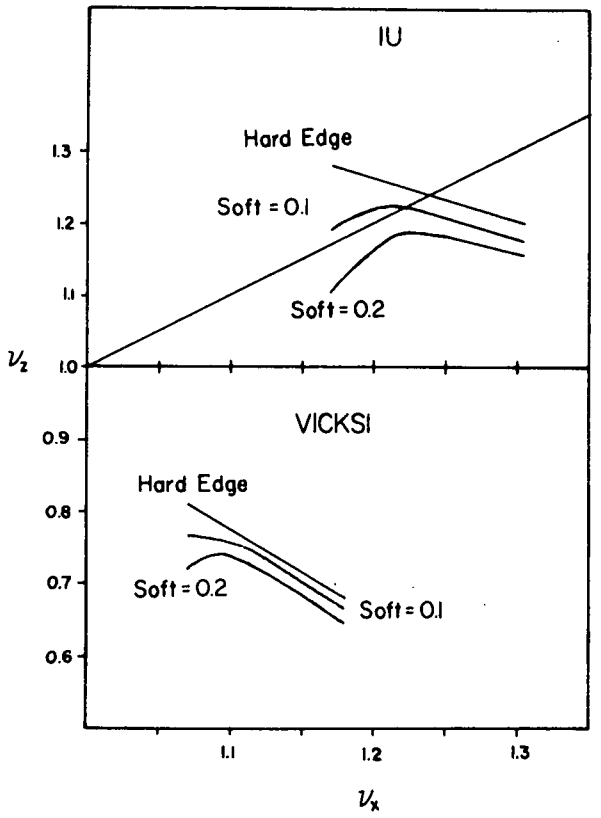

Fig. C2. Graphs of ν_x and ν_z for IUCF and VICKSI rings calculated for different edge-softness parameters.

The first-order matrix approach was further tested by writing another program, where the transfer matrices were calculated using the formulae for a general magnetic field given by Brown and Howry.[3] A field map for the IUCF injector cyclotron was provided by R. Pollack for testing. In order

to reduce the computing problems, we Fourier-analyzed this map and used the expansion coefficients in the code, instead of the actual field. The resulting values of ν_x and ν_z are compared with the hard- and soft-edge results from the code and shown in Table IIC-I. The discrepancy in x is probably due to the Fourier analysis, which results in fluctuating field derivatives that are not present in the real field. The general field code can also be used for studies of our cyclotron.

Table IIC-I

Various calculations of focussing frequencies for Indiana University Cyclotron (75 MeV protons)

Approximation	ν_x	ν_z
Exact Numerical	1.17	1.14
First Order Matrix	1.19	1.13
Hard Edge	1.17	1.28
Soft Edge (0.22)	1.17	1.14

[1] M. M. Gordon, Annals of Physics 50 (1968) 571.
[2] E. D. Courant and H. S. Snyder, Annals of Physics 3 (1958) 1.
[3] K. L. Brown and S. K. Howry, SLAC Rept. 91 (1970)

iii. Injection: Effects of Stripping

The cyclotron beam is to be injected into the ring by passing the stored burst and the incident burst simultaneously through a thin gas or foil stripper. The cyclotron beam particle must be a negative or partially charged ion in order to accomplish this stripping. Each passage through the stripper enlarges the stored beam burst and also slows the burst. The particle energy may be maintained by a small acceleration on each passage, but the gradual blow up of the beam will represent an upper limit on the storage time.

Consider a beam which occupies an area A in either the radial or vertical phase-space plane. If a first-order transfer-matrix approach is used, the incident beam will be contained in an ellipse

$$\gamma x^2 + 2\alpha xx' + \beta x'^2 = A/\pi = W$$

(See Courant and Snyder, for example) where x is either the horizontal or vertical displacement from the central orbit and x' is p_x/p. The natural units to use are mm and mr. After passing through the foil, the ellipse has been stretched in the x' direction by the multiple scattering.

A method of analysis which leads to an analytic expression starts by assuming a Gaussian function for the density in the transverse phase space. This function can be folded with the function for multiple scattering on each passage to generate a new density distribution of Gaussian form as shown in Fig. C3. This phase ellipse is transported by the ring so its behavior is determined by the periodic boundary conditions.

A computer program has been written which repeatedly performs the calculation described above. In particular, the storage ring application requires answering the question: "How many turns in the ring (or passages through the stripper) occur before the phase space area increases beyond a manageable point?" Fig. C4 shows graphs of storage time (number of turns) vs. particle energy for both the radial and vertical phase-space ellipses which were initially

$$(3.23)x^2 + 2(1.252)xx' + (.794)x'^2 = A/\pi$$

$$(1.35)z^2 + 2(.147)zz' + (.801)z'^2 = A/\pi$$

The initial phase space area was 10 mm-mr; the curves represent a doubling of this area. If the area is allowed to triple, the lifetime doubles.

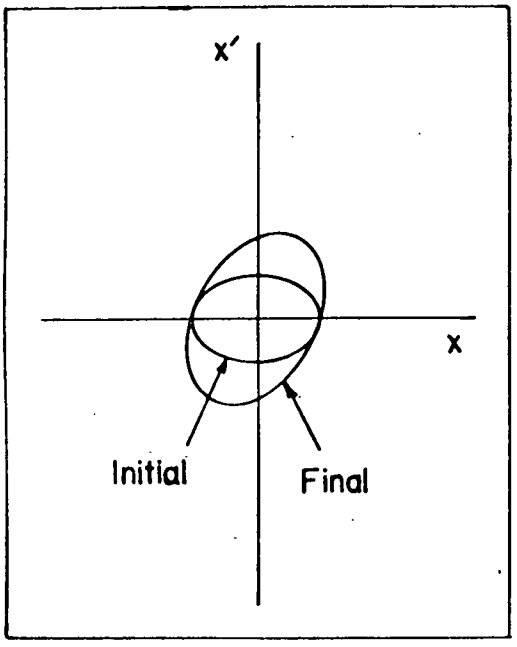

Fig. C3. An incident phase ellipse is distorted by multiple scattering on passage through the stripping foil to form the final ellipse.

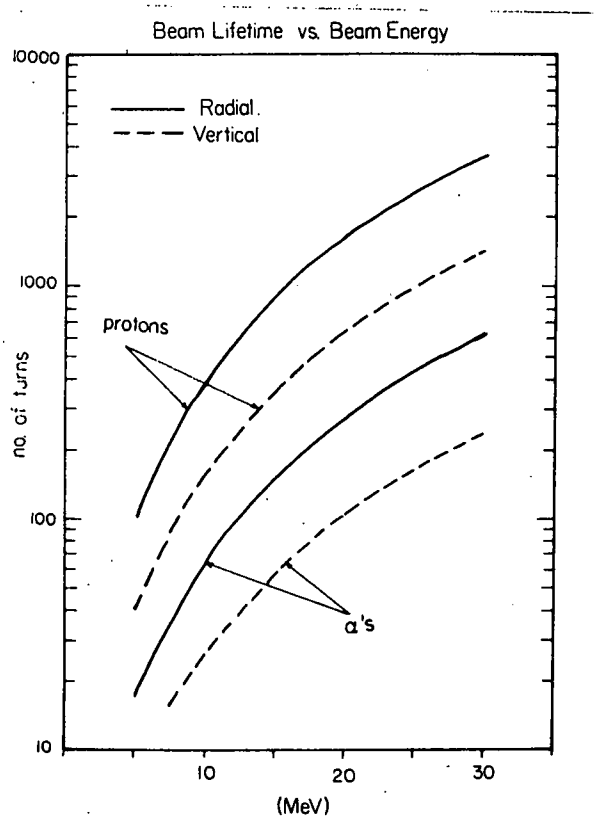

Fig. C4. Beam lifetime measured in number of passages through stripper foil before the initial phase ellipse doubles in area. The stripping foil is 5 $\mu g/cm^2$ carbon. Curves are given for protons and alpha particles as a function of energy.

iv. Extraction from the Storage Ring

The constraints on the extraction system are considerable. The extraction pulse must be of short enough duration to affect only one beam burst. The power delivered must be sufficient to deflect the pulse to separate completely the extraction orbit from the storage orbit. Once this separation is large enough, the extraction can be completed with an electrostatic deflector in combination with small magnets.

The amount of deflection (and hence the power) to extract the beam can be controlled with the size of the ring. The larger the ring, the smaller the required deflection angle. However, the cost of the ring increases dramatically with the size because the floor space and iron volume increase. Thus there is a trade-off between cost and deflection capability.

Our estimate for the power needed for extraction from the smallest possible 25 MeV proton ring is about 15 kW if electrostatic extraction is used. Such high power pulsers have been developed for fusion and high-power pulsed radar. However, none of these pulsers will run at the re-

quired repetition of ≈100 kHz. English Electric Valve has informed us that they make a special thyratron that can deliver 16 kV at 200 kHz with appropriate pulse characteristics. Using this tube, it may be possible to perform the extraction.

Magnetic extraction, using ferrites, may also be possible. This changes the power supply and switching requirements to low voltage and high current. We are just beginning to investigate this possibility.

v. Storage Ring Summary

The final decision on design strategy for the storage ring has been modified by conflicting design objectives and feasibility limits. Injection by stripping will permit storage of 27 MeV protons, 18 MeV deuterons, or 9 MeV ^{4}He. For ^{3}He and ^{4}He, energies are too low to be usable without a booster accelerator. Furthermore, extraction by beam pulsing is not assured. Alternative schemes of filling a ring and using time dependent r. f. fields to compress in phase and focus as necessary are also being considered. The final configuration should be such that the prototype device if built and tested can be used for research with the present machine.

c. The Mini-Cyclotron and Ion Source Testing

i. Construction of the Mini-Cyclotron

Our miniature cyclotron is now in use for ion source testing. This testing has been proceeding during the past summer with frequent periods of further instrumentation and improvements which will be described below. A picture of the apparatus as it currently exists is shown in Fig. C5.

At this time last year, the cyclotron consisted of a magnet, which previously was the model magnet for our large cyclotron, and a ten-inch diffusion pump. A copy of the hooded arc source used for years in this laboratory was constructed. The source became operational at limited power and stability after an old surplus power supply was modified to provide current and bias for the filament. Initial testing of plasma diagnostic equipment was carried out in this manner. Commercial power supplies with sufficient power and stability are now operational. A small r. f. system with a half-dee and puller has been installed. This r. f. system was reversibly adapted from the r. f. amplifier used for deflecting beam pulses outside of our big cyclotron. We will run with this small system, which provides up to 15 kV of accelerating potential at frequencies between 2 and 5 MHz until our full-size system, that will deliver 75 kV at 15 MHz, is completed. The large r. f. amplifier and support power supplies are presently being constructed or have been finished. Once the full power r. f. has been installed, construction will be completed so that measurements can

be carried on without interruption. As a part of this, a unique resonant dee and cavity design was developed by W. R. Smythe, as described below. In addition, a differential beam probe and Faraday cup have been installed. With these, actual cyclotron operation has been observed, and first-orbit currents of 40 microamps measured.

ii. Two-Turn Radio Frequency Cavity

A new type of compact r. f. cavity has been conceived for the ion source test facility. This cavity is designed to form a resonant circuit with the test dee so that it can be operated at up to 75 kV peak at a frequency of 15 MHz, thus duplicating the fields in the cyclotron at a frequency of interest. It also provides a rigid insulator-free support for the dee.

The cavity is best described as a two-turn coaxial cavity in which the current-carrying surface passes through itself to achieve the two-turn character, which greatly reduces the size of the cavity. The "passing through itself" is accomplished by means of posts passing through holes in the surface. At most points within the cavity, the voltage across gaps is approximately one half of the dee voltage.

Solutions of the electromagnetic wave equation in the cavity have been constructed by matching solutions for coaxial regions and solutions for radial regions. A computer program has been written employing these solutions to calculate the cavity impedance as a function of frequency. It also calculates voltage and current distributions and the power dissipated.

By use of the computer program, a relatively small cavity (60 cm diameter by 90 cm long) has been designed with the desired properties. The r. f. copper loss in the cavity is about 6 kW. This compact cavity design appears to have other useful applications, such as compact cyclotrons and beam bunchers. Investigation of tuning possibilities using a movable short indicates that a tuning range approaching 3:1 is possible.

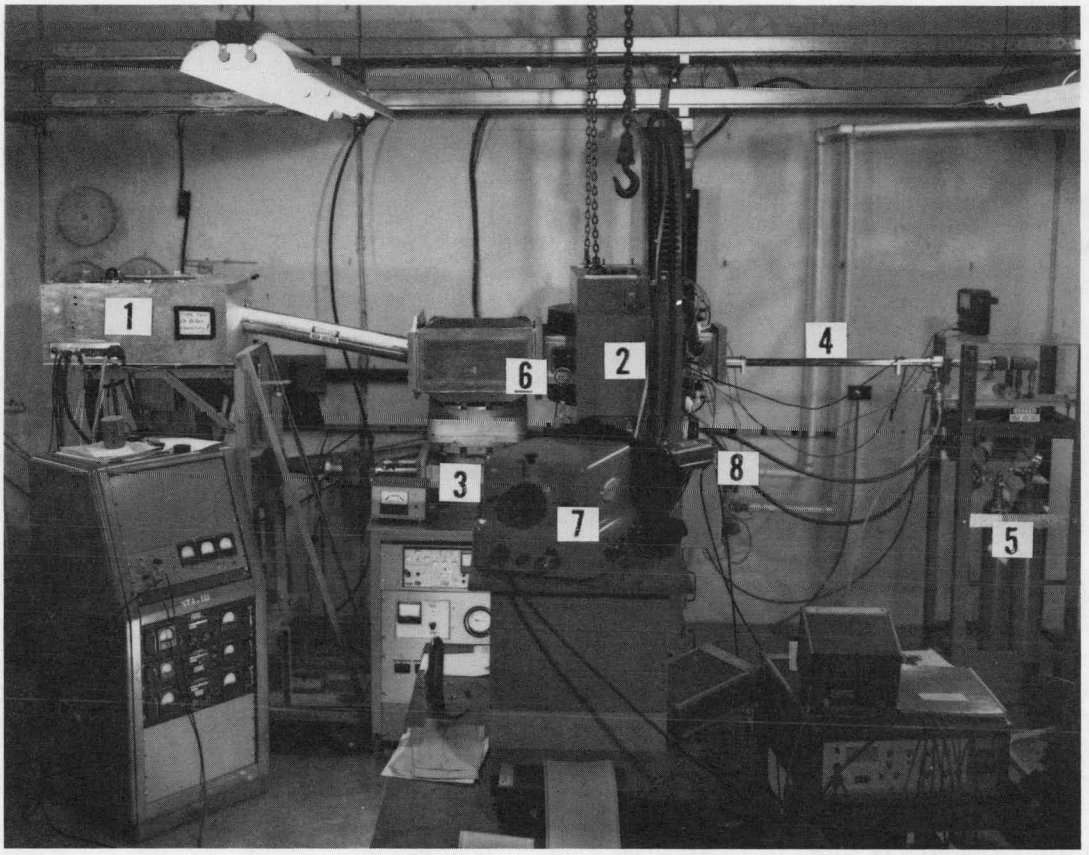

Fig. C5. The Miniature Cyclotron / Ion Source Test Facility

1. r. f. system
2. Magnet (12" diameter pole tip)
3. Vacuum system (w/ controls below)
4. Ion source support / supply rod (source inside vacuum)
5. Gas handling system
6. Lens 1
7. Monochromator
8. Photomultiplier tube

iii. Ion Source Development

We have initiated a study of the process through which the r. f. field extracts ions from a typical cyclotron source with a view to increasing beam current and upgrading source efficiency. The impetus for this work stems from our observations that, when beam extraction was repetitively suppressed over a number of r. f. cycles, the average beam current remained nearly constant, instead of decreasing. This indicates that sources are capable of much higher instantaneous beam currents than are delivered on the average. It implies that, with proper understanding of the interaction between r. f. field and source, more efficient operation should be possible.

In our view, the underlying physical process is the penetration of the r. f. field into the source plasma. While particle acceleration requires the r. f. frequency ω to be close to the cyclotron frequency ω_{ci}, a plasma is cut-off at $\omega/\omega_{ci}=1$, i.e., a thin sheath is present around the plasma which prevents penetration by electric fields (hence the term "cut-off"). Only the sheath of the source is accessible to the field as a source of particles. To increase penetration of the r. f. field into the plasma, coupling to a normal mode is required. This is feasible in the cyclotron geometry (r. f. field perpendicular to the magnetic field) at values of ω/ω_{ci} only slightly above unity, for instance via a small decrease in the local magnetic field in the immediate vicinity of the source. Under such conditions, field penetration and crossed-field ion-beam extraction have been recently observed. These and similar plasma effects may enhance beam extraction from accelerator sources.

To exploit these possibilities, a program of remote, non-perturbing diagnostic measurements was set up. The mini-cyclotron described above was arranged so the dee and vacuum chamber have ports and windows oriented so that the source plasma can be observed with low-f number optics. A mirror-lens arrangement projects an image of the source onto the slits of a monochromator. Optical emission from the source, or from a region within it, can now be spectrally resolved and detected by a fast photomultiplier tube. See Fig. C6. Real time instrumentation (box-car averager and phase-lock detector) process the light signal. Additional instrumentation consists of r. f. voltage pick-off from the dee and a differential beam probe and Faraday cup, located next to the dee.

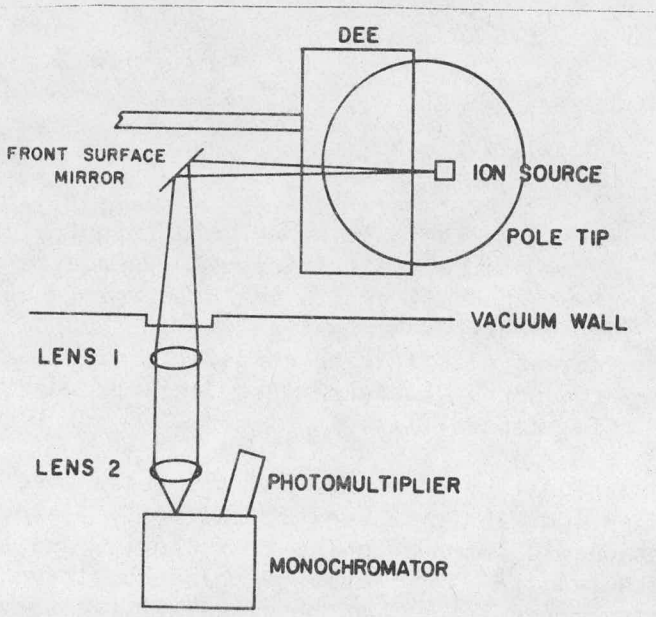

Fig. C6. Optics diagram (not to scale)

Initial tests were concerned with establishing the relation between optical line emission and ion density within the source. In hydrogen arcs this is indirect: line emission from neutrals is caused by electron collisions. Since ion and electron densities are nearly equal, variations in light and ion density should correspond very closely. At fixed arc voltage and gas pressure, the arc current J is proportional to the electron density. Thus the relationship between line emission intensity, I, and arc current will be the same as between line emission and ion density, n_i. A typical result, for the Balmer beta line at 4863 Å, is shown in Fig. C7.

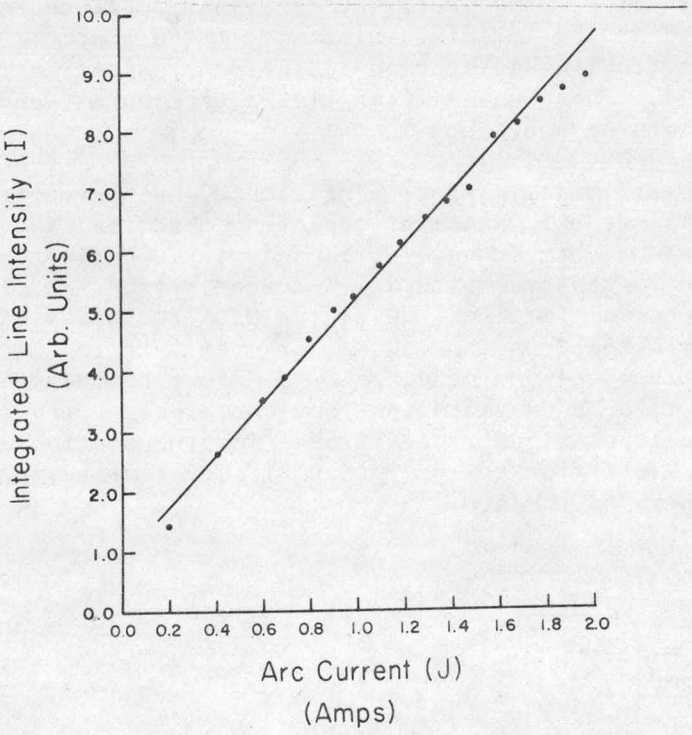

Fig. C7. Source arc optical emission (at 4863 Å) versus arc current.

This nearly linear dependence indicates that, under typical operating conditions, electrons in the source are sufficiently energetic to dissociate the H_2 molecule and simultaneously excite the atom. It should be noted that, to eliminate the effects of bremsstrahlung, the monochromator was operated with the narrowest slit setting compatible with the line width. Extensive tests were conducted to ensure that Stark broadening of the line was negligible for this slit setting.

Using the proportionality between I and n_i, tests were next conducted on the changes in ion density caused by the r. f. field. A 1 kHz square-wave modulation was imposed on the r. f. power, and the corresponding component extracted from I by means of phase-sensitive techniques. A number of significant observations was obtained. First, at $\omega/\omega_{ci} \approx 1$, the amount of light emission decreased during the portion of the 1000 Hz cycle when the r. f. power was on (Fig. c8). The decrease in I, and hence in n_i, was proportional to the average beam current. This indicates that, as expected, when the plasma is cut off the r. f. field can only drain charge from the sheath, leading to the observed decrease in the bulk density.

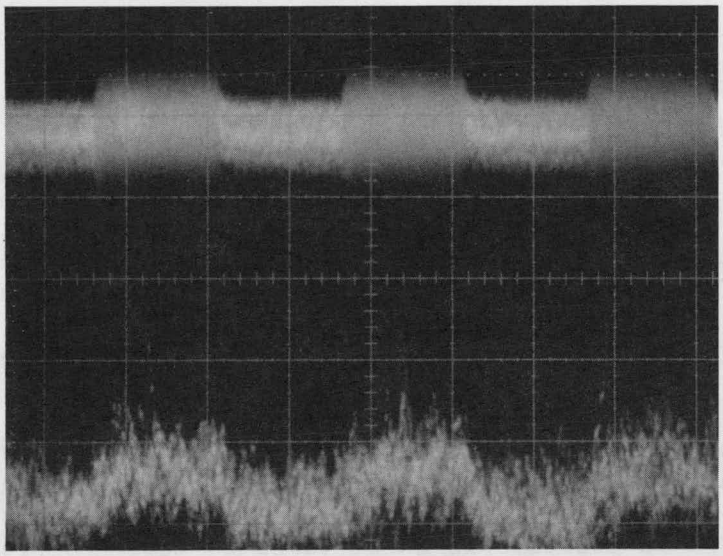

Fig. C8. Light emission changes during r. f. power pulses.
Horizontal scale: 0.5 msec/division.
Top trace: r. f. power, showing modulation.
Bottom trace: Photomultiplier signal output (note: increasing light corresponds to downward deflection of trace).

Secondly, at $\omega/\omega_{ci} \approx 2$, phase reversal was observed, i.e., I increased when the r. f. power was on. This corresponds to the expected penetration of the r. f. field into the bulk plasma, with consequent plasma heating leading to stronger atomic excitation. Third, preliminary tests indicate that light modulation during an individual r. f. cycle (i.e. on a time scale of the order of 100 nsec.) occurs under these conditions. This enables us to discriminate between density modulation (expected in normal-mode excitation) and macroscopic density increase resulting from excess ionization due to the r. f. field.

Additional measurements include detailed spectroscopy of the arc, showing several lines which exhibit modulation by the r. f. field, as above. Comparing intensity ratios of several lines should enable the electron temperature and its changes due to r. f. field penetration to be determined. Preliminary tests on helium arcs have also been carried out. Here, changes in ion density can be measured directly from the intensity of ionic lines.

In summary, a complete source diagnostic experiment has been constructed and brought into operation. Systematic, quantitative measurements have been performed and show that the details of r. f. field and source interac-

tions can be extracted. Our physical concepts appear to be confirmed, suggesting that understanding of the processes and their control can be achieved.

d. The 52" Cyclotron Development

i. Magnetic Field Analysis

The magnetic field data obtained in 1962 have been reanalyzed. These data consist of field maps of the main field at 7.5, 10.0, and 13.5 kG center fields and maps of trim coil excitations at each main field. All the data were Fourier analyzed with a program which allows for very rapid reduction of the data.

The results for the reliable data, which do not include the center region, are shown below in Figs. C9, C10, and C11. The average main field graph (Fig. C9) shows that the field decreases outside of 48 cm for the 13.5 kG field. This decrease is quite large so that isochronous acceleration cannot be maintained to 60 cm, which is the extraction radius. The magnitude of the fourth harmonic given in Fig. C10 reaches a maximum of about 30%. The difference produced in the average field by the trim coils indicates the effect of each trim coil as shown in Fig. C11. These results are consistent with those obtained in 1962.

The purpose of carrying out this analysis was to study the trimming of our field. A computer program has been written which uses the above data to calculate trim-coil currents that produce an isochronous field. These currents can be translated into potentiometer settings on the cyclotron console. The code works by producing a least squares fit to an ideal isochronous field calculated with a formula given by Hagedoorn and Verster.[1]

The results for protons in the 10 kG field are given in Table IIC-II. All the currents are well below the maximum possible. The largest difference between the ideal field and the calculated field between 20 cm and 60 cm is 2 gauss.

As expected, the program indicates that the 13.5 kG field cannot be made isochronous for protons. It is reasonable for alphas, however.

The data are not sufficient to carry out a program of providing computer-calculated tunes for all particles at all energies. There are no reliable central-region data so that the whole acceleration cycle can be studied. New data should be obtained in the near future so that we may completely analyze the operation of our cyclotron with the objective of improved operation for all particles and energies.

---

[1] H. L. Hagedoorn and N. F. Verster, Nucl. Instr. and Methods 18,19 (1962) 201.

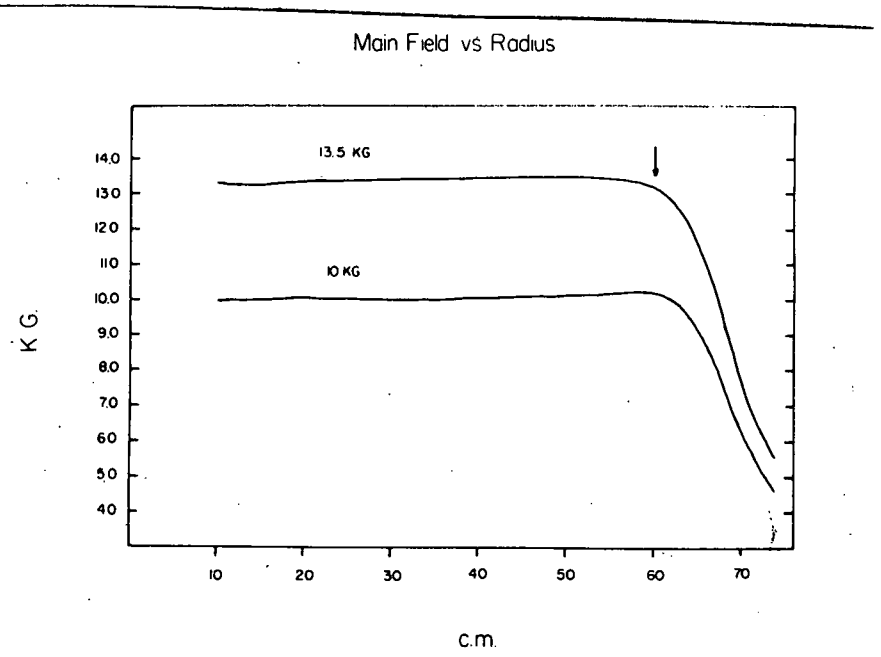

Fig. C9. Mean magnetic field versus radius for central fields, of 10 and 13.5 kG respectively. Arrow shows nominal extraction radius.

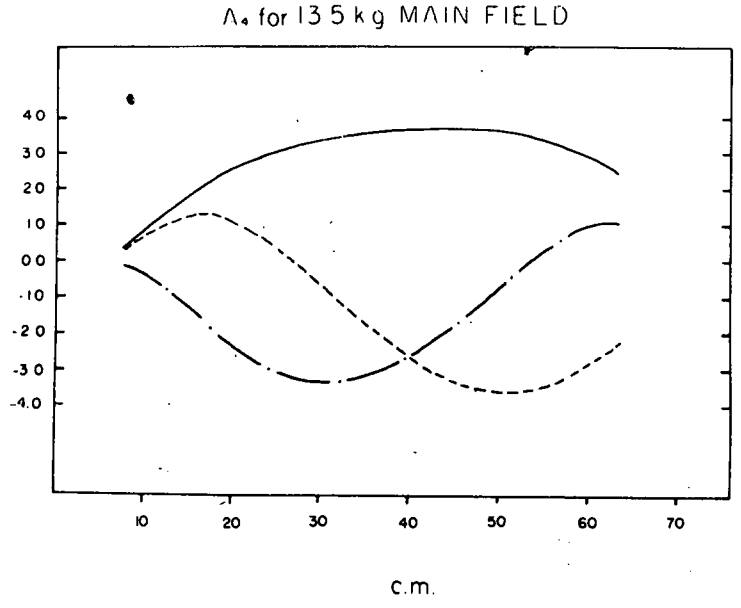

Fig. C10. Main magnetic field A_4 harmonic component versus radius. Amplitudes are in kG. Solid curve is amplitude. The two dashed curves represent the sine and cosine components.

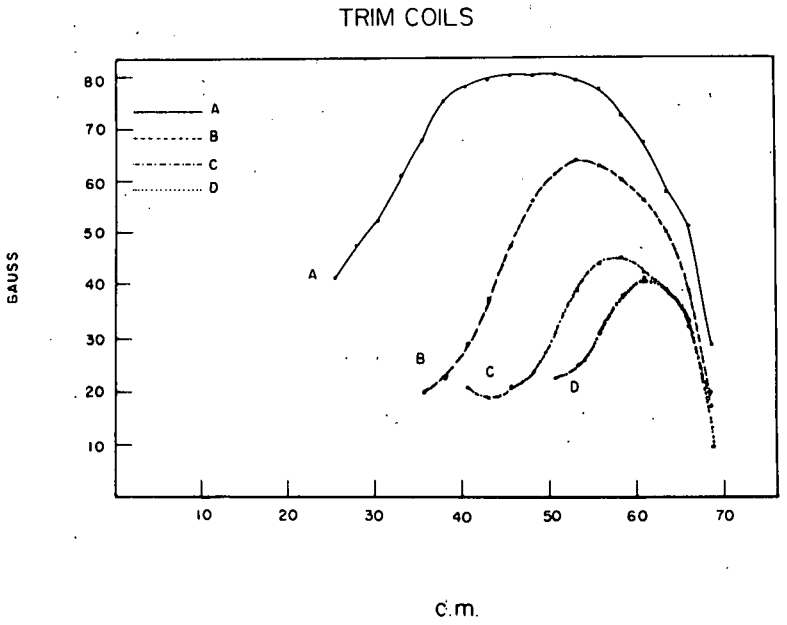

Fig. C11. A_0 components of trim coils as a function of radius for 150 amp excitation.

Table IIC-II

Trim coil currents for protons in 10 kG field

Coil	Current (Amperes)
A	130.0
B	52.1
C	104.0
D	242.9

ii. Magnetic Field Measurement

By the end of 1980 a complete remap of fields in the machine should be obtained. These data should allow us to understand completely the operation of the cyclotron and determine methods of shimming the field for improved operation. The cyclotron will have to be shut down for a period of 6 weeks.

We are currently designing and testing an instrument which consists of an arm that will rotate about the center of the cyclotron. This arm will contain 25 flip coils which will be flipped through 180° precisely. Each flip coil will have its own integrator. The 25 integrators will be multiplexed through an ADC. The system is quite similar to those used at Oak Ridge[1] and MSU.[2]

Since previous use of flip coil systems has suffered from temperature sensitivity, making a one part in 10^{-4} measurement difficult, we are paying careful attention to the thermal properties of the coil materials, integrating capacitors and operational amplifier units.

The mechanism for driving the sensor arm will be a modification of the large gear used in 1962. A stepping motor, placed outside the magnetic field, will drive a shaft and worm gear which in turn will move the large gear and platter.

---

[1] S. W. Mosko, E. D. Hudson, R. S. Lord, D. C. Hensley, and J. A. Biggerstaff, IEEE Transactions on Nuclear Science NS-24 (June 1977), 1269.

[2] P. Miller, H. Blosser, D. Gossman, B. Jeltema, D. Johnson, P. Marchand, IEEE Transactions on Nuclear Science NS-26 (April 1979), 2111.

iii. The Cyclotron Central Region

During the last year a substantial effort has been put into the development of hardware and software for a detailed study of the cyclotron central region. The quality of the ion beam produced by a cyclotron is critically dependent upon the emittance of the source and subsequent acceleration in the central region of the machine. It is expected that this study will lead to structural modifications of the central-region geometry in our cyclotron, giving improved beam quality.

The determination of ion trajectories in the region, which extends to a radius of approximately 18 cm., is made difficult because of the complicated nature of the electric field. The electric field resulting from the

ion source, puller, and dee structures cannot generally be described analytically. A full scale model of our cyclotron central region has been fabricated and will be used in an electrolytic tank which is nearing completion. The potential probe is driven by stepping motors via a CAMAC controller. Data, which we expect to be taking in the near future, will be collected by the PDP-11/34 system.

An alternative method currently under investigation is the numerical solution of the Laplace equation. Again, this is a complicated three-dimensional boundary value problem. The advantage is the ease with which the electric field can be determined for different central region geometries. The electrolytic-tank method would require remachining of the model for each new configuration. In an analogous manner the magnetic field could be determined by making use of the magnetic scalar potential. Due to the difficulty of solving the three-dimensional case, preliminary work on an approximate two-dimensional code is now underway. A two-dimensional graphics routine for use in specifying the structure boundaries has just been completed.

Once electric and magnetic field data become available, they will be used to calculate ion trajectories. A preliminary version of the central orbit code for computing these trajectories is now available for use. Ignoring space charge, the differential equations describing the ion motion may be derived beginning with the Lorentz force equation:

$$\vec{F} = q(\vec{E} + \vec{v} \times \vec{B}).$$

In Cartesian coordinates, the resulting seven first-order coupled differential equations are solved numerically with an explicit eighth-order Runge-Kutta routine. To test the code, median plane orbits have been computed for a constant magnetic field and a simple electric field, approximating the field of a single 180° dee. The contributions to the electric field from the ion source and puller have been ignored.

A schematic of the configuration used in these test calculations is shown in Fig. C12. The direction of the planar electric field is perpendicular to the dee edges. Outside the dee gap the magnitude of the electric field is taken to be zero, while inside it has the time dependent form $\cos(\omega t + \phi)$, where ω represents the r. f. angular frequency and ϕ the phase constant. Orbits for protons with different starting phases are shown in Fig. C13.

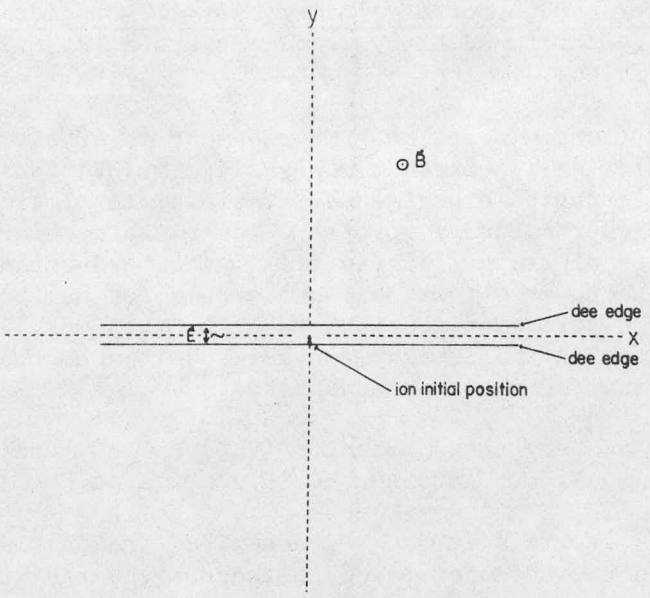

Fig. C12. Configuration used for testing the central orbit code.

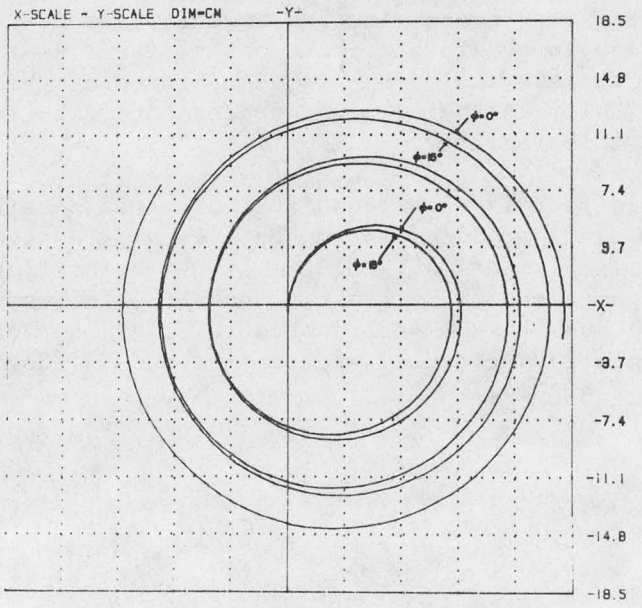

Fig. C13. Proton orbit for the case where the r. f. frequency equals the cyclotron frequency. ω = 10 MHz, B = 6.56 KG, ϕ = 0°,15°, and a dee voltage of 75 Kv were used.

2. Neutron Detector Development for TOF Studies - P. N. Craig, S. Dasgupta, D. A. Lind, T. G. Masterson, R. S. Raymond, C. D. Zafiratos.

The focus of work in detector development this year has again been the problem of outfitting a neutron time-of-flight (TOF) facility, with 9-meter and 30-meter flight path experimental stations, to provide high resolution, low background neutron energy spectra. Toward this end studies have been made in a variety of areas, ranging from better understanding of our standard neutron detectors to testing a new scheme for neutron-gamma ray discrimination. The following sections describe this work, as well as studies of the performance of two designs for large volume neutron detectors, and detector shielding for neutron detectors.

a. Very Large Detector (VLD) - P. N. Craig, T. G. Masterson, C. D. Zafiratos

In our 1978 progress report[1] we described the initial testing of a large volume neutron detector based on the designs and studies of Carlson et al.[2] This very large detector (VLD) consisted of an acrylic cell 36 cm x 21 cm dia) filled with NE 224 liquid scintillator. Results of these tests indicated a poorer time resolution in TOF spectra than had been hoped for; however, problems with the intrinsic time spread of the ^{3}He beam at that time were a major contribution to these results. The purpose of this new study was to obtain a measurement of the true time resolution of the VLD as well as make a side-by-side comparison of the performance of the VLD and the 2" "Colorado Style" neutron detector most commonly used in neutron studies at this facility.

The VLD used in this study consisted of a glass cell (active volume: 35 cm x 21.6 cm dia.) produced for us by a local glassblower. This cell was filled with 11.5 liters of NE213, a liquid scintillator with more favorable neutron-gamma ray discrimination characteristics than NE224, and viewed from both ends by RCA 4522 photomultipliers attached by acrylic adapters. A comparison of this detector and the 2" "Colorado Style" detector is shown in Fig. C14.

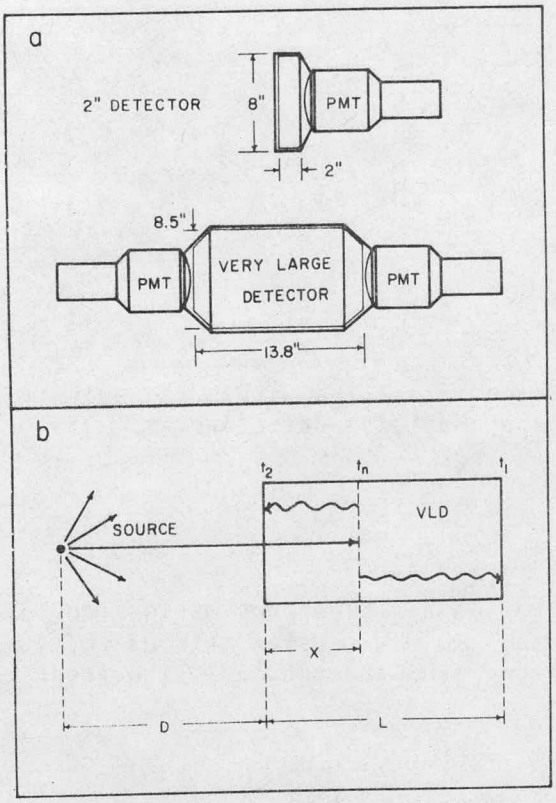

Fig. C14a. Side views of the 2" "Colorado Style" detector and the Very Large Detector (VLD). Fine outlines show the regions containing liquid scintillator. The PMT in all cases is the RCA 4522. Both detectors have cylindrical symmetry.
Fig. C14b. Schematic representation of method of compensating for the uncertainty of position of events in the VLD.

The method of compensating for the inherent uncertainty in position of a scintillation event in the VLD is shown schematically in Fig. C14b. A neutron produced by a source a distance D from the VLD produces a scintillation within the detector at a depth x and a time t_n. Light signals from the event propagate to each end of the VLD and are detected at times t_1 and t_2 given by:

$$t_2 = t_n + \left(\frac{x}{c/n}\right)f \qquad (1)$$

$$t_1 = t_n + \left(\frac{L-x}{c/n}\right)f \qquad (2)$$

where n is the index of refraction of the scintillator and f is a geometrical factor which expresses the fact that the average light path within the cell is not axial. Equations (1) and (2) can be solved for t_n and x:

$$t_n = \frac{1}{2}(t_1 + t_2) - \frac{nLf}{2c} \qquad (3)$$

$$x = \frac{c}{2fn}(t_2 - t_1) + \frac{L}{2} \qquad (4)$$

We now make the assumption that all neutron velocities within the scintillator may be replaced by a constant independent of neutron energy:

$$v_n \simeq \beta_0 c = \text{constant}$$

This is, of course, not strictly true, but is a good approximation provided the energy range of interest is less than ≈ 10 MeV. Using this assumption, we have for t_D (the flight time of neutrons from the source to the front face of the VLD):

$$t_D \simeq t_n - \frac{x}{\beta_0 c} \qquad (5)$$

Using equations (3) and (4), equation (5) becomes:

$$t_D \simeq G_1(t_1 - \alpha t_2) + G_2 \qquad (6)$$

where G_1 and G_2 are constant functions of β_0, n, f, and L_j, and α is:

$$\alpha = \frac{1 - \beta_0 nf}{1 + \beta_0 nf}$$

which is also constant for a constant β_0. Equation (6) is simple enough to permit timing signals from the two ends of the VLD to be easily reduced to depth-compensated time spectra for events in the detector. The constants G_1 and G_2 only serve to shift and compress the time spectra and thus contain no intrinsic spectroscopic information. In practice, time signals proportional to t_1 and t_2 are collected and combined in the relation

$t_1 - \alpha t_2$ using the KAOS data acquisition program on our PDP 11/34 computer.[3] This system permits simple variation of the parameter α to obtain empirically the optimum resolution for a particular energy spectrum.

Comparison spectra were taken for the VLD and the 2" detector using the reaction $^{9}Be(^{3}He,n)^{11}C$ with $E(^{3}He) = 25.5$ MeV. The detectors were both at a distance of 9 meters from the target and were oriented so $\theta(lab) = +4°$ for the VLD and $-4°$ for the 2" detector. Since VLD and 2" spectra were taken simultaneously, a direct comparison between detectors is allowed. One such pair of spectra is shown in Fig. C15. Table IIC-III gives the best time resolution of the ^{11}C ground state obtained for the two detectors during the course of the experiment. Also listed is the neutron peak-to-valley ratio for each detector which gives a measure of the neutron-gamma ray discrimination characteristics of each detector by measuring the ratio of the neutron peak height to the height of the valley between neutron and gamma ray peaks in a neutron-gamma ray spectrum. Both detectors suffer from a ≈1 nsec intrinsic time spread in the ^{3}He beam on target; however it is obvious that the VLD is giving an overall poorer performance than the 2" detector.

Table IIC-III

VLD - 2" Detector Comparison

Detector	Resolution (FWHM of ^{11}C g.s. in ns.)	n-γ Discrimination (neutron peak-to-valley ratio)
2"	1.10 ± .04	30 to 1
VLD	1.61 ± .03[1]	12 to 1

[1] Obtained for α=0.30

In order to estimate the effects of an intrinsic time spread in our results, a further study was conducted using a bench-top test set-up with a ^{60}Co source collimated to provide a 1" diameter beam of 1 MeV gamma rays axially through the detectors. Since ^{60}Co emits two simultaneous gamma rays, a second detector with very fast timing characteristics (≈140 picosec. resolution) was used to provide a timing mark for events in the neutron detectors. In this study a further comparison was relative to a 1" detector, which is identical to the 2" detector except that the effective volume of scintillator is halved by reducing the thickness to 1". The value of α was varied for data taken with the VLD until a value which gave optimum resolution was obtained. The effect of this variation is shown in Fig. C16. The negative value of α at optimum is due to the fact that the speed of the detected gammas exceeded that of scintillation light in the medium.

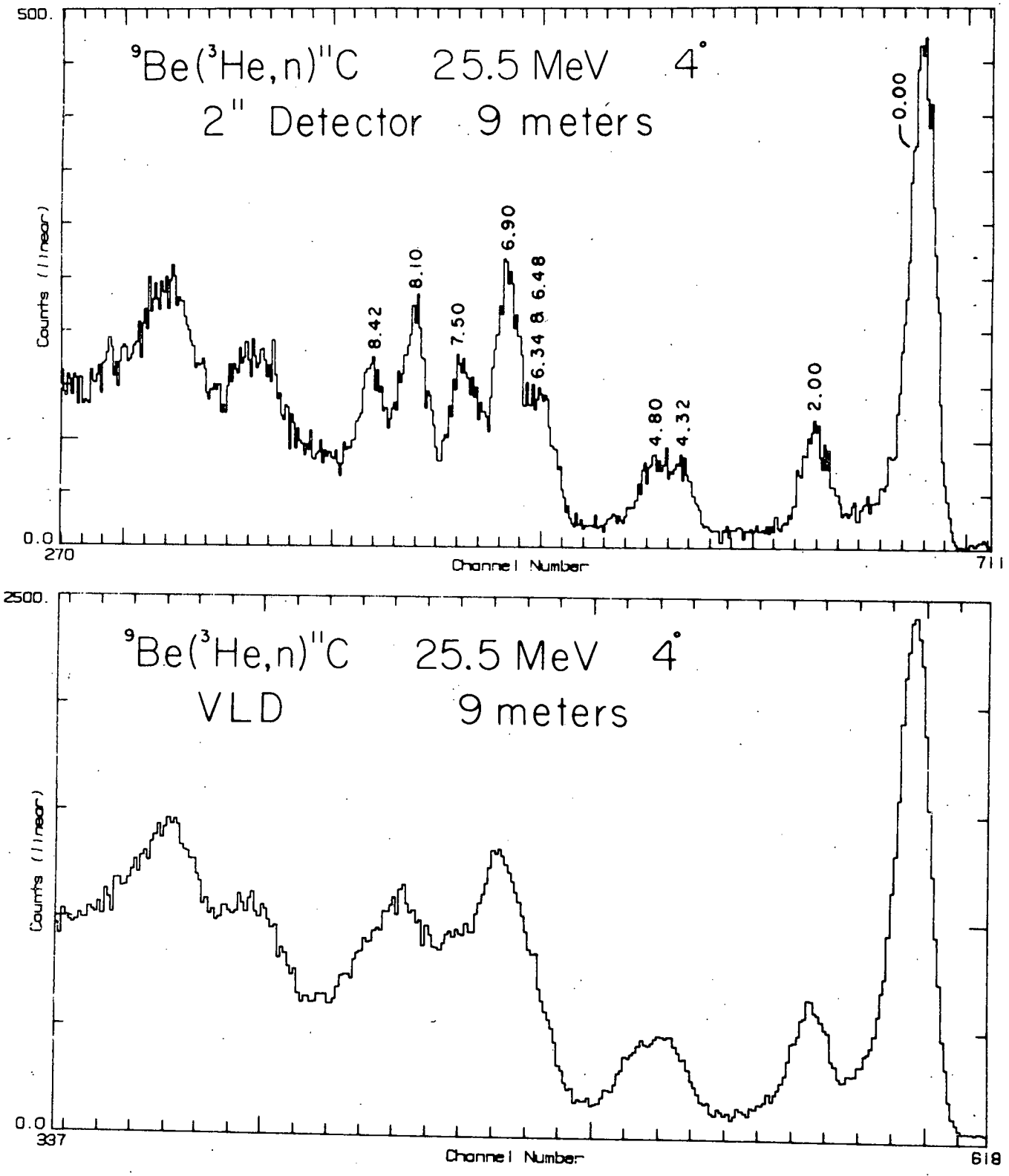

Fig. C15. Comparison of TOF spectra taken simultaneously by the 2" detector and the VLD. The first nine excited states in ^{11}C are labeled in the top spectrum. α=0.30 for the VLD spectrum. The FWHM of the ground state is 1.23 ns for the top spectrum and 1.61 ns for the bottom spectrum.

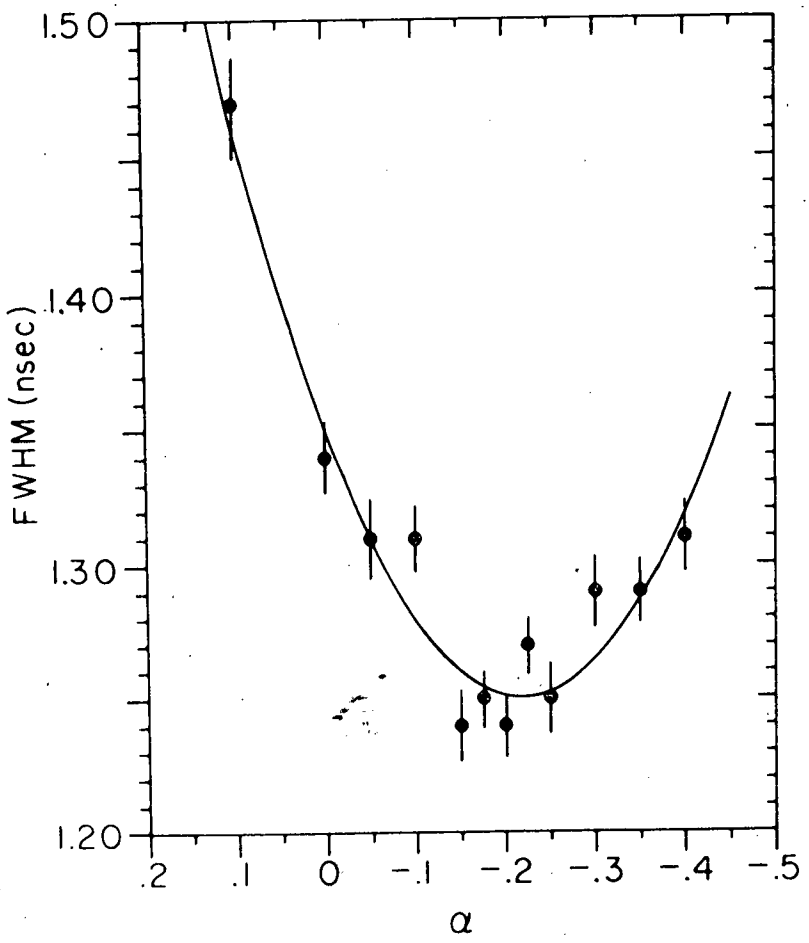

Fig. C16. Graph of the FWHM of a 1 MeV gamma ray timing peak versus the parameter α for the VLD. The curve represents a parabolic fit to the data. Error bars represent statistical uncertainties.

The results of the comparison of optimum resolution are shown in Table IIC-IV; the values quoted have had the time resolution of the timing scintillator unfolded to provide a measure of the true resolution of the detectors. The VLD resolution is much poorer than that of either of the other detectors. The improvement of only 0.1 ns between 2" and 1" detectors indicates that we are approaching the intrinsic time resolution of the detector system.

In constructing the VLD we had hoped to obtain a large volume detector with sub-nanosecond time resolution. While these tests show that we have failed in this case, efforts are proceeding in the hope that such a detector will eventually be developed.

Table IIC-IV

Gamma Ray Resolution Tests

Detector	Resolution[1] (FWHM of 1 MeV γ peak in nsec)
1"	0.70 ± .02
2"	0.79 ± .02
VLD	1.23 ± .02

[1] Effects of the timing scintillator have been unfolded

b. Long Cylindrical Detectors - S. Dasgupta, D. A. Lind, and R. S. Raymond

A problem with the VLD detector is that the signal-to-background ratio deteriorates markedly with lower neutron energy. An effort was made to develop large-volume detectors which could optimize the signal for a range of energies and achieve good n-γ discrimination. Square or rectangular cross sections give rather poor n-γ discrimination. Cylindrical units have given better performance if light is collected from both ends.

We constructed a unit 12.7 cm diameter x 102 cm long observed by RCA 4522 tubes at each end. The n-γ peak-to-valley ratio measure, as for the VLD, was about 10:1. The time resolution was a little better than the 21 cm diameter detectors. A considerable disadvantage was the large volume of detector phototubes and bases which must be contained within the shielded volume.

The problem of size and time resolution has led us back to development of very compact units which achieve about 0.5 ns time resolution. Improved time resolution allows such detectors to be placed close to the target yielding improved signal-to-noise ratio. Additional gains from higher pulse repetition rate and target thickness as well as primary beam pulse bunching all indicate that better time resolution is the most important factor for improving experimental capability.

c. The Multiple-Paddle Detector - P. N. Craig, T. G. Masterson, and C. D. Zafiratos

The primary emphasis of neutron detector development at this facility has been to improve the overall time resolution of our TOF detectors. It has long been felt that one of the factors hindering this effort has been the requirement of using liquid scintillators with pulse-shape discrimination characteristics. Since our work is done at relatively low neutron energies (upper limit ≈ 50 MeV), we are forced to set low energy thresholds on our detectors to obtain energy spectra with a large dynamic range. This requirement has the unfortunate effect of allowing energetic gamma rays produced in the target to be detected along with the neutrons. In order to deal with this problem, the standard procedure is to use a large liquid scintillator whose light output characteristics allow pulse-shape discrimination between neutron events and gamma-ray events.[4] This scheme usually leads to good gamma-ray rejection but time resolution only on the order of 1 nanosecond. Work at other facilities dealing with higher neutron energies, for which gamma ray rejection is effected by setting high energy thresholds, has resulted in far better time resolution using plastic scintillators with no pulse-shape discrimination. We are now investigating a method by which neutron-gamma ray discrimination can be performed using an array of plastic scintillators.

This new method of identifying neutrons and gamma rays exploits various aspects of the process by which these particles produce scintillation events. Neutrons interact with protons within the scintillator and these recoil protons produce scintillation events. Gamma rays, on the other hand, cause electrons within the scintillator to be Compton-scattered and it is the ionization produced by these electrons which causes the scintillations. Keeping in mind these effects, we now make three observations:

1) Gamma rays produced in our target reactions are less energetic (< 10 MeV) than most of the neutrons produced (≈ 20-40 MeV).
2) The electrons resulting from the Compton-scattering of these gamma rays produce less ionization (and thus fewer scintillations) per unit path length than do the recoil protons caused by the higher energy neutrons.
3) Compton electrons can be scattered through all angles while recoil protons must go forward.

Effects (1) and (2) can be exploited by using a scintillator whose thickness is less than the range of either the Compton electrons or the recoil protons. By doing this, neutron and gamma ray events could be identified by the amount of light emitted, and gamma rays could be rejected by setting a threshold on the amount of light that must be collected before an event is recorded. Effect (3) causes problems with this scheme, however, because it allows Compton electrons scattered at large angles to pass through a larger thickness of scintillator and thus produce a larger amount of light. Fortunately, this effect can be dealt with by stacking several isolated thicknesses of scintillator back-to-back and requiring a coincidence between events in adjacent scintillators before an event is accepted. The final result is a Multiple-Paddle Detector (MPD) made up of many thin isolated scintillator paddles stacked close together and tied together electronically in a coincidence circuit.

To illustrate this concept further, we will consider a specific example. Suppose we wish to discriminate between 10 MeV gamma rays and 40 MeV neutrons. The 10 MeV gamma rays can Compton scatter 10 MeV electrons which have a range of 5.3 cm in plastic and which initially deposit roughly 200 keV per mm of plastic.[5] The 40 MeV neutrons produce up to 40 MeV recoil protons which have a range of 1.4 cm in plastic and which initially deposit roughly 1.5 MeV per mm of plastic.[6] We will choose our plastic scintillator paddles to be 3 mm thick, so we will expect gamma ray events to deposit 0.6 MeV and neutron events to deposit at least 4.5 MeV in the paddles. We then check the technical data on plastic scintillators and find that for NE102 plastic scintillator the initial loss of 4.5 MeV by the protons produces roughly seven times as much light as the 0.6 MeV loss by the electrons.[7] Thus, it should be a relatively simple matter to set an energy threshold to reject gamma rays which produce forward scattered electrons. Further, since the range of both protons and electrons is much longer than the individual paddle thicknesses, a 3-fold coincidence requirement (or greater) between adjacent paddles should eliminate the effects of large-angle Compton-scattering producing anomalously large light outputs from electrons in individual paddles. Thus, using this simple two-step scheme, we perform neutron-gamma ray discrimination without relying upon pulseshape characteristics of a scintillation event.

A preliminary test of this discrimination scheme was conducted using a two-paddle arrangement and the $^{9}Be(\alpha,n)^{11}C$ reaction with E_{α} = 35 MeV. The detector was constructed using two paddles of Pilot B scintillator (203 cm x 15.2 cm x 6 mm), each connected at one end to an RCA 8575 photomultiplier via an acrylic light pipe. The two paddles were separated by a layer of aluminum foil and arranged so the PMT's were at opposite ends so that any coincident event in the two paddles could be mean-timed to compensate for differing light transit times in the paddles. Results of this test for various choices of energy threshold and coincidence requirements are given in Table IIC-V. As can be seen, the arrangement which provided the best compromise between gamma ray rejection and neutron collection was the one with the high energy-threshold setting and no coincidence requirement; while the corresponding arrangement with the added 2-fold coincidence requirement rejected about twice as many true neutron events. These results suffer from the fact that the paddles were thicker than we would have preferred, and that the use of only two paddles restricted us to looking at only 2-fold coincidences. Also, the best observed time resolution of 1.22 nsec FWHM for the ^{12}C ground state suffered from an large time spread in the α beam on target. However, the time resolution compared favorably with the resolution obtained by a fast scintillation detector monitoring the beam at the scattering chamber.

Table IIC-V

Double Paddle Test Results

Energy Threshold[1]	Coincidence Requirement	Neutron Count Rate (scaled)	Gamma Ray Count Rate (scaled)
low	no	1.00	1.00
high	no	0.60	0.02
low	yes	0.22	0.05
high	yes	0.19	≈0.00

[1] low threshold ≈ 2 MeV, high threshold ≈ 5.5 MeV

Further tests of this discrimination scheme are planned using a MPD presently under construction. This detector will use 5 Pilot F scintillator paddles (38 cm x 15 cm x3 mm), each viewed by an RCA 8575 PMT via an acrylic light pipe. Adjacent paddles will be separated by sheets of aluminum foil and will be viewed at opposite ends by their PMT's to allow mean timing of coincident events. Preliminary tests with individual paddles have uncovered a possible problem due to light attenuation within the thin plastic. The 3 mm thick plastic is observed to have an attenuation length of ≈ 28 cm, so setting a precise energy threshold for events occuring anywhere within the scintillator paddle will not be possible. However, it is hoped that the increased chances of coincidence events due to the decreased thickness of scintillator paddles will offset this effect and result in a useful detector.

d. Work in Progress - P. N. Craig and D. A. Lind

As noted in section (b), the problems of size and time resolution encountered with the VLD and Long Cylindrical Detectors have led us back to the development of smaller, more compact detectors with time resolutions on the order of 0.5 nsec. Toward this end we have returned to studying certain characteristics of the 1" and 2" "Colorado Style" detectors described in section (a) to determine if they could be improved by appropriate choices of photomultiplier tubes and detection geometries.

Time slewing that occurs with location of the scintillation event was investigated by use of collimated ^{60}Co gamma rays and cosmic ray muons. With 1 cm diameter collimated ^{60}Co gamma rays, coincidence timing using the 2.5 cm x 20 cm dia. detector was 0.5 nsec FWHM, but the time slewing from center to edge of the detector was 0.3 nsec. Tests of the time slewing and

light collection efficiency are in progress with a variety of 5 cm and 12.7 cm diameter photomultiplier tubes and different designs for light collection geometry. The 12.7 cm diameter phototubes (RCA 4522 and Amperex XP2041) have appreciably longer rise times coupled to the NE213 or NE224 scintillator than do the 5 cm diameter phototubes (RCA 8575 and RCA C31024). Also, the question of whether to detect light from a large scintillator by using an acrylic light funnel and a single large phototube or by clustering several small phototubes directly on the scintillator is being studied with a variety of phototubes and scintillator designs.

e. Detector Shielding for Neutron TOF Studies at Colorado - D. A. Lind, T. G. Masterson, R. S. Raymond and C. D. Zafiratos

In an effort to improve the shielding of neutron detectors, experiments were performed in the use of plastic scintillator panels as active shielding against cosmic-ray-produced neutrons. An enclosure was assembled consisting of a lead floor 5 cm thick, two lead walls, each 30 cm thick, 3 m long, and 25 cm apart, and a steel roof approximately 25 cm thick. The shielding represents 195 gm/cm^2 of steel, which is of the order of a 10-fold attenuation factor. The Fe-Pb shield was then covered with plastic scintillator panels, each 3 m x 0.6 m x 2.5 cm, on loan from Los Alamos. In the center we placed the very-large-detector (VLD) described in section (a) and shown in Fig. 1a. Standard n-γ discrimination electronics were used, and signals were fed to the PDP-11/34 computer, where two-dimensional gates were set around the neutron group. The threshold for detection was set at a neutron energy of 15 MeV with no upper limit on the energy range. The results are as follows:

No shielding	0.34 neutrons/sec
With Fe-Pb shielding	0.18 neutrons/sec
Fe-Pb shielding with cosmic ray veto outside	0.081 neutrons/sec

The difference between the shielded detector with and without cosmic-ray veto is probably the production of neutrons in the shield by cosmic ray flux.

A special problem exists in this area. The alluvial soil around the laboratory has abnormal levels of thorium and uranium with decay products so that very large gamma counting rates can occur. These do not directly contribute to the background but do affect the n-γ discrimination since that counting rate appears as a noise level on the discrimination signals.

f. Anti-coincidence Paddles for Indiana (p,n) Studies - T. Masterson, D. Lind, R. Raymond and E. Sugarbaker

The neutron detectors for the TOF system at Indiana are plastic scintillators in which the pulse shapes of protons and electrons (or muons) are indistinguishable. The large volume detectors see a cosmic ray flux comparable with the neutron flux in low counting rate experiments. In order to reduce this random backgroun we have shielded these detectors with large area (2 m x 0.6 m) anti-coincidence paddles (on loan from Los Alamos), as shown in Fig. C17. Each paddle counted at a rate of approximately 50 kHz and these signals were put in anti-coincidence with the neutron signals. The pulse width was approximately 20 ns and the resulting system dead time was 0.1 - 0.2%. The

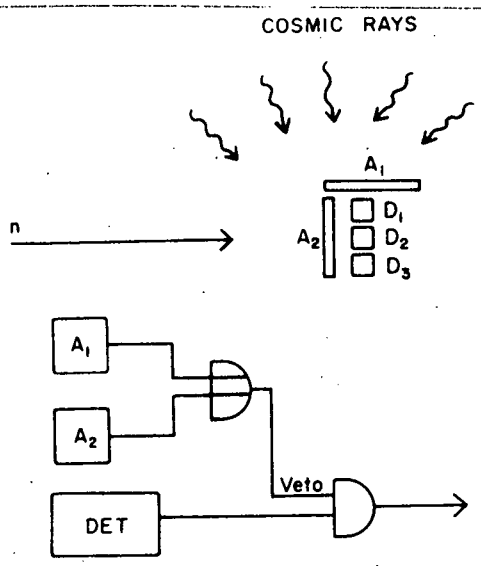

Fig. C17. Sketch of anti-coincidence paddle and neutron detector geometry and a schematic of the anti-coincidence electronics.

placing of detector A_2 in front of the detector array had the additional advantage that any charged particles produced by neutron interactions in the flight path were vetoed. The net effect was to reduce the background by a factor of 3.

---

[1] D. A. Lind et al., Univ. of Colorado NPL Technical Progress Report (1978) 153-158.

[2] J. D. Carlson, R. W. Finlay, and D. E. Bainum, Nucl. Inst. and Meth. 147 (1977) 353-360.

[3] D. E. Prull, Univ. of Colorado NPL Technical Progress Report (1979) 165.

[4] R. F. Bentley et al., Univ. of Colorado NPL Technical Progress Report (1971) 103.

[5] Ann T. Nelms, "Energy Loss and Range of Electrons and Positrons", Supplement to NBS Circular 577 (1958) 19.

[6] Joseph F. Janni, Calculations of Energy Loss, Range, Path Length, Straggling, Multiple Scattering, and the Probability of Inelastic Nuclear Collisions for 0.1 to 1000 MeV protons, (1966) 399.

[7] Nuclear Enterprises, "Plastic Scintillators; Light Pipes, and Cerenkov Detectors", p. 2.

3. New Computing Facilities - D. E. Prull

The computing facilities at the University of Colorado Nuclear Physics Laboratory were greatly expanded last year with the purchase of a Digital Equipment Corporation PDP-11/60 computer. Delivery and installation were completed in May, and system generation for RSX-11M version 3.2 was completed in early June.

The initial purchase consisted of a PDP-11/60 central processor, 256K bytes of ECC/MOS memory, memory management, cache memory, floating point, EIS, bootstrap loader, battery backup, and programmer's console. The peripherals include an LA120 DECwriter III system console and interface, an FP11 floating point processor, an RJM02 controller and one 67 megabyte RM02 disk pack drive, a TE16 800/1600 bpi magtape drive and controller, an RK11 controller, two VT100 alphanumeric display terminals, and a Printronix P600 lineprinter-plotter.

Several peripherals, including two Tektronix 4010 graphics terminals, a CR11 card reader and controller, an 8-line EIA terminal multiplexer and an RK05 cartridge disk drive were moved from our PDP-11/34 computer to the PDP-11/60. A second 67 megabyte RM02 disk pack drive was installed in late August, and another VT100 alphanumeric display terminal has been ordered.

Our primary goal in this purchase was an expansion which involved distributing the work load of the PDP-11/34 system over two systems. The PDP-11/34 can now be dedicated to on-line data acquisition tasks, with the PDP-11/60 providing all the required support functions, experiment setup capability, data analysis, and software development capability.

This expansion has been very successful. The PDP-11/60 computer is ideally suited to the small "number crunching" tasks required for data analysis and peak fitting and is fast enough to support several terminals in the multi-user environment of RSX-11M without degrading the system performance. All software development, including data acquisition software for the PDP-11/34, is now done on the PDP-11/60. Most of the data analysis, peak fitting, and playback of event tapes is also done on the PDP-11/60. In addition, several large programs which were previously run at the University's computing center have been converted and are now running on the PDP-11/60.

a. Data Acquisition Hardware - D. E. Prull

Our current data acquisition system is based on a Digital Equipment Corporation PDP-11/34 computer. It is interfaced to three Northern Scientific analog-to-digital converters and to CAMAC via a Kinetic Systems dedicated crate controller. This system, which runs under the RSX-11M operating system, also has three RK05 cartridge disk drives, a TE10 800 bpi magtape drive for multi-parameter event recording, a digital plotter, a character printer, and two terminals.

Several peripherals used primarily for data analysis functions were moved to the new PDP-11/60 computer this past year. The Tektronix 4010 graphics terminal was replaced by a Tektronix 4025 refresh graphics terminal in May. This new terminal has provided a dramatic improvement in the operation of our data acquisition software. Up to four histogram plots can be saved in the terminal's memory and quickly recalled for comparisons. Its function keys can be programmed with repetitive or special commands to save typing. It also provides split-screen scrolling, so histograms can be displayed on part of the screen with commands to the computer scrolled separately.

A major project this past year was the design of a second multiple analog-to-digital converter control unit. This new ADC control allows for independent or coincident operation of any combination of four ADC's and an eight bit routing register. Interfacing to the PDP-11/34 will be through a direct memory access port utilizing a Digital Equipment Corporation DR11-B general device interface. Construction of the ADC control has begun and final testing is expected in November. Work on the I/O driver and modifications required to add this controller to our data acquisition software are in progress.

We are also planning to expand our CAMAC interfacing. We requested and received funding for the purchase of a programmable, multiple DMA channel, CAMAC branch driver such as the BiRa Systems Model MBD-11. Our specifications have been completed and we are proceeding with the purchase. Once installed and operational, this CAMAC branch highway will provide the speed and flexibility required for our more sophisticated experiments.

b. Computer Program Development

CAMAC Driver - D. E. Prull

A driver for a Kinetic Systems 3912 dedicated CAMAC crate controller for RSX-11M was implemented on our PDP-11/34 computer last year. The driver is a modified version of the driver for a Kinetic Systems 3911A developed at Argonne National Laboratory by J. W. Tippie and P. H. Cannon[1]. The assistance provided by Argonne National Laboratory was a tremendous help in getting our system debugged and operational.

CAMAC as an I/O device for a computer has many unusual features and capabilities. When applied to data acquisition and control, it poses many unusual characteristics not common to classical I/O devices. A number of design considerations for the RSX-11M CAMAC driver were apparent:

1. The driver must be capable of coping with the CAMAC hierarchical structure of subaddress, module, crate, and highway in a logical way.

2. The driver must be capable of receiving a list of commands (FNA list) for the CAMAC hardware.

3. The driver must be capable of suspending execution of an FNA list pending an external hardware trigger (LAM).

4. When an FNA list is suspended, the driver must not appear to be busy for I/O to other modules.

To achieve these goals, a driver using nonstandard data structures (including a modified UCB structure) was implemented. The most significant departure from the classical driver is the "subchannel" concept. With this structure, multiple active I/O requests to a single controller are supported. All calls to the driver use the standard QIO procedures of the RSX-11M operating system.

The driver was incorporated into our operating system in May and has been used for some control functions without difficulty. It will be an integral part of the software supporting field mapping and model magnet design studies.

---

1. J. W. Tippie and P. H. Cannon, "CAMAC Driver for the RSX-11M v3 Operating System," Proceedings of the Digital Equipment Computer Users Society, Vol. 4, No. 2, 563.

c. Software Update - D. E. Prull and C. A. Crouch

One of the major projects this past year was updating all the software currently in use at the Laboratory. The primary goal in this effort was to clean up our program library while adding any missing documentation and fixing minor bugs. The remaining programs running on the PDP-9 computer were converted to the PDP-11 computers. All hardware dependence was removed from the data-analysis programs so that they can be run on either PDP-11 computer without modification. Finally, handbooks describing all available programs, along with operating instructions and sample input and output, were written.

FITIT - D. E. Prull

FITIT is a program to fit multichannel pulse-height spectra and extract peaks and peak areas using arbitrary peak shapes. Peak shapes are defined from user-supplied tables of counts versus x. A search is made on peak positions, peak normalizations (or scale factors), and peak widths (conversion from x to channels) to find a least squares fit to data in the region. Up to four different peak shapes may be used to fit a region containing up to 500 channels and 10 peaks. Peak positions and widths may be variable or linked to other peaks as desired. Fixed, variable, or predefined parabolic or linear backgrounds are used.

Searches are based on the non-linear least squares regression technique taken from LSQ11[1]. The current version of FITIT evolved from an earlier, more limited version developed at the laboratory in 1978[1].

1. D. E. Prull, Univ. of Colo. NPL Technical Progress Report (1978) 143.

EZREADER - D. E. Prull

Program EZREADER generates gated pulse-height spectra from multiparameter event data recorded on magnetic tapes. This program is a highly modified version of GAMMA[1] which was developed to analyze gamma-gamma coincidence data. Each event is checked to see if common gating conditions are satisfied. If the event is accepted, two of the ADC conversions, "A" and "B," are used to generate the pulse-height spectra. The user selects, via an input data file, which of these two conversions will be kept subject to gates on the other.

EZREADER will currently analyze six different types of event tapes. Up to 200 pulse-height spectra are placed on a scratch disk for each pass through the tapes. A separate program completes the sorting process by combining spectra from the scratch disk, subtracting random and background spectra, and creating data files compatible with the laboratory's data analysis program SPECTR.

1. D. E. Prull, Univ. of Colo. NPL Technical Progress Report (1979) 166.

TAPING - D. E. Prull

Program TAPING provides the capability of reading or writing blocked BCD nine-track magtapes. Its primary use is in handling magtapes from other facilities. Tape density is selectable at either 800 or 1600 bpi. The current version assumes fixed-length 80 character records with user-supplied blocking of from 1 to 10 records per block. Control functions are provided for rewinding the tape, skipping files, reading a file from the tape (either ASCII or EBCDIC format), writing a file on the tape, listing the first few lines of each file, and positioning the tape at the logical end of data.

XRF PROGRAM CONVERSION - C. A. Crouch

One of the major activities of the x-ray fluorescence (XRF) laboratory this past year has been program and data conversion from the PDP-9 computer to the PDP-11/34 and PDP-11/60 computers. A total of 11 programs have been modified to run on either PDP-11 computer. Three new programs were written to convert the XRF "Garr" data to a magnetic tape format suitable for PDP-11 use, and to provide back-ups of the new data tapes.

The XRF program and data conversion is very near completion. Last year a teletype interface was installed in the PDP-8E computer to facilitate communication with a PDP-11 computer. This hardware link has since been tested and software to transfer the XRF data to the PDP-11/60 computer is now in progress. Once this software has been completed, the XRF laboratory will perform all data acquisition and analysis using only the PDP-8E and PDP-11/60 computer systems.

DATA TAPE CONVERSION - C. A. Crouch

All data tapes recorded at the Nuclear Physics Laboratory prior to the use of the PDP-11/34 computer were written with the PDP-9 computer using 7-track magnetic tape. It is necessary to translate the 7-track data tapes to 9-track tapes in a format suitable for use with either PDP-11 computer. To accomplish this task, two programs have been written. The program which runs on the PDP-9 computer converts 7-track 18-bit binary data to 9-track 16-bit binary data. The PDP-11 program reads the 9-track tape and generates data files compatible with the PDP-11 data-analysis programs.

PLOTTING RCUTINES - C. A. Crouch

The software for the Tektronix 4662 interactive digital plotter was rewritten to incorporate a "block mode" of communication. In "block mode" transmission, the plotter controls the rate at which information is sent from the host (PDP-11/34 computer) by using a prompt to acknowledge to the host that sufficient memory space is available for another block of data. This method of data transfer prevents plotter buffer overflow and provides for error detection if a block is received incorrectly.

4. Electronics Maintenance and Development - J. A. Magyar

a. Cyclotron

i. Magnet System

Because of the demand for higher quality, more stable particle beams, the ripple content and long-term stability of the cyclotron magnet supplies are being examined.

The present unregulated valley and center coil supplies are of particular concern as a possible source of long-term drift. To correct this a new valley coil supply has been ordered, and two center coil supplies have been ordered and received. In the present system the upper and lower center coils are run in series from a single supply. Once the new supplies are installed each coil will be separately excited to allow fine tuning of the field symmetry in the vicinity of the ion source. It was not possible to locate commercially-made center coil supplies having a sufficiently low ripple at a reasonable price so auxiliary inductive reactors were also purchased for use in conjunction with the supplies. This combination has been tested and works well. All three supplies will be installed at the time of the planned magnetic field mapping early this winter.

ii. R. F. System

Because of the increased desire for maximum dee voltage at maximum frequencies, the inadequate output provided by the low level portion of the existing r. f. system is becoming a serious problem. In the present system a low-frequency r. f. oscillator is followed by several stages of frequency multiplication and the output of this chain is run from the cyclotron control room to the cyclotron vault, where it is used to drive an 8168 amplifier tube which then drives the final amplifier. The signal to the 8168 is inadequate at high frequencies. A new system has been designed to both eliminate this problem and simplify operation of the cyclotron by eliminating the various frequency multipliers. The final frequency is provided directly by an HP-3325A frequency synthesizer located in the control room. This signal is sent to the cyclotron vault and amplified by a 160 W transistorized broadband power amplifier. This amplifier is a slightly modified version of an existing Motorola[1] design. In order to obtain increased r. f. sinewave purity a higher power class A input stage has been substituted and the push-pull output stage is run with a much higher idle current. A large 0.09 °C/W heat sink cools the amplifier. When used with the proper impedance matching network the above amplifier easily provides adequate drive to the 8168 tube. A one-week operational test was entirely successful and this system is now being put into final form.

---

1. Motorola RF Data Manual, "Broadband Linear Power Amplifiers Using Push-pull Transistors," Helge O. Granberg, Motorola, Inc. 1978.

b. Experimental Support

i. ND 50/50 Data Acquisition System

The ND 50/50 multichannel analyzer has exhibited two types of failure during the past year. One problem has been the increasing inability of the analog portion of the ADC's to accept and interpret properly any reasonable range of input pulse shapes or heights. This has been corrected by minor modification of the peak detector circuitry.

The other problem has been the development of a persistent intermittent failure in the digital portion of the electronics which appear to be traceable to the ferrite core memory. Because the ND 50/50 has as its only output device the PDP-9 computer, which is being phased out, it has been decided to replace the ND 50/50 with a more modern system. A survey of the market is currently in progress for a multichannel analyzer system that will operate either on a stand-alone basis or in conjunction with the PDP-11/34 computer.

ii. Digital Current Integrator

The previous beam-current monitoring system, based on use of DYMEC current-to-frequency converters, has been partially replaced by installation of an ORTEC 439 Digital Current Integrator. With this change the ability to monitor accurately small beam currents has been improved by approximately ten-fold and currents of 10^{-9} A can now be measured with no noise problems. This conversion will be extended to include all experimental stations as soon as time permits.

iii. Target Ladder Controller

The existing microprocessor-based target-ladder-position controller has been subject to erratic operation for the past year or more. In view of the relative complexity of the system and the simplicity of the operational task involved, this is now being replaced with a much simpler and presumably more reliable hardwired controller. Design of this system is largely completed and construction just beginning. The new system should be in operation within a few months.

iv. Electrolytic Field-Mapping Tank

The design and construction of the power supply and driver units for the x- and y-axis probe-position stepping motors is now complete. These units have been tested and are ready for operation. The analog portion of the data acquisition electronics is also complete and tested with only the digital portion remaining to be done. When complete the entire measurement system will be controlled by the PDP-11/34 computer through parallel line CAMAC I/O ports. A single measurement sequence will take between 1 and 10 seconds starting with the application of a negative potential to the plates and stepping the voltage-measuring probe to its new x,y position. After waiting for a half period for the liquid motion to damp out the potential will be reversed and the probe

voltage will be reversed and the probe voltage will be read by a fast 12-bit ADC coupled to it through a high impedance amplifier. Two voltage readings, taken at successive zero crossings of a 60 Hz power line reference signal, will comprise a single measurement. In this way the effects of 60 Hz pickup may be averaged out exactly for each measurement position. After waiting for the completion of the second half period the next measurement cycle will begin. The sequential reversal of the plate polarities is used to minimize any electroplating effects that might occur. The completed system is expected to be in operation within the next few months.

v. Cyclotron Magnet Calibration System

Design work is now underway for a magnetic-field measuring system similar to the one used at Oak Ridge for mapping the ORIC magnetic field[1]. This system uses an array of flip-coils, each of which is coupled to a precision integrating amplifier. To take a field reading the coils are all flipped at one time after which the integrator voltages are read by a fast 16-bit ADC. The entire measurement process is computer controlled.

We plan to use the same Analog Devices 234L operational amplifiers and the fast 16-bit ADC-16Q successive approximation ADC used at Oak Ridge. Although a slower and much less expensive ADC of adequate accuracy has been located the estimated 200 hours saved in projected measurement time justifies the extra cost of the faster unit.

We are also investigating alternate flip-coil designs and are particularly interested in using smaller diameter coils wound on boron nitride forms with finer wire having a low coefficient of thermal expansion. It is hoped that this could significantly reduce the problems related to temperature effects in the probe assembly.

---

1. S. W. Mosko et al., IEEE Transactions on Nucl. Sic., v. NS-24, no. 3, pp. 1269-1271, June, 1977.

vi. Ion Source Test Facility

A substantial effort has been put into the ion source test facility. In order to run an arc as soon as possible, temporary filament and arc power supplies were installed. The permanent supplies have since been obtained and installed. These supplies are fully interlocked to the vacuum and water cooling systems and are remotely controlled and metered from a convenient location. This system is operating satisfactorily.

A temporary dee and r. f. system has also been installed. This system provides up to 6 kV peak across the dee gap at a frequency of 3MHz. The r. f. level may be modulated at audio frequencies to about 80% modulation depth.

Design and construction of the final r. f. system is in progress. When finished it will provide 75 kV peak accelerating voltage at 15 MHz. The dee structure and resonant tank are discussed elsewhere. The final r. f. amplifier uses a 4CW10,000A tetrode capable of providing 15 kW of power. At 15 MHz and 75 kV the expected loss in the dee-tank circuit is approximately 6 kW.

The final stage will be driven directly by a 160 W transistorized amplifier of the same design as that being installed in the cyclotron RF system. Tests show that with the proper matching network this amplifier easily provides the required grid voltage to the 4CW10,000A.

The detailed mechanical and electrical design of the final-stage amplifier is in progress. Design of the screen-voltage power supply and regulator is complete and these units are partially constructed. The 160 W driver amplifier is also partially built.

An old 30 kVA power supply previously converted to a lower-power use has been rebuilt in a more modern version and will provide up to 6500 V at 4 A to run the 4CW10,000A amplifier. This supply and its control wiring have been installed and tested. An adjustable 5 kV, 2 A supply has been purchased to satisfy the need previously met by the old 30 kVA supply. This new supply has also been installed and tested.

5. Space Usage - A. B. Phillips

The original plans to modify space to accommodate the new PDP-11/60 computer were changed due to cost and time factors. A different area was prepared in time to install the computer, which arrived in May, 1980.

In May, the bent crystal spectrometer was shipped to NBS, Washington, D.C. The spectrometer had been situated in a 13 x 16 foot stacked-concrete-block cave with 2-foot thick walls. When this cave is removed, experimenters will have much more space available around the gamma-line target chamber, now a cramped, cluttered area.

Space in the building is becoming very tight. Office space is saturated. Storage of not-in-use equipment and supplies has always been a problem. Set-up labs, the electronics shop, and the graphics area are overcrowded. Any increase in professional personnel may mean going to work space outside the laboratory building.

6. Photography - B. Hymel, C. Boozer, and S. Jackson

This year the laboratory has been doing its own photographic work at a great gain in convenience and at a savings in cost. Photographs for publications can now be prepared within twenty-four hours after the drawings are completed. The existing darkroom facilities have proven to be entirely adequate; only a 4" x 5" view camera and some floodlamps were needed.

7. Detector Cooling - B. Hymel

For several years we have routinely cooled our lithium-drifted silicon detectors with a system which circulates methanol through a heat exchanger cooled by a block of dry ice. Because of the inconvenience and expense of getting dry ice delivered to the laboratory, we have gone over this year to using a heat exchanger cooled by a 1/3 horsepower mechanical refrigerator operating with freon. An electric resistance heater mounted on a separate heat exchanger is used for detector warmup. Electric automotive fuel pumps are used to circulate the methanol through either heat exchanger and the detector mounting block. An automotive fuel tank selector valve is used to select either the cooling or warming path of methanol circulation.

The new system is somewhat slower than the old system in cooling down the detectors but it is appreciably more convenient.

8. A Heavy-Ion Detector for the Energy-Loss Spectrometer- R. C. Weiss

For reaction products heavier than ^{4}He, the helical cathode proportional chamber (HCPC) backed with a plastic scintillator commonly used in the spectrometer focal plane does not provide adequate particle identification and background rejection. A combination gridded ionization chamber - HCPC similar to one in use at Los Alamos[1] has been constructed and put into use for the study of (^{3}He,^{7}Be) reactions. This device does provide the particle selectivity needed for the study of multi-nucleon transfer reactions having very small cross sections.

As shown in Fig. C18, the new detector has an active length of 64 cm and a depth of 24 cm, adequate to stop particles with ranges of up to 25 mg/cm^2 in isobutane. This corresponds to 16 MeV ^{4}He or 50 MeV ^{7}Li at 300 Torr. For the (^{3}He,^{7}Be) measurements the gas pressure was maintained at 300 Torr. The ionization region is bounded on one side by an aluminum cathode maintained at -500 V and on the other side by a split anode formed from a copper-coated G-10 circuit board. The anodes are biased at +400 V. The total energy (E) signal is taken from the cathode, the ΔE signal is taken from the narrow anode section. The two grids isolate the ionization region from the anodes so that the signal amplitudes are independent of the transverse displacement of the particle trajectory.

Position detection along the length of the detector is accomplished with a HCPC. Electrons produced by the charged particles as they enter the ionization region drift through the helix structure, which is maintained at the anode potential, into the proportional chamber region where a single anode wire is at +2000 V. The induced pulse on the helical delay line yields the position information to a precision of a millimeter or so FWHM. The HCPC structure must be heavily shielded from the ionization region to reduce coupling of the proportional chamber signals into the E and ΔE signals.

The effectiveness of the gridded ionization chamber for particle identification is shown in Fig. C19. This figure displays the energy signal vs the ΔE signal, and clearly shows well-defined particle groups from the ^{58}Ni(^{3}He,^{7}Be) reaction. A position spectrum for the same reaction is shown in Fig. C20.

Further developments with this detector will stress improvements in position resolution by a careful study of dispersion compensation. The detector will be used in a series of experiments, the first of which will be a study of the effect of increasing mass number on differential cross sections for the (^{3}He,^{7}Be) reaction.

1. S. D. Orbesen, E. R. Flynn, D. L. Hanson and J. W. Sunier, Los Alamos Report LA-6843-MS (1977).

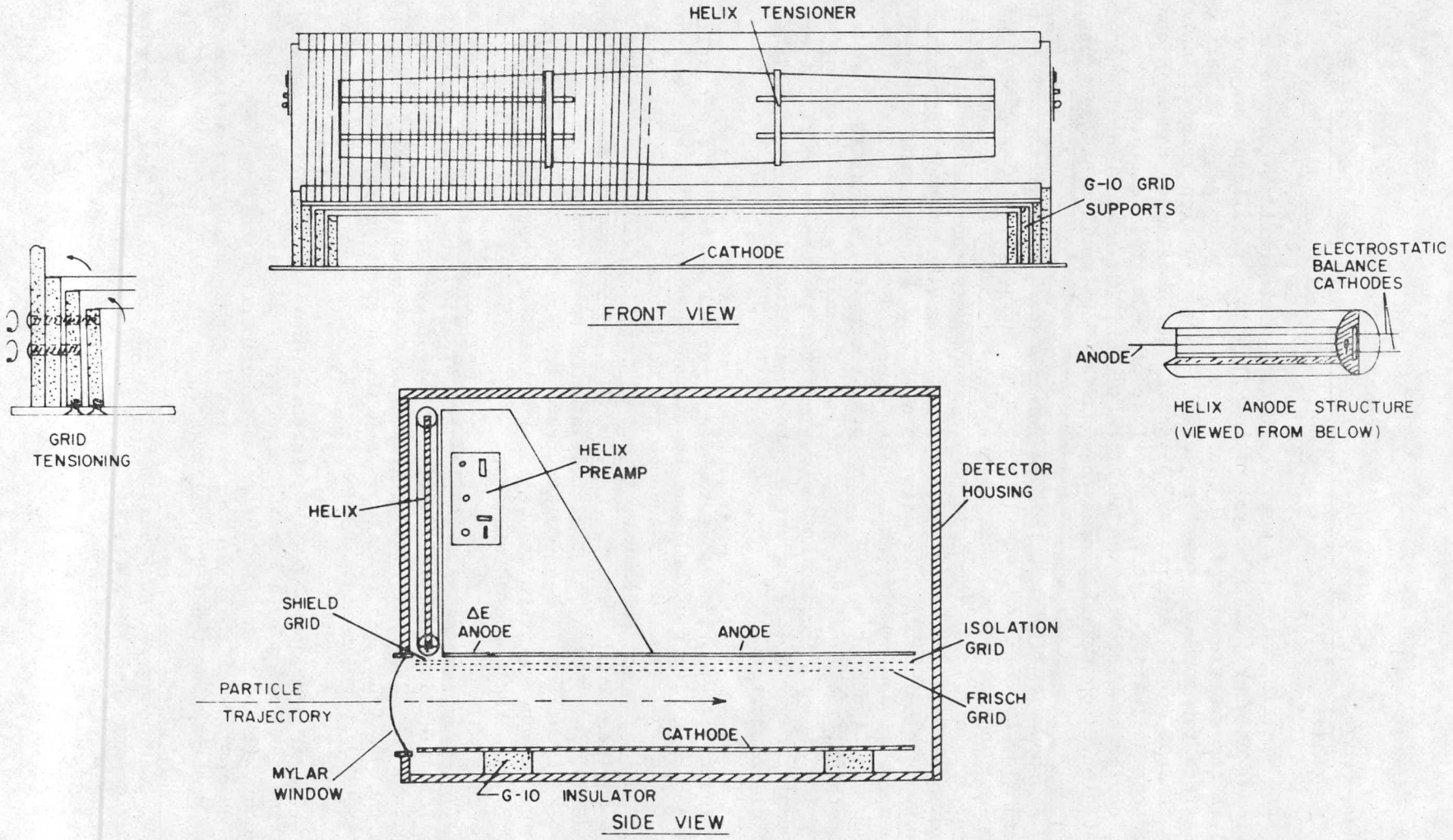

Fig. C18. Sectional views of the heavy-ion detector.

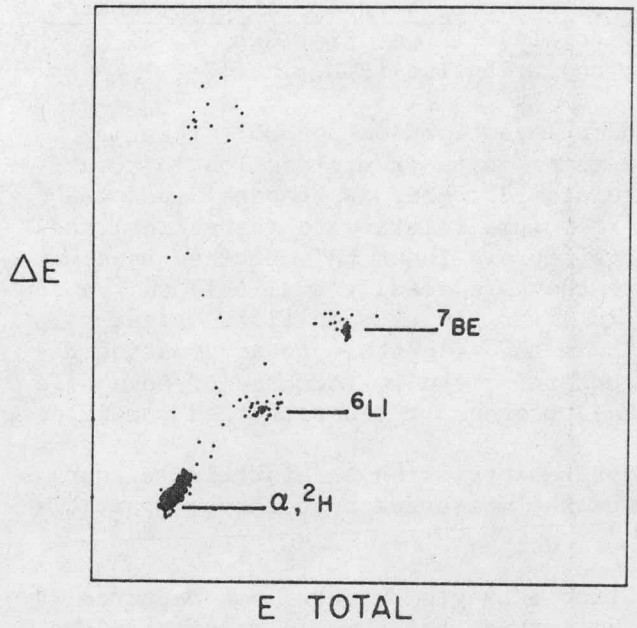

Fig. C19. Particle identification for the $^{58}Ni(^{3}He,^{7}Be)^{54}Fe$ reaction at 43 MeV.

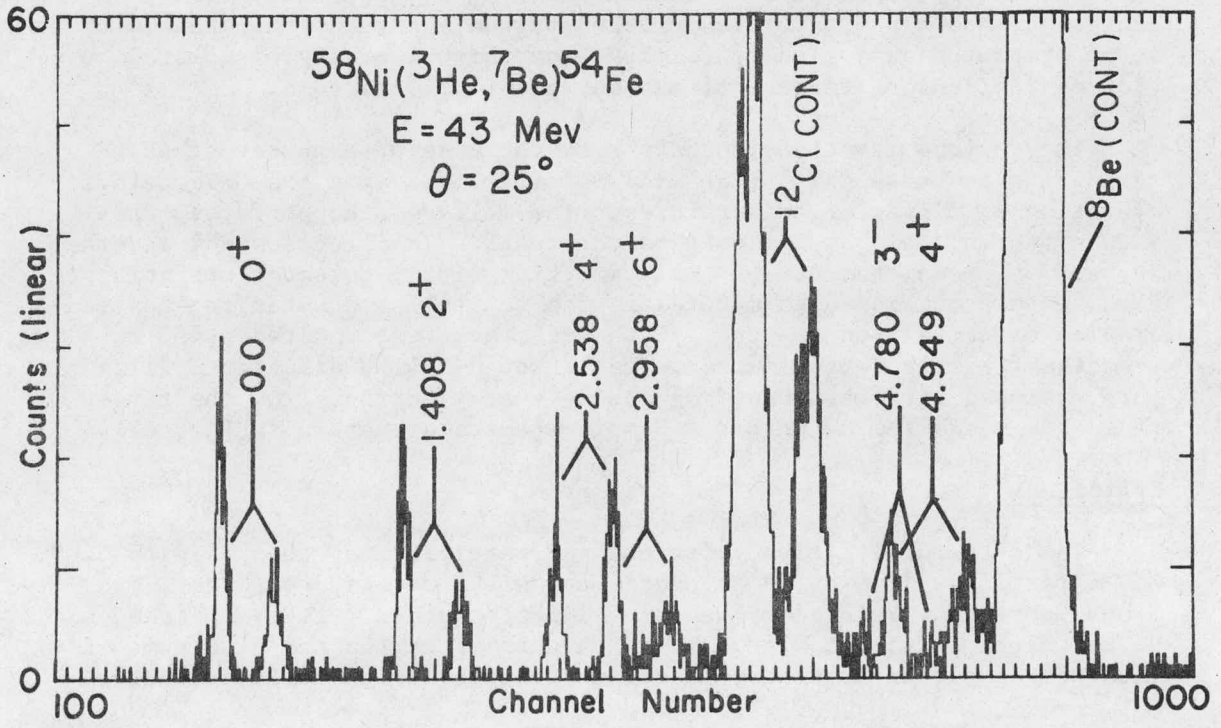

Fig. C20. A spectrum of states in ^{54}Fe observed with the heavy-ion detector and energy-loss spectrometer. Each state appears as a doublet because the ^{7}Be ejectile is emitted either in its ground state or first excited state.

9. An Evaluation of a CdTe Detector as a Practical Spectrometer for Energetic Charged Particles - R. A. Ristinen, R. J. Peterson, J. J. Hamill; and G. Entine (RMD, Inc.)

CdTe detectors have been under investigation for more than 15 years[1] with the primary interest being in their application to x-rays and γ rays where the high average atomic number is responsible for a high detection efficiency per unit volume relative to the silicon and germanium devices now commonly available. These CdTe devices have now been developed to the point where they are readily available on the commercial market[2] for application in a variety of specialized situations. To our knowledge there is in the literature no information derived from direct measurements concerning the performance of CdTe as a spectrometer for energetic (>5 MeV) protons or other charged particles.

We have made a number of measurements which should help to characterize the performance of CdTe for the measurement of charged particle spectra.

Our measurements were made with a single detector manufactured by RMD, Inc. The device was about 2 mm thick and 8 mm in diameter. The measurements included the detector response to conversion electrons from a ^{207}Bi source, alpha particles from an ^{241}Am source, and protons, deuterons, and alpha particles emitted by nuclear reactions induced by beams of protons and alpha particles from the University of Colorado cyclotron incident on targets of carbon, aluminum, and gold.

The various reaction products were detected at a number of scattering angles between 20° (lab) and 90° (lab) and with the CdTe detector operating at different temperatures, bias voltages, count rates, and with different main amplifier time constants. In all cases the reverse current was less than 100 nA. A 5 mm thick Si(Li) detector operating at room temperature was also mounted in the scattering chamber for the generation of comparison spectra. Both detectors were located at 20 cm from the target and viewed the target through 2.5 mm diameter collimators equipped with permanent magnets so that electrons from the target would not reach the detectors. Sample spectra are shown in Fig. C21.

Efficiency

The detector efficiency for charged particles was checked with 5.49 MeV α particles from an ^{241}Am source and with protons, deuterons, and alpha particles produced by beams of 14 MeV protons, 22 MeV protons, and 35 MeV alpha particles, incident on targets of carbon and aluminum. Efficiencies were in each case measured relative to the Si(Li) detector.

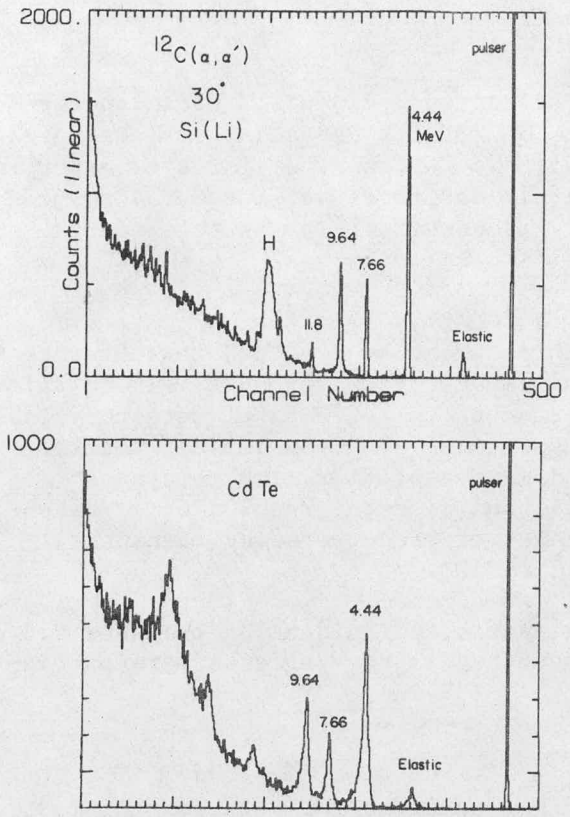

Fig. C21. A comparison of spectra obtained under identical conditions with a Si(Li) detector and a CdTe detector. In both cases the target was ^{12}C, the scattering angle was 30°, and the α beam energy was 35.2 MeV. The gains are not equal in the two spectra.

For protons, the CdTe efficiency was found to rise with increasing energy and to attain a maximum value of about 80%. For alphas and deuterons the efficiency appears to decrease with increasing energy. At this point we can offer no explanation for this behavior; perhaps the observed efficiency is characteristic of only this particular CdTe detector.

Energy Resolution

The detector energy resolution was determined for a variety of particles and energies. A pulser peak was present in each spectrum to ensure that the noise contribution to the line width from the electronics was negligible. Typically this contribution was no greater than about one-fourth the total line width. Si(Li) line widths were measured under conditions identical to those used for the CdTe line width determination and thus include all contributions due to energy spread in the incident beam, target thickness, kinematic broadening, and electronics. The line width due to the CdTe detector alone was about 470 keV, or about 2% for alpha particles in the range of 20 to 30 MeV. Similarly, for protons of 8 to 12 MeV the line width due to the CdTe device alone was approximately 187 keV, about 2%.

Linearity

The dependence of signal pulse height on incident particle energy was examined for protons in the range of 3 to 12 MeV and for alpha particles in the energy range of 7 to 35 MeV. Within the limits of experimental uncertainty, both CdTe and Si(Li) detectors were observed to produce output pulse amplitudes linearly proportional to particle energy.

Other Factors

There are a number of factors which might be expected to influence detector operation, but which were not investigated exhaustively in this work. We did make a cursory examination of the effects of detector bias voltage (20 V to 80 V), detector temperature (-50°C to +25°C), total count rate (1,000 to 10,000 cps), and main amplifier time constants (0.25 to 8.0 μsec) on signal amplitude and detector resolution. The observed effects over the indicated ranges of each operating parameter were not dramatic, in the range of 10 to 50%.

All measurements were made with particles incident on the same 2.5 mm dia. spot on the detector front surface, so edge effects were not investigated.

Conclusions

These early studies of a single CdTe device as a particle spectrometer indicate that the devices are linear in pulse height versus energy and that the energy resolution is intermediate between Si(Li) and scintillators such as NaI. There may be a serious problem, however, with an energy-dependent efficiency, possibly only for this particular device, that remains to be understood before CdTe can be seriously employed for nuclear physics investigations. Further studies will include similar measurements on other CdTe detectors and measurements of radiation damage effects due to fast neutrons.

---

[1] For a recent review of progress in CdTe devices, see:
R. C. Whited and M. M. Schieber, Nucl. Instr. and Meth. 162 (1979) 113.

[2] Radiation Monitoring Devices, Inc., 44 Hunt St., Wetertown, MA 02172.

10. Time-of-Flight Spectrometer for EPICS - T. G. Masterson

A fast particle time-of-flight system was assembled to monitor the relative number of pions, muons, and electrons in the EPICS channel at LAMPF. The micro-structure time interval between beam pulses is 5 ns and the system was designed to operate within this time range.

The system consisted of two very fast Pilot U scintillators mounted on the fastest commercially available RCA phototubes (C31024). The measured intrinsic time resolution of the phototube-scintillator combina-

tion was 140 ps. The two scintillators were separated by 4 m and placed in the direct pion beam just downstream of the scattering target. The scintillators were capable of handling instantaneous rates of several megahertz and the direct beam rates approached this value. Although the fast electronics could handle this rate comfortably, the slow electronics (digitizing the time intervals) could not and a random sampling device was designed to reduce this rate. A schematic of the electronics and a typical flight time spectrum are shown in Figs. C22 and C23.

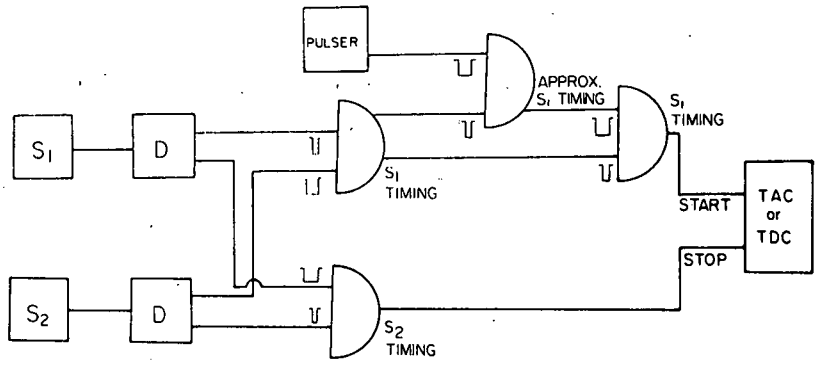

Fig. C22. Schematic of electronics for fast time-of-flight system. The coincidence units in the start and stop legs of the circuit ensure that only valid events reach the TDC. The pulser unit allows sampling at any desired rate.

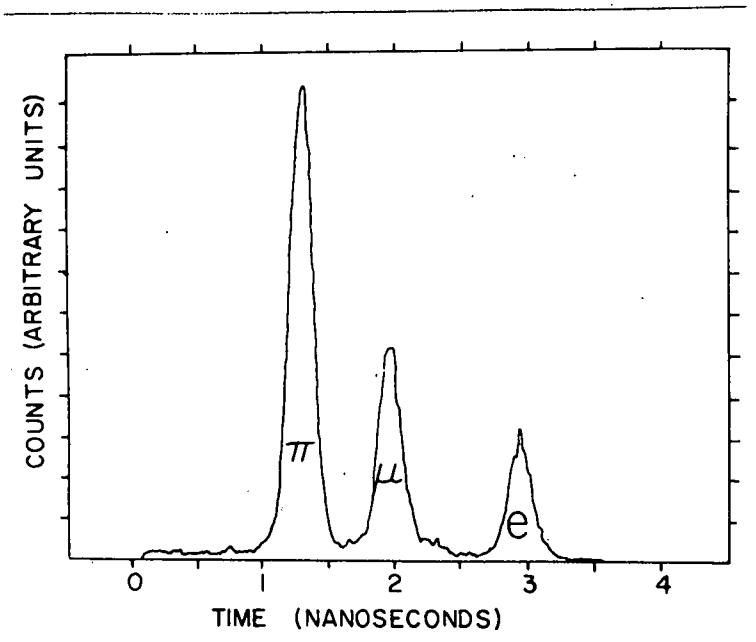

Fig. C23. Time-of-flight spectrum showing clear separation of π's, μ's and e's within a 5 ns time interval.

11. Energy-Time Distribution of the Cyclotron Beam - T. Masterson, D. Murdock, R. Raymond, P. Smith and C. Zafiratos

This laboratory has developed large-volume neutron detectors with reasonable (1 ns) time resolution for very-long-flight-path neutron time-of-flight spectroscopy. An alternative approach involves the use of sub-nanosecond resolution detectors at conventional distances of about 10 meters. Sub-nanosecond beam bursts are required and two avenues to this goal are being investigated. One involves modification of the cyclotron and is being pursued as reported elsewhere in this report. The other would use a buncher operating at 200 MHz with amplitudes of about 100 kV. In either case we will need to measure the distribtuion of the beam in E-t phase space.

A solid state detector will give the required time resolution of about 0.1 nanosecond. The energy resolution of such detectors at cyclotron beam energies is, however, marginal for this purpose. Nonetheless, the simplicity of a direct E-t correlation with a single detector led us to pursue this possibility.

A 28 MeV alpha beam was extracted in a single-turn mode from the cyclotron. A small chamber which held a target and solid state detector was inserted in the switchyard beam line about 7-1/2 meters from the exit of the deflector. A 170 $\mu g/cm^2$ Au foil was used to scatter beam particles into the detector at 90°. A biased amplifier and biased time-to-amplitude converter (TAC) were used to provide sufficient dispersion in both E and t. The stop signal for the TAC was taken from the cyclotron r. f.

A two-dimensional plot of E vs. t is shown in Fig. C24. The events extending downward from the elastic alpha group are caused by inelastic scattering. The horizontal line of events is due to a pulser. The events at an earlier time and at higher energy than the elastic alphas are presumably due to a different turn partially extracted from the cyclotron. The extreme widths of the elastic group are about 150 keV in energy and 1 ns in time.

To determine whether the detector had adequate resolution at this energy, it was then placed in the scattering chamber of the energy-loss spectrometer. A strip of gold 0.7 mm wide was evaporated onto a carbon backing. With the beam swinger operating in the dispersion mode this strip intercepted a 12 keV wide slice of the dispersed 28 MeV alpha beam. The observed width of the elastic alpha peak seen with the detector was 42 keV FWHM. Thus we concluded that the detector resolution was just adequate to make the results in Fig. C24 useful.

The energy distribution of the 28 MeV alpha beam was then measured by stepping the gold strip target across the dispersed beam profile. The results are shown in Fig. C25. The FWHM of the beam is seen to be about 55 keV. However, the distribution is broad at the base and asymmetric. The profile in Fig. C25 is consistent with an extreme distribution near 150 keV width. Correlated time measurements could not

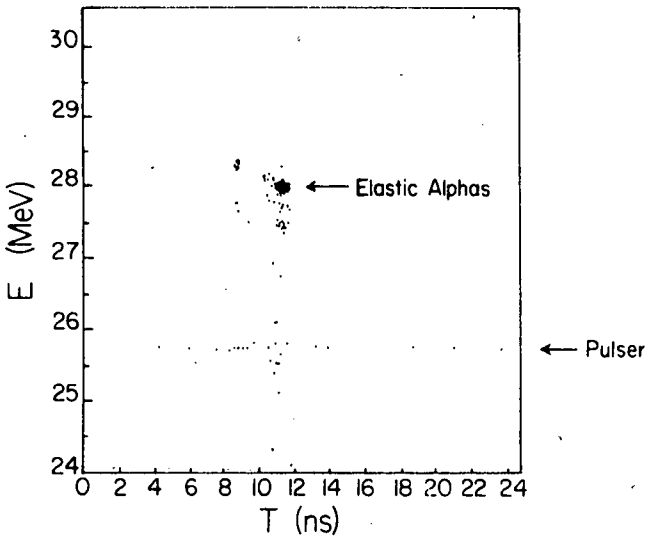

Fig. C24. Energy vs. time for a 28 MeV alpha beam. These data were obtained with a silicon detector observing alphas scattered by a gold foil. The events below elastic alphas represent inelastic scattering. The weak group to the upper left is presumably a different turn extracted from the cyclotron.

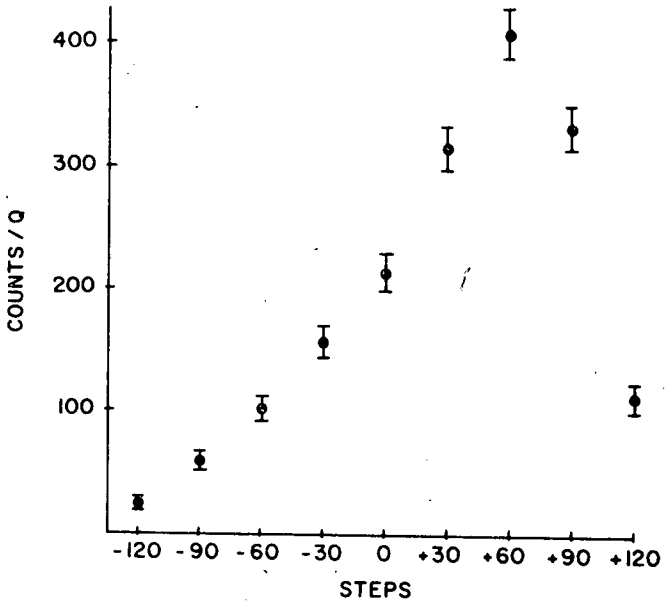

Fig. C25. Beam intensity vs. energy as measured in the magnetic spectrometer for the conditions of Fig. C24. Each step on the horizontal axis represents 0.5 keV.

be made with the magnetic spectrometer because of the non-isochronous trajectories followed by beam particles in the dispersion mode of operation.

We now plan to use a smaller volume, higher resolution solid state detector to study a variety of beams at the switchyard location. Some time smearing of the beam caused by energy spread occurs even at the switchyard. For the 28 MeV alpha beam a 100 keV spread produces over 1/3 ns of time spread in the 7-1/2 m flight from the cyclotron. The possibility of operating in the cyclotron target box will be investigated.

D. Cyclotron Operation - A. B. Phillips

Operation for the period 1 September 1979 to 31 August 1980 is covered below. Table D-I shows hours of cyclotron operation by purpose. Table D-II shows hours of operation by particle and energy range. An additional 73 hours were spent on tests of cyclotron components without beam.

Of the 8784 hours in the leap year, the cyclotron was available for use 89% of the year, and was running for experiments 64% of the year. Actual beam-on-target time was 4308 hours, equal to 77% of cyclotron running time or 49% of the year.

The cyclotron was out of commission for various reasons for 991 hours, or 11% of the year. 492 hours were spent on scheduled maintenance, 91 hours on scheduled repairs, and 408 hours on unscheduled repairs. Of the scheduled repairs, the biggest item was 72 hours for repairing an internal water leak in the cyclotron. The repair actually took 2-1/2 weeks, but most of it was done concurrently with the two weeks of down time scheduled for annual maintenance.

Also included in scheduled repairs are 6 hours which had to be taken out of operating time last October for spraying for an infestation of black widow spiders. At least 31 dead spiders were counted. Luckily, we caught it before anybody was hurt.

Major non-scheduled repairs, meaning those which wiped out scheduled experiment runs, consisted of the following:

1. 114 hours - 45° magnet power supply repairs, choke failure.
2. 16 hours - RF repairs
3. 96 hours - repairs to beam flapper (pulser)
4. 160 hours - internal water leak (same one noted in scheduled repairs.)

Of the minor non-scheduled repair times, two are worth noting. One evening the experimenters were plagued by recurrent fire alarms--and fire trucks--due to a dirty smoke detector, which shut them down temporarily. The other case is that of one of the main mechanical vacuum pumps, which sprung a leak into the vacuum pumping chambers from the water cooling jacket. Only a few hours were lost because we had an exact replacement which had been given to us by another campus laboratory when they declared it surplus two years ago.

Listed on the next page are experiments in collaboration with experimenters from other laboratories.

Collaboration

57 hours - Two runs for Yale Medical School, studies in the use of ^{48}Ca as a stable medical tracer isotope.
68 hours - R. De Vries, LASL.
116 hours - N.S.P. King, LASL.
98 hours - P. M. Walker, Michigan State University.
70 hours - S. D. Schery, New Mexico Tech, Socorro, NM.
131 hours - W. P. Alford, Univ. of Western Ontario, London, Ontario, Canada.
110 hours - D. Dehnhard, Univ. of Minnesota.
149 hours - N. Roughton, Regis College, Denver, CO.
799 hours total

Table D-III is a list of scheduled visitors to the laboratory during the period.

Table D-1

Hours of Cyclotron Operation - PURPOSE

Month	Cyclotron Development & Test	Research		Service		Subtotal Hrs/mo.
		Staff	Collaborate	Staff	Irradiations Outside & Collaborate	
Sept. 79	--	374	68	--	--	442
Oct.	--	565	--	--	--	565
Nov.	50	468	13	--	--	531
Dec. 79	29T	247	145	--	--	392
Jan. 80	--	283	173	--	--	456
Feb.	2T	308	154	--	--	462
March	--	458	40	--	--	498
April	3T	271	38	--	--	309
May	18T	399	--	--	--	399
June	21T	412	31	--	--	443
July	--	566	27	--	--	593
Aug.	--	531	--	--	--	531
Totals	50 + 73T	4,882	689	--	--	5,621 + 73T

Table D-II
Hours of cyclotron operation - PARTICLE

Month	Protons 6-28 MeV	Deuterons 14-17 MeV	H_2^+ 8 MeV	^3He 25-44 MeV	^4He 2-43 MeV	Subtotal Hrs/mo.
Sept. 79	13	46	--	202	181	442
Oct.	9	--	--	212	344	565
Nov.	5	--	--	492	34	531
Dec. 79	7	--	--	201	184	392
Jan. 80	70	--	11	125	250	456
Feb.	29	--	--	131	302	462
March	123	19	--	194	162	498
April	139	80	--	90	--	309
May	--	99	--	56	244	399
June	17	--	--	241	185	443
July	--	--	--	336	257	593
Aug.	80	--	--	245	206	531
Totals	492	244	11	2,525	2,349	5,621

Table D-III

Scheduled Visitors - 9-1-79 to 8-31-80

Date	No.	From
10-27-79	19	Foreign exchange students, CIRES, Boulder
11-10-79	25	Physics classes, U.C. Denver
11-12-79	16	C.U. classes, Astrogeophysics and Physics
1-17-80	16	Soc. Physics students, USC, Pueblo, CO
1-17-80	8	C.U. Health Physics class
1-30-80	6	C.U. Health Physics class
3-12-80	8	C.U. Physics 214 class
3-13-80	9	C.U. Physics 214 class
3-17-80	3	Moscow, Kharkov, USSR
3-18-80	8	C.U. Health Physics class
3-24-80	5	Warren Tech. Center, Golden, CO
4-1-80	6	C.U. Health Physics class
4-10-80	30	Open house - C.U. graduate students
4-11-80	4	South Dakota School of Mines
4-21-80	17	Physics class, Colorado College, Colo. Spgs., CO
5-3-80	20	Physics classes, U.C. Denver
5-6-80	2	Physics class, U. of Wyoming, Laramie, WY
5-9-80	52	Physics class, Gateway H.S., Aurora, CO
6-20-80	24	C.U. High School Science Teachers' Conference
6-23-80	22	C.U. High School Science Teachers' Conference
7-12-80	20	Physics classes, U.C. Denver
8-18-80	125	C.U. Eng.-Annual High School Honors Conference
8-19-80	60	C.U. Eng.-Annual High School Honors Conference
Total	505	

III. THEORETICAL PROGRAM

A. A Weak-Coupling Analysis of the ^{205}Tl(p,t)^{203}Tl Reaction - E. Rost

Several low-lying states of ^{203}Tl have been calculated by Covello and Sartoris[1], who used a weak-coupling model involving a proton hole ($s_{1/2}$, $d_{3/2}$, or $d_{5/2}$) coupled to a ^{204}Pb core (either 0^+ or 2^+). This model can be tested by measuring relative cross sections in the ^{205}Tl(p,t)^{203}Tl reaction. An additional test of the model is obtained by comparison to the strengths of the ^{204}Pb core-state excitations.

In order to apply the model the states of ^{203}Tl and ^{205}Tl are expanded

$$\psi^J_M = \sum_{jNR} C^J_{jNR} \left[\phi^j \chi^R_{(N)}\right]^J_M$$

in terms of hole states ϕ^j and core states $\chi^R_{(N)}$ involving an N-phonon state of angular momentum R. The expansion coefficients are taken from ref. 1 and are assumed to be the same for ^{205}Tl and ^{203}Tl. The form factor for a (p,t) reaction, assuming a spectator hole state, is then proportional to

$$\begin{aligned}
\langle \psi^{J_B}_{M_B} | V | \psi^{J_A}_{M_A} \rangle &= \sum_{jNRN'R'\lambda} C^{J_A}_{jNR} C^{J_B}_{jN'R'} \\
&\times \langle \left[\phi^j \chi^{R'}_{(N')}\right]^{J_B}_{M_B} | V^\lambda_{M_B - M_A} | \left[\phi^j \chi^R_{(N)}\right]^{J_A}_{M_A} \rangle \\
&= -\sum_{jNRN'R'\lambda} (\lambda J_A M_B - M_A M_A | J_B M_B)(-1)^{R+R'-J_A-J_B} C^{J_A}_{jNR} C^{J_B}_{jN'R'} \\
&\times \sqrt{(2R'+1)(2J_A+1)}\, W(\lambda R J_B j; R' J_A) \langle \chi^{R'}_{(N')} || [V^j \chi^R_{(N)}]^{R'} \rangle \qquad (2)
\end{aligned}$$

The reduced matrix elements are, in turn, proportional to those of creation (destruction) operators for a phonon of type λ

$$\langle \chi^{R'}_{(N')} || [V^\lambda \chi^R_{(N)}]^{R'} \rangle \propto \langle N'R' || b_\lambda + b^\dagger_\lambda || NR \rangle \qquad (3)$$

and have been tabulated by Raz[2]. To obtain the normalization constants we use the experimental ^{206}Pb(p,t)^{204}Pt data and standard DWBA calculations

$$\left(\frac{d\sigma_{EX}}{d\Omega}\right) = \frac{\epsilon_\lambda}{2\lambda+1} \left| \langle 1\lambda || b^\dagger_\lambda || 00 \rangle \right|^2 \left(\frac{d\sigma_{DW}}{d\Omega}\right) = \epsilon_\lambda \left(\frac{d\sigma_{DW}}{d\Omega}\right) \qquad (4)$$

thereby defining enhancement factors ϵ_λ.

The $^{205}Tl(p,t)^{203}Tl$ cross sections are then obtained from eqs. 2, 3, and 4 by summing over M_A and M_B leading to the final result

$$\left(\frac{d\sigma_{TH}}{d\Omega}\right)^{J_B} = \frac{\varepsilon_j}{2j+1}\Big| \sum_{jNRN'R'} \sqrt{(2J_B+1)(2R'+1)}\, W(\lambda R J_B j; R' J_A)(-1)^{R+R'} \times C^{J_A}_{jNR}\, C^{J_B}_{jN'R'} \langle N'R' \| b_\lambda + b_\lambda^+ \| NR\rangle^2 \left(\frac{d\sigma_{EX}}{d\Omega}\right)_\lambda \tag{5}$$

In Table III-I the calculated enhancement factors are presented for the six lowest states in ^{203}Tl for which the Covello and Sartoris[1] model applies. The agreement is quite good. In particular, the ground state transition is seen to carry the same strength as the $^{206}Pb(p,t)^{204}Pb$ transition and the five $\lambda=2$ transitions are correctly ordered in energy and in relative strength. Thus the weak-coupling model is able to account for all the strong L=2 states below 1400 keV.

Table III-I

Calculated and experimental excitation energies and enhancement factors for the $^{205}Tl(p,t)^{203}Tl$ reaction.

E_{EX}(keV)	E_{TH}(keV)	J^π	λ	ε_{EX}	ε_{TH}	$\varepsilon_{TH}/\varepsilon_{EX}$
0.0	0.0	$1/2^+$	0	5.88	6.11	1.04
279	593	$3/2^+$	2	0.46	0.66	1.44
681	683	$5/2^+$	2	3.20	2.38	0.74
1045	1049	$3/2^+$	2	0.83	0.89	1.07
1066	1207	$5/2^+$	2	0.47	0.22	0.47
1325	1314	$3/2^+$	2	0.20	0.08	0.40

A paper presenting these results has been submitted to Nuclear Physics.

[1] A. Covello and G. Sartoris, Nucl. Phys. A93 (1967) 481.
[2] B. J. Raz, Phys. Rev. 114 (1959) 1116.

B. Finite-Range Two-Nucleon Transfer - P. D. Kunz

The two-nucleon transfer reaction induced by light ions has been calculated[1-6] in finite range by many authors. While most of the calculations have been done in a configuration-space representation, Charlton[4] has formulated a momentum-space calculational technique[8-10]. This method efficiently evaluates the finite-range integrals needed for the cross sections and is incorporated into the computer code DWUCK5[11]. We will present the changes from the formulation of Charlton[4] in calculating the form factor used in the code.

The differential cross section for the usual DWBA treatment of the reaction A(p,t)B can be written as

$$\frac{d\sigma}{d\Omega} = \frac{(T_B 1 N_B 1 | T_A N_A)^2}{(2s_a+1)(2J_A+1)} \sum_{m_a M_A} \sum_{m_b M_B} |T_{m_a M_A m_b M_B}|^2 ,$$

where the transition amplitude is given by

$$T_{m_a M_A m_b M_B} = \int dr_1 dr_2 dr_a$$

$$x \; \psi^{-*}_{m_b}\left(\frac{r_1+r_2+r_a}{3} - R_B\right) V_{m_a M_A m_b M_B} \psi^{+}_{m_a}(r_a - R_A).$$

Here T_A and T_B are the initial and final nuclear isotopic spins with projections N_A and N_B and the $\psi^{\pm}_m$ are the initial and final distorted waves.

The nuclear matrix element integrated over the dineutron relative coordinate may be written

$$\int V_{m_a M_A m_b M_B} dr = \int \langle \Psi_{I_B M_B}(\xi_B) \phi^*_{t j_b m_b}(r,\rho) \left| V(r_1 - r_a) + V(r_2 - r_a) \right|$$

$$\times \Psi_{I_A M_A}(\xi_B, r_1, r_2)\, \chi_{j_a m_a}(\sigma_p) \rangle\, dr$$

$$= \sum_{LSJ\ell sj} F_{LJ\ell js}(R,\rho)\ \ (I_B J\, M_B M \,|\, I_A M_A)$$

$$\times (j_a j\, m_a m \,|\, j_b m_b)(L s M_L m_s \,|\, J\, M)$$

$$\times (\ell s m_\ell m_s \,|\, j\, m)\ i^{\ell - L}\ Y^*_{LM_L}(R)\ Y_{\ell m_\ell}(\rho).$$

The coordinates are defined by

$$R = (r_1 + r_2)/2$$

$$r = (r_2 - r_1)$$

$$\rho = r_a - R\ .$$

The triton is defined to be in a spatially symmetric s state and its wave function has the form

$$\phi_{t m_b}(r,\rho) = \phi_t(r,\rho)[\chi(\sigma_1)\chi(\sigma_2)]_{00}\chi_{m_b}(\sigma_a)$$

The spatial part of the wave function is taken from a variational calculation of Tang and Herndon[12] with the normalization

$$\int \left| \phi_t(r,\rho) \right|^2 dr\, d\rho = 1.$$

The overlap between the initial and final target states is expressed by

$$\langle \Psi_{I_B M_B} \,|\, \Psi_{I_A M_A} \rangle_J = u_{\ell_1 j_1 \ell_2 j_2}(r_1, r_2) \sum_{S=0,1} [(\ell_1 \tfrac{1}{2}) j_1 (\ell_2 \tfrac{1}{2}) j_2 \,|\, (\ell_1 \ell_2) L (\tfrac{1}{2}\tfrac{1}{2}) S]_J$$

$$\times \left\{ [Y_{\ell_1}(r_1) Y_{\ell_2}(r_2)]_L [\chi(\sigma_1)\chi(\sigma_2)]_S \right\}_J .$$

The radial function above is generally a product of two single-particle orbitals generated from a Wood-Saxon potential adjusted to give a binding energy equal to half the two-neutron separation energy.

The computer code DWUCK5 requires as input the Fourier transform of the form factor in the form

$$f_{LJ\ell j}(Q,P) = \frac{1}{4\pi} \int e^{-iQ\cdot R}\, e^{ip\cdot P}\; F_{LJ\ell j}(R,\rho) Y^{*}_{LM_L}(R)\; Y_{\ell m_\ell}(\rho)$$

$$\times\; dR\; d\rho\; Y_{LM_L}(Q) Y^{*}_{\ell m_\ell}(\rho)\; dQ\; dP/Q^{L}P^{\ell}$$

which reduces to

$$f_{LJ\ell j}(Q,P) = 4\pi \int_0^\infty \int_0^\infty F_{LJ\ell j}(R,\rho)(Q^{-L}) j_L(QR)(p^{-\ell}) j_\ell(p\rho) R^2 dR\; \rho^2 d\rho.$$

In order to calculate the momentum-space form factor it is convenient to transform the product of the potentials and triton wave function,

$$[V(r_1-r_a) + V(r_2-r_a)]\; \Phi_t(r,\rho) = (2\pi)^{-6} \int g_o(p,q) e^{ip\cdot\rho} e^{iq\cdot r} dq\; d\rho$$

where we have kept only the lowest angular momentum component of the triton. Similarly the target state function is expanded into momentum space:

$$[(\ell_1 \tfrac{1}{2}) j_1 (\ell_2 \tfrac{1}{2}) j_2 | (\ell_1 \ell_2) L (\tfrac{1}{2}\tfrac{1}{2}) S]_J\; u_{\ell_1 j_1 \ell_2 j_2}(r_1,r_2) [Y_{\ell_1}(r_1) Y_{\ell_2}(r_2)]_L$$

$$= (2\pi)^{-L} \int h_L(q_1,q_2)\; [Y_{\ell_1}(q_1) Y_{\ell_2}(q_2)]_L e^{iq_1\cdot r_1}\; e^{iq_2\cdot r_2} dq_1 dq_2.$$

We make use of the technique of Bayman and Kallio[13] to transform q_1 and q_2 to the center-of-mass and relative-momentum coordinates

$$Q = q_2 + q_1$$

$$q = (q_2 - q_1)/2$$

to give

$$h_L(q_1,q_2)[Y_{\ell_1}(q_1)Y_{\ell_2}(q_2)]_L$$

$$\equiv (2\pi)^3 \sum_{L_1L_2} Q^L H_{L_1L_2}(Q,q) \; [Y_{L_1}(R)\; Y_{L_2}(q)]_L .$$

This expression inverted gives

$$H_{LO}(Q,q) = \frac{1}{8\pi^3} \; \frac{(2\ell_1+1)^{1/2}(2\ell_2+1)^{1/2}\int dq\; h_L(q_1,q_2)[D_0/2 + \sum_{m>0} D_m]}{(2L+1)^{1/2}}$$

where $D_m = (\ell_1 \ell_2 m-m|LO)\; d_{\ell_1 m}(\theta_1) d_{\ell_2 -m}(\theta_2)$

as defined in ref. 13.

The form factor then becomes a straightforward numerical integration over q,

$$f_{LJ01/2}(Q,P) = \int q^2 dq\; g_0(P,q)\; H_{LO}(Q,q).$$

The potentials used to generate the triton wave function are taken from ref. 12,

$$V(r) = V_0(r)\; P_0 + V_1(r)\; P_1$$

with

$$V_i = -V_i \exp[\; -\kappa_i(r-r_c)] \;, \qquad r>r_c$$

$$= \infty \qquad\qquad\qquad\qquad , \qquad r<r_c .$$

The P_i are the projection operators for the singlet and triplet states and the parameters are

r_c = 0.45 fm

V_o = 277.07 MeV, κ_o = 2.211 fm^{-1}

V_1 = 549.26 MeV, κ_1 = 2.735 fm^{-1}.

Because of the discontinuity in the slope of the wave functions at $r=r_c$ it is necessary to include a term[14] in the potential of the form

$$V'(r) = \frac{\hbar^2}{M} \delta(r-r_c^+) \frac{\partial}{\partial r} .$$

This term is important and for the Tang-Herndon wave functions, the (p,t) cross sections are reduced by a factor of 0.46 from the case where the V' term is not included. The shapes of low energy (p,t) reactions are not changed.

A computer code THREE has been constructed to calculate the Fourier transform of the product $V\phi_t$. The output of this program is read into DWUCK5 which then constructs the Fourier transforms of the target form factor and does the necessary integration over the variable q. The two-nucleon transfer option has been thoroughly checked against DWUCK4 by using the zero range option in DUWCK5 and also the usual finite-range calculation with separable forms of $V\phi_t$ in the coordinates ρ and r. The time for a typical case for an L=0 transfer is about 50 seconds on a CDC-6400.

1. B. F. Bayman, Nucl. Phys. A168 (1971)1;
   B. F. Bayman and D. H. Feng, ibid., A205 (1973) 513.
2. T. Takemasa, Nucl. Phys. A220 (1973) 31.
3. N. S. Chant, Nucl. Phys. A211 (1973) 269.
4. L. A. Charlton, Phys. Rev. C 12 (1975) 351.
5. M. R. Strayer and W. F. Werby, J. Phys. G 3 (1977) L179.
6. T. Takemasa, T. Tamura, and T. Udagawa, Nucl. Phys. A321 (1979) 269.
7. D. H. Feng, M. A. Nagarajan, M. R. Strayer, M. Vallieres, and W. T. Pinkston, Phys. Rev. Lett. 44 (1980) 1037.
8. D. Robson and R. D. Koshel, Phys. Rev. C 6 (1972) 1125.
9. L. A. Charlton, Phys. Rev. C 8 (1973) 146.
10. L. A. Charlton and D. Robson, Florida State University Technical Report No. 5 (unpublished).
11. P. D. Kunz, Computer code DWUCK5 (unpublished).
12. Y. C. Tang and R. C. Herndon, Phys. Lett. 18 (1965) 42.
13. B. F. Bayman and A. Kallio, Phys. Rev. 156 (1967) 1121.
14. J. Dobes, Nucl. Phys. A235 (1974) 199.

C. Effects of Deuteron Continuum States in Stripping Reaction - P. D. Kunz

The description of deuteron elastic scattering via a three-body model has been considered by several groups[1,2,3]. This model treats the system as a neutron, proton, and inert nucleus with the nuclear internal degrees of freedom evident only through the imaginary part of the nucleon-nucleus potential. The solution to this three-body Hamiltonian is expanded in deu-

teron eigenstates keeping only a few of the lowest partial waves. The different methods differ primarily in their treatment of the continuum states of the deuteron. Johnson and Soper[1] use a single state and the adiabatic approximation while Rawitscher[2] and Farrel et al.[3] use finite momentum bins. An alternative solution which we use is to quantize the states in a spherical box of finite but large radius. This method avoids the disadvantages of the binning procedure where one either uses an average energy[2] for the bin or a numerically complicated bin integration scheme[3].

The Hamiltonian for the three-body system is given by

$$H = T_R + T_r + V_{np}(r) + V_n(r_n) + V_p(r_p)$$

where T_R and T_r are the kinetic energies of the center-of-mass and internal motion of the deuteron, respectively. The potential $V_{np}(r)$ is chosen to be the separable potential of Yamaguchi[4] and V_n and V_p are the optical potentials of the proton and neutron on the nucleus A at half the deuteron incoming kinetic energy.

The solution to the Hamiltonian is expanded in eigenstates of

$$[T_r + V_{np}(r)]\ \phi_i(r) = \varepsilon_i \phi_i(r)$$

$$\Psi(R,r) = \sum_{i=0}^{\infty} \chi_i(R)\phi_i(r)$$

where $\chi_0(R)$ for the deuteron ground state has the boundary condition of incoming plane wave plus outgoing scattered wave and $\chi_n(R)$ for $n>0$ have the boundary conditions of outgoing waves only. The $\phi_n(r)$ are restricted in this work to be only relative s wave states satisfying a boundary condition

$$\phi_n(r_{max}) = 0$$

The solution of the Schrodinger equation then reduces to an infinite set of coupled equations of the form

$$(E_i - T_R - V_{ii})\ \chi_i(R) = \sum_{j\neq i} V_{ij}\chi_j(R)$$

where

$$V_{ij} = \langle \phi_i(r) \left| V_n(R + r/2) + V_p(R - r/2) \right| \phi_j(r) \rangle$$

and $E_i = E - \varepsilon_i$.

This set of equations is then truncated to give a finite set of coupled equations which can be solved by usual methods, e.g. by the computer code CHUCK.

The radius r_{max} is chosen so as to give 5 or 6 states for the deuteron center-of-mass energy between zero and the maximum energy. The states near zero energy for the center-of-mass motion are found to contribute insignificantly to the elastic scattering. For a total energy of the system of 22 MeV the value of r_{max} was about 24 fm. The comparison of our method with the calculations of Farrel et al.[3] gave very close quantitative agreement as shown in Fig. 1.

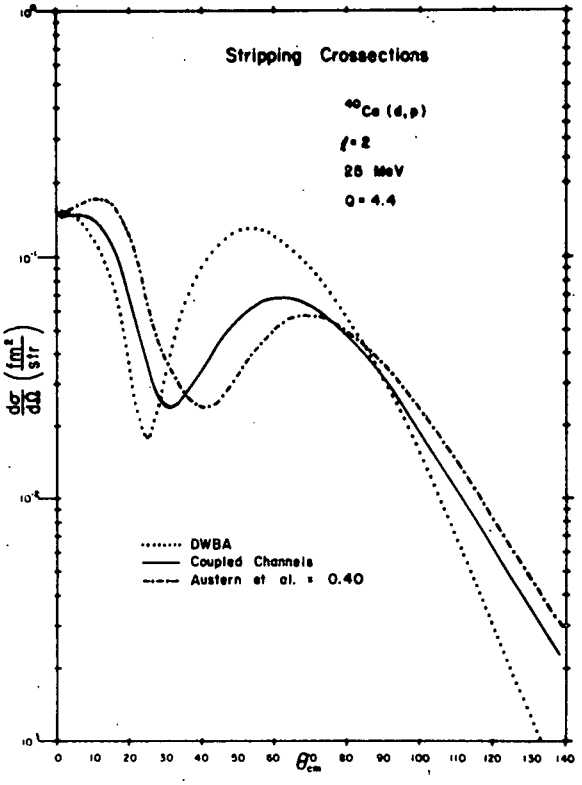

Fig. 1. Comparison of the coupled channels calculations with the DWBA and calculations by Austern et al. The Austern et al. result has been renormalized to agree with the coupled channels calculation at 0°.

1. R. C. Johnson and P. J. R. Soper, Phys. Rev. C 1 (1970) 976.
2. G. H. Rawitscher, Phys. Rev. C 9 (1974) 2210.
3. J. P. Farrel, Jr., C. M. Vincent, and N. Austern, Ann. Phys. (NY) 96 (1976) 333. Ibid, 114 (1978) 93.
4. Y. Yamaguchi, Phys. Rev. 95 (1954) 1628.

D. Non-locality Effects in Nuclear Reactions - H. Haghbin and P. D. Kunz

It is well known that the nucleon-nucleus optical potential is non-local. The non-locality can be parameterized following refs. 1 and 2 in the form:

$$V(\bar{r}_1,\bar{r}_2) = V_c(r_1)\delta^3(\bar{r}_1-\bar{r}_2) + H_1(R)\ U(r) + iH_2(R)W(r)$$

$$\bar{r} = \bar{r}_2-\bar{r}_1\ ,\ \bar{R} = \frac{\bar{r}_2+\bar{r}_1}{2}$$

where U and W are nuclear potential shapes chosen to be of Wood-Saxon form and H_1 and H_2 are non-local shape functions. Assuming reasonable shapes and ranges for H_1 and H_2 one solves the Schrodinger equation using momentum-space techniques, leading to a Lippmann-Schwinger equation (LSE). We have modified the matrix inversion method of reference (3) by treating the principle-value singularity in the LSE carefully as is required for application to high energy reactions.

The LSE we are concerned with is of the form:

$$R(k_1k_0) = U(k_1k_0) + \frac{2}{\pi}\ P\int_0^\infty \frac{f(k')dk'}{k'^2-k_0^2} \qquad (1)$$

We may break this integral into three terms:

$$P\int_0^\infty \frac{f(k')}{k'^2-k^2}dk' = \int_0^{k_1} \frac{f(k')dk'}{k'^2-k_1^2} + P\int_0^{k_2} \frac{f(k')}{k'^2-k_0^2}\ dk' + \int_{k_2}^\infty \frac{f(k')dk'}{k'^2-k_0^2}$$

where $k_1k_2=k_0^2$.
To evaluate the second integral we expand f(k') about k_o and keep the first two terms:

$$f(k') = f(k_0) + f'(k_o)(k'-k_0) + \ldots$$

The first term does not contribute since

$$P\int_{k_1}^{k_2} \frac{dk'}{k'^2-k_0^2} = 0$$

while the second term is free of the singularity and is elementary:

$$P\int_{k_1}^{k_2} \frac{f'(k_0)(k'-k_0)dk'}{k'^2-k_0^2} = f'(k_0)\ell n \frac{k_0+k_2}{k_0+k_1} .$$

The correction terms are negligible if we choose k_1 and k_2 close enough to k_0. Now we make the transformations

$$k = \begin{cases} k_0 \tanh X, & \text{for } k < K_0 \\ k_0 \coth X, & \text{for } k > K_0 . \end{cases}$$

The LSE then takes the form

$$R(k_1 k_0) = U(k,k_0) + \frac{2k_0}{\pi} \int_0^{X_0} \phi(x)dx - \frac{2k_0}{\pi} \int_0^{X_0} \xi(x)dx$$

$$+ \frac{2}{\pi} f(k_0) \ell n \frac{k_0}{k_1}$$

where

$$\phi(x) = U(k,k')R(k',k_0)$$

$$\xi(x) = U(k,k')R(k',k_0) .$$

This method was tested by comparing our wave functions and scattering amplitudes with those obtained by conventional configuration-space calculations at 700 and 800 MeV. The relativistic Schrodinger equation was used with the Coulomb potential method outlined in ref. 4.

The Fourier transforms of H_1 and H_2 were chosen to be

$$G_1(K^2) = \frac{1}{1-\lambda_1\beta^3/\alpha^3} \left[e^{-k^2\alpha^2/16} - \lambda\beta^3/\alpha^3 \, e^{-k^2\beta^2/16}\right]$$

$$G_2(K^2) = \frac{1}{1-\lambda_2} \left[1 - e^{-k^2\lambda^2/16}\right] .$$

In practical calculations, it is convenient to replace the non-local potential by an energy-dependent local equivalent potential (ref. 2). The parameters of non-local shapes were chosen to reproduce the energy dependences of the real and imaginary central potential depths compiled in ref. 5.

The work will continue by starting with the G-matrix as input for calculation of an optical potential. This potential is non-local due to G-matrix non-locality and anti-symmetrization effects. The effects of this non-locality on nuclear reactions at intermediate energy will then be studied.

1. F. Perey and B. Buck, Nucl. Phys. 32 (1962) 353.
2. H. Fiedeldey, Nucl. Phys. 77 (1966) 149.
3. M. I. Haftel and F. Tabakin, Nucl. Phys. A158 (1970) 1.
4. C. M. Vincent and S. C. Phalak, Phys. Rev. C 10 (1974) 391.
5. G. Passatore, Nucl. Phys. A95 (1967) 694.

E. Studies of the Sensitivity of the Ratio of π^+ Elastic Cross Sections to the rms Charge Radius of Light Nuclei - T. Masterson, E. Rost and M. Stanton

The elastic scattering[1] of low energy π^- from light nuclei has indicated that the ratio of elastic cross sections from different isotopes is very sensitive to neutron matter radius differences between the isotopes. Differences accurate to a few hundredths of a fermi have been obtained in this manner. Although theoretical studies [1-3] indicate model sensitivity to be minimal, a more conclusive test of this method is to perform the analogous experiment and analysis with positively charged pions which would then be sensitive to proton matter radius differences. Since proton matter radii are independently measured using electron scattering or muonic x-ray studies, comparison of π^+ experiments with these measurements would test the validity of the π^- method.

One such π^+ study has already been undertaken [3] but its accuracy ($\pm$.02 fm for a comparison of ^{11}B and ^{12}C proton radius differences) was better than either the muonic x-ray data[4] ($\pm$.06fm) or the electron scattering data[5] ($\pm$.12 fm). A further experimental study is needed using isotopes such as ^{14}N, $^{16,18}O$ where the charge radius and radius differences are adequately known.

We have calculated the π^+ elastic scattering ratios for $^{14}N/^{16}O$ and $^{16}O/^{18}O$ comparative studies using the pion-nucleus optical potential program DUMIT[6]. These are shown in Figs. 2 and 3 respectively. Calculations have been made with the global parameters

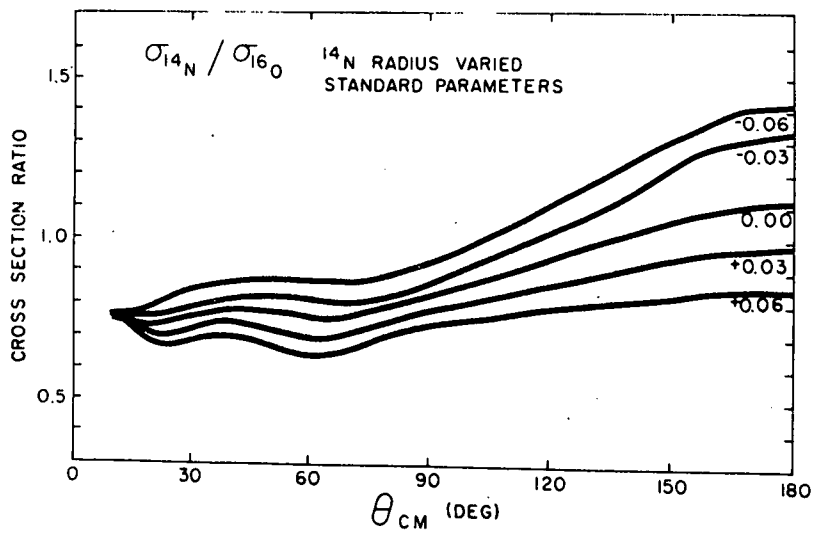

Fig. 2. Effect on elastic cross section ratio $\sigma(\pi^+ + ^{14}N)/\sigma(\pi^+ + ^{16}O)$ of variation of radius parameter 'a' by ±0.03 f and ±0.06 f. Only the standard optical potential parameters were used.

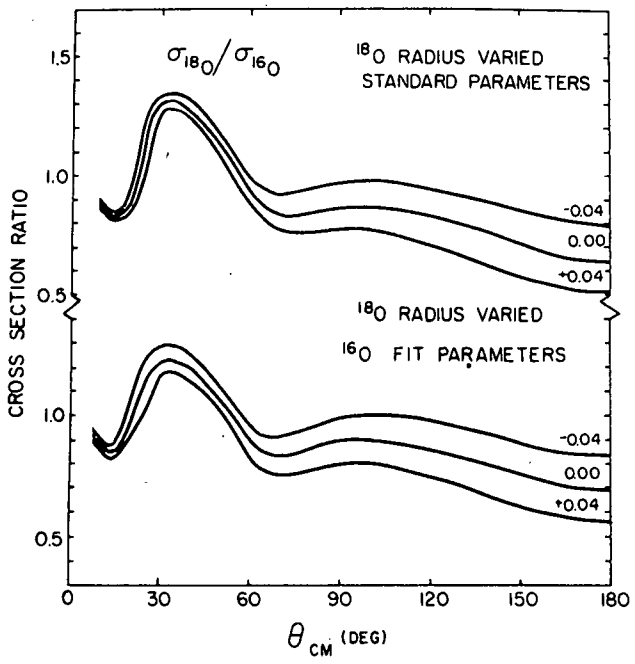

Fig. 3. Effect on elastic cross section ratio $\sigma(\pi^+ + ^{18}O)/\sigma(\pi^+ + ^{16}O)$ of variation of radius parameter 'a' by ±0.04 f. The top set of curves are for the standard optical potential parameters while the bottom set are for the best fit parameters.

described in ref. 6. For ^{14}N and ^{16}O the neutron density distribution was assumed to be the same as the proton distribution although this makes very little difference as the π^+ probe is insensitive to large variations in the neutron distribution. The measured[1] ^{18}O neutron radius was used for the $^{16}O/^{18}O$ comparison.

The figures indicate that the cross section ratios are very sensitive to small changes in the radius of the proton distribution and experimental accuracies of ±0.02 fm can be expected. The ^{14}N - ^{16}O rms proton radius difference is 0.17±0.02 fm while the ^{16}O - ^{18}O difference is .07±.01 fm. Calculations have also been made by first fitting the elastic π^+ on ^{16}O scattering data[7] of Malbrough et al. to obtain optical potential parameters. The quality of this fit is excellent as shown in Fig. 4. The ratios obtained with these parameters are also shown in Fig. 3 and are very similar to those calculated with the global parameters even though the absolute magnitude of the cross section has changed considerably. Both sets of parameters are listed in Table III-II.

1. R. R. Johnson et al., Phys. Rev. Lett. 43 (1979) 844.
2. Univ. of Colo. Annual Report (1979) p. 190.
3. B. M. Barnett et al., submitted to Phys. Lett.
4. G. A. Beer et al., contribution 1B27 to Eighth International Conference High Energy Physics and Nuclear Structure, Vancouver, Canada, Aug., 1979, and A. Olin, private communication.
5. C. W. de Jager et al., At. Data & Nucl. Data Tables 14 (1974) 479.
6. A. Rosenthal, Thesis, Univ. of Colo., 1978, and N. J. DiGiacomo et al., Phys. Lett. 66B (1977) 421.
7. D. J. Malbrough et al., Phys. Rev. C 17 (1978) 1395.
8. G. Rowe, M. Salomon, R. Landau, TRIUMF Report TRI-PP-78-1 (1978).

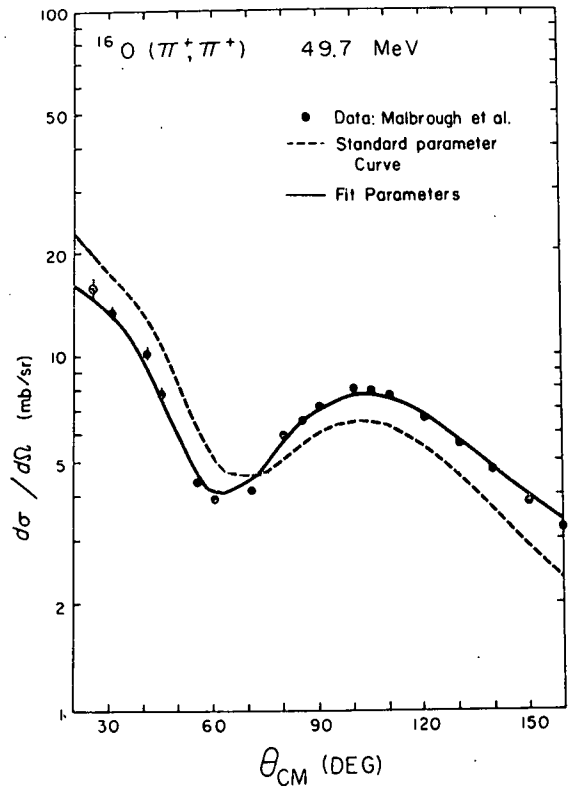

Fig. 4. A comparison of the π^++^{16}O differential cross section calculated from the standard parameters with the cross section calculated from the best fit parameters obtained by fitting to the data of Malbrough[7] et al.

Table III-II

Optical potential parameters for $\pi^{+}+{}^{16}O$.

	Standard	Best fit
πN phases	R.S.L. [8]	R.S.L. [8]
B_o	(-0.41,0.41)	(-0.60,0.11)
C_o	(0,0)	(0.17,0.23)
ξ	1.0	0.38
r,α [5]	2.789,1.544	2.789,1.544

F. Systematics of the Intermediate Energy (p,d) Reaction - J. R. Shepard

A reasonably large amount of cross section data now exists for the (p,d) and (d,p) reactions on light nuclei (A<40) at bombarding energies between 100 and 800 MeV. In addition, several analyzing power measurements have recently been made at energies below 400 MeV. In general the exact finite-range DWBA reproduces cross section data quite well when input quantities are treated carefully. (On the other hand, analyzing powers are poorly reproduced, even at the lower bombarding energies[1].)

Recently we have examined the existing data without reference to a specific model and have found some interesting systematics. The origin of these systematics is not readily apparent in the DWBA formulation and suggests that, while the DWBA may be correct in many of its particulars, it is likely that a simpler model can be used to understand the dynamics of the reaction.

Fig. 5 shows that when the analyzing power angular distributions for the ${}^{13}C(p,d){}^{12}C$ (g.s.) reaction for 65 MeV<T_p<400 MeV are plotted versus an effective momentum transfer, a striking correspondence is observed. This effective momentum transfer is defined to be

$$q \equiv \left| \bar{K}'_p - \bar{K}'_d \right|,$$

where the proton and deuteron wave-numbers are evaluated using the kinetic energy each particle has at the center of its optical model potential well. This crude treatment of distortion is essential for obtaining the correspondence shown in Fig. 5.

When the effective momentum transfer defined above is employed, similar systematics also appear in cross section data. Fig. 6 shows this for the $^4He(p,d)^3He$ reaction at T_p=200, 400 and 770 MeV. It may be noted that such systematic behavior is not observed when these data are plotted versus

$$q' \equiv \left| \frac{3}{4} \vec{K}_p - \vec{K}_d \right| \quad \text{or} \quad \left| \frac{3}{4} \vec{K}_p' - \vec{K}_d' \right|$$

which is the relevant momentum transfer in the plane wave Born approximation (PWBA) and, by extension, in the DWBA. In Fig. 6 the cross sections are seen to have a roughly exponential fall-off with respect to q with a rate that is independent of energy. Furthermore, there is an energy-independent oscillatory structure superimposed on this fall-off which is more clearly evident in Fig. 7 which shows the cross sections with the exponential falloff (the straight lines of Fig. 6) divided out. This oscillatory structure can be well described as the (smeared) modulus of $\cos(qR_{osc})$ where R_{osc} is a characteristic length describing the frequency of the oscillation. This length happens to have roughly the same value (1.7 fm) as that which governs the exponential fall-off via $\exp(-qR_{falloff})$.

Although the oscillations are less pronounced, a similar situation is observed for $^{13}C(p,d)^{12}C$ (g.s.) cross sections for $121<T_p<800$ MeV,

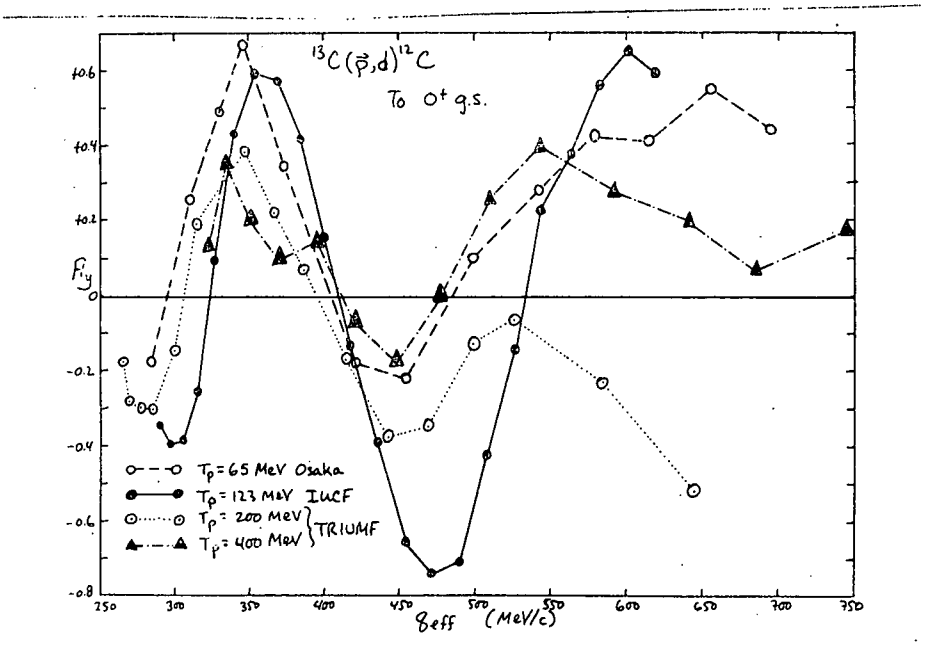

Fig. 5. Analyzing powers for the $^{13}C(p,d)^{12}C$ (0^+g.s.) reaction are plotted versus q_{eff} (see text) for several different energies.

except that the lengths are larger (3.7 fm) and the oscillations behave like $|\sin(qR)|$. Note that this transition has $\ell_{tr}=1$ whereas for ^{4}He(p,d), where the oscillations were like $|\cos(qR)|$, a $\ell_{tr}=0$ transition occurred. An exponential drop-off with oscillations superimposed, both being governed by similar length parameters of 3.2 fm, is also observed for ^{16}O(d,p)^{17}O(5/2$^+$ g.s.) at T_d=700 MeV. In this instance the oscillations behave like $|\cos(qR)|$ for the $\ell_{tr}=2$ transition.

These systematics and the hint of a phase rule governing the oscillations suggest that a relatively simple geometrical model such as that successfully applied to intermediate energy (p,p') cross sections and analyzing powers could be fruitfully employed here. The development of such a model is presently underway.

1. J. R. Shepard, E. Rost and P. D. Kunz, Proc. of Fifth Int. Symp. on Pol. Phenom. in Nuclear Physics, Santa Fe, NM, August, 1980.
2. R. D. Amado, J.-P. Dedonder and F. Lenz, Phys. Rev. C 21 (1980) 647, and R. D. Amazdo, F. Lenz, J. A. McNeil and D. A. Sparrow, preprints and to be published.
3. G. Bruge, rapport interne (Saclay) DPh-N/ME/78-1.
4. H.T. Fortune et al., Phys. Rev. C 12 (1975) 1723.

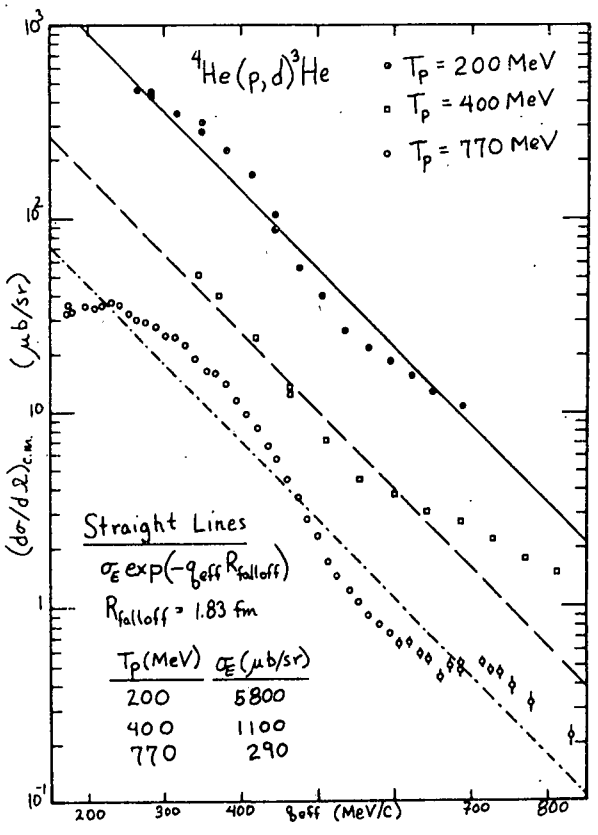

Fig. 6. Cross sections for the ^{4}He(p,d)^{3}He reaction are plotted versus q_{eff} (see text) for T_p=200, 400 and 770 MeV.

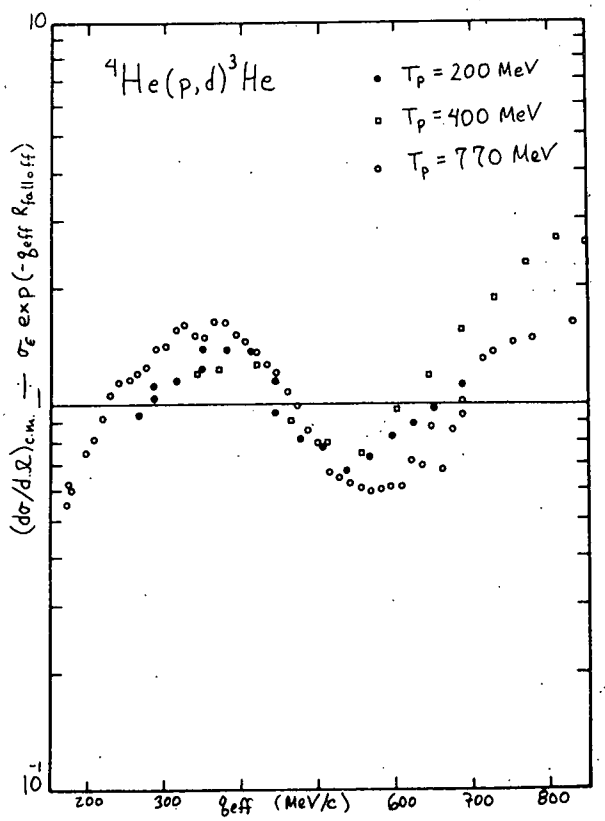

Fig. 7. Same as Fig. 6, but cross sections are divided by the exponential factor represented by the straight lines in Fig. 6.

G. Failure in the DWBA Analysis of (p,d) - J. R. Shepard, E. Rost and P. D. Kunz

The distorted wave Born approximation (DWBA) has generally been quite successful in reproducing (p,d) cross sections over a wide range of bombarding energies extending up to T_p=800 MeV. However, it does not reproduce analyzing powers nearly so well, although qualitative agreement is frequently achieved. In many cases, however, agreement is quite poor and can only be improved by arbitrary and physically unjustified adjustment of input parameters, such as potential strengths or geometries. The origin of the difficulty is not well understood although the possibilities are myriad. Isolating and identifying these problems would provide guidance for developing an improved theoretical understanding of the (p,d) reaction mechanism.

We have analyzed recent measurements for which the DWBA fails in a most spectacular fashion. Specifically, we have looked at cross section and analyzing power measurements for the $^{24}Mg(p,d)^{23}Mg(2.36\ MeV\ 1/2^+)$ transition at T_p=94 MeV. While similar failures have been observed by us for transitions in other light nuclei in this energy regime, this particular one is the most severe and has been the focus of our attention. We have examined the influence on the DWBA of several frequently ignored effects in an attempt to identify the source of the difficulty.

Fig. 8 combines the data with "standard" DWBA calculations employing phenomenological proton[3] and deuteron [4] optical model potentials and target wave functions tied to electron scattering densities[5]. Both exact-finite-range (calculations performed as in ref. 5) and zero-range results are shown with cross sections normalized using the theoretical spectroscopic factor of Chung and Wildenthal as reported in ref. 7. While some

differences can be perceived between the two calculations, they are insignificant when compared to the discrepancy with the data. The calculations overestimate the cross sections by at least an order of magnitude and the pronounced oscillatory structure observed in the asymmetry data is in no way reproduced.

These discrepancies appear not to be due to the use of improper optical potentials since significant improvement was not achieved by use of several other potential sets, including one which contained a tensor (T_R) interaction in the deuteron potential.

The effect of the deuteron continuum on (p,d) and (d,p) cross sections has been frequently studied. Approximate treatments such as the Johnson-Soper prescription[8] have resulted in improved agreement with cross section data in many cases. Full coupled-channels formulation of the three-body problem[9,10] is much more difficult and extended comparisons with data have not yet been made. Farrell, Vincent and Austern[9] suggest that continuum or break-up effects are most pronounced for low partial waves in the nuclear interior. This is just the region emphasized in momentum-mismatched reactions such as the one discussed here. We therefore

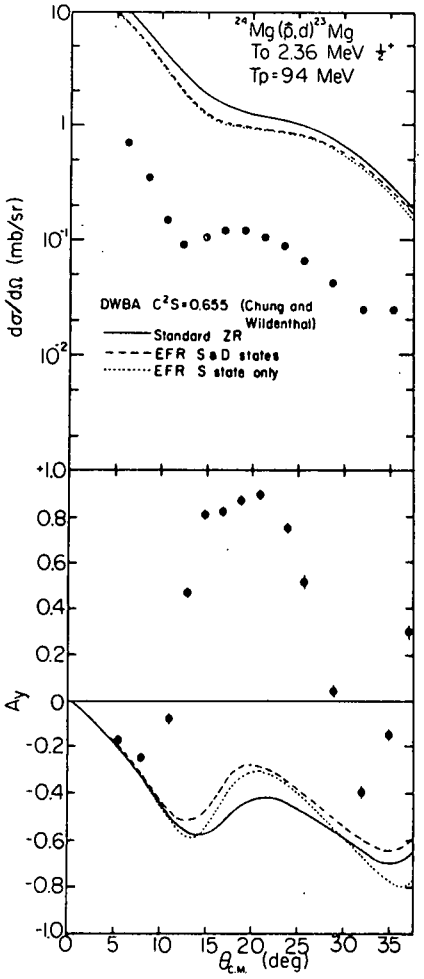

Fig. 8. Zero-range and exact-finite-range DWBA calculations are compared with data.

performed coupled-channels calculations in the spirit of ref. 9 using five continuum channels and a separable nucleon-nucleon potential. A comprehensive discussion of the calculational techniques used appears elsewhere in this Progress Report. These calculations appear in Fig. 9. The dashed curves of Fig. 9 correspond to DWBA calculations using unfolded nucleon-nucleus potentials[11] and are therefore equivalent to the Johnson-Soper method[8]. A folded or Watanabe-type potential[12] was used in the DWBA to generate the dotted curve; this corresponds to a limiting case of the coupled-channels calculations where only the deuteron bound

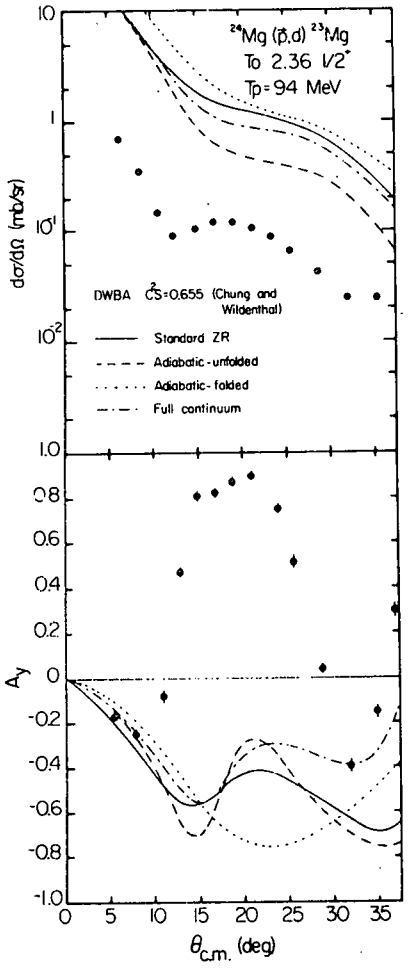

Fig. 9. DWBA calculations with and without continuum contributions are compared with data. See text for explanation.

state contribution is retained. Examination of the calculated analyzing powers displayed in Fig. 9 shows that, as asserted in ref. 9, the Johnson--Soper prescription yields a better approximation to the full calculation than the Watanabe model although no distinct preference can be inferred from the cross sections. In any case, no matter how the breakup contributions are treated, Fig. 9 shows that they do not appreciably improve agreement with the data.

^{24}Mg and ^{23}Mg are known to be strongly deformed nuclei. Consequently relatively large multistep contributions are possible in single-nucleon transfer reactions. These effects have been examined in detail for the ^{24}Mg(d,t) and (d,^{3}He) reactions by Nelson and Roberson[13]. We have used their amplitudes generated from shell model or band-mixed rotational model analyses in a CCBA extension of the DWBA to assess the influence of two-step contributions. The effect of two-step contributions was found to be quite small both for cross sections and analyzing powers, especially when compared to the discrepancies with data.

The highly oscillatory A_y angular distribution observed in the ^{24}Mg(p,d) reaction is qualitatively similar to that observed for elastic scattering of strongly-absorbed particles which can qualitatively be described using strong-absorption models which exploit the localized nature of the reaction[14]. We used several means of artificially introducing such localization into the DWBA calculations. All gave similar results and resulted in greatly improved agreement with the data. Examples appear in Fig. 10 where the dotted and dashed curves were obtained by multiplying the form factor by

$$f(r) = 1 - \{1 + \exp[(r-R_{co})/a_{co}]\}^{-1}$$

with a_{co}=0.5 fm and R_{co}=3.2 and 4.0 fm (or 1.11 x $24^{1/3}$ and 1.39 x $24^{1/3}$) respectively. In effect this amounts to a smoothed lower radial cut-off with cut-off parameters arbitrarily chosen to give the vastly improved agreement with the A_y data shown in the bottom half of Fig. 10. Not surprisingly, a similar effect can be achieved by greatly increasing absorption in the optical potentials. This is illustrated by the dashed-dot curve in Fig. 10 which was generated using the ZR DWBA without a cut-off, but with the imaginary deuteron potential strength increased by a factor of three. The top of Fig. 10 shows that the cut-off chosen to give optimum agreement with the A_y data also greatly improves agreement with the measured cross sections. Fig. 11 indicates that measured A_y values for strong ℓ=2 and ℓ=1 transitions are also much better reproduced. Cross section calculations using the Chung and Wildenthal spectroscopic factors are also in better agreement for these transitions.

Such general improvement using cut-offs suggests that delicate cancellations between one- and two-step amplitudes are not responsible for the poor agreement between the DWBA and experiment for the $^{24}Mg(p,d)^{23}Mg$ (2.36 MeV $1/2^+$) reaction. It does suggest that the cut-offs are mocking up important physical effects neglected in the DWBA even when the many refinements discussed above are included. The calculations are obviously very sensitive to contributions from the nuclear interior and apparently the DWBA, even in its more refined formulations, does not treat these contributions correctly. In the present case, this incorrect treatment results in catastrophic disagreement with experiment. We are continuing to investigate the origins of this disagreement.

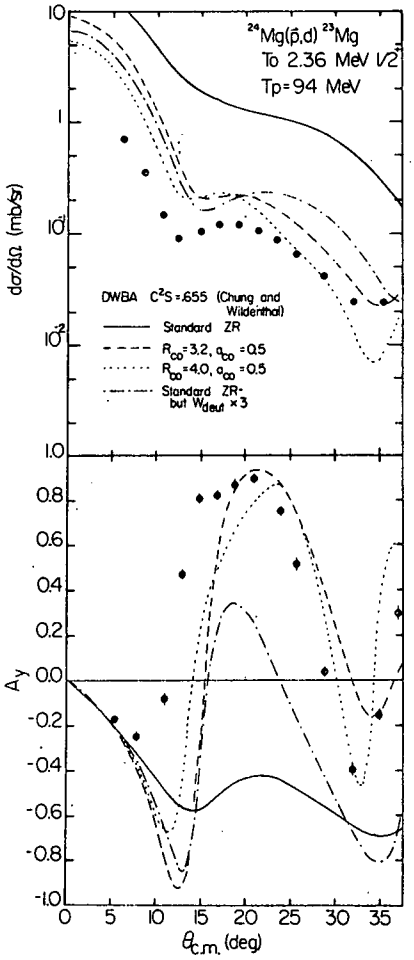

Fig. 10. Zero-range DWBA calculations with and without surface localization are compared with the data. The dashed and dotted curves reflect the use of cut-offs. The dashed-dot curve reflects the use of increased deuteron absorption.

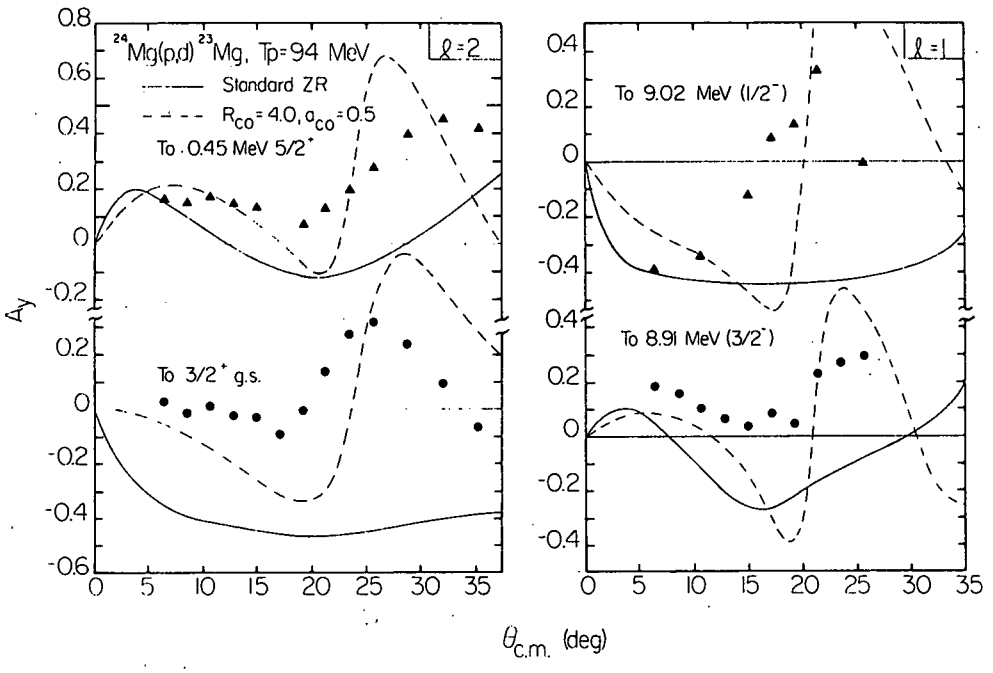

Fig. 11. Zero-range DWBA calculations with and without cut-offs are compared with the data.

1. K. Hoshono et al., contribution to the Fifth Intl. Symp. on Pol. Phenom. in Nuclear Physics, Santa Fe, NM, August, 1980.
2. D. W. Miller et al., Bull. Am. Phys. Soc. 25 (1980) 522, and to be published.
3. Y. S. Horowitz, Nucl. Phys. A193 (1972) 438.
4. J. Childs and W. W. Daehnick, Bull. Am. Phys. Soc. 20 (1975) 626.
5. J. R. Shepard and P. Kaczkowski, Bull. Am. Phys. Soc. 22 (1977) 529 (1977).
6. T. S. Bauer et al., Phys. Rev. C 21 (1980) 757.
7. D. W. Miller et al., Phys. Rev. C 21 (1979) 2008.
8. R. C. Johnson and P. J. R. Soper, Phys. Rev. C 1 (1970) 976.
9. J. P. Farrell, Jr., C. M. Vincent and N. Austern, Ann. Phys. 96 (1976) 333 and N. Austern, C. M. Vincent and J. P. Farrell, Jr., Ann. Phys. 114 (1978) 93.
10. G. H. Rawitscher, Phys. Rev. C 11 (1975) 1152.
11. H. H. Duhm, Nucl. Phys. A118 (1968) 563.
12. S. Watanabe, Nucl. Phys. 8 (1958) 484.
13. R. O. Nelson and N. R. Roberson, Phys. Rev. C 6 (1972) 2153.
14. e.g., R. D. Amado, F. Lenz, J. A. McNeil, and D. A. Sparrow, preprint.

H. Relativistic Generalization of Simple Pion-Nucleon Models - R. J. McLeod and D. J. Ernst (Texas A & M University)

A relativistic, partial wave N/D dispersion theory[1] has been developed for low energy, pion-nucleon interactions. For simplicity the P-wave crossing cut was generated from the right-hand physical cut by using the infinite-mass crossing relations. The no-crossing approximation was used for the S-waves. Elastic scattering phase shifts were calculated with coupling to inelastic channels taken from experiment. A form factor for the pion-nucleon vertex was chosen to be $\exp(-q^2/\beta^2)$ where q is the pion momentum and β is the only adjustable parameter in the model.

Three models were examined: pseudoscalar coupling (PSC), pseudovector coupling (PVC), and a PSC model in which the intermediate antinucleon states are removed from the propagator (PSC-N). This last model is motivated by the success of the Chew-Low model[2]. In the Chew-Low model the nucleon is assigned an infinite mass, thus the pion does not couple to the antinucleon. In this sense, the PSC-N model may be considered a relativistic extension of Chew-Low. In the PSC-N model, the angular integrals that arise cannot be done analytically. By expanding in terms of $\kappa=2q^2/(M^2+2q^2)$, where M is the nucleon mass, a convergent series was obtained.

In the PSC and PVC models, the parameter β was adjusted to reproduce the resonance in the P_{33} channel. For the PSC model, β was found to be 1100 MeV. In the P_{33} channel we have obtained detailed quantitative agreement with the experimental phase shifts for pion laboratory energies less than 1.2 GeV (solid curve Fig. 12). This agreement is much better than previous N/D results, but no better than a Chew-Low calculation[2] with a β of 764 MeV. Similar results were found for the PVC model. The PSC-N model did not fit the P_{33} phase shifts as well as the other models did (dashed curve in Fig. 12). In Fig. 12 a β of 2525 MeV was used which gives the best overall fit, but which predicts a resonance at too high an energy and with too narrow a width. This is due to the large contribution of the antinucleon. In Fig. 13 the nucleon pole term without the form factor (N) is plotted for the various models. A large difference can be seen for the various models. There are two important conclusions. First, adjusting β can compensate for the different amplitudes of the models, up to a point. Thus the results for the PSC and Chew-Low are comparable in the P_{33} channel. The PSC-N amplitudes, however, are outside the effective adjustable range of β, thus they do not fit in the resonance region. Second, coupling to the antinucleon gives a large contribution in the P_{33} channel of the PSC model, larger than of order M^{-1} as is usually implied in the literature. Models that do not include the antinucleon degrees of freedom are found to be unphysical. For this reason, the successs of the Chew-Low model is due to its connection to relativistic dispersion relations rather than underlying pion-nucleon physics.

THIS PAGE
WAS INTENTIONALLY
LEFT BLANK

in the sense that the phases were smaller than they were for the PSC model. However, the signs of the phase shifts were opposite to the data in both channels. The large antinucleon contribution in the S-waves can be seen in Fig. 14 where the S_{11} channel is plotted. It is seen that complete removal of the antinucleons did not supply sufficient attraction to agree with the experimental phase shifts. In the S_{31} channel, the phase shifts are again found to be much smaller than the experimental data. Thus, the S-wave problems in the PSC model are probably due to incorrect physical input and not to the presence of the antinucleons.

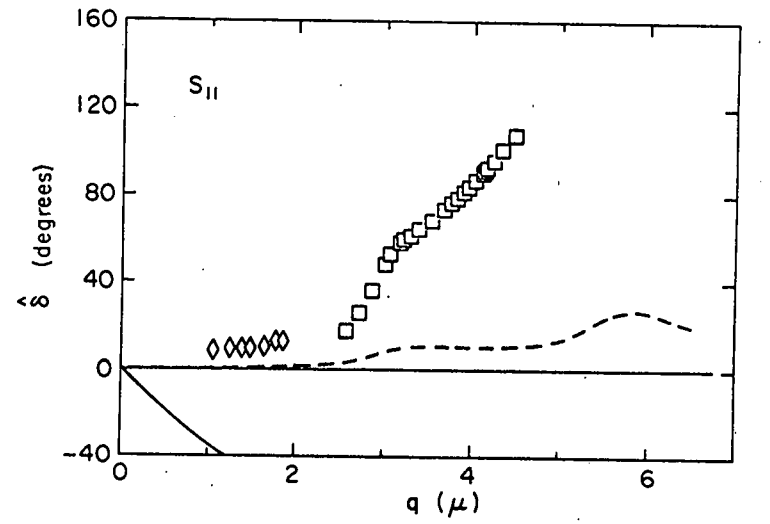

Fig. 14. The phase shifts versus the center-of-mass momentum in the S_{11} channel. The symbols are experimental data points. The solid curve is for the PSC model and the dashed curve is for the PSC-N model.

1. For a more complete account of this study, see R. J. McLeod, Texas A & M Univ., Ph.D. thesis, (1979), unpublished, and "Relativistic Generalizations of Simple Pion-Nucleon Models," R. J. McLeod and D. J. Ernst, submitted to Phys. Rev. C.
2. D. J. Ernst and M. B. Johnson, Phys. Rev. C 17 (1978) 247.

I. Pion-Nucleon Scattering Calculations - R. J. McLeod

Although there are good experimental data for pion-nucleon scattering at low energies, there is not a good dynamic theory to explain them. The existing models either do not reproduce the data in some channels or require several adjustable parameters to do so. Furthermore, most models rely on a dispersion-theory calculation which is based on a Low equation. The results of such calculations do not solve the original Low equations from which they were derived.

Recently, McLeod and Ernst[1] used a partial wave N/D dispersion theory for the pseudoscalar coupling model that put the crossing cut into the numerator function instead of the denominator function as had been done previously. For the simplest field-theoretic model, the Chew-Low model, this leads to a different high energy behavior than has been found previously[2]. Implications for a possible solution to the Low equation for the Chew-Low model are being studied. Also in ref. 1, it was found that the S-wave problems inherent to the pseudoscalar coupling model were not due to the presence of nucleon-antinucleon pairs. The calculation was done in the no-crossing approximation for the S-waves. Preliminary results show that isospin crossing has a large effect on the S-wave phase shifts. Also, ρ exchange has a significant effect. Further work is needed to determine if adding these factors as dynamic input into the model will improve agreement with experimental data.

---

1. See previous article.
2. D. J. Ernst and M. B. Johnson, Phys. Rev. C 17 (1978) 247.

J. Separable Approximation to the Reid Potential - R. J. McLeod and D. J. Ernst (Texas A & M University)

Separable potential forms are useful because they are easy to work with. A separable form of a two-body interaction will reduce a three-body problem to a one-dimensional integration. The general form of a separable approximation V_S of rank N to a local potential V is given by[1]

$$V_S = \sum_{ij=1}^{N} V|f_i\rangle M_{ij} \langle f_j|V$$

where

$$\sum_j M_{ij} \langle f_j|V|f_k\rangle = \delta_{ik}.$$

A polynomial basis set for $|f_i\rangle$ leads to good results at low energy but requires increasing-rank separable potentials with increasing energy. Choosing[2] $\langle r|f_i\rangle = j_i(k_i r)$ leads to a separable approximation that can be adjusted to fit V at some predetermined energy by adjusting the k_i's. This means that the higher-energy parts of V can be fitted with a lower-rank V_S.

In ref. 2 the above technique was applied to an exponential potential with good results. Presently, the technique is being applied to the Reid soft core potential which is a more realistic local potential. In Fig. 15

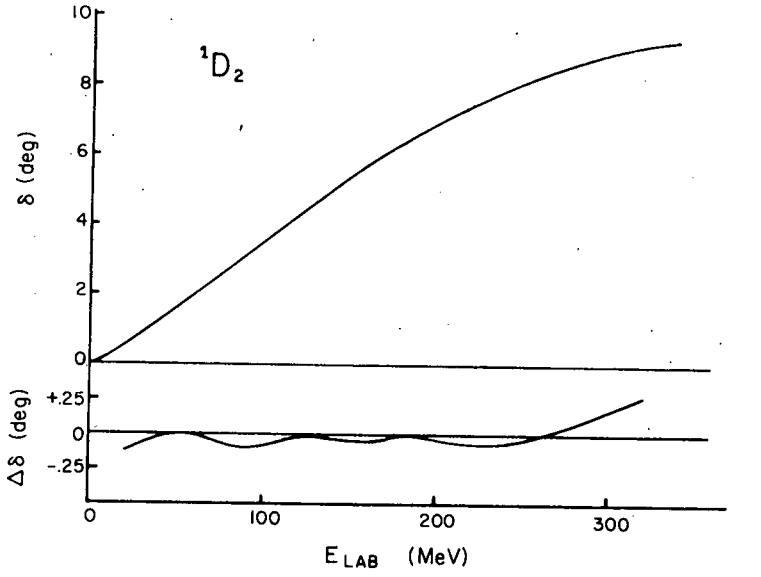

Fig. 15. The energy dependence of the phase shifts for the $^1D_2$ channel, the Reid soft core potential, and $\Delta\delta$, the difference between the exact phase shifts and those calculated using the approximation described in the text.

the phase shift for the $^1D_2$ channel is plotted as well as $\Delta\delta$, the difference between the exact results and that approximated by a separable potential of rank three. It is seen that the separable potential fits well over the entire range for which the Reid potential is assumed to be valid. The largest errors are near the ends of the energy range by choice. Smaller ranges could be fit more accurately if desired or the whole range could be fit better with a V_s of larger rank. Similar results are found for the other channels except for the coupled channels which are currently being calculated. Upon completion of the coupled-channels calculations this work will be submitted for publication.

1. D. J. Ernst, C. M. Shakin, and R. M. Thaler, Phys. Rev. C 10 (1974) 2176.
2. R. J. McLeod and D. J. Ernst, Phys. Rev. C 18 (1978) 1060.

K. Computer Program Development - E. Rost

The computing speed and, especially, the convenience of the newly installed PDP 11/60 computer has stimulated the conversion of most of the nuclear reaction computer programs to this machine. In particular, DWUCK (distorted waves) and DUMIT (pion optical model) have been converted without restriction whereas CHUCK (coupled channels) and ALICE (cascade calculations) can be run with moderate size cases. In addition, several utility programs were developed, viz. an angular momentum package (ANGMOM) and optical model search routines including polarization and tensor searches (OPUCK). A library of theory programs is resident on the PDP 11/60 disk memory and has been used extensively this summer.

IV. PUBLICATIONS AND REPORTS

A. Published Articles

A Simple Function for the Description of Cyclotron Magnetic Fields. D. H. Haynes and P. A. Smith, Nucl. Inst. and Meth. 166 (1979) 315.

Possible Methods for Improving the Resolution of Neutron Time-of-Flight Measurements of Direct Reaction Spectra. P. A. Smith, Nucl. Inst. and Meth. 166 (1979) 229.

Evidence for Pion Exchange Currents in the Analysis of the $^{4}He(p,d)^{3}He$ Reaction at Intermediate Energies. J. R. Shepard, E. S. Rost, and G. R. Smith, Phys. Lett. 89B, 13 (1979).

The (^{3}He,n) Reaction on Isotopes of Krypton. W. P. Alford, R. E. Anderson, P. A. Batay-Csorba, R. A. Emigh, D. A. Lind, P. A. Smith, and C. D. Zafiratos, Nucl. Phys. A330 (1979) 77.

Experimental Capabilities - Present and Future. C. D. Zafiratos, Proceedings of the Telluride Conference on the (p,n) Reaction and the Nucleon-Nucleon Force, Edited by C. D. Goodman, S. M. Austin, S. D. Bloom, J. Rapaport, and G. R. Satchler, Plenum Press, p. 313 (1980).

The ^{7}Li and $^{12}C(p,d)$ Reactions at T_p=800 MeV. T. S. Bauer, G. S. Adams, G. J. Igo, G. Pauletta, C. A. Whitten, G. R. Smith, J. R. Shepard, R. E. Anderson, R. L. Boudrie, N. J. DiGiacomo, J. J. Kraushaar, R. J. Peterson, and G. Hoffman, Phys. Rev. C 21 (1980) 757.

Low Lying Excited States of ^{106}Ag Studied with the $^{103}Rh(\alpha,n\gamma)^{106}Ag$ and $^{104}Pd(\alpha,pn\gamma)^{106}Ag$ Reactions. L. E. Samuelson, R. A. Emigh, D. E. Prull, R. E. Anderson, J. J. Kraushaar, and R. A. Ristinen, Z. Phys. A294 (1980) 353.

The ($\vec{t}$,p) Reaction on ^{56}Fe, $^{58,60,64}Ni$: Structure and Reaction Mechanism Effects. W. P. Alford, R. N. Boyd, E. R. Sugarbaker, D. L. Hanson, and E. R. Flynn, Phys. Rev. C 21 (1980) 1203.

Thick-Target Measurements and Astrophysical Thermonuclear Reaction Rates, Proton-Induced Reactions. N. A. Roughton, M. J. Fritts, R. J. Peterson, C. S. Zaidins, and C. J. Hansen, Atomic Data and Nuclear Data Tables 23, 177 (1980).

Nuclear Structure Effects Revealed by Inelastic Pion Scattering, R. J. Peterson, Nucl. Phys. A335, (1980) 365.

Spin and Isospin Transfer in the $^{12}C(\pi^+,\pi^{+\prime})$ Reaction. R. J. Peterson, R. L. Boudrie, J. J. Kraushaar, R. A. Ristinen, J. R. Shepard, G. R. Smith, C. F. Moore, W. J. Braithwaite, N. S. P. King, C. L. Morris, H. A. Thiessen, and J. Piffaretti, Phys. Rev. C 21 (1980) 1030.

Microscopic Investigation of Octupole Modes of Oscillation via Analyzing Power Measurements. D. Ardouin, R. E. Brown, J. Cizewski, E. R. Flynn, J. Sunier, W. P. Alford, and E. R. Sugarbaker, Phys. Rev. C 22 (1980) 432.

Neutron-Hole States in ^{204}Tl. P. A. Smith, R. J. Peterson, R. A. Emigh, and R. E. Anderson, Nucl. Phys. A342 (1980) 437.

A Search for Nuclear Structure Dependence of Analyzing Powers for the $(\vec{t},p)$ Reaction in Medium Mass Nuclei. R. E. Brown, J. A. Cizewski, J. W. Sunier, E. R. Flynn, W. P. Alford, and E. R. Sugarbaker, D. Ardouin, Phys. Rev. C 21 (1980) 2663.

Analyzing Power Measurements for Two-Nucleon Transfer Reactions in a Shape Transitional Nucleus. E. R. Flynn, R. E. Brown, J. A. Cizewski, J. Sunier, W. P. Alford, and E. R. Sugarbaker, D. Ardouin, Phys. Rev. C 22 (1980) 43.

Acute Nickel Intoxication by Dialysis. J. D. Webster, T. F. Parker, A. C. Alfrey, W. R. Smythe, H. Kubo, G. Neal, and A. R. Hull, Annals of Internal Medicine 92 (1980) 631.

(π^+,p) Absorption in $^{6,7}Li$ at 75 and 175 MeV. J. Kallne, J. Davis, P. C. Gugelot, J. S. McCarthy, G. R. Smith, R. L. Boudrie, B. Hoistad, and C. L. Morris. Phys. Rev. C 21 (1980) 2681.

High Spin States of ^{89}Y studied with the $^{87}Rb(\alpha,n\gamma)^{89}Y$ Reaction. C. A. Fields and L. E. Samuelson, Phys. Rev. C 20 (1979) 2442.

A Method for Determining the Neutron Multiplicity for Gamma Rays from (particle,xnγ) Reactions. C. A. Fields, F. W. N. de Boer, R. A. Ristinen, L. E. Samuelson, and P. A. Smith, Nucl. Inst. and Meth. 169 (1980) 173.

Gamma-Ray Spectroscopy of ^{87}Y. C. A. Fields, F. W. N. de Boer, J. J. Kraushaar, W. W. Pratt, R. A. Ristinen, and L. E. Samuelson, Z. Phys. A295 (1980) 365.

Analysis of $(^6Li,d)$ and $(d,^6Li)$ Reactions in the Nickel and Tin Regions. A. Vitturi, L. Ferreira, P. D. Kunz, H. M. Sofia, P. F. Bortignon, and R. A. Broglia, Nucl. Phys. A340 (1980) 183.

DWBA Form Factor for Three-Particle Transfer Reaction. T. Kammuri, H. Shimaoka, P. D. Kunz, S. Kato, K. Okada, M. Kondo, K. Hosono, T. Saito, N. Matsuoka, S. Nagamachi, T. Noro, K. Ogino, and Y. Kadota, Phys. Lett. 90B (1980) 197.

The Sequential Transfer Mechanisms in (p,n) Reactions. P. D. Kunz, Proceedings of the Telluride Conference on the (p,n) Reaction and the Nucleon-Nucleon Force, Edited by C. D. Goodman, S. M. Austin, S. D. Bloom, J. Rapaport, and G. R. Satchler, Plenum Press, (1980) p. 451.

A Search for Isobaric Analogues of M1 States and Giant Spinflip Resonances in the ^{208}Pb(p,n) Reaction. D. J. Horen, C. D. Goodman, C. C. Foster, C. A. Goulding, M. B. Greenfield, J. Rapaport, D. E. Bainum, E. Sugarbaker, T. G. Masterson, F. Petrovich, and W. G. Love, Phys. Lett. 95B (1980) 27.

B. Articles Accepted or Submitted for Publication

A Method of Estimating the Effect of Multiple Scattering in a Stripper on the Phase Space of a Charged Particle Beam. P. A. Smith, accepted by Nucl. Inst. and Meth.

Proton Radius Determination from the Ratio of π^+ Elastic Scattering from ^{11}B and ^{12}C. B. M. Barnett, W. Gyles, R. R. Johnson, K. L. Erdman, J. Johnstone, J. J. Kraushaar, S. Lepp, T. G. Masterson, E. S. Rost, D. R. Gill, A. W. Thomas, J. Alster, I. Navon, R. H. Landau, Accepted for publication in Phys. Lett.

Elastic Scattering of 13.9 MeV Positive Pions from ^{12}C. D. R. Gill, K. L. Erdman, E. W. Blackmore, W. Gyles, B. M. Barnett, C. Oram, R. R. Johnson, T. G. Masterson, N. Grion, Submitted to Physical Review Communications.

Analyzing Power Measurements for the $^{13}C(\vec{p},d)^{12}C$ Reaction at 200 and 400 MeV. R. P. Liljestrand, J.M Cameron, D. A. Hutcheer, W. J. MacDonald, R. McDonald, C. A. Miller, W. C. Olsen, J. J. Kraushaar, J. R. Shepard, J. G. Rogers, J. T. Tinsley, and C. E. Strouach, Submitted to Phys. Lett.

Semi-Microscopic Analysis of Multi-Nucleon Transfer and the $^{40}Ca(\alpha,p)^{43}Sc$ Reaction. P. A. Smith and R. J. Peterson, Submitted to Nucl. Phys.

The Tetraneutron Revisited. F. W. N. de Boer, J. J. van Ruyven, A. W. B. Kalshoven, H. Verheul, R. Vis, E. R. Sugarbaker, C. A. Fields, and C. S. Zaidins, Accepted for publication in Nucl. Phys.

Aligned Octupole Bands in Deformed N=90 and N=92 Nuclei. F. W. N. de Boer, C. A. Fields, G. Marro, E. R. Sugarbaker, J. Konijn, H. Verheul, and P. M. Walker, Accepted for publication in Phys. Lett.

Decay Pathways and Entry-State Population in $(\alpha,xn\gamma)$ and $(^3He,xn\gamma)$ Reactions on ^{150}Nd. C. A. Fields, F. W. N. de Boer, D. E. Prull, R. A. Ristinen, L. E. Samuelson, P. A. Smith, and E. R. Sugarbaker, Submitted to Nucl. Phys.

High Spin States of ^{90}Nb. C. A. Fields, F. W. N. de Boer, J. J. Kraushaar, R. A. Ristinen, L. E. Samuelson, and E. R. Sugarbaker, Submitted to Nucl. Phys.

A Study of $^{80,82,84}Sr$ by the $^{A}Kr(\alpha,2n\gamma)^{A+2}Sr$ Reactions. C. A. Fields, F. W. N. de Boer, E. R. Sugarbaker, and P. M. Walker, Submitted to Nucl. Phys.

High-Spin States in in ^{86}Sr. C. A. Fields, F. W. N. de Boer, B. J. Diana, E. R. Sugarbaker, and P. M. Walker, Submitted to Z. Phys. A.

Fluorine: Its Mineralogical Residence in the Mahogany Zone of the Green River Formation, Piceance Creek Basin, Colorado, U. S. A. O.M Saether, D. D. Runnells, R. A. Ristinen, and W. R. Smythe, Accepted for publication in Chemical Geology.

The ^{12}C(^{9}Be,n)^{20}Ne Reaction. E. R. Sugarbaker, R. N. Boyd, D. Elmore, and H. E. Gove, Accepted for publication in Nucl. Phys.

Energy Systematics of the Giant Gamow-Teller Resonance and a Charge-Exchange Dipole Spin-Flip Resonance. D. J. Horen, D. E. Bainum, C. C. Foster, C. D. Goodman, C. Gaarde, C. A. Goulding, M. B. Greenfield, J. Rapaport, T. N. Taddeucci, and E. R. Sugarbaker, Submitted to Phys. Lett.

Single-Nucleon Transfer Reactions to ^{100}Ru, R. J. Peterson, R. A. Emigh, and R. E. Anderson, Accepted for publication in Nucl. Phys.

The Reaction ^{10}B(d,n)^{11}C as an Ion Temperature Plasma Diagnostic. F. E. Cecil, L. K. Len, and R. J. Peterson, Accepted for publication in Nucl. Instr. and Methods.

Proton Stripping to High Spin States of ^{13}N. R. J. Peterson and J. J. Hamill, Accepted for publication in Phys. Rev.

Proton Stripping to ^{14}N. R. J. Peterson and J. J. Hamill, Submitted to Nucl. Phys.

Analyzing Power Measurements for the ^{13}C($\vec{p}$,d)^{12}C Reaction at 200 and 400 MeV. R. P. Liljestrand, J. M. Cameron, D. A. Hutcheon, W. J. MacDonald, R. McDonald, A. M. Miller, W. C. Olsen, J. J. Kraushaar, J. R. Shepard, J. G. Rogers, J. T. Tinsley, and C. E. Stronach, Accepted for publication in Phys. Lett. B.

A Study of the Particle-Vibration Multiplets in ^{203}Tl using the ^{205}Tl(p,t)^{203}Tl, ^{208}Pb(p,t)^{206}Pb and ^{206}Pb(p,t)^{204}Pb Reactions. R. C. Weiss, R. E. Anderson, J. J. Kraushaar, R. A. Ristinen, and E. S. Rost, Submitted to Nucl. Phys.

High Spin States in ^{90}Mo. F. W. N. de Boer, C. A. Fields, B. J. Diana, and E. R. Sugarbaker, Submitted to Nucl. Phys.

The Level Structure of ^{152}Sm. F. W. N. de Boer, C. A. Fields, and E. R. Sugarbaker, J. Konijn, H. Verheul, and P. M. Walker, Submitted to Nucl. Phys.

The Level Structure of ^{162}Dy. F. W. N. de Boer, C. A. Fields, E. R. Sugarbaker, P. M. Walker, and L. K. Peker, Submitted to Nucl. Phys.

The Level Structure of ^{156}Gd Studied by Means of the (α,2nγ) Reaction. F. W. N. de Boer; J. Konijn, A. van Poelgeest, W. H. A. Hesselink, M. J.A deVoigt, H. Verheul, and O. Scholten, Accepted for publication in Nucl. Phys.

Relativistic Generalizations of Simple Pion-Nucleon Models. R. J. McLeod and D. J. Ernst, Submitted to Phys. Rev. C.

Prsence and Formation of Cobalamin Analogues in Multivitamin-Mineral Pills. H. Kandu, M. J. Bindu, J. F. Kolhouse, W. R. Smythe, E. R. Podell, and R. H. Allen, Submitted to The New England Journal of Medicine.

C. Published Abstracts, Conference Presentations and Reports

Excitation of Giant Resonances in ^{118}Sn via 130 MeV Pion Scattering, R. S. Raymond, R. E. Anderson, R. L. Boudrie, J. Piffaretti, N. S. P. King, T. G. Masterson, C. L. Morris, R. J. Peterson, R. A. Ristinen, Proceedings of the International Conf. on Nuclear Physics, Berkeley (1980) 265.

Measurement of Nuclear Charge Distribution by π^+ Scattering, T. G. Masterson, J. J. Kraushaar, S. Lepp, E. S. Rost, B. Barnett, W. Gyles, R. R. Johnson, D. Gill, A. W. Thomas, J. Alster, Bull. Am. Phys. Soc. 25 (1980) 594.

Study of ^{12}C Levels with $18 \leq Ex \leq 20$ MeV Using the ^{11}B(h,d)^{12}C Reaction, J. R. Shepard, R. A. Emigh, R. J. Peterson, T. G. Masterson, M. D. Rayman, N. S. P. King, Bull. Am. Phys. Soc. 25 (1980) 594.

Comparison of (^{3}He,t) and (^{3}He,^{3}He') Yields to Analog states in A=13, R. J. Peterson, J. R. Shepard, R. A. Emigh, M. Rayman, T. G. Masterson, D. Dehnhard, Bull. Am. Phys. Soc. 25 (1980) 593.

Giant Resonances Observed in the ^{112,124}Sn(p,n)^{112,124}Sb Reactions, E. R. Sugarbaker, D. A. Bainum, C. C. Foster, D. J. Horen, C. Gaarde, C. D. Goodman, C. A. Goulding, M. Greenfield, T. G. Masterson, J. Rapaport, Proceedings of the International Conf. on Nuclear Physics, Berkeley (1980) 207.

Search for Isobaric Analogues of M1 States and Spin-Flip Resonances in ^{206,208}Pb(p,n) Reactions, D. J. Horen, C. D. Goodman, C. C. Foster, G. A. Goulding, M. B. Greenfield, J. Rapaport, D. E. Bainum, E. R. Sugarbaker, T. G. Masterson, F. Petrovich, W. G. Love, Proceedings of the International Conf. on Nuclear Physics, Berkeley (1980) 272.

Analyzing-Power Measurements for ^{24}Mg($\vec{p}$,d) at 95 MeV, D. W. Miller, D. W. Devins. W. W. Jacobs, W. P. Jones, and J. R. Shepard, Bull. Am. Phys. Soc. 25 522 (1980).

The Search for the Tetraneutron, F. W. N. de Boer, P. A. Smith, A. W. B. Kalshover, J. J. van Ruyven, H. Verheul, and R. Vis, Bull. Am. Phys. Soc. 24 818 (1979).

The Band Structure of ^{156}Gd, J.Konijn, F. W. N. de Boer, H. Verheul, and O. Scholter, Proc. Int. Conf. on Band Structure and Nuclear Dynamics v. 1 (Tulane Univ. 1980) p. 33.

Incident Angular Momentum Window in Light-Ion Induced Compound Nuclear Reactions, C. A. Fields, F. W. N. de Boer, R. A. Ristinen, L. E. Samuelson, P. A. Smith, and E. R. Sugarbaker, Proceedings of the International Conf. on Nuclear Physics, Berkeley (1980) p. 455.

One-Step Approach to Equilibrium Model for Pre-Equilibrium Neutron Emission, C. A. Fields, F. W. N. de Boer, R. A. Ristinen, L. E. Samuelson, P. A. Smith, and E. R. Sugarbaker, Proceedings of the International Conf. on Nuclear Physics, Berkeley (1980) p. 457.

High-Temperature Maxwellian Evaporation of Neutrons by Compound Nuclei, C. A. Fields, F. W. N. de Boer, R. A. Ristinen, L. E. Samuelson, P. A. Smith, and E. R. Sugarbaker, Proceedings of the International Conf. on Nuclear Physics, Berkeley (1980) p. 458.

Additional ^{4}He Induced Thermonuclear Rates Using Thick Target Techniques, N. A. Roughton, T. Intrator, C. Hansen, R. J. Peterson, and C. S. Zaidins, Bull. Am. Phys. Soc. 24 (1979) 821.

Excitation Functions of States in ^{12}C from π^{+} Inelastic Scattering, W. Cottingame, K. Allbright, W. J. Braithwaite, S. Greene, C. Harvey, D. B. Holtkamp, R. J. Joseph, I. B. Moore, C. F. Moore, J. Piffaretti, C. L. Morris, N. King, R. L. Boudrie, J. J. Kraushaar, R. J. Peterson, R. A. Ristinen, and G. R. Smith, Bull. Am. Phys. Soc. 24 (1979) 821.

Spectroscopy of Mass 12 at High Excitation Energies, J. R. Shepard, R. A. Ristinen, J. J. Kraushaar, M. D. Rayman, G. R. Smith, R. J. Peterson, N. S. P. King, W. W. Jacobs, and A. D. Bacher, Bull. Am. Phys. Soc. 24 (1979) 829.

Inelastic Scattering of Tritons and ^{3}He at 23 MeV from ^{13}C, D. Dehnhard, G. C. Idzorek, S. J. Tripp, R. E. Brown, J. A. Cizowski, E. R. Flynn, C. L. Morris, R. J. Peterson, Bull. Am. Phys. Soc. 25 (1980) 593.

The ^{13}C(^{3}He,d)^{14}N Reaction, J. J. Hamill and R. J. Peterson, Bull. Am. Phys. Soc. 25 (1980) 593.

Target Mass Dependence of the Pre-Equilibrium (α,2nγ) Reaction Mechanism, C. A. Fields, F. W. N. de Boer, R. A. Ristinen, P. A. Smith, and E. R. Sugarbaker, Bull. Am. Phys. Soc. 25 (1980) 594.

Systematics of Neutron-Deficient Strontium Isotopes, C. A. Fields, F. W. N. de Boer, E. R. Sugarbaker, and P. M. Walker, Proc. Int. Conf. on Band Structure and Nuclear Dynamics v. 1 (Tulane Univ. 1980) 20.

Aligned Octupole Bands in A=90 and A=92 Nuclei, F. W. N. de Boer, C. A. Fields, G. Marro, E. R. Sugarbaker, J. Konijn, H. Verheul, and P. M. Walker, Proc. Int. Conf. on Band Structure and Nuclear Dynamics v. 1 (Tulane Univ. 1980) 98.

In Vivo and In Vitro Measurements of Liver Cadmium in Uraemia, A. Alfrey, H. Baddeley, P. W. Craswell, L. Ibels, W. R. Smythe, and B. J. Thomas, Australian and New Zealand Journal of Medicine, Feb., 1980, Vol. 10, No. 1, p. 12.

Trace Element Abnormalities in Chronic Uraemia, A. Alfrey, P. Craswell, L. Ibels, and R. Smythe, Australian and New Zealand Journal of Medicine, Feb., 1980, Vol. 10, No. 1, p. 120.

Development of the Very Large Detector (VLD) for Long Flight Path Neutron Time-of-Flight, P. N. Craig and C. D. Zafiratos, Journal of the Colorado-Wyoming Academy of Sciences, vol 12, no. 1, 1980, p. 62.

The $^{46,48}Ti(\vec{p},\alpha)^{43,45}Sc$ Reaction, R. N. Boyd, S. L. Blatt, T. R. Donoghue, H. J. Hausman, E. R. Sugarbaker, and S. E. Vigdor, 5th International Symposium on Polarization Phenomena in Nuclear Physics, August, 1980, Santa Fe.

D. Theses

Decay Pathways and Entry State Population in the 35 MeV $^{150}Nd(\alpha,xn\gamma)$ Reactions. Christopher Albert Fields, M. S., 1980.

A Heavy-Ion Detector and its Use in Alpha-Transfer Reactions. Robert Claude Weiss, M. S., 1980.

A Nuclear Plasma Diagnostic Technique. Thomas Paul Intrator, M. S., 1980.

V. PERSONNEL

A. Academic and Scientific

F. D. Becchetti[1]	Visiting Professor
F. W. N. de Boer[2]	Visiting Professor
H. C. Bhang[3]	Research Associate
S. S. Dasgupta[4]	Research Associate
R. A. Emigh[5]	Research Associate
E. F. Gibson[6]	Visiting Professor
J. J. Kraushaar	Professor
P. D. Kunz	Professor
D. A. Lind	Professor
T. G. Masterson	Assistant Professor
R. J. McLeod	Research Associate
R. J. Peterson	Professor, Chairman of Laboratory
R. S. Raymond	Research Associate
R. A. Ristinen	Professor
E. S. Rost	Professor
J. R. Shepard	Assistant Professor
E. R. Siciliano[7]	Assistant Professor
P. A. Smith	Accelerator Physicist
W. R. Smythe	Professor
R. Stern	Professor, Dept. of Astrogeophysics
E. R. Sugarbaker	Visiting Assistant Professor
M. Yasue[7]	Research Associate
C. D. Zafiratos	Professor and Chairman, Dept. of Physics
C. S. Zaidins[8]	Professor

B. Technical and Support Staff

R. C. Armstrong	Research Aide
C. A. Crouch	Computer Programmer A
E. C. DeGabain	Research Fabricator
C. A. Fields[9]	Professional Research Assistant
B. C. Hymel	Research Aide
J. A. Magyar	Professional Research Assistant
A. B. Phillips	Cyclotron Engineer
D. E. Prull	Scientific Programmer
J. N. Sonnenberg	Staff Assistant
R. C. Weiss[9]	Professional Research Assistant
A. K. Wiles	Equipment Fabricator

C. Research Assistants

J. E. Benage[9]	D. H. Haynes
T. L. Chenevert[10]	S. H. Lepp[10]
P. N. Craig	D. P. Murdock[9]
B. J. Diana[9]	M. D. Rayman[10]
S. A. Dickey[9]	R. E. Rodenburg[9]
H. Haghbin	M. A. Rumore[9]
J. J. Hamill	L. K. Smith[9]
G. N. Hassold[10]	

D. Other Students (part-time)

A. Alaniz
A. Ash
C. Boozer
H. Cockburn
M. Covey
D. Crook
M. Gordon
T. Herbert
D. Hermann
S. Jackson
G. Marro
P. Mattingly[9]
S. Morrison
G. Olbright[9]
G. Shea
R. Sinton[9]
C. Somps
M. Stanton
B. Walsh[9]
T. Woolf[9]

E. Summer Visitor (supported in part by contract funds)

N. Roughton (Regis College, Denver)

---

[1] On leave from University of Michigan, Ann Arbor, starting Sept., 1980.
[2] On leave from Vrije Universiteit, Amsterdam, appointment ended Sept. 1980.
[3] Appointment began October, 1980.
[4] Appointment ended January, 1980.
[5] Appointment ended June, 1980.
[6] On leave from California State University, Sacramento, Spring semester.
[7] Appointment began September, 1980.
[8] On leave to I.P.N., Orsay, France.
[9] Appointment began 1980.
[10] Appointment ended 1980.

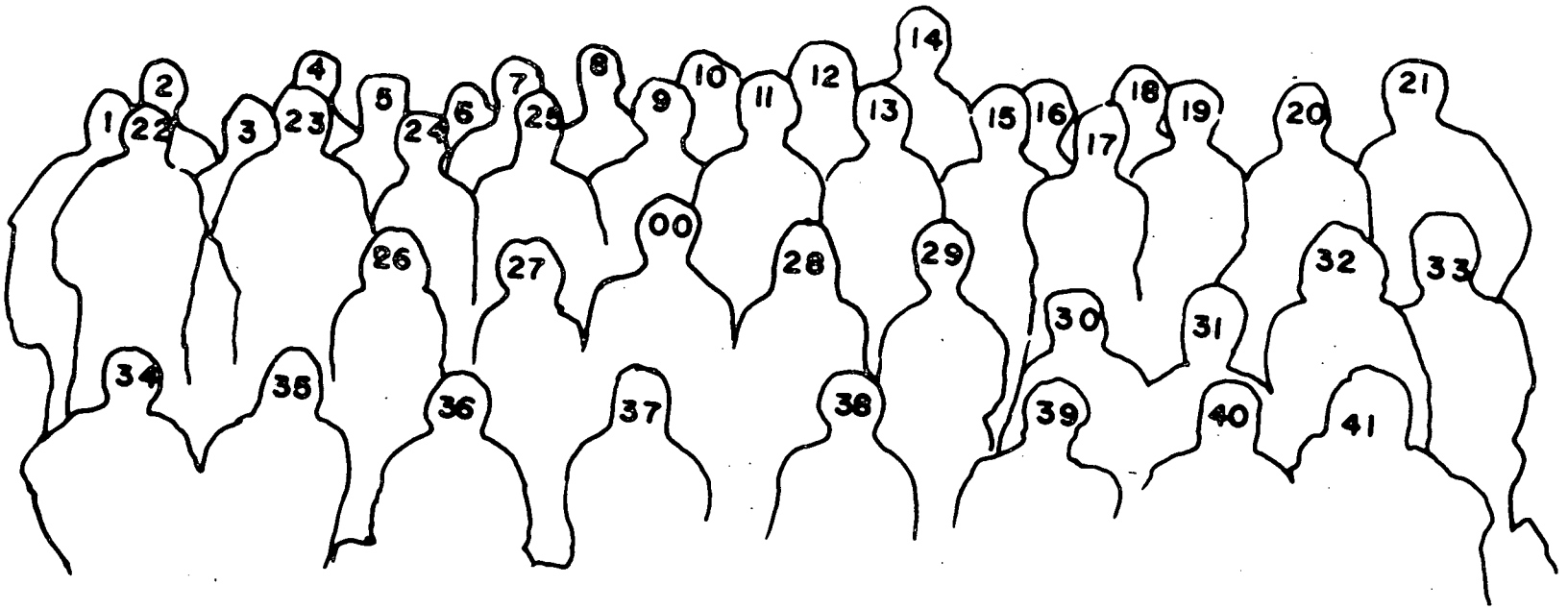

1. A. K. Wiles
2. D. E. Prull
3. M. Gordon
4. D. Hermann
5. R. A. Ristinen
6. C. A. Fields
7. E. Sugarbaker
8. J. J. Hamill
9. R. J. McLeod
10. P. N. Craig
11. G. N. Hassold
12. B. C. Hymel
13. R. C. Weiss
14. M. Yasue
15. F. D. Becchetti
16. W. R. Smythe
17. H. Haghbin
18. F. W. N. de Boer
19. M. B. Chen
20. P. A. Smith
21. R. Stern
22. R. C. Armstrong
23. J. J. Kraushaar
24. T. G. Masterson
25. A. B. Phillips
26. S. Jackson
27. C. A. Crouch
28. B. J. Diana
29. J. N. Sonnenberg
30. P. D. Kunz
31. E. S. Rost
32. R. E. Rodenburg
33. D. A. Lind
34. J. A. Magyar
35. S. A. Dickey
36. J. R. Shepard
37. R. S. Raymond
38. D. H. Haynes
39. G. Shea
40. A. Alaniz
41. D. P. Murdock
00. R. J. Peterson

Not Shown:

C. D. Zafiratos
E. R. Siciliano
L. Smith
C. S. Zaidins
E. C. DeGabain
C. Boozer
J. Benage
M. Rumore